

**Escherichia coli metabolism under dynamic conditions  
The tales of substrate hunting**

Vasilakou, E.

**DOI**

[10.4233/uuid:6708acd8-92a7-449b-9275-d311bbfb06aa](https://doi.org/10.4233/uuid:6708acd8-92a7-449b-9275-d311bbfb06aa)

**Publication date**

2020

**Document Version**

Final published version

**Citation (APA)**

Vasilakou, E. (2020). *Escherichia coli metabolism under dynamic conditions: The tales of substrate hunting*. [Dissertation (TU Delft), Delft University of Technology]. <https://doi.org/10.4233/uuid:6708acd8-92a7-449b-9275-d311bbfb06aa>

**Important note**

To cite this publication, please use the final published version (if applicable).  
Please check the document version above.

**Copyright**

Other than for strictly personal use, it is not permitted to download, forward or distribute the text or part of it, without the consent of the author(s) and/or copyright holder(s), unless the work is under an open content license such as Creative Commons.

**Takedown policy**

Please contact us and provide details if you believe this document breaches copyrights.  
We will remove access to the work immediately and investigate your claim.

***Escherichia coli* metabolism under dynamic conditions:**

**The tales of substrate hunting**

Dissertation

for the purpose of obtaining the degree of doctor

at Delft University of Technology

by the authority of the Rector Magnificus Prof.dr.ir. T.H.J.J. van der Hagen,

chair of the Board for Doctorates

to be defended publicly on

Monday 9 November 2020 at 12:30 o'clock

by

**Eleni VASILAKOU**

Master of Science in Chemical Engineering,

National Technical University of Athens, Greece

born in Ioannina, Greece

This dissertation has been approved by the

Promotor: Prof.dr.ir. M.C.M. van Loosdrecht

Copromotor: Dr. S.A. Wahl

Composition of the doctoral committee:

Rector Magnificus,	chairperson
Prof.dr.ir. M.C.M. van Loosdrecht	Delft University of Technology, promotor
Dr. S.A. Wahl	Delft University of Technology, copromotor

Independent members:

Prof.dr.ir. H. Noorman	Delft University of Technology
Prof.dr. M. Oldiges	Forschungszentrum Jülich GmbH, Germany
Prof.dr. F.J. Bruggeman	Vrije Universiteit Amsterdam, The Netherlands
Dr.ir. I. Rocha	Universidade NOVA de Lisboa, Portugal
N. Banke	Glycom A/S, Denmark
Prof.dr. P. Daran-Lapujade	Delft University of Technology, reserve member

The research presented in this thesis was performed at the Cell Systems Engineering section, Department of Biotechnology, Faculty of Applied Sciences, Delft University of Technology, The Netherlands.

This project was part of the ERA-IB funded consortium DYNAMICS (ERA-IB-14-081) and was also financed by the Netherlands Organization for Scientific Research (NWO) under the code 053.80.724.

All research data and code supporting the findings described in this thesis are available in 4TU.Centre for Research Data at: <https://doi.org/10.4121/uuid:44a6b4eb-c4b6-4199-b023-39a97ab0eae8>.

Cover design by: N. Margaritis and K. Patsiogianni

© 2020, Eleni Vasilakou

All rights reserved

**ISBN: 978-94-6366-329-8**

Printed by Ipskamp Printing

*Dedicated to my family*

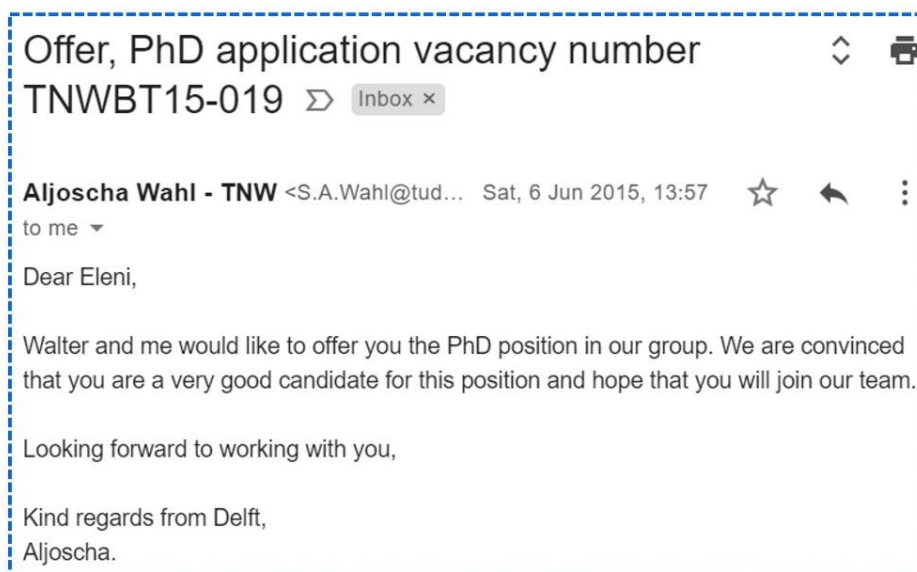
**“Just like a single cell, the character of our lives is determined not by our genes,  
but by our responses to the environmental signals that propel life.”**

**Bruce H. Lipton** in

The biology of belief: Unleashing the power of consciousness, matter and miracles.  
Mountain of Love/Elite Books (2005).



## Preface



This was how it all began. A very important e-mail, a very important day, which was the start of an unforgettable journey.

My decision to pursue a PhD in Biotechnology was mainly driven by some very passionate people in the field, whom I had the luck to meet and work with, at the Bioenergy Group of Prof. Angelidaki, at the Technical University of Denmark, for the purpose of my Diploma thesis. My supervisors (whom I personally thank in the Acknowledgements section) showed me the irresistible side of scientific research and motivated my career choices.

September 1<sup>st</sup>, 2015 was the first day I walked into the Department of Biotechnology in TU Delft, our old but beloved building, of major historical significance in the world of microbiology. A day of too many thoughts and feelings: Was that the right choice? Am I ever going to be a “Doctor”? How can it be so cold and rainy in the first day of September?!

4.5 years later, I definitely know the answer to my first two questions. The last one will probably require many more years of research to be answered, surely not by me.

My research was characterized by both successes and failures, moments of pride and moments of disappointment, challenges, self-development, friendships and collaborations, all worth it. This PhD thesis is a tiny piece of the puzzle of understanding bacterial metabolism. I am optimistic that it will provide new knowledge to the readers, form critical opinions, inspire and engage more people to get involved with scientific research. If none of these happens, I at least hope that you will enjoy the reading!

**Eleni Vasilakou**

**Delft, May 2020**



## Days in the lab



**Figure 1.** My beloved reactor, with which I spent 4 full years (days and nights). This is the setup needed to grow bacterial cells (yes they are inside the yellow broth!).

**Figure 2.** Science is often full of surprises. This is what happens after forgetting an LB media for many days in the fridge. Microorganisms created their own art.

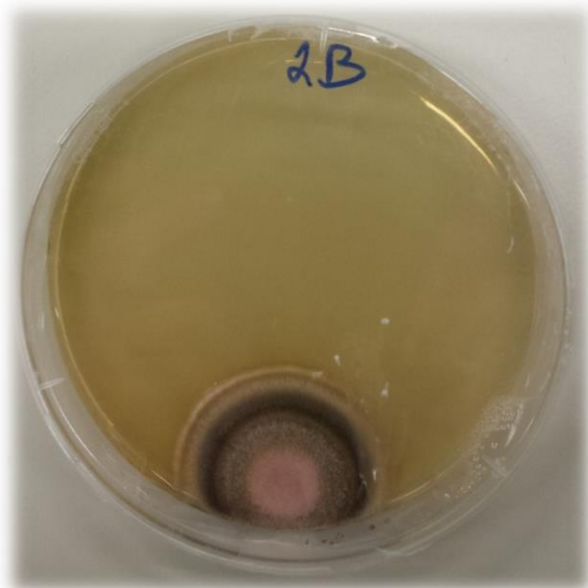






## Table of Contents

Abbreviations.....	1
Summary/Samenvatting .....	3
<u>Chapter 1</u> – General Introduction .....	11
<u>Chapter 2</u> – Current state and challenges for dynamic metabolic modeling ....	23
<u>Chapter 3</u> – <i>Escherichia coli</i> metabolism under short-term repetitive substrate dynamics: Adaptation and trade-offs.....	41
<u>Chapter 4</u> – Model-based identification of cellular mechanisms during the transition of <i>Escherichia coli</i> from steady-state to dynamic environments .....	93
<u>Chapter 5</u> – Proteomic and metabolomic analysis of <i>Escherichia coli</i> adaptation strategies to substrate fluctuations .....	139
<u>Chapter 6</u> – Conclusions and Outlook .....	199
Acknowledgements .....	209
About the author .....	217



## Abbreviations

<b>2PG</b>	2-phosphoglycerate	<b>Lys</b>	Lysine
<b>3PG</b>	3-phosphoglycerate	<b>M1P</b>	Mannitol-1-phosphate
<b>6PG</b>	6-phosphogluconate	<b>M6P</b>	Mannose-6-phosphate
<b>ADP</b>	Adenosine diphosphate	<b>Mal</b>	Malate
<b>AEC</b>	Adenylate energy charge	<b>Meth</b>	Methionine
<b>AIC</b>	Akaike information criterion	<b>MOMA</b>	Minimization of metabolic adjustment
<b>aKG</b>	Alpha-ketoglutarate	<b>mRNA</b>	Messenger ribonucleic acid
<b>Ala</b>	Alanine	<b>MS</b>	Mass spectrometry
<b>AMP</b>	Adenosine monophosphate	<b>NMR</b>	Nuclear magnetic resonance
<b>Asn</b>	Asparagine	<b>ODE</b>	Ordinary differential equation
<b>Asp</b>	Aspartate	<b>PEP</b>	Phosphoenolpyruvate
<b>ATP</b>	Adenosine triphosphate	<b>pfk</b>	Phosphofruktokinase
<b>BPG</b>	Bisphosphoglyceric acid	<b>PFR</b>	Plug flow reactor
<b>BWF</b>	Block-wise feeding	<b>pgi</b>	Phosphoglucoisomerase
<b>cAMP</b>	Cyclic adenosine monophosphate	<b>pgk</b>	Phosphoglycerate kinase
<b>CCR</b>	Carbon catabolite repression	<b>Phe</b>	Phenylalanine
<b>CDW</b>	Cell dry weight	<b>ppk</b>	Polyphosphate kinase
<b>Cit</b>	Citrate	<b>PPP</b>	Pentose phosphate pathway
<b>Cys</b>	Cysteine	<b>Pro</b>	Proline
<b>DHAP</b>	Dihydroacetonephosphate	<b>PTS</b>	Phosphotransferase system
<b>DNA</b>	Deoxyribonucleic acid	<b>PWA</b>	Piecewise affine
<b>DO</b>	Dissolved oxygen	<b>pyk</b>	Pyruvate kinase
<b>E4P</b>	Erythrose-4-phosphate	<b>RCF</b>	Reference constant feeding
<b>eno</b>	Enolase	<b>Rib5P</b>	Ribose-5-phosphate
<b>F6P</b>	Fructose-6-phosphate	<b>rRNA</b>	Ribosomal ribonucleic acid
<b>FBA</b>	Flux balance analysis	<b>S7P</b>	Sedoheptulose-7-phosphate
<b>fba</b>	Fructose biphosphate aldolase	<b>SEM</b>	Scanning electron microscopy
<b>FBP</b>	Fructobiphosphate	<b>Ser</b>	Serine
<b>Fum</b>	Fumarate	<b>SRE</b>	Stimulus response experiment
<b>G1P</b>	Glucose-1-phosphate	<b>STR</b>	Stirred tank reactor
<b>G6P</b>	Glucose-6-phosphate	<b>Suc</b>	Succinate
<b>GAP</b>	Glyceraldehydphosphate	<b>T6P</b>	Trehalose-6-phosphate
<b>gap</b>	Glyceraldehyde 3-phosphate	<b>TCA</b>	Tricarboxylic acid
<b>GC</b>	Gas chromatography	<b>Thr</b>	Threonine
<b>GDP</b>	Guanosine diphosphate	<b>tmRNA</b>	Transfer-messenger ribonucleic acid
<b>Gln</b>	Glutamine	<b>TOC</b>	Total organic carbon
<b>Glu</b>	Glutamate	<b>tpi</b>	Triosephosphate isomerase
<b>Gly</b>	Glycine	<b>Tre</b>	Trehalose
<b>GTP</b>	Guanosine triphosphate	<b>tRNA</b>	Transfer ribonucleic acid
<b>His</b>	Histidine	<b>Trp</b>	Tryptophan
<b>iCit</b>	Isocitrate	<b>Tyr</b>	Tyrosine
<b>IDMS</b>	Isotope dilution mass spectrometry	<b>UDP</b>	Uridine diphosphate
<b>Ile</b>	Isoleucine	<b>UTP</b>	Uridine triphosphate
<b>LC</b>	Liquid chromatography	<b>Val</b>	Valine
<b>Leu</b>	Leucine	<b>Xyl5P</b>	Xylose-5-phosphate



# Summary / Samenvatting

## Summary

Dynamic environmental conditions govern microbial metabolism and affect cellular growth. Many applications in biotechnology require cultivating microorganisms in large-scale bioreactors. These environments are commonly characterized by physicochemical gradients, due to imperfect mixing and have been the cause of reduced performance of cell factories in industry. Changes in substrate and gas concentrations, pH and temperature are some example of the generated gradients.

The aim of this thesis is to unravel and understand the effects of repetitive substrate fluctuations on the cellular behaviour of *Escherichia coli* K12 MG1655, using experimental and modelling approaches.

**Chapter 1** is a general introduction to biotechnology and its applications, with a focus on upstream bioprocesses. In addition, the role of the bacterium *Escherichia coli* as a model organism, as well as a working horse of biotechnology, is discussed.

In **Chapter 2**, the quantitative experimental and kinetic modelling approaches, currently used for studying microbial metabolism under dynamic conditions, are summarized and discussed. Current challenges and future perspectives finalize this chapter.

In the experimental **Chapter 3**, a block-wise feeding regime was applied to an aerobic *E.coli* culture, with the aim to grow cells under substrate (glucose) gradients, following a reference chemostat (steady-state) growth. This regime was called “fast feast-famine”, as cells experienced periods of substrate excess, limitation and depletion in a time-scale of seconds. The regime was characterized by repetitive cycles of 20 s feeding and 380 s without feeding. The perturbations were applied for at least 8 generations, allowing the cells to adapt to the dynamic environment (highly reproducible cellular response). The specific substrate and oxygen consumption (average) rates increased during the feast-famine regime, compared to the reference steady-state cultivation. The increased rates at same (average) growth rate led to a reduced biomass yield (30% lower), while there was no significant by-product formation. Such observation suggests the emergence of energy spilling reactions. With the increase in extracellular substrate concentration, the cells rapidly increased their uptake rate. Within 10 seconds after the beginning of the feeding, the glucose uptake rate was higher (4.68  $\mu\text{mol/g}_{\text{CDW}}/\text{s}$ ) than reported during batch growth (3.3  $\mu\text{mol/g}_{\text{CDW}}/\text{s}$ ). The high uptake led to an accumulation of several intracellular metabolites, during the feast phase, accounting for up to 34% of the carbon supplied. Although the intracellular metabolite concentrations changed rapidly, the cellular energy charge remained homeostatic, suggesting a well-controlled balance between ATP producing and ATP consuming reactions.

The importance of combining experimental perturbation studies and kinetic modelling, in order to reveal metabolic strategies for coping with dynamic conditions is highlighted in the following Chapter 4.

In **Chapter 4**, a published kinetic model for central carbon metabolism by Peskov K, et al. was used to investigate if the experimental observations from Chapter 3 could be reproduced with a model originating from steady-state calibration. Only after parameter optimization, with significant changes, could the data be reproduced, highlighting significant alterations in the enzymatic kinetics of glycolysis during feast-famine, compared to steady-state growth. Post-transcriptional modifications were assumed to explain the sudden decrease in the substrate uptake rate, observed while glucose was still in excess. To reflect such change in the modelling approach, the feast-famine cycle was split into two phases and the experimental uptake rate was used as fixed input. Nevertheless, this was not yet sufficient to fully reproduce the experimental observations. The time course of the glycolytic intermediates could only be reproduced when introducing glycogen synthesis and assimilation in the model. Here, glycogen acted as a storage pool, providing carbon and energy to reinitiate growth during famine conditions. Furthermore, ATP-spilling reactions were needed to reproduce the observed adenylate energy homeostasis. Additionally, a continuous draining of ATP supported the hypothesis of increased maintenance during the feast-famine regime.

In **Chapter 5**, multi-omics approaches, i.e. shotgun cellular proteomics and <sup>13</sup>C-labelled metabolomics were used for untargeted analysis and generation of new hypotheses on cellular regulatory mechanisms, when cells were subjected to fluctuations in substrate availability. The extracellular dynamics were expected to trigger global stress responses, in line with the observed reduced biomass yield. Surprisingly, this was not the case – stress-related proteins did not alter from steady-state to feast-famine conditions. On the other hand, the cellular proteome adjusted for specific functional categories, including biosynthesis and translation processes (ribosomes). This increase can be explained by either increased protein production to support the rapid growth changes, during the short time of substrate availability, or ribosome stalling due to amino acid limitation during the famine phase. During substrate-limited growth (constant feeding) cells have an overcapacity of metabolic enzymes (involved in central carbon pathways), which is used under nutrient up-shift to handle rapid increase in metabolic fluxes. The down-regulation of several enzymes in glycolysis, TCA cycle and pentose phosphate pathway, as well as, transporter proteins, revealed that cells respond more to the substrate excess period than the starvation period during the block-wise feeding regime. This is also in accordance with the observed down-regulation of the glyoxylate-shunt enzymes. Moreover, the increased levels of polyphosphate kinase indicated the use of a polyphosphate pool as a putative buffer for energy homeostasis.



Glycogen production and degradation was verified by the proteomic and  $^{13}\text{C}$  tracing analysis and is suggested to contribute to the ATP spilling (biomass yield losses), along with the increased protein turnover, which was identified by an increased section of the cellular proteasome.

The generated insights of the whole thesis are summarized in **Chapter 6**. Additionally, open questions are discussed. The future challenges include scale-down experiments, research on the effects of dynamics on production hosts, the use of mutant strains for validation experiments and data integration toward multi-scale modeling.

## Samenvatting

De dynamische condities in de omgeving van een cel bepalen het microbiële metabolisme en hebben invloed op de celgroei. Vele biotechnologische toepassingen vereisen de cultivatie van micro-organismen in grootschalige bioreactoren. Deze reactoren worden gewoonlijk gekarakteriseerd door fysisch-chemische gradiënten, die ontstaan door onvolledige menging. Dit veroorzaakt een verminderde productopbrengst van in industriële biotechnologische processen. Gradienten in concentraties van substraat en zuurstof, pH en temperatuur zijn enkele voorbeelden van dergelijke gradiënten.

Het doel van dit proefschrift was het ontrafelen en begrijpen van de effecten van repetitieve substraatfluctuaties op het cellulaire gedrag van *Escherichia coli* K12 MG1655, door gebruik te maken van zowel experimentele als modelmatige benaderingen.

**Hoofdstuk 1** is een algemene introductie tot de biotechnologie en haar toepassingen, met een focus op upstream bioprocessen. Daarnaast wordt ook de rol van de bacterie *Escherichia coli* als modelorganisme en als werkpaard van de biotechnologie besproken.

In **Hoofdstuk 2** worden de kwantitatieve experimentele en kinetische modelmatige benaderingen, die op dit moment in gebruik zijn voor het onderzoeken van het microbiële metabolisme onder dynamische condities, samengevat en besproken. Dit hoofdstuk wordt afgesloten met een overzicht van huidige uitdagingen en toekomstperspectieven.

In het experimentele **Hoofdstuk 3**, is een bloksgewijs voedingsregime opgelegd aan een aerobe *E.coli* cultuur, met het doel om de cellen te laten groeien onder substraat (glucose) gradiënten, na een initiële chemostaat (steady-state) groei als referentieconditie. Dit regime werd "fast feast-famine" genoemd, aangezien cellen perioden van substraatovervloed, en substraatuitputting ervaren op een tijdsschaal van seconden. Het regime werd gekarakteriseerd door repetitieve cycli van 20 s voeding en 380 s zonder voeding. Deze verstoringen werden minimaal 8 generaties lang toegepast, om de cellen de kans te geven om zich aan te passen aan de dynamische omgeving. De specifieke (gemiddelde) substraat en zuurstof consumptiesnelheden namen gedurende het feast-famine regime toe in vergelijking met de referentie steady-state cultivatie. Deze toegenomen snelheden bij dezelfde (gemiddelde) groeisnelheid leidden tot een gereduceerde biomassaopbrengst (30% lager), terwijl er geen significante productie van bijproducten was. Een dergelijke observatie suggereert het ontstaan van energieverspillende reacties. Met de verhoging in extracellulaire substraatconcentratie verhoogden de cellen vlug hun opnamesnelheid. Binnen 10 seconden na het begin van de voeding was de opnamesnelheid hoger ( $4.68 \mu\text{mol}/\text{g}_{\text{CDW}}/\text{s}$ ) dan wordt gerapporteerd voor de maximale snelheid tijdens batchgroei ( $3.3 \mu\text{mol}/\text{g}_{\text{CDW}}/\text{s}$ ). Deze hoge opnamesnelheid leidde tot een accumulatie van verscheidene intracellulaire metabolieten,

die, gedurende de feast-fase, goed was voor 34% van de aangeboden koolstof. Alhoewel de intracellulaire metabolietconcentraties snel veranderden, bleef de cellulaire energiestatus homeostatisch, hetgeen suggereert dat er een bijzonder gecontroleerd evenwicht bestaat tussen ATP-producerende en ATP-consumerende reacties.

In het volgende Hoofdstuk 4 wordt het belang van het combineren van experimentele verstoringstudies en kinetisch modellen, om metabole strategieën voor het omgaan met dynamische condities te bestuderen, benadrukt.

In **Hoofdstuk 4** is een door Peskov et al. gepubliceerd model voor het centrale koolstofmetabolisme gebruikt om te onderzoeken of de experimentele waarnemingen uit Hoofdstuk 3 gereproduceerd konden worden met een model dat op steady-state condities gekalibreerd is. Enkel na parameteroptimalisatie, met significante veranderingen, konden de data gereproduceerd worden, hetgeen de significante aanpassingen in de enzymatische kinetiek van de glycolyse gedurende feast-famine ten opzichte van steady-state groei benadrukt. Post-transcriptionele modificaties werden verondersteld om de plotselinge vermindering in de substraatopnamesnelheid, geobserveerd terwijl glucose nog steeds in overmaat aanwezig was, te verklaren. Om een dergelijke verandering in de modelmatige benadering te kunnen reflecteren, is de feast-famine cyclus opgesplitst in twee fases en is de experimentele opnamesnelheid gebruikt als invoerparameter. Desalniettemin was dit niet voldoende om de experimentele observaties volledig te kunnen reproduceren. Het tijdsverloop van de glycolytische intermediären kon alleen worden gereproduceerd wanneer glycogeen synthese en assimilatie in het model werden geïntroduceerd. In dit geval trad glycogeen op als een opslagpool, die koolstof en energie verschaft om de groei tijdens de famine-condities mogelijk te maken. Verder waren ATP-verspillende reacties nodig om de geobserveerde adenylaat energiehomeostase te kunnen reproduceren. Dit continue aftappen van ATP ondersteunt bovendien de hypothese dat de onderhoudsenergie behoefte tijdens feast-famine hoger is.

In **Hoofdstuk 5** werden multi-omics benaderingen, dat wil zeggen, shotgun cellular proteomics en <sup>13</sup>C-labelled metabolomics, gebruikt voor ongerichte analyse en generatie van nieuwe hypotheses over cellulaire regulatie mechanismen, wanneer cellen blootgesteld werden aan fluctuaties in substraatbeschikbaarheid. De verwachting was dat de extracellulaire dynamiek globale stress reacties op gang zou brengen, in lijn met de geobserveerde verlaagde biomassaopbrengst. Verrassend genoeg was dit niet het geval – stressgerelateerde eiwitten veranderden niet tussen steady-state en feast-famine condities. Anderzijds paste het cellulaire proteome zich wel aan in specifieke functionele categorieën, waaronder biosynthese en translationele processen (ribosomen). Deze toename kan

verklaard worden door enerzijds een verhoogde eiwitproductie om de snelle veranderingen in groei tijdens de korte tijdsinterval van substraatbeschikbaarheid mogelijk te maken of anderzijds door het vastlopen van de translatie naar eiwitten door beperkingen in de beschikbaarheid van aminozuren tijdens de famine-fase. Tijdens de substraatgelimiteerde groei (constante voeding) hebben cellen een overcapaciteit aan metabole enzymen (betrokken bij de centrale koolstofroutes), die wordt gebruikt om tijdens nutriënttoename de snelle verhoging in metabole fluxen te kunnen verwerken. De neerwaartse regulatie van verscheidene eiwitten in de glycolyse, citroenzuurcyclus en pentosefosfaatroute en ook van transport eiwitten, laat zien dat cellen meer reageren op de periode van substraatovervloed dan op de periode van verhongering tijdens het bloksgewijze voedingsregime. Dit is ook in overeenkomst met de geobserveerde neerwaartse regulatie van de glyoxylaatshunt eiwitten. Bovendien wijzen de verhoogde niveaus van polyfosfaatkinase op het gebruik van een polyfosfaatpool als vermoedelijke buffer voor energiehomeostase. Glycogeen productie en degradatie werd geverifieerd door de proteomics analyse en  $^{13}\text{C}$  tracing analyses en draagt vermoedelijk bij aan de ATP verspilling (biomassaopbrengstverliezen), samen met de verhoogde eiwitomzetting, die geïdentificeerd werd op basis van een verhoogde sector van het cellulaire proteasoom.

De gegenereerde inzichten van het gehele proefschrift zijn samengevat in **Hoofdstuk 6**. Hiernaast worden open vragen besproken. De toekomstige uitdagingen omvatten nieuwe scale-down experimenten, onderzoek naar de effecten van dynamische condities op industriële productiestammen, het gebruik van mutantstammen voor validatie-experimenten en data-integratie in de richting van multi-scale modelleren.



Chapter



**General Introduction**

## **1.1 The power of Biotechnology**

### **1.1.1 Definition and landmarks**

Hungarian agricultural engineer Karl Ereky was the first one to introduce the term “Biotechnology” in 1919, as the technology to convert raw materials to useful products, utilizing living organisms [1]. However, the applications of biotechnology dated several thousand years back, when people were for example using microorganisms to bake bread or brew beer and vinegar in ancient civilizations (Egypt, Greece, Mesopotamia). Since then, biotechnology has developed to a broader field, which combines various disciplines, such as biology, chemistry, physics and mathematics, with the aim to develop processes and high value-added products, exploiting organisms, cells or cellular components.

Crop breeding, beer and wine brewing, as well as producing bread are some of the oldest examples of biotechnology [2]. Nevertheless, the study of biotechnology began at the 17<sup>th</sup> century, when Antonie van Leeuwenhoek discovered bacteria and protozoa using the first microscope in 1677 [3]. Significant scientific breakthroughs in the field occurred in the next centuries, including the first smallpox vaccine by Edward Jenner in 1798 [4], the discovery of the bacterial nature of fermentation by Louis Pasteur in 1862 [5] and the discovery of genetic inheritance laws by Gregor Mendel in 1863 [6]. Biotechnology in the 20<sup>th</sup> century was also characterized by major contributions, such as the discovery of penicillin, the first antibiotic, by Alexander Fleming in 1928 [7], the development of submerged fermentation as a cultivation method by Albert J. Kluyver [8], the description of the DNA structure by James D. Watson and Francis Crick in 1953 [9] and the first successful recombinant DNA experiment with bacterial genes by Stanley N. Cohen and Herbert Boyer in 1973 [10]. The biotechnological progress continues in the current century, where several advances already occurred. The first draft sequence of the human genome (led by Craig Venter) [11] is an example of the recent scientific developments in the field. More landmarks of biotechnology are well reviewed in the work of Bhatia S [12].

### **1.1.2 Range of biotechnological applications**

Biotechnology provides products and technologies to improve the quality of life, while reducing environmental impact, mainly related to [12, 13]:

1. Environment: development of technologies to clean contaminated water, air and soil through oxidation or reduction of the contaminants by microorganisms.
2. Health (“red biotechnology”): development of tools to detect diseases and treatments, as well as, medicines to combat them.

3. Agriculture (“green biotechnology”): advances in agriculture for higher crop yields, increased farming sustainability and development of nutrient-rich nutrition.
4. Biorefineries (“white biotechnology”): use of enzymes and microbes in fermentation processes in order to produce biofuels and biochemicals (reducing use of petrochemicals and contributing to the decrease of greenhouse gas emissions), utilize biomass waste products and optimize manufacturing process efficiency.

This thesis specifically contributes to industrial biotechnology, which is the sector of biotechnology referring to the large-scale manufacturing of bioproducts (ranging from food to antibiotics and polymers) from renewable raw materials, employing microorganisms and enzymes. These processes are based on the ability of microbial cells to convert nutrients (mainly sugars) into products through their metabolism. In addition, enzymes which are involved in these metabolic processes can be used as biocatalysts, for example in detergent production.

### **1.1.3 Bioprocesses in a nutshell**

All bioprocesses consist of upstream processing, including all the steps until fermentation, and downstream processing, which characterizes the purification and recovery of the final product [14]. Figure 1.1 shows a simplified outline of the main steps in both upstream and downstream processing. More steps may be included depending on the nature and the needs of each process. In addition, during upstream processes, raw material development and strain engineering are interconnected in several steps, to achieve economic efficiency.



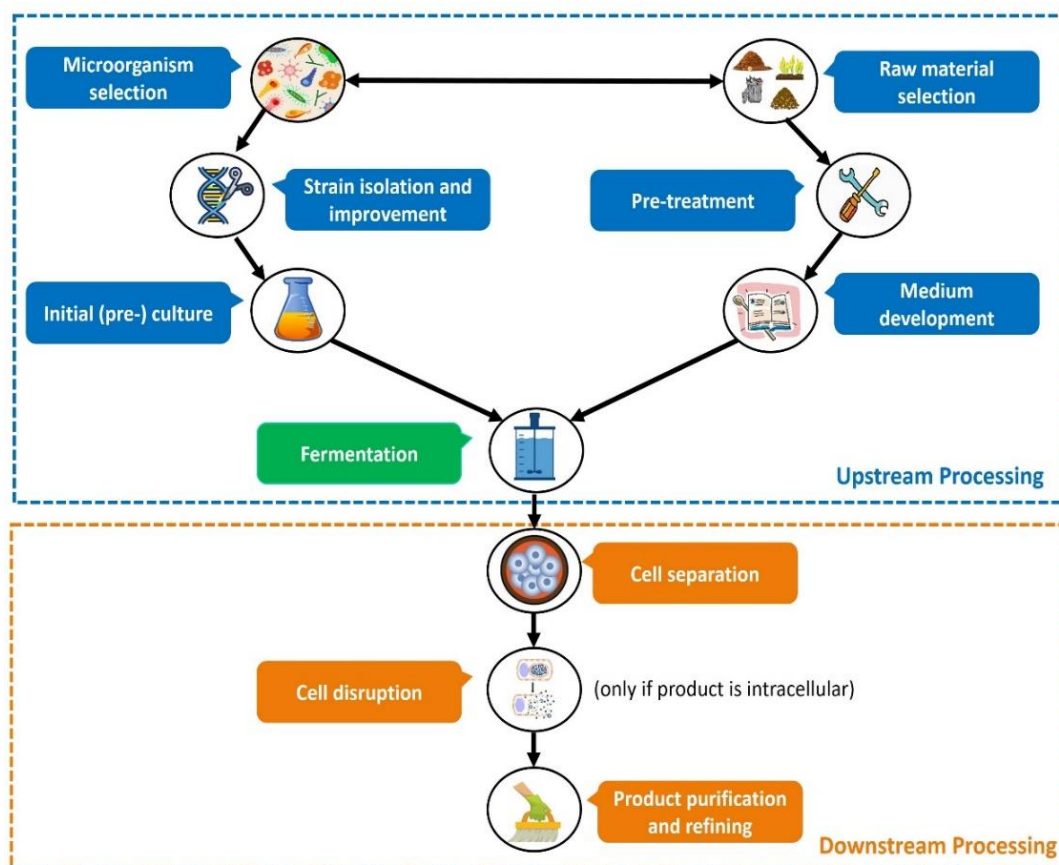


**Figure 1.1** Schematic outline of upstream and downstream bioprocesses.

#### 1.1.4 Fermentation and cultivation environment

The focus of this thesis is the last step of the upstream processing, the fermentation. In industrial terms, fermentation is the enzymatic decomposition of organic sources (“substrates”) by microorganisms or eukaryotic cells and their subsequent conversion to products (e.g. acids and alcohols). In large-scale production, this is occurring inside tanks with various sizes and geometries, called “bioreactors”. Continuous stirred tank reactors and bubble columns are some of the most frequently used types of bioreactors.

The performance of microbial cells is influenced by the cultivation environment, which in industrial bioprocesses represents the inside of a bioreactor. During a microbial cultivation, several physical or chemical extracellular parameters may vary over time and lead to the formation of a “dynamic” environment. The large scale of industrial bioreactors (hundred to several thousand litres), necessary to enable sufficient production capacity with low costs, usually causes microorganisms to experience dynamic gradients during their cultivation [15]. For example, imperfect mixing can lead to heterogeneities in different parts of the reactor (e.g. substrate and dissolved gas concentrations, pH, temperature, shear stress and more) [16]. Since substrates are added at only one point in the reactor, they represent the largest

gradients. The effects of substrate gradients on cellular behaviour constitute the subject of this thesis.

## 1.2 The protagonist of this thesis: *Escherichia coli*

A wide range of microorganisms are used in bioprocesses, such as bacteria, yeast and fungi. One of the most studied microbes and with numerous applications in biotechnology, is the bacterium *Escherichia coli* (*E.coli*), the central “character” of this thesis. *E.coli* is a gram-negative, facultative anaerobic bacterium (i.e. respiration takes place in the presence of oxygen and fermentation in its absence), discovered in 1885 by Theodor Escherich, to whom owes its name [17]. The term “*coli*” was derived by the common natural habitat of *E.coli*, which is the colon (lower intestine) of vertebrates [18]. Cells are rod-shaped and their sizes vary, depending on the particular strain and growth conditions, with an average length of 2  $\mu\text{m}$  and diameter ranging from 0.25–1  $\mu\text{m}$  [19, 20] (Figure 1.2). *E.coli* is a member of the Enterobacteriaceae group and while it is mostly harmless, some pathogenic strains have also been identified [21].

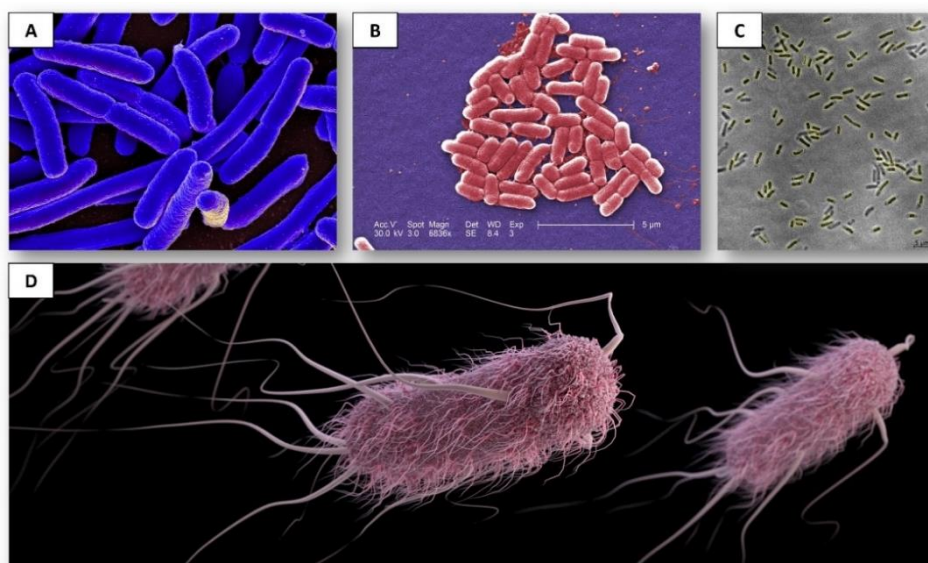


**Figure 1.2** How do they look like? **A)** Digitally-colored scanning electron micrograph (SEM) depicts numbers of *E.coli* bacteria. Produced by the National Institute of Allergy and Infectious Diseases (NIAID) (<https://phil.cdc.gov/Details.aspx?pid=18160>). **B)** SEM digitally-colored image of a growing cluster of O157:H7 pathogenic *E.coli* bacterial strain, under a high magnification of 6836X. Credits to Janice Haney Carr. Image was provided by the National Escherichia, Shigella, Vibrio Reference Unit at CDC (<https://phil.cdc.gov/Details.aspx?pid=10068>). **C)** Optical microscope image of *E.coli* cells published by Konokhova AI, et al. [22]. **D)** Three-dimensional (3D), computer-generated image of a group of *E.coli* extended-spectrum  $\beta$ -lactamase-producing (ESBLs) bacteria. The artistic recreation was based upon SEM imagery. Visual example of the long, whip-like, peritrichous flagella, sprouting from what appear to be random points on the organism’s exterior, as well as the numerous shorter, and finer fimbriae, imparting a furry look to the bacteria. Created by Alissa Eckert (2016) and provided by CDC/ Antibiotic Resistance Coordination and Strategy Unit (<https://phil.cdc.gov/Details.aspx?pid=21915>).

*E.coli* is considered one of the most important model organisms in microbiology, in which DNA cloning was first developed [10], which laid the foundations of metabolic engineering and shaped the future of biotechnology [23, 24]. *E.coli* possesses some distinct traits which make it a popular host for the industrial production of various compounds. These properties include:

- Rapid growth, doubling time of about 20 minutes [25]
- Ability to grow in high cell density cultures [26], particularly useful for achieving high volumetric productivities
- Capability of synthesizing all essential amino acids and vitamins, thus growing on inexpensive culture medium
- Extensive knowledge of its genome, which was sequenced in 1997 (for *E.coli* K12 MG1655) [27], as well as transcriptome, proteome and metabolome.
- Availability of genetic tools for strain engineering, such as gene deletion approaches [28]

The widespread use of *E.coli* in biotechnology has led to the development of various industrial strains (especially K12 and B types), used as cell factories in large-scale bioprocesses. *E.coli* is a very popular host in the biopharmaceutical industry and produces nearly 30% of the approved therapeutic recombinant proteins [29], with significant advantages over other microbes, such as the yeast *Saccharomyces cerevisiae* [30, 31]. The first recombinant pharmaceutical compound to enter the market was insulin, as treatment to diabetes, produced in *E.coli* in 1982 [32]. In addition, more bio-based products, derived by genetically engineered *E.coli*, include amino acids for the food industry and biopolymers. A detailed review on all the biochemicals, produced so far by engineered *E.coli*, has been published by Chen X, *et al.* [24] and a metabolic estimate of its potential on producing even more non-native compounds has been computationally investigated by Zhang X, *et al.* [33].

Representing a microbe of high industrial interest, *E.coli* was chosen as the working horse of this study. The laboratory K12 MG1655 strain was chosen, due to the considerable amount of information known about its physiology and genome.

### 1.2.1 A peek inside *E.coli* cell factories

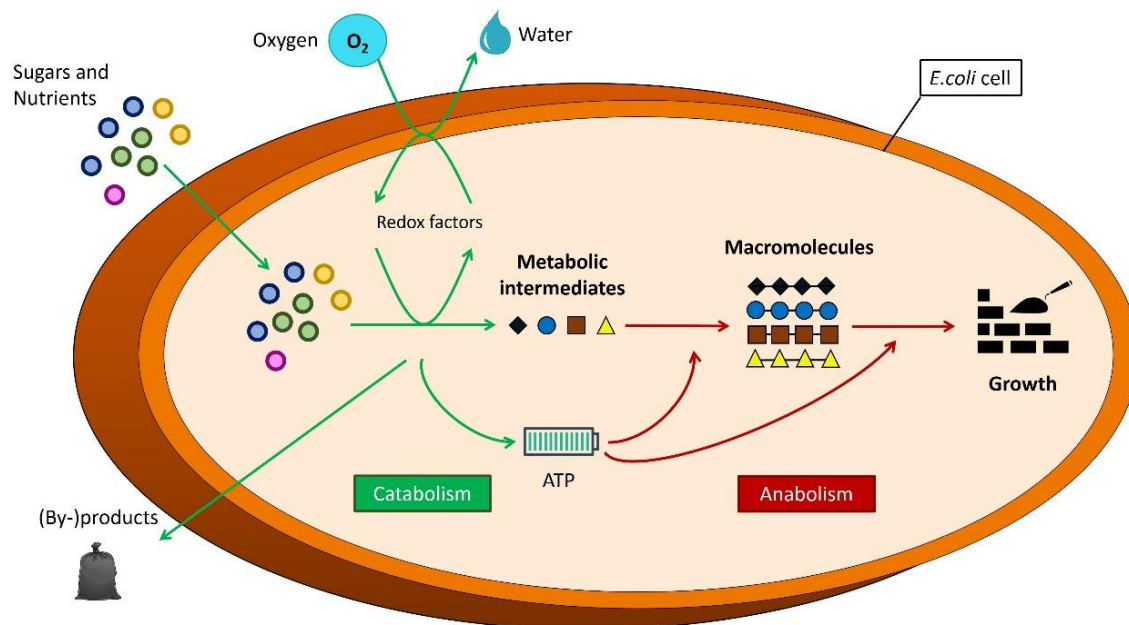


**Figure 1.3.** Schematic representation of the bacterial aerobic metabolism. Catabolism of carbon sources (sugars) leads to intermediates for biomass synthesis and (by-)products, as well as, energy generation (direct and via respiration). The intermediates and energy are used to generate biomass components (anabolism).

Metabolism is a set of chemical reactions occurring inside the cell, which controls its survival. The main characteristics of bacterial aerobic metabolism are shown in Figure 1.3 and will be briefly explained. Cells receive nutrients from their extracellular environment, such as sugars (carbon) and oxygen (energy). These nutrients are then converted to metabolic intermediates, through a series of chemical reactions, which compose catabolism. Catabolism requires the transfer of electrons from organic compounds to electron acceptors (such as oxygen) (via redox factors) and produces energy in the form of adenosine triphosphate (ATP) molecules. At the same time by-products are produced and excreted out of the cell, such as carbon dioxide, organic acids and ethanol. All these chemical reactions are categorized in different metabolic pathways, such as glycolysis, pentose phosphate pathway, tricarboxylic acid cycle and the respiratory chain. The energy and precursors derived by catabolism are subsequently used for anabolism, where macromolecules (proteins, polysaccharides, lipids, nucleic acids) are synthesized by building block compounds (amino acids, monosaccharides, fatty acids and nucleotides). Finally, these macromolecules are assembled in the cellular structure generating cellular growth.

With the growing needs of the bio-industry, higher productivities and lower costs need to be achieved. One way to accomplish these goals is the construction of more powerful and robust strains. However, one of the main requirements is a deep understanding of cellular functions under different cultivation environments. Despite the overwhelming and detailed knowledge

of *E.coli* biology, the integration of all mechanisms, composing the dynamic cellular regulation, is not yet fully unravelled. Novel insights related to *E.coli* metabolism come to light almost every day, as confirmed by very recent publications [34-39]. The full potential and capabilities of *E.coli* in biotechnology will still continue to surprise us.

### 1.3 Scope of the thesis

Microbial metabolism responds to different types of gradients occurring simultaneously in industrial large-scale cultivations (e.g. nutrients, dissolved gases, pH etc.), due to imperfect mixing. The purpose of this thesis was to investigate the behaviour of *E.coli* cells under these dynamic environmental conditions, with a particular interest on the effects of fluctuations in substrate availability, separate from the other gradients. Except from a better understanding of the cell factory, this work aims to demonstrate how experimental observations and metabolic models can be integrated towards designing methods to develop better performing strains for industrial applications.

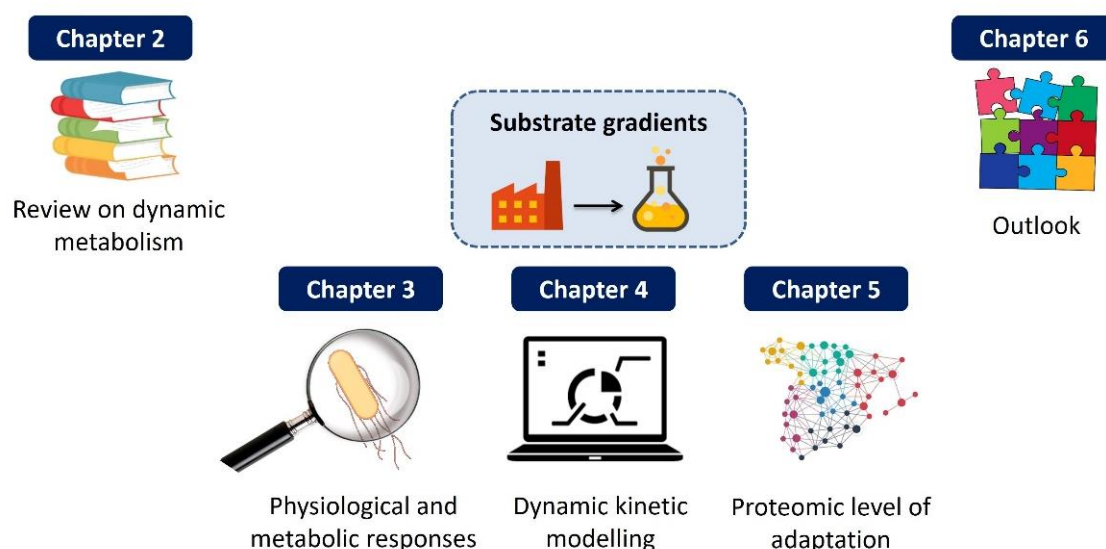


**Figure 1.4.** Schematic outline of the chapters of this thesis.

The cellular responses to environmental stimuli have been extensively studied. Thus, in **Chapter 2**, the quantitative experimental and kinetic modelling approaches used for studying dynamic metabolism, as well as the current challenges, were reviewed.

In **Chapter 3**, glucose perturbations were enforced in an *E.coli* lab-scale aerobic cultivation, by block-wise feeding, with the aim to mimic the aspect of substrate gradients in large-scale conditions. Short time-scales were used for the applied perturbations, similar to the industrial mixing timeframes, but also able to allow for sampling and process monitoring. This approach allowed to study the cellular adaptation of cells, which experienced dynamics for several generations. Their physiological and metabolic responses were monitored *in vivo* under this

so-called feast-famine regime and were compared to a reference continuous feeding cultivation. Metabolomics were also employed to estimate intracellular fluxes under the different cultivation conditions. Several metabolic strategies were revealed, including the importance of storage metabolism and energy-spilling mechanisms.

The challenge of combining experimental perturbations with dynamic kinetic modelling was addressed in **Chapter 4**. A published kinetic model [40], which was developed under steady-state conditions, was used to evaluate its ability in predicting the dynamic cellular responses quantified in Chapter 3. Kinetic parameter optimization and the implementation of storage pathways in the model were used as approaches to unravel significant cellular functions under block-wise substrate feeding conditions.

A multi-omics analysis was then performed in **Chapter 5**, consisting of untargeted proteomics and <sup>13</sup>C-tracing metabolomics, for a deeper understanding of the cellular regulatory mechanisms under dynamic conditions. The aim was to identify and locate the main components and routes of dynamic regulation inside the cell, when block-wise substrate feeding was applied.

Finally, **Chapter 6** describes the major contributions of this work and discusses open questions and challenges for future research.

## References

1. Ereky K: *Biotechnologie der Fleisch-, Fett-, und Milcherzeugung im landwirtschaftlichen Grossbetriebe: für naturwissenschaftlich gebildete Landwirte verfasst*. Berlin: P. Parey; 1919.
2. Verma AS, Agrahari S, Rastogi S, Singh A: **Biotechnology in the realm of history**. *J Pharm Bioallied Sci* 2011, **3**:321-323.
3. Lane N: **The unseen world: reflections on Leeuwenhoek (1677) 'Concerning little animals'**. *Philos Trans R Soc Lond B Biol Sci* 2015, **370**.
4. Riedel S: **Edward Jenner and the history of smallpox and vaccination**. *Proc (Bayl Univ Med Cent)* 2005, **18**:21-25.
5. Robbins L: *Louis Pasteur and the hidden world of microbes*. New York: Oxford University Press; 2001.
6. Lewis CA: **Gregor Mendel: The Friar Who Grew Peas**. *Catholic Library World* 2007, **77**:261-262.
7. Hugh TB: **Howard Florey, Alexander Fleming and the fairy tale of penicillin**. *Med J Aust* 2002, **177**:52-53; author reply 53.
8. Kluyver AJ, Perquin LHC: **Zur Methodik der Schimmelstoffwechseluntersuchung**. *Biochem Z* 1933, **266**.
9. Watson JD, Crick FH: **The structure of DNA**. *Cold Spring Harb Symp Quant Biol* 1953, **18**:123-131.
10. Cohen SN, Chang AC, Boyer HW, Helling RB: **Construction of biologically functional bacterial plasmids in vitro**. *Proc Natl Acad Sci U S A* 1973, **70**:3240-3244.
11. Venter JC, Smith HO, Adams MD: **The Sequence of the Human Genome**. *Clin Chem* 2015, **61**:1207-1208.
12. Bhatia S: **History, scope and development of biotechnology**. In *Introduction to Pharmaceutical Biotechnology, Volume 1*. pp. 1-1-1-61: IOP Publishing; 2018: 1-1-1-61.
13. Gavrilesco M, Chisti Y: **Biotechnology-a sustainable alternative for chemical industry**. *Biotechnol Adv* 2005, **23**:471-499.
14. Stanbury PF, Whitaker A, Hall SJ: *Principles of fermentation technology*. Third edition. edn. Amsterdam: Butterworth-Heinemann, an imprint of Elsevier; 2017.
15. Straathof AJJ, Wahl SA, Benjamin KR, Takors R, Wierckx N, Noorman HJ: **Grand Research Challenges for Sustainable Industrial Biotechnology**. *Trends Biotechnol* 2019, **37**:1042-1050.
16. Lara AR, Galindo E, Ramirez OT, Palomares LA: **Living with heterogeneities in bioreactors: understanding the effects of environmental gradients on cells**. *Mol Biotechnol* 2006, **34**:355-381.
17. Escherich T: **Die Darmbakterien des Neugeborenen und Sauglings**. *Fortschritte der Medizin* 1885, **3**:515-522.
18. Berg RD: **The indigenous gastrointestinal microflora**. *Trends Microbiol* 1996, **4**:430-435.
19. Grossman N, Ron EZ, Woldringh CL: **Changes in cell dimensions during amino acid starvation of Escherichia coli**. *J Bacteriol* 1982, **152**:35-41.
20. Zaritsky A, Woldringh CL: **Chromosome replication rate and cell shape in Escherichia coli: lack of coupling**. *J Bacteriol* 1978, **135**:581-587.
21. Garrity G, Brenner DJ, Krieg NR, Staley JR: *Bergey's Manual® of Systematic Bacteriology: Volume 2: The Proteobacteria, Part B: The Gammaproteobacteria*. Springer US; 2007.
22. Konokhova AI, Gelash AA, Yurkin MA, Chernyshev AV, Maltsev VP: **High-precision characterization of individual E. coli cell morphology by scanning flow cytometry**. *Cytometry A* 2013, **83**:568-575.
23. Russo E: **The birth of biotechnology**. *Nature* 2003, **421**:456-457.
24. Chen X, Zhou L, Tian K, Kumar A, Singh S, Prior BA, Wang Z: **Metabolic engineering of Escherichia coli: a sustainable industrial platform for bio-based chemical production**. *Biotechnol Adv* 2013, **31**:1200-1223.

25. Fossum S, Crooke E, Skarstad K: **Organization of sister origins and replisomes during multifork DNA replication in Escherichia coli.** *EMBO J* 2007, **26**:4514-4522.
26. Shiloach J, Fass R: **Growing E. coli to high cell density--a historical perspective on method development.** *Biotechnol Adv* 2005, **23**:345-357.
27. Blattner FR, Plunkett G, 3rd, Bloch CA, Perna NT, Burland V, Riley M, Collado-Vides J, Glasner JD, Rode CK, Mayhew GF, et al: **The complete genome sequence of Escherichia coli K-12.** *Science* 1997, **277**:1453-1462.
28. Xu W, Klumbys E, Ang EL, Zhao H: **Emerging molecular biology tools and strategies for engineering natural product biosynthesis.** *Metabolic Engineering Communications* 2020, **10**:e00108.
29. Selas Castineiras T, Williams SG, Hitchcock AG, Smith DC: **E. coli strain engineering for the production of advanced biopharmaceutical products.** *FEMS Microbiol Lett* 2018, **365**.
30. Ferrer-Miralles N, Domingo-Espin J, Corchero JL, Vazquez E, Villaverde A: **Microbial factories for recombinant pharmaceuticals.** *Microb Cell Fact* 2009, **8**:17.
31. Sanchez-Garcia L, Martin L, Manges R, Ferrer-Miralles N, Vazquez E, Villaverde A: **Recombinant pharmaceuticals from microbial cells: a 2015 update.** *Microb Cell Fact* 2016, **15**:33.
32. **Human insulin receives FDA approval.** *FDA Drug Bull* 1982, **12**:18-19.
33. Zhang X, Tervo CJ, Reed JL: **Metabolic assessment of E. coli as a Biofactory for commercial products.** *Metab Eng* 2016, **35**:64-74.
34. Bottomley AL, Peterson E, Iosifidis G, Yong AMH, Hartley-Tassell LE, Ansari S, McKenzie C, Burke C, Duggin IG, Kline KA, Harry EJ: **The novel E. coli cell division protein, YtfB, plays a role in eukaryotic cell adhesion.** *Scientific Reports* 2020, **10**:6745.
35. Ma ZZ, Zhou H, Wei YL, Yan S, Shen J: **A novel plasmid-Escherichia coli system produces large batch dsRNAs for insect gene silencing.** *Pest Manag Sci* 2020.
36. Govender K, Naicker T, Lin J, Baijnath S, Chuturgoon AA, Abdul NS, Docrat T, Kruger HG, Govender T: **A novel and more efficient biosynthesis approach for human insulin production in Escherichia coli (E. coli).** *AMB Express* 2020, **10**:43.
37. Fredens J, Wang K, de la Torre D, Funke LFH, Robertson WE, Christova Y, Chia T, Schmied WH, Dunkelmann DL, Beranek V, et al: **Total synthesis of Escherichia coli with a recoded genome.** *Nature* 2019, **569**:514-518.
38. Xu Y, Zhao Z, Tong W, Ding Y, Liu B, Shi Y, Wang J, Sun S, Liu M, Wang Y, et al: **An acid-tolerance response system protecting exponentially growing Escherichia coli.** *Nat Commun* 2020, **11**:1496.
39. Melson EM, Kendall MM: **The sRNA DicF integrates oxygen sensing to enhance enterohemorrhagic Escherichia coli virulence via distinctive RNA control mechanisms.** *Proc Natl Acad Sci U S A* 2019, **116**:14210-14215.
40. Peskov K, Mogilevskaya E, Demin O: **Kinetic modelling of central carbon metabolism in Escherichia coli.** *FEBS J* 2012, **279**:3374-3385.





# Chapter



## Current state and challenges for dynamic metabolic modeling

Published as: Vasilakou E, Machado D, Theorell A, Rocha I, Noh K, Oldiges M, Wahl SA: Current state and challenges for dynamic metabolic modeling. *Curr Opin Microbiol* 2016, 33:97-104.

DOI: 10.1016/j.mib.2016.07.008

## **Abstract**

While the stoichiometry of metabolism is probably the best studied cellular level, the dynamics in metabolism can still not be well described, predicted and, thus, engineered. Unknowns in the metabolic flux behaviour arise from kinetic interactions, especially allosteric control mechanisms. While the stoichiometry of enzymes is preserved *in vitro*, their activity and kinetic behaviour differs from the *in vivo* situation. Next to this challenge, it is infeasible to test the interaction of each enzyme with each intracellular metabolite *in vitro* exhaustively. As a consequence, the whole interacting metabolome has to be studied *in vivo* to identify the relevant enzymes properties. In this review we discuss current approaches for *in vivo* perturbation experiments, that is, stimulus response experiments using different setups and quantitative analytical approaches, including dynamic carbon tracing. Next to reliable and informative data, advanced modeling approaches and computational tools are required to identify kinetic mechanisms and their parameters.

## 2.1 Introduction

Modeling of microbial systems has two major aims: (1) to provide a systemic understanding of cellular behaviour and (2) to guide the design of microbial host, to optimize, for example, the production of chemicals. Metabolic network analysis has guided the genetic engineering of cells, leading to significantly improved production hosts [1, 2]. Especially, steady-state analysis has delivered insights to metabolic fluxes in many different microorganisms [3]. This includes the discovery of unknown pathways and activities including unusual routes in carbohydrate metabolism in pathogenic hosts [4], amino acid degradation pathways [5] or uncommon shunts in cyanobacteria [6].

However, most current models fail to predict cellular operation [7]. The metabolic flux not only depends on the enzyme concentration, but a variety of cellular functions and mechanisms, like transcription, translation, post-translational modifications and allosteric control. For each level, techniques have been developed to monitor changes *in vivo*, but the integration of data and its interpretation remain highly challenging. Experimental data sets for modeling are often derived from well-defined and controlled environmental conditions, whereas cells in production processes are faced with sub-optimal conditions, for example, limited oxygen, switching substrate availability or product inhibition. Such environmental factors are one source leading to a limited accuracy of model predictions for dynamic process conditions.

Without doubt, metabolism is the best studied cellular level. For most common hosts like *Escherichia coli*, *Saccharomyces cerevisiae*, *Bacillus subtilis*, *Corynebacterium glutamicum* and many more, the metabolic network stoichiometry is arguably completely described [8, 9]. Unknowns in metabolic activity arise from kinetic interactions, especially allosteric control mechanisms. While the stoichiometry of enzymes is preserved *in vitro*, its activity and behaviour differs from the *in vivo* situation [10]. As a consequence, the whole interacting metabolome has to be studied to identify the enzymatic properties *in vivo* [11]. Experiments and modeling of enzyme kinetic networks have been pioneered by Theobald U, *et al.* [12],[13] using stimulus-response experiments (SRE). While crucial new insights have been generated, these approaches only partly succeeded to identify enzyme mechanisms (structural) or kinetic (quantitative) parameters [7].

There are different aspects that lead to non-identifiability (i.e., the inability of the data to sufficiently determine the model's structure and its quantitative parameters): (1) Carbon effluxes from central carbon metabolism cannot be quantified with sufficient accuracy during the short term of the experiment. (2) Parallel reaction rates and reaction cycles cannot be distinguished. (3) Parameter estimation quality remains low because of high correlations of

the model parameter and limited regulatory information content of intracellular concentration measurements [14].

The review focuses on approaches to overcome named challenges, especially approaches that (1) increase the information content by addition of isotopic tracers, like  $^{13}\text{C}$ , (2) combinatorial approaches that allow for inference of different enzyme kinetic mechanisms, (3) novel developments in parameter estimation.

## **2.2 Coupling experimental observations with modeling approaches**

Identification of *in vivo* kinetic mechanisms is challenging as the system can only be perturbed by extracellular stimuli and/or genetic modifications (Figure 2.1). The experiments have therefore to be designed with the modeling and the required model resolution and accuracy in mind. In particular, the experimental data must show precise quantitative properties to distinguish between the different hypotheses and deliver sufficient accuracy and coverage for the parameter identification. These criteria, coming from the study aim and the modeling approach, define the measurements and approaches needed, that is, to decide whether additional, quantitative metabolite measurements need to be developed or complementary observables, like carbon labelling [15], are required.

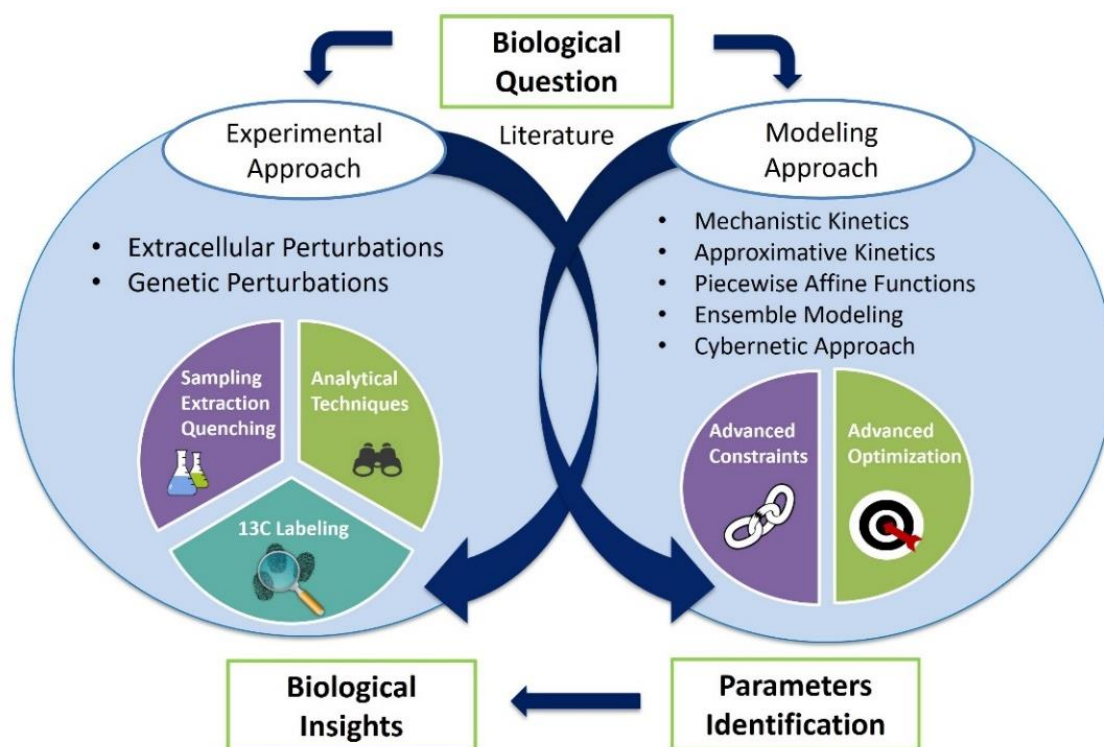


**Figure 2.1** Modeling and the experimental approach are determined by the biological question, that is, the approaches need to be fine-tuned to identify the relevant parameters. The biological system needs to be perturbed by modification of the metabolic network (using genetic modifications) and/or the extracellular conditions (substrate pulse, temperature, among others). The response of the system is monitored using (advanced) analytical methods including  $^{13}\text{C}$  tracing, to provide the researcher with quantitative *in vivo* data. The data is then used to calibrate metabolic models, which need to be chosen based on the biological question and available data. Modeling and parameter estimation deliver information on the intracellular kinetics, including kinetic features of the reaction steps and allow for new biological insights.

### 2.3 Experimental approaches

The aim to reach predictive kinetic models requires sufficient informative experimental data for parameter identification. In this context, the term ‘informative’ means accurate, robust and quantitative data gathered for relevant conditions. Commonly, metabolic flux is observed under steady-state conditions, while dynamic flux estimation is more challenging in several experimental and computational aspects. The aim of this review article is not a complete description of all variants of experimental approaches, but to emphasize how they contribute to the construction of kinetic metabolic models. All these experimental approaches have in common that they must be conducted under well-controlled, reproducible conditions.

To identify kinetic parameters from steady-state experiments, the analysis of a series of different steady-states is required [16-18]. An obvious challenge in such a series of experiments is to keep the cellular properties comparable. To this end, continuous cultivation in chemostat with different dilution rates has been employed.

To keep the enzymatic properties constant while gathering sufficient information on the kinetic mechanisms, the so called stimulus–response experiment was proposed by Theobald U, *et al.* [12] and became a widely-used, yet very challenging approach. More specifically, the cells are exposed to strong and abrupt perturbations in substrate supply in a short timeframe, that is, much shorter than protein turnover times. Pioneering work has been performed in yeast and bacteria by substrate pulses [12, 18-23]. An experimental challenge in SREs is the rapid monitoring of intracellular metabolites, that is, rapid sampling, quenching and analysis of the low concentrated intracellular metabolites by quantitative analytical techniques. The available setups range from fast manual sampling [13] to automated sampling devices coupled to conventional bioreactors [24, 25] or plug-flow bioreactor units like the BioScope [26, 27].

Besides precise analytical determination of metabolite concentrations, the quantification at intracellular levels is influenced by imperfect quenching procedures that have to be considered [28, 29], that is, aspects of metabolite leakage or significant presence of metabolites already in culture supernatant. However, procedures like the differential method with total broth extraction [30] or metabolite balancing including error propagation with all three types of samples (i.e. cell extract, quenching and culture supernatant) [31] have been developed to overcome this. Nevertheless, such methods need to be validated for each novel microbial species.

SREs generate a comprehensive time course of intracellular metabolite concentrations in time, that can be used to identify reaction kinetic parameters [32] and putative regulatory mechanisms [33]. For example, Chassagnole C, *et al.* [19] designed a dynamic model accounting for the phosphotransferase system (PTS), glycolysis and the pentose-phosphate pathway in *E.coli*. Using the data of intracellular metabolite concentrations after the disturbance of steady-state with a glucose pulse, it was shown that the PTS adjusts in sub-seconds to the new condition and exhibits a major flux control in *E.coli* metabolism.

The SRE approach has also been applied to other microorganisms with the aim to highlight the importance of compartmentation for the regulation of glycolysis in yeast [12], to shed light on the valine/leucine pathway kinetics in *C. glutamicum* [20], or to study the dependency of penicillin-G production on the mechanisms of transport of phenylacetic acid and the product over the cell membrane in *Penicillium chrysogenum* [18, 23].

While SREs with single pulse are highly informative to obtain insights into microbial kinetics and metabolic responses, it is not yet clear if this type of perturbation mimics well the ‘non-laboratory’ biotechnological conditions experienced by cells in large-scale bioreactors, especially when the network has been conditioned to the substrate limited steady-state

before the perturbation. There is evidence from literature that the metabolic response of the first substrate pulse differs from a series of perturbations in *E.coli* [34].

To study such ‘training’ phenomena, where metabolic networks are ‘trained’ under periodically changing conditions, a series of scale-down approaches have been applied. Block-wise feeding regimes have been used in scale-down experiments, generating a repetitive dynamic environment. One of the first studies applying block-wise feeding investigated the impact of dynamics on the energy metabolism in yeast strains [35], especially evaluating the yield of biomass and products in comparison to steady-state conditions. Later, this type of feast/famine experiments was used to study metabolism *in vivo*, with focus on storage metabolism in *P. chrysogenum* [36] and *S. cerevisiae* [33].

Suarez-Mendez CA, *et al.* [33], also, showed that this kind of experimental regime not only simulates the cell transition from substrate excess to starvation conditions, but also facilitates the reproducibility of metabolic response measurements. Especially, several (identical) cycles can be sampled allowing for higher time-resolution and replicate measurements compared to the single-pulse experiment.

Continuous dynamic perturbations can also be generated in two-compartment bioreactors that mimic large-scale conditions. This efficient scale-down approach can simulate inhomogeneity inside large-scale bioreactors, by circulating cells between either two stirred-tank reactors (STR-STR) or from one STR to a plug flow reactor (PFR) [37, 38].

While all these experimental setups can generate frequent observations and high coverage of metabolic concentration profiles, the relevant information for the identification of kinetic parameters might still be limited, especially for branch-point metabolic nodes [39]. In recent years, these limitations have been overcome with the use of <sup>13</sup>C tracer experiments, a powerful method that enables the quantification of intracellular fluxes and provides reliable information on parallel or bidirectional reactions [40, 41]. In <sup>13</sup>C based metabolic flux analysis (MFA), <sup>13</sup>C-labeled substrates are fed and the labeling enrichment is traced through the metabolic network by either mass spectrometry-based techniques or nuclear magnetic resonance spectroscopy (NMR) [42]. In the traditional isotopic steady-state method only the labeling data of the metabolites is required to inform about the particular flux distribution, whereas under isotopic dynamic conditions, both the labeling and concentrations of metabolites need to be measured [14]. Link H, *et al.* [43] used <sup>13</sup>C isotopic labeling to identify allosteric metabolite-protein interactions (allosteric mechanisms) that have an impact on the switch between gluconeogenesis to glycolysis in *E.coli*. The cells were cultured on filter material allowing for a very fast exchange of the cultivation medium, for example switching from glucose to pyruvate. The authors measured the metabolic response to such shifts and



applied a modeling approach, using a large set of different kinetic hypothesis to identify the most relevant allosteric mechanisms.

## 2.4 High-throughput opportunities and developments

The experimental approaches discussed can only generate results for one strain under one perturbation condition. In recent years, high-throughput experimental approaches have been developed to miniaturize the experiments and study more strains and conditions in parallel. A first characterization of metabolic phenotypes can be obtained from the analysis of the extracellular space (metabolic footprinting) [44].

Fuhrer T, *et al.* [45] screened the intracellular metabolome of several *E.coli* mutants, using a microtiter cultivation system coupled to flow-injection mass-spectrometry. This system allows for up to 1400 sample measurements per day. Hollinshead WD, *et al.* [46] have applied metabolic fingerprinting together with  $^{13}\text{C}$  tracing using a series of different tracer substrates, allowing to identify key metabolic flux phenotypes of less common microorganisms.

While the classical millilitre scale cultivation can only be performed in batch mode, novel systems combine automated liquid-handling and optical sensors to control small scale cultivation [47]. For example, the Biolector system can handle 48 parallel cultivation wells [48]. Heux S, *et al.* [49] developed a robotic flux profiling system from isotopic fingerprints that enables the generation of 20 flux profiles per day though.

## 2.5 Analytical techniques

To obtain as much information as possible about the  $^{13}\text{C}$  patterns of metabolites, advanced analytical techniques are of major importance. Mass spectrometry and tandem mass spectrometry are the most common devices. With the ambition of kinetic modeling in mind, the focus in this review is on quantitative approaches, while untargeted approaches are only briefly touched.

The ambition of quantitative intracellular measurements not only requires highly sensitive instruments to detect the low concentrated metabolites, but also a careful sample preparation. Continuous improvements and validation of protocols for new organisms are crucial to ensure good data quality. Especially, the cellular matrix is challenging, as ionization is sensitive to varying backgrounds. Standard addition or introduction of internal standards is required to correct for matrix effects. In 2005, Mashego MR, *et al.* [50], [51] introduced an internal standard for each metabolite, by the addition of U- $^{13}\text{C}$  labelled cell extract, which is, since then, frequently applied in current quantitative metabolomics. This internal standard

can be added at an early stage of the sample processing and enables to correct for losses during the processing [31, 52].

For measuring isotopic labeling, precisely the mass isotopomer distribution of intracellular metabolites, mass spectrometry, coupled to gas-chromatography or liquid chromatography, has shown significant advances in recent years. Tandem mass spectrometry has proven to enhance the sensitivity and additionally increase the resolution, with respect to the labeling composition by MS/MS [53]. Therefore, the metabolic flux estimation can be improved, compared to single MS or NMR based techniques [14, 54, 55].

Next to these targeted, quantitative approaches, untargeted approaches are necessary for the determination of novel metabolites and pathways. Since they provide broader coverage, untargeted metabolomics data is extremely complex and software tools are indispensable. Examples are the XCMS platform [56] for traditional metabolomics and X<sup>13</sup>CMS [57], and DynaMet [58], MathDAMP [59], or MID Max [60] for identification of isotopic labeling enrichments in detected metabolites.

## 2.6 Modeling approaches

The parameterized kinetic model should be able to (1) reproduce the experimental observations, (2) allow for the prediction of genetic or environmental perturbation. With predictive models at hand, optimization of the host and the process conditions will deliver more efficient bioprocesses. The advances in technology have enabled the construction of detailed mechanistic models that link metabolite concentrations with enzyme activities. Major limitations of practical applicability are the sheer amount of model parameters lacking identifiability, the size of the network or the accuracy of the kinetic expressions [61]. Here it is important to recognize that for predictive models not necessarily all parameters are required to be well determined [62]. This perception unlocks the use of sampling approaches, where average model predictions over a range of parameters are investigated. Approximative kinetic formats are a suitable alternative, as they are represented by canonical equations and usually contain fewer parameters. Some of the earliest approaches include power-law formats (GMA, S-Systems) and linearized formats (log-lin, lin-log). However, these formats can lead to inconsistent thermodynamic states, a problem that is addressed by recent formats such as modular rate laws and convenience kinetics [61, 63].

Although kinetic parameters can often be found in the literature, they are determined using *in vitro* experiments that can differ significantly from *in vivo* conditions. Hence, the final step to obtain a working model is to calibrate its parameters using *in vivo* data. The quality of calibration will depend on the model complexity and amount of available data. True estimates

of some parameters may not be possible due to structural or practical identifiability problems [64].

Ensemble modeling approach is a powerful approach to tackle these problems [65-69]. It consists on building an ensemble of alternative models that complies with experimental observations. In especial, models with different complexity are generated and compared with respect to their ability to reproduce key features of the data. To overcome data scarcity and inaccuracies (noise), sampling based approaches have become popular to yield surrogates for missing knowledge in parameter values. Sampling of metabolite concentrations, kinetic parameters, enzyme levels and fluxes have been used to identify average properties on a system level, even when the available data is insufficient for actual parameter inference [70-73]. Having fast simulators and smart stochastic sampling schemes at hand, Bayesian approaches could emerge as the 'Swiss army knife' that unlocks the consistent incorporation of all prior knowledge.

Irrespective of the biological question, modeling includes several common elements. In particular, fast and accurate numerical integrators, robust parameter fitting and advanced statistical tools are required, capable to deal with the non-linear and often ill-posed dynamic problems. Particularly, badly determined or non-identifiable parameters, often non-intuitively correlated pose distinct numerical challenges to model calibration. Parameter uncertainty is addressed by the calculation of confidence intervals, often using the Fisher information matrix, bootstrapping or profile likelihoods. For addressing uncertainty in potentially non-identifiable parameters, profile likelihoods have proven the most reliable [74]. With a dynamic model at hand, analysis for the rate limiting and controlling steps can be performed. One frequently used approach is Metabolic Control Analysis, a sensitivity analysis framework [75-77]. MCA computes the effects of small parameter perturbations resulting in flux control coefficients which describe the effect of a change in the activity of an enzyme on all network fluxes.

## **2.7 Conclusions and Outlook**

With predictive kinetic models at hand, the design and understanding of microbial cell factories could receive a boost in development. The construction of valid metabolic models is highly challenging and requires further developments, in both experimental and computational approaches:

- Design experimental systems that generate sufficient perturbations, while still being representative for natural and industrial environments and allow for accurate monitoring of the cellular dynamics.

- Develop these platforms for high-throughput analysis, to study a series of external and internal conditions.
- Rigorous dynamical systems theory and systems analysis to elucidate mathematical structures that can be beneficially exploited [78].
- New computational tools for parameter exploration and identification in high-dimensional (>100) spaces.
- Enhancement of model building frameworks (like KiMoSys [79] for kinetic modeling) by various features to assist modellers with the complex tasks of gathering and integrating the available information.
- Establish comprehensive model databases (like Bio- Models [80] for kinetic modeling). To this end, standards, structured repositories for the experimental omics data and associated protocols (meta-data) are needed [81].

Ultimately, predictive metabolic models could then integrate into whole-cell models, which also include transcription, translation and post-translational mechanisms [82]. Next to cell-focused models, the integration of the extracellular environment with spatial inhomogeneity due to transport limitation (mixing) are relevant for the development of industrial bioprocesses [83, 84].

## References

1. *Systems Metabolic Engineering*. Springer; 2012.
2. Lee SJ, Lee DY, Kim TY, Kim BH, Lee JW, Lee SY: **Metabolic engineering of *Escherichia coli* for enhanced production of succinic acid, based on genome comparison and in silico gene knockout simulation**. *Applied and Environmental Microbiology* 2005, **71**:7880-7887.
3. Chubukov V, Gerosa L, Kochanowski K, Sauer U: **Coordination of microbial metabolism**. *Nat Rev Microbiol* 2014, **12**:327-340.
4. Beste DJV, Bonde B, Hawkins N, Ward JL, Beale MH, Noack S, Nöh K, Kruger NJ, Ratcliffe RG, McFadden J: **13C Metabolic Flux Analysis Identifies an Unusual Route for Pyruvate Dissimilation in *Mycobacteria* which Requires Isocitrate Lyase and Carbon Dioxide Fixation**. *PLOS Pathogens* 2011, **7**:e1002091.
5. Veiga T, Solis-Escalante D, Romagnoli G, ten Pierick A, Hanemaaijer M, Deshmukh AT, Wahl A, Pronk JT, Daran JM: **Resolving phenylalanine metabolism sheds light on natural synthesis of penicillin G in *Penicillium chrysogenum***. *Eukaryot Cell* 2012, **11**:238-249.
6. Knoop H, Grundel M, Zilliges Y, Lehmann R, Hoffmann S, Lockau W, Steuer R: **Flux balance analysis of cyanobacterial metabolism: the metabolic network of *Synechocystis* sp. PCC 6803**. *PLoS Comput Biol* 2013, **9**:e1003081.
7. Wiechert W, Noack S: **Mechanistic pathway modeling for industrial biotechnology: challenging but worthwhile**. *Current Opinion in Biotechnology* 2011, **22**:604-610.
8. Orth JD, Conrad TM, Na J, Lerman JA, Nam H, Feist AM, Palsson BØ: **A comprehensive genome-scale reconstruction of *Escherichia coli* metabolism**. *Mol Syst Biol* 2011, **7**:535-535.
9. Rocha I, Forster J, Nielsen J: **Design and application of genome-scale reconstructed metabolic models**. *Methods Mol Biol* 2008, **416**:409-431.
10. Teusink B, Passarge J, Reijenga CA, Esgalhado E, van der Weijden CC, Schepper M, Walsh MC, Bakker BM, van Dam K, Westerhoff HV, Snoep JL: **Can yeast glycolysis be understood in terms of in vitro kinetics of the constituent enzymes? Testing biochemistry**. *Eur J Biochem* 2000, **267**:5313-5329.
11. Lindsley JE, Rutter J: **Whence cometh the allosterome?** *Proc Natl Acad Sci U S A* 2006, **103**:10533-10535.
12. Theobald U, Mailinger W, Baltus M, Rizzi M, Reuss M: **In vivo analysis of metabolic dynamics in *Saccharomyces cerevisiae* : I. Experimental observations**. *Biotechnol Bioeng* 1997, **55**:305-316.
13. Theobald U, Mailinger W, Reuss M, Rizzi M: **In vivo analysis of glucose-induced fast changes in yeast adenine nucleotide pool applying a rapid sampling technique**. *Anal Biochem* 1993, **214**:31-37.
14. Wahl SA, Nöh K, Wiechert W: **13C labeling experiments at metabolic nonstationary conditions: An exploratory study**. *BMC Bioinformatics* 2008, **9**.
15. Buescher JM, Antoniewicz MR, Boros LG, Burgess SC, Brunengraber H, Clish CB, DeBerardinis RJ, Feron O, Frezza C, Ghesquiere B, et al: **A roadmap for interpreting (13)C metabolite labeling patterns from cells**. *Curr Opin Biotechnol* 2015, **34**:189-201.
16. Kotte O, Heinemann M: **A divide-and-conquer approach to analyze underdetermined biochemical models**. *Bioinformatics* 2009, **25**:519-525.
17. Canelas AB, Ras C, ten Pierick A, van Gulik WM, Heijnen JJ: **An in vivo data-driven framework for classification and quantification of enzyme kinetics and determination of apparent thermodynamic data**. *Metabolic Engineering* 2011, **13**:294-306.
18. Douma RD, Deshmukh AT, de Jonge LP, de Jong BW, Seifar RM, Heijnen JJ, van Gulik WM: **Novel insights in transport mechanisms and kinetics of phenylacetic acid and penicillin-G in *Penicillium chrysogenum***. *Biotechnol Prog* 2012, **28**:337-348.
19. Chassagnole C, Noisommit-Rizzi N, Schmid JW, Mauch K, Reuss M: **Dynamic modeling of the central carbon metabolism of *Escherichia coli***. *Biotechnol Bioeng* 2002, **79**:53-73.

20. Magnus JB, Hollwedel D, Oldiges M, Takors R: **Monitoring and modeling of the reaction dynamics in the valine/leucine synthesis pathway in *Corynebacterium glutamicum***. *Biotechnol Prog* 2006, **22**:1071-1083.
21. Kremling A, Fischer S, Sauter T, Bettenbrock K, Gilles ED: **Time hierarchies in the *Escherichia coli* carbohydrate uptake and metabolism**. *Biosystems* 2004, **73**:57-71.
22. Zhang J, Sassen T, Pierick AT, Ras C, Heijnen JJ, Wahl SA: **A fast sensor for in vivo quantification of cytosolic phosphate in *Saccharomyces cerevisiae***. *Biotechnol Bioeng* 2014.
23. Deshmukh AT, Verheijen PJ, Maleki Seifar R, Heijnen JJ, van Gulik WM: **In vivo kinetic analysis of the penicillin biosynthesis pathway using PAA stimulus response experiments**. *Metab Eng* 2015, **32**:155-173.
24. Schaefer U, Boos W, Takors R, Weuster-Botz D: **Automated sampling device for monitoring intracellular metabolite dynamics**. *Anal Biochem* 1999, **270**:88-96.
25. Buziol S, Bashir I, Baumeister A, Claassen W, Noisommit-Rizzi N, Mailinger W, Reuss M: **New bioreactor-coupled rapid stopped-flow sampling technique for measurements of metabolite dynamics on a subsecond time scale**. *Biotechnol Bioeng* 2002, **80**:632-636.
26. Visser D, van Zuylen GA, van Dam JC, Oudshoorn A, Eman MR, Ras C, van Gulik WM, Frank J, van Dedem GW, Heijnen JJ: **Rapid sampling for analysis of in vivo kinetics using the BioScope: a system for continuous-pulse experiments**. *Biotechnol Bioeng* 2002, **79**:674-681.
27. Mashego MR, van Gulik WM, Vinke JL, Visser D, Heijnen JJ: **In vivo kinetics with rapid perturbation experiments in *Saccharomyces cerevisiae* using a second-generation BioScope**. *Metabolic Engineering* 2006, **8**:370-383.
28. Millard P, Massou S, Wittmann C, Portais JC, Letisse F: **Sampling of intracellular metabolites for stationary and non-stationary (<sup>13</sup>C) metabolic flux analysis in *Escherichia coli***. *Anal Biochem* 2014, **465**:38-49.
29. Bolten CJ, Kiefer P, Letisse F, Portais JC, Wittmann C: **Sampling for metabolome analysis of microorganisms**. *Anal Chem* 2007, **79**:3843-3849.
30. Taymaz-Nikerel H, de Mey M, Ras C, ten Pierick A, Seifar RM, van Dam JC, Heijnen JJ, van Gulik WM: **Development and application of a differential method for reliable metabolome analysis in *Escherichia coli***. *Anal Biochem* 2009, **386**:9-19.
31. Tillack J, Paczia N, Nöh K, Wiechert W, Noack S: **Error Propagation Analysis for Quantitative Intracellular Metabolomics**. *Metabolites* 2012, **2**:1012-1030.
32. Rizzi M, Baltés M, Theobald U, Reuss M: **In vivo analysis of metabolic dynamics in *Saccharomyces cerevisiae*: II. Mathematical model**. *Biotechnol Bioeng* 1997, **55**:592-608.
33. Suarez-Mendez CA, Sousa A, Heijnen JJ, Wahl A: **Fast "Feast/Famine" Cycles for Studying Microbial Physiology Under Dynamic Conditions: A Case Study with *Saccharomyces cerevisiae***. *Metabolites* 2014, **4**:347-372.
34. Sunya S, Bideaux C, Molina-Jouve C, Gorret N: **Short-term dynamic behavior of *Escherichia coli* in response to successive glucose pulses on glucose-limited chemostat cultures**. *J Biotechnol* 2013, **164**:531-542.
35. van Kleeff BH, Kuenen JG, Heijnen JJ: **Heat flux measurements for the fast monitoring of dynamic responses to glucose additions by yeasts that were subjected to different feeding regimes in continuous culture**. *Biotechnol Prog* 1996, **12**:510-518.
36. de Jonge L, Buijs NA, Heijnen JJ, van Gulik WM, Abate A, Wahl SA: **Flux response of glycolysis and storage metabolism during rapid feast/famine conditions in *Penicillium chrysogenum* using dynamic (<sup>13</sup>C) labeling**. *Biotechnol J* 2014, **9**:372-385.
37. Lorantfy B, Jazini M, Herwig C: **Investigation of the physiological response to oxygen limited process conditions of *Pichia pastoris* Mut(+) strain using a two-compartment scale-down system**. *J Biosci Bioeng* 2013, **116**:371-379.
38. Neubauer P, Junne S: **Scale-down simulators for metabolic analysis of large-scale bioprocesses**. *Curr Opin Biotechnol* 2010, **21**:114-121.

39. Abate A: **Piecewise affine approximations of fluxes and enzyme kinetics from in vivo  $^{13}\text{C}$  labeling experiments.** *International Journal of Robust and Nonlinear Control* 2012;1120-1139.
40. Iwatani S, Yamada Y, Usuda Y: **Metabolic flux analysis in biotechnology processes.** *Biotechnol Lett* 2008, **30**:791-799.
41. Wiechert W:  **$^{13}\text{C}$  metabolic flux analysis.** *Metab Eng* 2001, **3**:195-206.
42. Kohlstedt M, Becker J, Wittmann C: **Metabolic fluxes and beyond-systems biology understanding and engineering of microbial metabolism.** *Appl Microbiol Biotechnol* 2010, **88**:1065-1075.
43. Link H, Kochanowski K, Sauer U: **Systematic identification of allosteric protein-metabolite interactions that control enzyme activity in vivo.** *Nat Biotech* 2013, **31**:5.
44. Allen J, Davey HM, Broadhurst D, Heald JK, Rowland JJ, Oliver SG, Kell DB: **High-throughput classification of yeast mutants for functional genomics using metabolic footprinting.** *Nat Biotechnol* 2003, **21**:692-696.
45. Fuhrer T, Heer D, Begemann B, Zamboni N: **High-throughput, accurate mass metabolome profiling of cellular extracts by flow injection-time-of-flight mass spectrometry.** *Anal Chem* 2011, **83**:7074-7080.
46. Hollinshead WD, Henson WR, Abernathy M, Moon TS, Tang YJ: **Rapid metabolic analysis of *Rhodococcus opacus* PD630 via parallel  $^{13}\text{C}$ -metabolite fingerprinting.** *Biotechnol Bioeng* 2016, **113**:91-100.
47. Heux S, Philippe B, Portais JC: **High-Throughput Workflow for Monitoring and Mining Bioprocess Data and Its Application to Inferring the Physiological Response of *Escherichia coli* to Perturbations.** *Applied and Environmental Microbiology* 2011, **77**:7040-7049.
48. Rohe P, Venkanna D, Kleine B, Freudl R, Oldiges M: **An automated workflow for enhancing microbial bioprocess optimization on a novel microbioreactor platform.** *Microb Cell Fact* 2012, **11**:144.
49. Heux S, Pointot J, Massou S, Sokol S, Portais JC: **A novel platform for automated high-throughput fluxome profiling of metabolic variants.** *Metabolic Engineering* 2014, **25**:8-19.
50. Mashego MR, Wu L, Van Dam JC, Ras C, Vinke JL, Van Winden WA, Van Gulik WM, Heijnen JJ: **MIRACLE: mass isotopomer ratio analysis of U- $^{13}\text{C}$ -labeled extracts. A new method for accurate quantification of changes in concentrations of intracellular metabolites.** *Biotechnology and Bioengineering* 2004, **85**:620-628.
51. Wu L, Mashego MR, van Dam JC, Proell AM, Vinke JL, Ras C, van Winden WA, van Gulik WM, Heijnen JJ: **Quantitative analysis of the microbial metabolome by isotope dilution mass spectrometry using uniformly  $^{13}\text{C}$ -labeled cell extracts as internal standards.** *Anal Biochem* 2005, **336**:164-171.
52. Wahl SA, Seifar RM, Ten Pierick A, Ras C, van Dam JC, Heijnen JJ, van Gulik WM: **Quantitative Metabolomics Using ID-MS.** *Methods Mol Biol* 2014, **1191**:91-105.
53. Mairinger T, Steiger M, Nocon J, Mattanovich D, Koellensperger G, Hann S: **Gas Chromatography-Quadrupole Time-of-Flight Mass Spectrometry-Based Determination of Isotopologue and Tandem Mass Isotopomer Fractions of Primary Metabolites for C- $^{13}$ -Metabolic Flux Analysis.** *Analytical Chemistry* 2015, **87**:11792-11802.
54. Antoniewicz MR: **Tandem mass spectrometry for measuring stable-isotope labeling.** *Curr Opin Biotechnol* 2013, **24**:48-53.
55. Niedenführ S, Pierick AT, van Dam PT, Suarez-Mendez CA, Nöh K, Wahl SA: **Natural isotope correction of MS/MS measurements for metabolomics and C fluxomics.** *Biotechnol Bioeng* 2015.
56. Smith CA, Want EJ, O'Maille G, Abagyan R, Siuzdak G: **XCMS: processing mass spectrometry data for metabolite profiling using nonlinear peak alignment, matching, and identification.** *Anal Chem* 2006, **78**:779-787.
57. Huang X, Chen YJ, Cho K, Nikolskiy I, Crawford PA, Patti GJ: **X13CMS: global tracking of isotopic labels in untargeted metabolomics.** *Anal Chem* 2014, **86**:1632-1639.

58. Kiefer P, Schmitt U, Müller JE, Hartl J, Meyer F, Ryffel F, Vorholt JA: **DynaMet: a fully automated pipeline for dynamic LC-MS data.** *Anal Chem* 2015, **87**:9679-9686.
59. Baran R, Kochi H, Saito N, Suematsu M, Soga T, Nishioka T, Robert M, Tomita M: **MathDAMP: a package for differential analysis of metabolite profiles.** *BMC Bioinformatics* 2006, **7**:530.
60. McCloskey D, Young JD, Xu S, Palsson BO, Feist AM: **MID Max: LC-MS/MS Method for Measuring the Precursor and Product Mass Isotopomer Distributions of Metabolic Intermediates and Cofactors for Metabolic Flux Analysis Applications.** *Anal Chem* 2016, **88**:1362-1370.
61. Srinivasan S, Cluett WR, Mahadevan R: **Constructing kinetic models of metabolism at genome-scales: A review.** *Biotechnology Journal* 2015, **10**:1345-1359.
62. van Mourik S, Ter Braak C, Stigter H, Molenaar J: **Prediction uncertainty assessment of a systems biology model requires a sample of the full probability distribution of its parameters.** *PeerJ* 2014, **2**:e433.
63. Costa RS, Machado D, Rocha I, Ferreira EC: **Hybrid dynamic modeling of Escherichia coli central metabolic network combining Michaelis-Menten and approximate kinetic equations.** *Biosystems* 2010, **100**:150-157.
64. Chis OT, Banga JR, Balsa-Canto E: **Structural identifiability of systems biology models: a critical comparison of methods.** *PLoS One* 2011, **6**:e27755.
65. Tran LM, Rizk ML, Liao JC: **Ensemble modeling of metabolic networks.** *Biophys J* 2008, **95**:5606-5617.
66. Tan Y, Rivera JG, Contador CA, Asenjo JA, Liao JC: **Reducing the allowable kinetic space by constructing ensemble of dynamic models with the same steady-state flux.** *Metab Eng* 2011, **13**:60-75.
67. Haunschild MD, Freisleben B, Takors R, Wiechert W: **Investigating the dynamic behavior of biochemical networks using model families.** *Bioinformatics* 2005, **21**:1617-1625.
68. Lee Y, Lafontaine Rivera JG, Liao JC: **Ensemble Modeling for Robustness Analysis in engineering non-native metabolic pathways.** *Metab Eng* 2014, **25**:63-71.
69. Saha R, Chowdhury A, Maranas CD: **Recent advances in the reconstruction of metabolic models and integration of omics data.** *Curr Opin Biotechnol* 2014, **29**:39-45.
70. Saa P, Nielsen LK: **A general framework for thermodynamically consistent parameterization and efficient sampling of enzymatic reactions.** *PLoS Comput Biol* 2015, **11**:e1004195.
71. Chakrabarti A, Miskovic L, Soh KC, Hatzimanikatis V: **Towards kinetic modeling of genome-scale metabolic networks without sacrificing stoichiometric, thermodynamic and physiological constraints.** *Biotechnology Journal* 2013, **8**:1043-U1105.
72. Andreatti S, Miskovic L, Hatzimanikatis V: **iSCHRUNK - In Silico Approach to Characterization and Reduction of Uncertainty in the Kinetic Models of Genome-scale Metabolic Networks.** *Metabolic Engineering* 2016, **33**:158-168.
73. Murabito E, Verma M, Bekker M, Bellomo D, Westerhoff HV, Teusink B, Steuer R: **Monte-Carlo modeling of the central carbon metabolism of Lactococcus lactis: insights into metabolic regulation.** *PLoS One* 2014, **9**:e106453.
74. Fröhlich F, Theis FJ, Hasenauer J: **Uncertainty Analysis for Non-identifiable Dynamical Systems: Profile Likelihoods, Bootstrapping and More.** In *Computational Methods in Systems Biology; 2014//; Cham*. Edited by Mendes P, Dada JO, Smallbone K. Springer International Publishing; 2014: 61-72.
75. Chassagnole C, Fell DA, Rais B, Kudla B, Mazat JP: **Control of the threonine-synthesis pathway in Escherichia coli: a theoretical and experimental approach.** *Biochem J* 2001, **356**:433-444.
76. Hoefnagel MHN, Starrenburg MJC, Martens DE, Hugenholtz J, Kleerebezem M, Van S, II, Bongers R, Westerhoff HV, Snoep JL: **Metabolic engineering of lactic acid bacteria, the combined approach: kinetic modelling, metabolic control and experimental analysis.** *Microbiology* 2002, **148**:1003-1013.



77. Arnold A, Nikoloski Z: **A quantitative comparison of Calvin-Benson cycle models.** *Trends Plant Sci* 2011, **16**:676-683.
78. Wiechert W, Nöh K, Weitzel M: **Metabolic isotopomer labeling systems. Part III: Path tracing.** *Mathematical Biosciences* 2013, **244**:1-12.
79. Costa RS, Verissimo A, Vinga S: **KiMoSys: a web-based repository of experimental data for Kinetic MOdels of biological SYStems.** *BMC Syst Biol* 2014, **8**:85.
80. Chelliah V, Juty N, Ajmera I, Ali R, Dumousseau M, Glont M, Hucka M, Jalowicki G, Keating S, Knight-Schrijver V, et al: **BioModels: ten-year anniversary.** *Nucleic Acids Res* 2015, **43**:D542-548.
81. Miskovic M: **Comparison of tolerance of venlafaxine, paroxetine and amitriptyline in depression therapy.** *Med Arch* 2015, **69**:107-109.
82. Karr JR, Takahashi K, Funahashi A: **The principles of whole-cell modeling.** *Curr Opin Microbiol* 2015, **27**:18-24.
83. Wang G, Tang W, Xia J, Chu J, Noorman H, van Gulik WM: **Integration of microbial kinetics and fluid dynamics toward model-driven scale-up of industrial bioprocesses.** *Engineering in Life Sciences* 2015, **15**:20-29.
84. Noorman H: **An industrial perspective on bioreactor scale-down: What we can learn from combined large-scale bioprocess and model fluid studies.** *Biotechnology Journal* 2011, **6**:934-943.





# Chapter



## *Escherichia coli* metabolism under short-term repetitive substrate dynamics: Adaptation and trade-offs

Published as: Vasilakou E, van Loosdrecht MCM, Wahl SA: *Escherichia coli* metabolism under short-term repetitive substrate dynamics: adaptation and trade-offs. *Microb Cell Fact* 2020, 19:116.

DOI: 10.1186/s12934-020-01379-0

## Abstract

**Background:** Microbial metabolism is highly dependent on the environmental conditions. Especially, the substrate concentration, as well as oxygen availability, determine the metabolic rates. In large-scale bioreactors, microorganisms encounter dynamic conditions in substrate and oxygen availability (mixing limitations), which influence their metabolism and subsequently their physiology. Earlier, single substrate pulse experiments were not able to explain the observed physiological changes generated under large-scale industrial fermentation conditions.

**Results:** In this study we applied a repetitive feast-famine regime in an aerobic *Escherichia coli* culture in a time-scale of seconds. The regime was applied for several generations, allowing cells to adapt to the (repetitive) dynamic environment. The observed response was highly reproducible over the cycles, indicating that cells were indeed fully adapted to the regime. We observed an increase of the specific substrate and oxygen consumption (average) rates during the feast-famine regime, compared to a steady-state (chemostat) reference environment. The increased rates at same (average) growth rate led to a reduced biomass yield (30% lower). Interestingly, this drop was not followed by increased by-product formation, pointing to the existence of energy-spilling reactions. During the feast-famine cycle, the cells rapidly increased their uptake rate. Within 10 seconds after the beginning of the feeding, the substrate uptake rate was higher ( $4.68 \mu\text{mol}/\text{g}_{\text{CDW}}/\text{s}$ ) than reported during batch growth ( $3.3 \mu\text{mol}/\text{g}_{\text{CDW}}/\text{s}$ ). The high uptake led to an accumulation of several intracellular metabolites, during the feast phase, accounting for up to 34% of the carbon supplied. Although the metabolite concentrations changed rapidly, the cellular energy charge remained unaffected, suggesting well-controlled balance between ATP producing and ATP consuming reactions. The role of inorganic polyphosphate as an energy buffer is discussed.

**Conclusions:** The adaptation of the physiology and metabolism of *Escherichia coli* under substrate dynamics, representative for large-scale fermenters, revealed the existence of several cellular mechanisms coping with stress. Changes in the substrate uptake system, storage potential and energy-spilling processes resulted to be of great importance. These metabolic strategies consist a meaningful step to further tackle reduced microbial performance, observed under large-scale cultivations.

### 3.1 Introduction

Microorganisms are widely used for the production of chemicals, ranging from small organic acids to large proteins, including biopharmaceuticals, biochemicals and bulk biofuels [1-3]. In order to meet the cost targets and demands, large-scale production cultivations are and will be required [4]. However, scale-up of microbial processes is not a trivial process, as strain performance usually declines from lab to industrial-scale bioreactors [5-7]. One root of this problem is the mixing limitations, which characterize large-scale bioreactors, and lead to several heterogeneities in the cultivation environment. Important parameters, affected by the constraints in mass and heat transfer, are nutrient concentrations, pH, dissolved gases, temperature and other parameters, which have been extensively reported in many studies and reviews [8-13].

Substrate gradients are frequently considered as a main reason for performance reduction. Commonly, the substrate concentration should be kept at low levels to avoid overflow metabolism [14-17]. To achieve such conditions, fed-batch or chemostat regimes are applied. At large scale with mixing limitations, this leads to varying concentration of the substrate in different areas of the reactor [8, 18-20]. Especially, for most large-scale bioreactors, there is one feeding inlet; close to that point the substrate concentration is (very) high, while it becomes lower in the other parts of the reactor. Thus, cells inside the reactor circulate between zones of substrate excess and zones of substrate limitation. Depending on the scale and the type of the reactor, the timeframes are in order of seconds to minutes [11, 12, 18]. The presence and origin of these gradients has also been demonstrated by computational fluid dynamic simulations [18, 21-23].

It is known that such heterogeneities have a big impact on the cellular metabolism, from physiology to metabolic fluxes and gene expression, and subsequently on product formation. Cells traveling close to the feeding zone will increase their substrate uptake rates, which may lead to increased overflow metabolism leading to unwanted products and energy spilling. Additionally, the high uptake rate leads to high oxygen demands, potentially inducing oxygen depletion in this zone [24-26]. On the other hand, cells passing through areas with low substrate concentration may re-consume overflow metabolites and/or activate stress response pathways, due to substrate limitations [12]. For example, *Escherichia coli* cultures, cyclically circulating from high to low glucose levels, have shown decreased biomass yields and by-product formation [8, 19].

Two approaches to improve the cell performance in large-scale bioprocesses are: 1) Optimization of bioreactor design and operating conditions preventing gradients, and/or 2) Development of more robust strains which can cope with these conditions.

Especially, for designing more robust strains a mechanistic understanding of the (metabolic) responses to the environment dynamics is required. The cellular regulation mechanisms to cope with frequently changing environments have been, and still are, key questions in microbiology, not only for industrial applications, but also for understanding microbial ecosystems such as the natural habitat of *E.coli*, involving the lower intestine of humans and animals, water, sediment and soil [27].

The cellular behaviour, under substrate dynamic conditions, has been studied using numerous scale-down experiments, for many types of microorganisms (for reviews check [28, 29]). Commonly these studies derived observations on the physiology, such as average rates of growth, substrate uptake, product formation and respiration, but focused less on the metabolic network and the underlying mechanisms of the cellular responses. For example, the energetic state of the cell, storage accumulation, futile cycles and more phenomena, occurring under dynamic conditions, need further investigation. In addition, the fact that microorganisms, cultivated in large-scale bioreactors, face substrate gradients in a cyclic mode (alternating from substrate excess to limitation), has been highly neglected. Most of the scale-down experiments assessed the behaviour of the culture shortly after applying a single perturbation event. However, we strongly consider that cells develop different adaptation strategies, when facing variations in environmental conditions, over long time periods (not long enough for genetic evolution). Several researchers studied such conditions [30-34] and suggested significant changes in physiology, metabolic fluxes, as well as transcription and translation, when the cells moved between different stress zones repeatedly, eventually leading to reduced growth and productivity [6]. Therefore, the long-term responses to successive substrate gradients will be different than those which would occur in short-term (<5 generations) or after a sudden perturbation. Suarez-Mendez CA, *et al.* [35] applied repetitive glucose perturbations to *Saccharomyces cerevisiae* culture, using a feast-famine regime, proving that the dynamic responses of the adapted culture showed many differences compared to stimulus-response experiments, such as the absence of the ATP paradox [36]. A similar study has been performed for *Penicillium chrysogenum* [37]. However, only a few studies have been previously performed with *E.coli*, assessing the effects of substrate gradients in long-term. Pickett AM, *et al.* [38] were the first ones to apply repeating square-wave glucose perturbations, studying the effects on growth and composition of *E.coli* ML30. However, they applied cycles of 2 hours duration, which are not able to capture the metabolic responses occurring in timescales of seconds in large-scale bioreactors. Sunya S, *et al.* [39] characterized the dynamic behaviour of *E.coli* DPD2085 imposed in 4 successive cycles, of 7 min duration each, of glucose pulses in different intensities. All cycles were compared to each other, in terms of specific formation and consumption rates. Nonetheless, the profiles of O<sub>2</sub> and CO<sub>2</sub> concentration were still changing

after 4 cycles of successive perturbations, indicating that the microorganism did not yet reach a metabolic steady response. In addition, the intracellular metabolic activity was not monitored.

The main goal of this study was to investigate the cellular responses of bacteria under changes in substrate availability, separated from other gradients. For this reason, a feast-famine regime was applied, for the first time, in a physiologically adapted *E.coli* K12 aerobic culture, with successive glucose perturbations and both intracellular and extracellular metabolic responses, occurring in short-time scale (seconds), were quantitatively described.

## 3.2 Materials and Methods

### 3.2.1 Strain and cultivation medium

*Escherichia coli* wild-type strain K12 MG1655, obtained from The Netherlands Culture Collection of Bacteria (NCCB, 3508 AD, Utrecht, The Netherlands), was used in all the experimental work of this study. The cultivation (and preculture) medium consisted of (per litre): 0.151 mol glucose ( $C_6H_{12}O_6 \cdot 1H_2O$ ), 0.5 g  $MgSO_4 \cdot 7H_2O$ , 0.5 g NaCl (Avantor J.T.Baker, Gliwice, Poland), 1.25 g  $(NH_4)_2SO_4$ , 1.15 g  $KH_2PO_4$ , 6.75 g  $NH_4Cl$  (Merck KGaA, Darmstadt, Germany), 0.001 g thiamine-HCl (Sigma-Aldrich, St. Louis, Missouri, USA) and 2 mL of trace elements solution [40]. The pH of the medium was adjusted to 7.0 by the addition of 1 M  $K_2HPO_4$ , before filter sterilization (pore size 0.2  $\mu m$ , cellulose acetate, FP 30/0.2, Whatman GmbH, Dassel, Germany).

### 3.2.2 Preculture

Culture aliquots, previously stored in 80% v/v glycerol at  $-80^\circ C$ , were used for the preculture. Cells were grown in shake-flasks filled with 100 mL of the above-mentioned mineral medium, in an incubator ( $37^\circ C$ , 220 rpm) and were used as inoculum for the bioreactor cultivation.

### 3.2.3 Cultivation conditions

The cultivation was performed in a 1.2 L stirred tank bioreactor (Applikon Biotechnology B.V., Delft, The Netherlands), with 0.95 L working volume, controlled by weight. The bioreactor was aerated with pressurized air at  $0.44 L min^{-1}$  (0.5 vvm), using a Smart series mass flow controller 5850S (Brooks Instrument, PA, USA). The bioreactor was operated at 0.3 bar overpressure, at  $37^\circ C$  and a stirrer speed of 700 rpm. pH was controlled at 7.0 by automatic addition of either 4 M KOH or 2 M  $H_2SO_4$ . Antifoam (Basildon Chemicals Ltd, UK) was added manually, when necessary, during the batch phase. During the whole experiment, pH, temperature, medium and effluent vessel weight, base and acid addition were monitored online. In addition, the dissolved oxygen in the broth was measured by a polarographic ADI



sensor (Applisens, Applikon, Delft, The Netherlands). A gas analyser (NGA 2000, Rosemount, Emerson, USA) was used to measure on-line the oxygen ( $O_2$ ) and carbon dioxide ( $CO_2$ ) concentrations in the offgas. After the batch phase was completed (indicated by the decrease of carbon dioxide and the increase of dissolved oxygen), the medium feeding was switched on and a chemostat phase began at a dilution rate of  $0.044\text{ h}^{-1}$ . After 114 hours (5 residence times), samples for metabolite and biomass quantification were withdrawn.

### 3.2.4 Dynamic feast-famine regime

After sampling of the reference chemostat, the regime was changed to an intermittent feeding. The feast-famine setup is shown in Figure 3.1. Successive cycles of 400 s were applied by a continuous medium feeding for 20 s, followed by a period of 380 s of no feeding. The feeding pump was controlled automatically by a timer (Omega, CT, USA). The waste outflow was controlled by a scale, on top of which the reactor operated, maintaining the broth volume at 0.95 L. The regime was designed to feed the same amount of medium over time, as in the chemostat culture, leading to an average dilution rate of  $0.047\text{ h}^{-1}$ . Aeration rate was increased to  $0.7\text{ L min}^{-1}$  (0.8 vvm), to avoid oxygen limitation. The rest of the cultivation conditions remained the same as the reference chemostat. After 180 hours (8 residence times) of the intermittent feeding, samples for biomass and metabolite quantification were withdrawn.

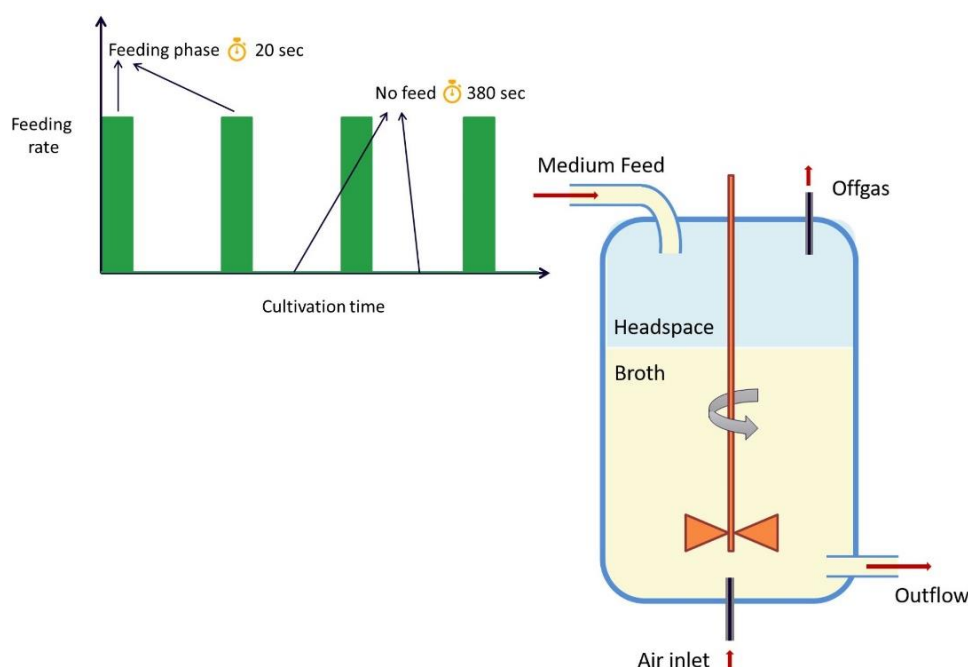


**Figure 3.1** Schematic representation of the feast-famine setup used in this work. The medium, containing glucose as a substrate, was fed block-wise (20 s on, 380 s off) through a head-plate port. A constant volume was maintained by weight control. Successive cycles run for about 200 h in total.

### **3.2.5 Sample analysis**

#### ***Cell dry weight measurements***

For the determination of the biomass concentration (dry weight), 2 mL of broth were collected and centrifuged (Heraeus Biofuge Stratos centrifuge) at 4°C for 5 min at 13800 g. The supernatant was then discarded and the pellet was resuspended in 1 mL Milli-Q water. Centrifugation and resuspension were repeated, the sample was then transferred to a previously dried (for 48 h at 70°C) and weighted glass vial and dried at 70°C for at least 48 h. The vials were then weighted again (after cooling down to room temperature inside a desiccator) and the cell dry weight was calculated as the difference between the final weight and the empty vial weight. The average of four replicate samples was used for the steady-state culture, six replica were used for the feast-famine regime.

#### ***Total organic carbon***

Total broth samples (2 mL each) were withdrawn from the reactor and immediately stored at -80°C. Supernatant samples were acquired by centrifuging total broth samples (Heraeus Biofuge Pico microcentrifuge) at room temperature for 1 min at 10400 g. The supernatant was then filtrated (pore size 0.2 µm filter, cellulose acetate, FP 30/0.2, Whatman GmbH, Dassel, Germany) and stored at -80°C. The total amount of organic carbon (TOC) was quantified with a TOC Analyzer (TOC-L CSH, Shimadzu), using the “difference method”: TOC was calculated from the difference between total carbon and inorganic carbon. Calibration standards were obtained from LPS b.v. (Oss, The Netherlands).

#### ***Extracellular metabolite sampling***

For the determination of extracellular metabolite concentrations, 2 mL of broth were withdrawn into a tube (Eppendorf) and immediately centrifuged (Heraeus Biofuge Pico microcentrifuge) at room temperature for 1 min at 10400 g. The supernatant was then filtrated (pore size 0.2 µm filter, cellulose acetate, FP 30/0.2, Whatman GmbH, Dassel, Germany) into an empty tube, submerged into liquid nitrogen and stored at -80°C until analysis. Centrifugation was used before filtration to prevent blocking of the filter, due to the high biomass concentration of the samples. For GC-MS and LC-MS analysis, 60 µL of <sup>13</sup>C cell extract were added to 300 µL of sample, as internal standard mix, before freezing with liquid nitrogen and storage at -80°C until further analysis.

#### ***Intracellular metabolite sampling***

For the determination of intracellular metabolite concentrations, the differential method was applied with some modifications [41]. For the total broth measurement, 1 mL of broth was withdrawn from the reactor into a tube filled with 5 mL aqueous methanol quenching solution

(60% v/v) at  $-40^{\circ}\text{C}$ , to rapidly stop metabolic activity. The sample was immediately vortexed to ensure homogeneity and then weighted. 120  $\mu\text{L}$  of  $^{13}\text{C}$  cell extract (production method described in [42]) were added to the sample, as internal standard mix. For the extraction of metabolites, 5 mL of aqueous ethanol solution (75% v/v), preheated at  $70^{\circ}\text{C}$ , were added to the sample and the tube was then placed into a water bath at  $95^{\circ}\text{C}$  for 4 minutes. After the boiling extraction, the sample was immediately cooled down to  $-40^{\circ}\text{C}$  in a cryostat.

The ethanol-water mixture in all samples was then evaporated in a Rapid-Vap (Labconco, MO, USA) at  $30^{\circ}\text{C}$ , under vacuum. The dried sediment was resuspended in 600  $\mu\text{L}$  Milli-Q water, vortexed and transferred to eppendorf tubes. The samples were centrifuged at 15000 g for 5 minutes at  $1^{\circ}\text{C}$  (Heraeus Biofuge Stratos centrifuge). The supernatants were transferred to new empty tubes and centrifuged again under the same conditions. The filtrate was stored in screw-cap vials, at  $-80^{\circ}\text{C}$ , until further analysis. The intracellular concentrations were obtained from the difference between total broth and extracellular measurements.

### **Analytical methods**

Extracellular concentrations of organic acids (acetate, lactate, formate) and ethanol were determined by HPLC (BioRad HPX-87H 300\*7.8 mm column, at  $59^{\circ}\text{C}$ ,  $0.6\text{ mL}\cdot\text{min}^{-1}$ , 1.5 mM phosphoric acid in Milli-Q water as eluent, coupled to a Waters 2414 RI detector and a Waters 2489 UV detector at 210 nm).

Processed extracellular and total broth samples were analysed by GC-MS/MS, GC-MS and LC-MS/MS. Metabolites of the central carbon pathways (glycolysis, pentose phosphate pathway (PPP), tricarboxylic cycle (TCA)) were quantified with GC-MS/MS (7890A GC coupled to a 7000 Quadrupole MS/MS, both from Agilent, Santa Clara, CA, equipped with a CTC Combi PAL autosampler, CTC Analytics AG, Zwingen, Switzerland), as described in [43] and/or anion-exchange LC-MS/MS [44]. GC-MS was used for the quantification of amino acids, as described in [45]. Ion-pair reversed phase LC-MS/MS was used for the quantification of nucleotides, as described in [46]. The isotope dilution mass spectrometry (IDMS) method, described in [42, 47], was used for the metabolite quantification.

## **3.3 Results**

The adaptation of *Escherichia coli* to repetitive, dynamic perturbations was evaluated with respect to short and long-term physiological and metabolic characteristics:

- 1) Comparison between average metabolic rates and yields under repetitive dynamic conditions and steady-state (reference) conditions, at the same dilution rate.

- 2) Comparison of the metabolic response between repetitive dynamics, single perturbations (pulse experiments) and steady-state levels.

It was assumed that cells were adapted after five residence times under the feast-famine regime, and a repetitive metabolic response was obtained. This assumption was supported by the observation that the online measurements of dissolved oxygen (DO) and offgas ( $O_2$  and  $CO_2$ ) concentrations (Figure 3.2) and the  $R_{CO_2}$  production rate (Appendix A.1), showed a highly reproducible pattern over the cycle.

### **3.3.1 *Escherichia coli* physiological behaviour under substrate dynamics**

#### ***Extracellular environment***

During the first 100 seconds of the cycle the residual glucose concentration (Figure 3.2A) was higher than the reported glucose affinity constant ( $K_M = 10 \mu M$ ) of the microorganism [48]. This time period will be referred to as (substrate) feast phase. The concentration increased from 0.01 to 0.32 mM, which was the maximum value, during the first 20 s of the cycle. Then, glucose depleted after 100 s ( $< 10 \mu M$ ), leading to a (substrate) famine phase.

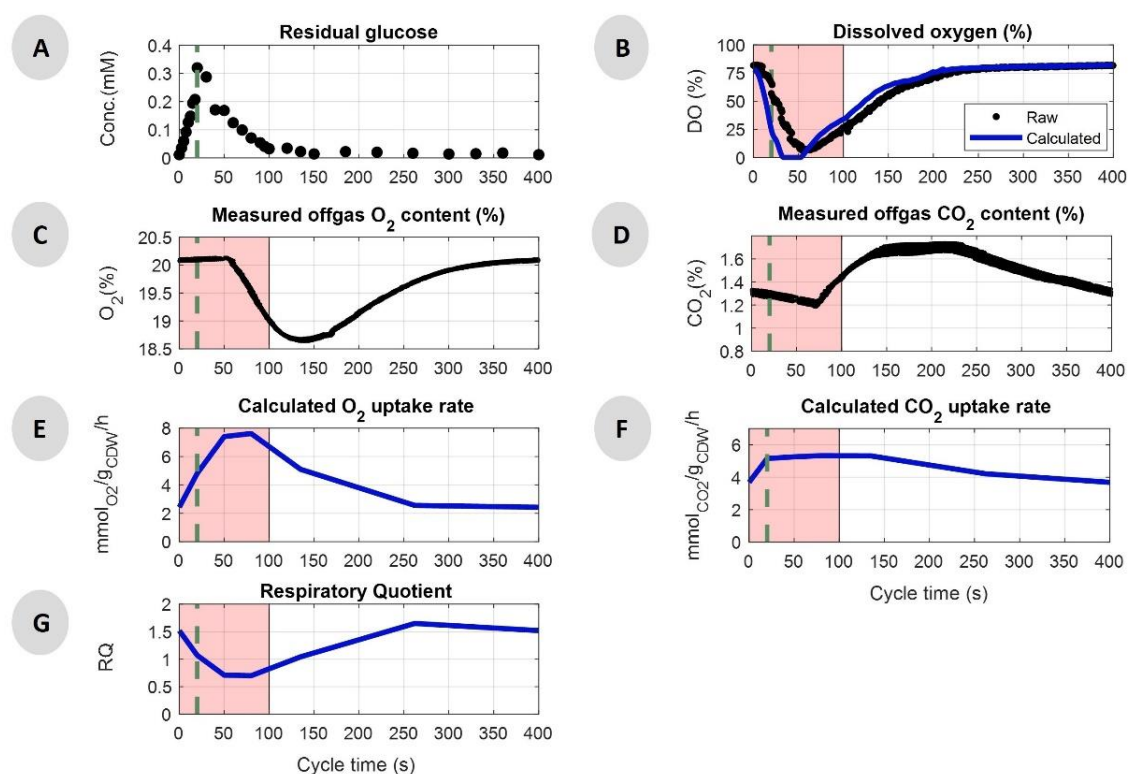


**Figure 3.2** Measured concentrations and calculated rates during the feast-famine cycle (s), approximately 8 generations after the beginning of the regime. **A)** Residual glucose concentration (mM), quantified by GC-MS/MS. **B)** Dissolved oxygen concentration (%) in the broth, raw data (black) and calculated, eliminating delays of the used Clark probe, (blue). **C)** Measurements of oxygen content in offgas (%). **D)** Measurements of carbon dioxide content in offgas (%). **E)** Calculated oxygen uptake rate ( $\text{mmol}_{\text{O}_2}/\text{g}_{\text{CDW}}/\text{h}$ ) based on the headspace and tubing offgas delays. **F)** Calculated carbon dioxide production rate ( $\text{mmol}_{\text{CO}_2}/\text{g}_{\text{CDW}}/\text{h}$ ) based on the headspace, tubing offgas delays and bicarbonate in the broth. **G)** Respiratory quotient (RQ) over time derived from the calculated  $q_{\text{O}_2}$  and  $q_{\text{CO}_2}$ . Data of 16 successive cycles are overlapped for DO,  $\text{O}_2$  and  $\text{CO}_2$  (B, C, D). The pink area in the plots represents the substrate feast phase. Green vertical dashed lines show the end of the feeding (20 s).

The broth dissolved oxygen profile was estimated by deconvolution (Figure 3.2(B) blue line), i.e. accounting for the dynamics of the Clark electrode (see Appendix A.2 for details).

With the supply of substrate, a decreased dissolved oxygen concentration was observed, suggesting a (high) oxygen consumption during the substrate feast period. The same behaviour was expected for the offgas measurements. The minimum  $\text{O}_2$  concentration (and maximum  $\text{CO}_2$ ) was observed only after the end of the feast phase. This delay can be explained by the headspace and tubing gas hold-up [49]. The  $\text{O}_2$  uptake rate and  $\text{CO}_2$  production rate over time (Figure 3.2 (E-F)) were therefore calculated, taking into account these delays (Appendix A.3). For the  $\text{CO}_2$  production, the interconversion of dissolved carbon dioxide to bicarbonate in the broth, due to the neutral pH 7 was, also, taken into account. The respiratory quotient (RQ) was then derived from these rates over time (Figure 3.2G). We observed that the RQ decreased from 1.5 to 0.7 during the first 50 s of the feast phase, and

increased back to the initial value after approximately 200 s, indicating that the electrons, from 20 to 120 s of the regime ( $RQ < 1$ ), are transferred to oxygen, while the respective carbon is not found in the form of  $CO_2$ . Therefore, we expect a form of intracellular storage compound (with electron to carbon ratio  $e^-/C < 3$ ), synthesized in the feast phase and degraded in the famine phase. Further discussion on this follows after the metabolome section.

### **Average biomass specific rates and yields**

In order to compare the physiology of the cells between steady-state and feast-famine conditions, the respective biomass specific conversion rates were calculated (Table 3.1). For the steady-state culture, rates were derived from the respective mass balances. During the intermittent feeding regime, all of the glucose supplied over one cycle was consumed, according to the GC-MS/MS measurements. Therefore the average glucose uptake rate ( $q_{glc}$ ) was calculated as the amount of substrate fed over the total cycle time. Taking into consideration the 20 h average doubling time of *Escherichia coli* at a dilution rate of  $0.05\text{ h}^{-1}$ , we expected the biomass concentration to vary by 0.5% during one cycle. This small change could not be determined experimentally, therefore a constant specific growth rate ( $\mu$ ) was considered within a cycle and calculated using the average of six cell dry weight measurements. To calculate the average  $O_2$  uptake and  $CO_2$  production rates, the respective online measurements were first integrated (trapezoidal method) over time, and then averaged for 16 successive cycles.

The extracellular by-product (acetate, lactate, formate and ethanol) concentrations (Appendix A.4), obtained from HPLC measurements, were also integrated over the cycle and their average formation rates were then calculated from their mass balances (raw data can be found in Appendix A.5). The average acetate production did not exceed  $0.02\text{ mmol/g}_{CDW}/\text{h}$ , both during steady-state and feast-famine conditions. The absence of high amounts of by-products in *E.coli* cultivations has been observed in previous studies, both during chemostat (usually at lower dilution rates (up to  $0.3\text{ h}^{-1}$ )) and after glucose or oxygen perturbations [50-54]. The by-product formation is related to overflow metabolism, a common phenomenon in *E.coli* cultivations in glucose-containing medium, where acetate is produced even when the culture is fully aerated [55-57]. Here, overflow metabolism was not significantly affected by the transition of the cells from steady-state to long-term dynamics.

The biomass specific rates were reconciled using the approach described in [58], using element conservations as constraints and the total organic carbon (TOC) measurements of the broth and the filtrate. A constant biomass composition of  $CH_{1.73}N_{0.24}O_{0.35}S_{0.006}P_{0.005}$  ( $\gamma_x=4.38$ ,  $M_w=23.2\text{ g/Cmol}$ ) [59] was used for all calculations. The phenomenon of cell lysis

was also introduced in the reconciliation to account for carbon and electrons of non-viable biomass.

**Table 3.1** Steady-state and average feast-famine biomass specific rates with their associated standard deviations. All the results presented in the table were calculated using data reconciliation. Raw data can be found in Appendix A.5.

	Steady-state	Feast-famine (cycle average)	log2-fold changes between the two regimes
<b>Biomass Concentration</b> (g L <sup>-1</sup> )	9.33 ± 0.01	6.28 ± 0.03	- 0.6
<b>Biomass Growth <math>\mu</math></b> (g g <sub>CDW</sub> <sup>-1</sup> h <sup>-1</sup> )	0.044 ± 0.002	0.048 ± 0.003	+ 0.1
<b>Lysis rate</b> (g g <sub>CDW</sub> <sup>-1</sup> h <sup>-1</sup> )	-	0.008 ± 0.006	-
<b>q<sub>Glucose</sub></b> (mmol <sub>glc</sub> g <sub>CDW</sub> <sup>-1</sup> h <sup>-1</sup> )	-0.73 ± 0.01	-1.12 ± 0.02	+ 0.6
<b>q<sub>O<sub>2</sub></sub></b> (mmol <sub>O<sub>2</sub></sub> g <sub>CDW</sub> <sup>-1</sup> h <sup>-1</sup> )	-2.08 ± 0.02	-4.42 ± 0.06	+ 1.1
<b>q<sub>CO<sub>2</sub></sub></b> (mmol <sub>CO<sub>2</sub></sub> g <sub>CDW</sub> <sup>-1</sup> h <sup>-1</sup> )	2.30 ± 0.02	4.53 ± 0.06	+ 1.0
<b>Respiratory Quotient</b>	1.11 ± 0.01	1.03 ± 0.02	- 0.1
<b>Total Biomass Yield</b> (g <sub>CDW</sub> g <sub>glc</sub> <sup>-1</sup> )	0.31 ± 0.01	0.21 ± 0.01	- 0.5
<b>Oxygen to Substrate ratio</b> (mmol <sub>O<sub>2</sub></sub> mmol <sub>glc</sub> <sup>-1</sup> )	2.85 ± 0.05	3.94 ± 0.08	+ 0.5

The most evident observation is that the calculated rates for glucose and oxygen uptake and CO<sub>2</sub> production were higher (+0.6, +1.1, +1.0 log<sub>2</sub>-fold times respectively) for the intermittent feeding, compared to the reference continuous regime. More specifically, during the reference chemostat operation, the oxygen to substrate consumption ratio was 2.85 ± 0.05 mol<sub>O<sub>2</sub></sub>/mol<sub>glc</sub>, which is comparable to the values reported in literature for similar cultivation conditions, ranging from 2.74 – 3.62 mol<sub>O<sub>2</sub></sub>/mol<sub>glc</sub> [50, 51, 59-61]. When the cells were subjected to feast-famine cycles, the average oxygen to substrate ratio increased, reaching 3.94 ± 0.08 mol<sub>O<sub>2</sub></sub>/mol<sub>glc</sub>.

Introducing potential cell lysis in the reconciliation, we observed that the lysis rate during the steady-state was calculated as negative (while positive by definition), with a high standard deviation and therefore the steady-state lysis was assumed zero.

The intermittent feeding, resulted in decreased average cell dry weight concentration and subsequent 0.5 log<sub>2</sub>-fold decrease (-30.3%) of the total biomass yield. The biomass yield was calculated as the ratio of the total biomass growth rate (including lysed biomass) over the glucose uptake rate. A decrease in biomass yield has also been reported in previous studies for *E. coli*, when varying the substrate availability. Many studies attributed this phenomenon either to overflow metabolism, due to high growth rates (>0.15 h<sup>-1</sup>) [25, 39], or to oxygen limitation. For example, Neubauer P, *et al.* [62] observed a 10% decrease in yield for cells circulating from zones of glucose excess to glucose starvation in a scale-down

two-compartment reactor (continuous stirred and plug flow), compared to reference conditions. This was explained by the oxygen limitation occurring in high-concentrated regions of glucose. However, this was not the case in our experimental setup. Only minor amounts of acetate were produced as a by-product and did not increase under the dynamic conditions. In addition, we did not observe any changes (elemental analysis) in the biomass composition or morphology, during the reference conditions compared to the one during the feast-famine regime (Appendix A.6) Lower biomass yields were also reported for other microorganisms, such as *Saccharomyces cerevisiae* (almost 25% decrease), subjected to an intermittent feeding (similar to the regime used here) [63].

The ratio of CO<sub>2</sub> produced per glucose consumed, during the steady-state regime, was  $3.16 \pm 0.05 \text{ mol}_{\text{CO}_2}/\text{mol}_{\text{glc}}$ , while for the feast-famine a value of  $4.05 \pm 0.08 \text{ mol}_{\text{CO}_2}/\text{mol}_{\text{glc}}$  (+ 28.1%) was observed. Together with the increase in O<sub>2</sub> consumption, it indicates that more glucose was used for respiration, rather than biomass production, during the feast-famine cycles [8].

### **3.3.2 Glucose uptake dynamics: a matter of seconds**

The feast-famine setup allows to measure the short-term responses of *E.coli* cells with high time resolution and repeated measurements. Especially, samples can be obtained from repetitive cycles (Figure 3.2B, C, D), which allowed for distributing sampling over several cycles.

Special focus was to obtain a high-resolution uptake profile as substrate uptake has a major impact on the intracellular metabolic behaviour of the microorganism. To calculate the short-term glucose uptake profile, a piecewise affine (PWA) rate approximation [64] was calculated. The breakpoints used were timepoints of 0, 2, 15, 18, 110 and 400 s. These breakpoints were chosen based on the highest goodness of fit ( $R^2$  was used), among various combinations [65]. The flux between the breakpoints followed a first order linear function (Figure 3.3). Note that the first and last breakpoint were coupled (cyclic regime). The rate was normalized using the reconciled biomass concentration of  $6.28 \text{ g L}^{-1}$ .



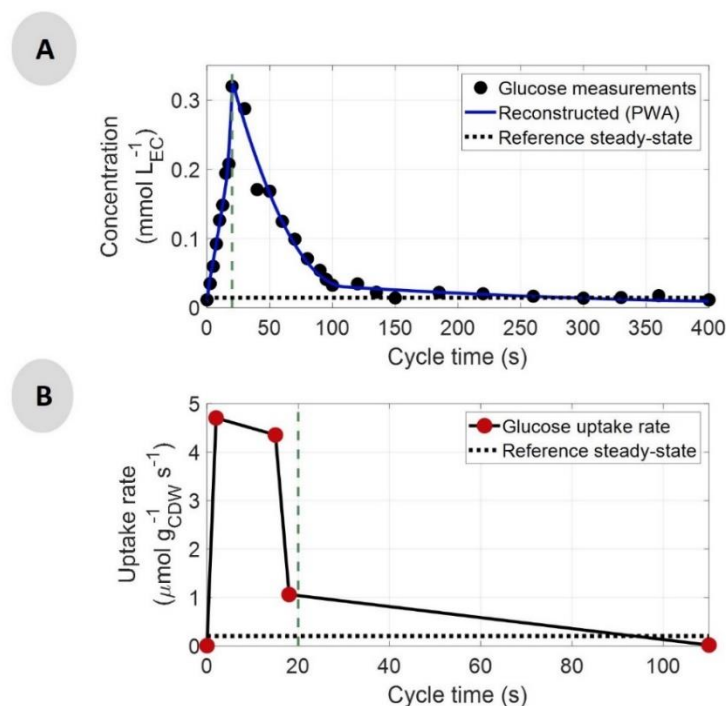


**Figure 3.3 A)** Residual glucose concentration in mM (black dots) and the PWA fitted profile (blue line) over one cycle time (s). **B)** Glucose uptake rate ( $-q_{\text{glc}}$ ) in  $\mu\text{mol}_{\text{glc}}/\text{g}_{\text{CDW}}/\text{s}$  over one cycle time (s). The red dots represent the breakpoints. Note that for the rate only the first 110 s are shown. For  $t > 110\text{s}$ , the flux was zero until the end of the cycle. Green vertical dashed lines show the end of the feeding (20 s) and the horizontal dotted lines represent the average steady-state levels.

There was no obvious correlation between the glucose uptake rate and the extracellular glucose concentration. The rate reached its highest value ( $4.68 \mu\text{mol}/\text{g}_{\text{CDW}}/\text{s}$ ) immediately after the beginning of the feeding and then decreased slightly until the end of the feeding, followed by significant decrease between 15 s and 18 s, i.e. from  $4.40$  to  $1.04 \mu\text{mol}/\text{g}_{\text{CDW}}/\text{s}$ .

This contradiction is explained by the activity of the phosphotransferase system (PTS) [66], which is the main substrate uptake system in *E.coli* under glucose excess ( $K_m$  is in the range of  $3\text{-}10 \mu\text{M}$  [48, 67]). Therefore, the glucose transport did not depend only on the extracellular concentration, but also on the intracellular concentrations of other metabolites like glucose-6-phosphate (G6P), phosphoenolpyruvate (PEP) and pyruvate, which are key components of the PTS.

The overshoot in the glucose uptake rate has been previously observed in cells exposed to excess of substrate after a starvation period, in different experimental setups [52, 60, 62]. However, the main difference of our work is that we described an adapted microorganism, which has sustained substrate perturbations for more than 8 generations, while the above-mentioned studies reported the behaviour of the cells right after applying a perturbation for the first time.

The highest estimated uptake rate in our work was significantly higher than the maximum observed during batch cultivations for the same strain (3.06 [68] and 3.30 [52]  $\mu\text{mol}/\text{g}_{\text{CDW}}/\text{s}$ ), proving that the microorganism has a higher uptake capacity than the one observed under maximum growth. It is, however, puzzling that the glucose uptake rate was decreasing already (mainly after 18 s), while glucose was still in excess (above the glucose affinity constant). An additional test experiment was performed under the same cultivation conditions, with a shorter feeding phase (13 s) but the same cycle length (400 s) and the same total amount of glucose fed over the cycle. The glucose uptake rate calculated (data not shown) exhibited the same decreasing pattern 2 seconds before the end of the feeding phase (at 11 s), while glucose was still in excess. Raw observations of this test experiment are included in Table A-2 (Appendix A.5). Therefore, it is concluded that the specific feeding time, chosen for the experimental setup of this study, was not an influencing factor of this behaviour. This decrease suggests that there was another limitation in further metabolizing glucose, which arose early in the feast phase. Another critical observation is that the uptake of glucose was decoupled from the oxygen uptake. While there was no glucose uptake after 100 s (Figure 3.3B), oxygen was still consumed (Figure 3.2E), suggesting that an intracellular compound was oxidised during the substrate famine phase. Different hypotheses for both observations will be derived (see Discussion) based on the analysis of the intracellular metabolite measurements (section 3.3.3).

### **3.3.3 Metabolite dynamics in the intracellular space**

The highly dynamic glucose uptake rate, discussed in the previous section, was expected to result in significant fluctuations in the intracellular metabolite levels. Therefore, it is important to observe how *E.coli* is regulating its metabolic network to handle the increased fluxes under these rapidly changing conditions, without detrimental effects on its survival. For this aim, a broad range of intracellular metabolites were quantified during the reference chemostat regime and the feast-famine cycle regime, including glycolysis, tricarboxylic acid (TCA) cycle, pentose phosphate pathway (PPP) intermediates and amino acids. These measurements originated from one experiment, but metabolites were sampled densely in time, over several cycles. The clear trends of the measurements showed high technical reproducibility (i.e. sampling and analysis).

#### ***Glycolysis and Pentose Phosphate Pathway***

The intracellular flux profiles over time were estimated by (dynamic) Flux Balance Analysis (FBA) for the glycolytic and pentose phosphate reaction steps. The stoichiometric network included reactions of central carbon metabolism, where the intermediates could be measured (otherwise lumped, see Appendix A.7 for details). The glucose uptake rate, derived previously, was used as input for the PTS flux. For the steady-state flux determination it was assumed

that 70% of the PTS flux was directed towards glycolysis, while the rest was directed towards the pentose phosphate pathway; this ratio is a recurring value reported in literature [59, 69-71]. For the dynamic flux determination during the feast-famine cycles, instead of setting the PTS flux split ratio, we used the minimization of the squared difference between the dynamic and the steady-state phosphoglucoisomerase (PGI) and PPP fluxes as the optimization target (i.e. minimization of metabolic adjustment – MOMA) [72]. It has been suggested that mutant *E.coli* strains redistribute their metabolic fluxes in such way to minimally divert from the wild-type metabolic network [72-74]. Our work is a comparable case, where the perturbation of the cells was not genetic, but kinetic, as a result of an intermittent substrate feeding. It was, therefore, assumed for our analysis that the optimal flux distribution after the perturbation required the smallest change from the steady-state metabolism, the same way the genetic engineered strains adapt with respect to the wild-type.

The simple network used in FBA is shown in Figure 3.4, along with the measured metabolite concentrations and the estimated fluxes over time. MOMA was performed in Matlab R2018a, The MathWorks, Inc., using quadratic programming. The derived fluxes in the chosen breakpoints can be found in Appendix A.8.

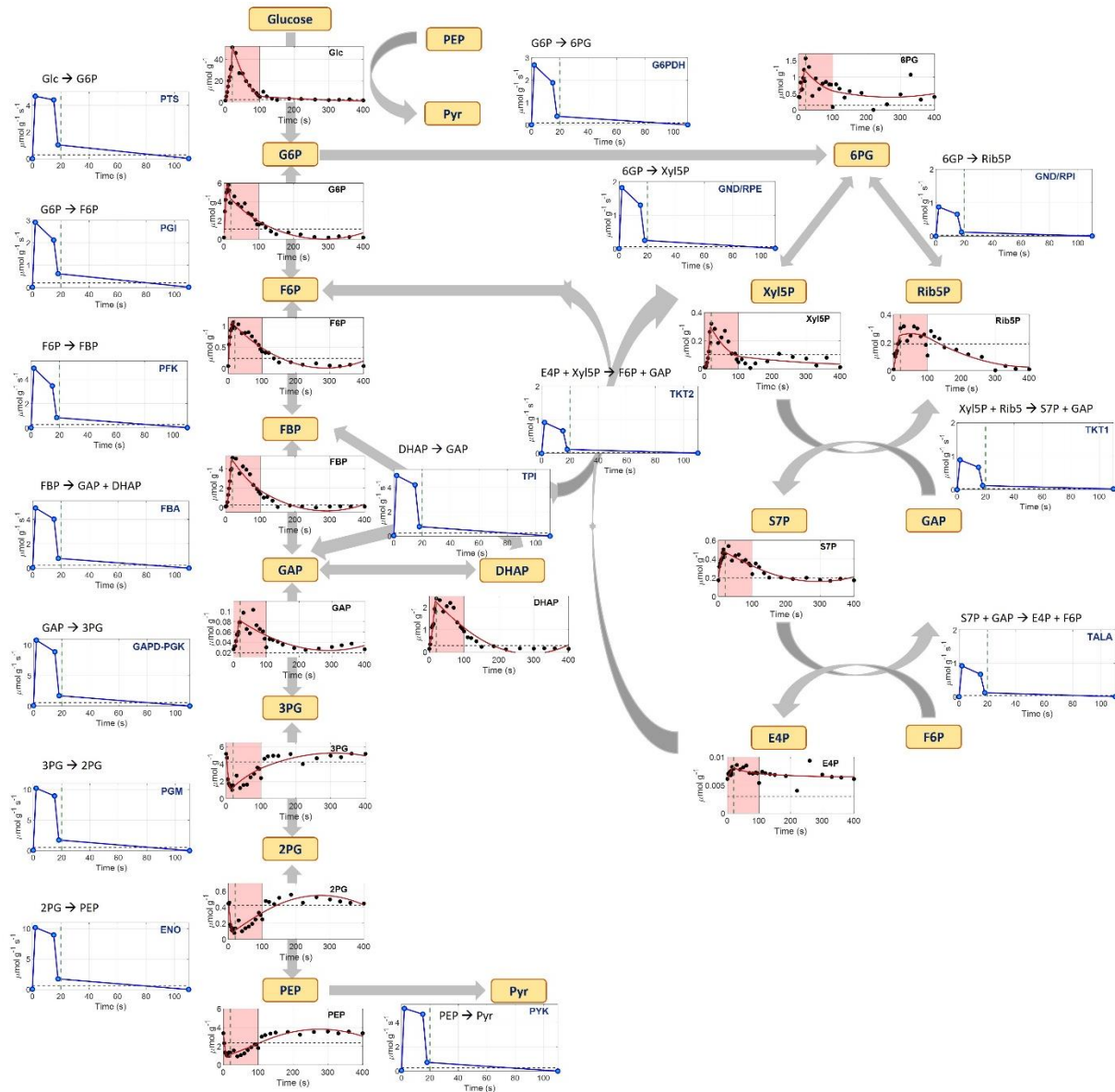


**Figure 3.4** Network model used for the flux balance analysis. Metabolite names are shown in yellow text boxes. Under each metabolite, its intracellular concentration ( $\mu\text{mol/g}_{\text{CDW}}$ ) (extracellular only for glucose) over time (s) is shown. Black dots represent the measurements, the red line is the PWA fitted line and black dashed lines represent the average steady-state levels. Green vertical dashed lines show the end of the feeding (20 s). The pink area represents the substrate feast phase. The blue line plots show the FBA estimated flux profiles in  $\mu\text{mol}_{\text{reaction\_substrate}}/\text{g}_{\text{CDW}}/\text{s}$ , where the blue dots are the values at the breakpoints. Fluxes are shown up to 110 seconds and they were all zero afterwards until the end of the cycle.

Looking at the dynamics in terms of concentration profiles, we observed that the microorganism transported the glucose from the extracellular to the intracellular space, causing all the upper glycolytic metabolites to increase during the first 20 s, in agreement with the extracellular glucose decrease. After fast filling of the pools, depletion also followed the extracellular concentration profile, i.e. very low concentration levels were observed during the famine phase ( $>100$  s). The measured concentrations were significantly higher than the steady-state levels (e.g. up to 20 fold change for FBP), due to the short-term overshoot of

carbon flux. The opposite trend was observed for the lower glycolytic metabolites (3PG, 2PG, PEP), whose concentration immediately decreased in the first seconds of the feast phase (3-6 fold change from steady-state). The reason behind this drop is based on the PTS system. In order to import and phosphorylate glucose to G6P, PEP needs to be produced and then converted to pyruvate. Unfortunately, pyruvate could not be quantified in this experiment. PEP concentration showed negative correlation with G6P, as it reached its lower concentration after 12.5 s, the same time the maximum concentration of G6P was reached. This behaviour has been observed before in *E.coli* responses to glucose pulses [50, 75-77]. Even in lower concentrations PEP was always available, during the whole cycle, for the import of glucose, therefore no limitation in the glucose transport system of *E.coli* was observed.

The metabolites of pentose phosphate pathway related well to the dynamics observed in glycolysis, as they exhibited the same behaviour of rapid accumulation in the beginning of the feast phase and later decrease to the initial levels. The pool of 6PG responded directly to the changes occurring in its precursor, G6P, reaching its maximum concentration at 20 s (7.5 s delay compared to G6P). This peak was observed slightly later in the rest of the metabolites, with the exception of Xyl5P, which responded equally fast.

Looking at the flux profiles, we observed that the glucose uptake rate dynamics propagated through glycolysis. The peak observed in the PTS flux right at the beginning of the feeding, also occurred in the succeeding reactions towards the formation of PEP and they all decreased significantly after 15 s. After 110 s all metabolite pools remained constant, while there was no more flux running in glycolysis. The same trend was also observed in all the reaction steps of the pentose phosphate pathway.

Compared to the steady-state levels, the immediate increase of the PTS flux (16 fold) led to a higher change in all the glycolytic fluxes (18-19 fold) and an even higher increase in the flux towards PPP (30 fold). This observation, together with the fact that 62.4% of the PTS flux was directed into glycolysis (less than the 70% assumed in steady-state), gives an indication that the cells may increase the flux to pentose phosphate pathway, under these dynamic conditions, therefore enhancing the production of NADPH, assumingly for redox balance purposes. Similar increase was observed after a single-pulse of glucose in an aerobic *E.coli* culture, which was used to further support the calculated increase in growth rate during the feast phase [52]. NADPH was, therefore, needed to support the increased growth. This behaviour has, also, been observed as a response to oxidative stress for *E.coli* [78, 79] and other organisms [80, 81].

### TCA Cycle

In the case of the TCA cycle, only a few metabolites could be precisely quantified, which are shown in Figure 3.5.

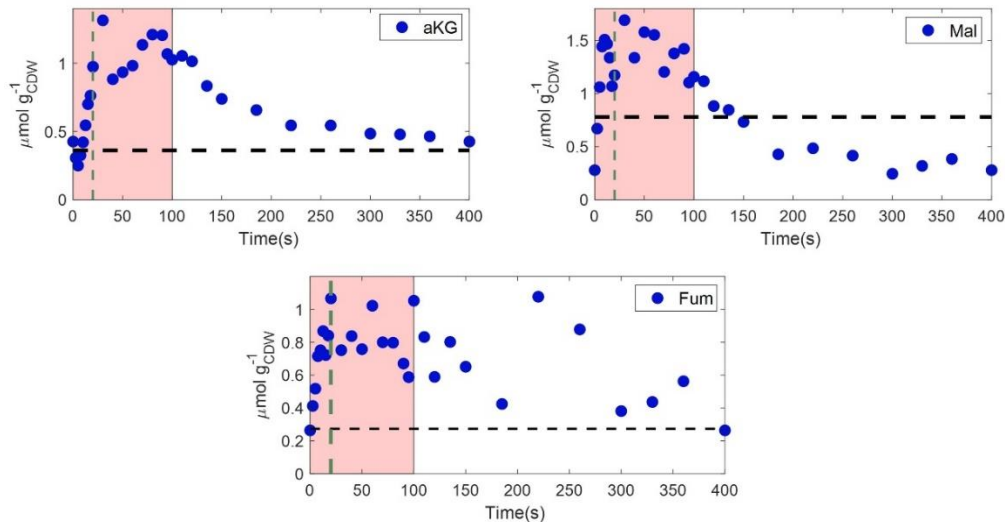


**Figure 3.5** Intracellular concentrations ( $\mu\text{mol}/\text{g}_{\text{CDW}}$ ) of TCA metabolites (a-ketoglutarate, malate and fumarate), over a feast-famine cycle (s). Black horizontal dashed lines represent the average steady-state levels. Green vertical dashed lines show the end of the feeding (20 s). The pink area represents the substrate feast phase.

Following glycolysis, also the TCA metabolites showed a dynamic profile over time. We observed that aKG and malate reached their highest concentration 30 s after the beginning of the feast-famine cycle (Figure 3.5), displaying a delay of 10 s compared to the glucose profile (Figure 3.3). This delay was also evident during the famine phase, as the metabolite levels reached low levels much later than the glycolytic ones (>100 s). Fumarate showed a more oscillating profile over time, but a general increase of the pool during the feast phase and a following decrease, to the initial levels at the end of the cycle, was detected. The highest concentration change during the cycle was observed for malate (6.1 fold), which was still lower than the dynamics of the upper glycolytic metabolites, such as G6P (31.7 fold) and F6P (18.8 fold).

### Amino acids

Amino acids are relevant precursors for protein synthesis. At the same time, several amino acids are closely connected with their respective central carbon metabolism precursor. For example alanine is only one (equilibrium) reaction step from pyruvate. Thus, on the one hand one could expect homeostasis to ensure balanced growth, on the other hand a high dependency on central carbon metabolism (Appendix A.9). Amino acids derived from E4P (Figure A-3, Appendix A.9) displayed a similar dynamic profile with their precursor, with delays in reaching their highest values. The same trend was observed for the amino acids derived

from aKG (Figure A-7, Appendix A.9) and the ones from pyruvate (Figure A-6, Appendix A.9). They all increased and decreased over time related to the concentration of their precursors, with some exhibiting more pronounced and faster dynamics (e.g. glutamine, alanine, leucine) than others (e.g. lysine, proline). On the other hand, serine, tryptophan and glycine were not significantly affected by the profile of their precursor, 3PG, as they displayed small changes over time, remaining close to their steady-state values (Figure A-4, Appendix A.9). The amino acids, derived from oxaloacetate, also, displayed various trends, either rapidly increasing (e.g. threonine) or decreasing (e.g. aspartate, cysteine) during the feast phase (Figure A-5, Appendix A.9).

The largest deviation of concentrations from the steady-state ranged from 1 to 3 fold times for most of the amino acids, more modest than the changes in their precursors. Cysteine was the only exception, as its concentration was measured to be 200 fold higher than the steady-state, in the beginning of the feast-famine regime (Figure A-5, Appendix A.9). Interestingly, while all amino acid concentrations decreased at the end of the cycle towards biomass synthesis, some even reaching their low steady-state levels, the opposite trend was observed for aspartate. Aspartate decreased rapidly during the feast phase and then increased during the famine phase, reaching a concentration of around  $6 \mu\text{mol}/\text{g}_{\text{CDW}}$ , while its steady-state concentration was  $2.6 \mu\text{mol}/\text{g}_{\text{CDW}}$  (Figure A-5, Appendix A.9).

### Nucleotides and Energy Homeostasis

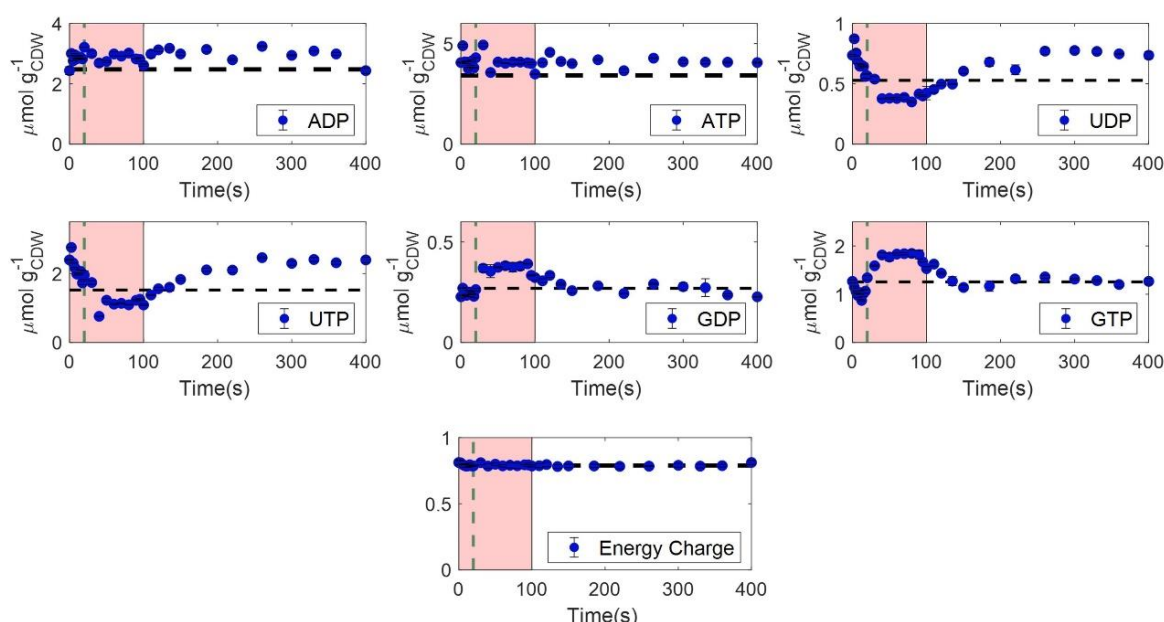


**Figure 3.6** Intracellular concentrations ( $\mu\text{mol}/\text{g}_{\text{CDW}}$ ) of nucleotides, as well as the adenylate energy charge (AEC), over a feast-famine cycle (s). Black horizontal dashed lines represent the average steady-state levels. Green vertical dashed lines show the end of the feeding (20 s). The pink area represents the substrate feast phase.

Nucleotide responses to the feast-famine regime are of high interest and especially the ATP/ADP levels, which reflect the adenylate energy state ( $AEC = \frac{ATP + \frac{1}{2}ADP}{ATP + ADP + AMP}$  [82]) of a cell and can provide insights on how the cells encounter the dynamic perturbations energetically. As expected, but still surprising, the AEC of the cell showed stability throughout the cycle (average value of 0.79), indicating that the total rate of ATP production is equal to the one of ATP consumption. The average AxP (sum of ATP and ADP) concentration was in the range of 6.99  $\mu\text{mol/g}_{\text{CDW}}$ , while the energy turnover is expected in the range of 0.4 to 1 second, using a normal P/O ratio (2.98) for *E.coli* [59]. Therefore, such balancing occurred in sub-seconds. Under glucose-limited and batch growth conditions the AEC, in most microorganisms, ranges between 0.7-0.95 [83-86]. AMP concentration was at noise level and therefore not quantified. Its contribution on the AEC calculations was neglected.

Our findings are in agreement with results from single pulse experiments [50, 52, 87], as well as two-compartment scale-down cultivations [34], in *E.coli* K12, where the energy homeostasis was also reported during glucose excess (AEC ranging from 0.8 to 0.85 in the different studies). However, in these studies, the AEC was decreasing during the famine phase, sometimes reaching values even lower than 0.7 [34], which was not the case in our experiment. Link H, *et al.* [88] also observed that the AEC remained unaffected, ranging between 0.7-0.8, after transferring fed-batch grown cells to batch reactors.

In contrast to AxP's, UDP and UTP were not homeostatic. They decreased over the feast phase and increased during the famine phase. Also, GDP and GTP were dynamic with a trend opposite to UxP's (Figure 3.6).

### **Total Metabolome**

From the extracellular observations, it was observed that the carbon uptake and excretion were significantly shifted. While the substrate carbon was consumed only during the first 100 s, excretion in the form of CO<sub>2</sub> was observed over the whole cycle (400 s). The specific glucose uptake rate was higher than at the reference steady-state and there was no significant accumulation of by-products. This suggests high intracellular accumulation of carbon during the feast phase and degradation during the (extracellular) famine phase.

The total amount of intracellular carbon during steady-state and feast-famine was calculated from the measured metabolites at every timepoint and is shown in Figure 3.7.



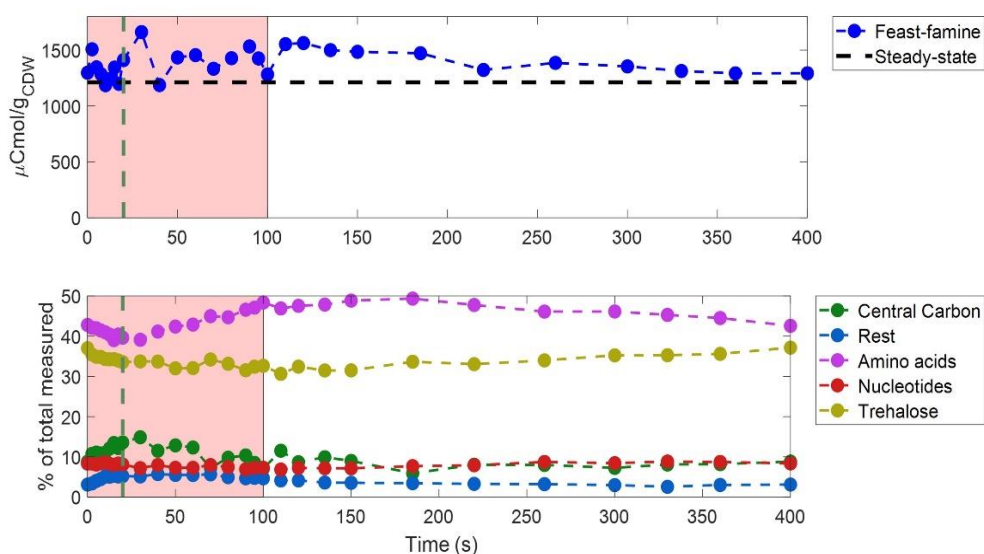


**Figure 3.7 Top:** Total amount of intracellular metabolites measured (in  $\mu\text{Cmol/g}_{\text{CDW}}$ ) over a feast-famine cycle (s). The black horizontal dashed line represents the average steady-state levels. **Bottom:** The carbon distribution (% of the total intracellular metabolome measured) in metabolites of different categories/pathways, over a feast-famine cycle (s). Green vertical dashed lines show the end of the feeding (20 s). The pink area represents the substrate feast phase. The detailed list of metabolites for each category can be found in Appendix A.10.

The total amount of metabolites was changing over time, during the feast-famine regime. We observed a small decrease in the total metabolome during the first 10 seconds of the cycle, followed by an increase until the highest point (1661  $\mu\text{Cmol/g}_{\text{CDW}}$ ), at 30 s (Figure 3.7-top). After this point, the concentrations remained constant (around 1420  $\mu\text{Cmol/g}_{\text{CDW}}$ ) until approximately 120 s. Then a constant decrease, until reaching the initial level, was observed. Significantly, the total amount of carbon in the measured metabolome was, at all timepoints, higher than the steady-state levels, resulting from the overshoot in the glucose uptake.

But which metabolites accounted for the highest changes? In Figure 3.7 (bottom) metabolites have been divided in different categories, based on their pathways, and the carbon percentage of the total metabolome that they represented was plotted over time. Amino acids were found to contain most of the total carbon during the whole cycle, ranging from 39 to 49%, with glutamate contributing the most to this observation, being the most abundant pool measured. Trehalose was also a significant pool, accounting for approximately 34% of the total carbon, remaining however, constant over time. In the first 20 s of the feast-famine regime, the carbon percentage of central carbon intermediates (glycolysis, PPP and TCA) was increasing, in addition to the metabolites M6P, T6P, UDP-glucose, M1P and G1P (representing the rest in Figure 3.7-bottom). Besides increasing metabolites in central carbon metabolism, there were also several metabolites with the contrary response (see metabolites of lower glycolysis – Figure 3.4). Because of this, the change in the central carbon metabolites (Figure 3.7-bottom) seems less dynamic than the concentration profiles shown in Figure 3.4. The

highest change was attributed to citrate (2-6% of the total carbon measured) (Figure 3.7-bottom). After 20 s, while glucose uptake rate was already lower, the filling of the amino acid pools was evident, as their carbon percentage increased during the feast, as well as the first 100 s of the famine phase. Nucleotides remained constant over time, as discussed earlier in this section.

From the oxygen uptake profile (Figure 3.2E), we derived that 41.5% of the total oxygen consumption occurred during the first 110 s of the cycle (feast). However, oxygen was still consumed in the famine phase, with a lower rate, until approximately 250 s when it reached the initial uptake level and remained constant until the end of the cycle. Since glucose was depleted during that phase and by-product concentrations were not changing over time, the electrons consumed must have been supplied either by an intracellular storage compound or other accumulated intermediates, as is also shown from the RQ calculation (Figure 3.2G).

The most common storage polysaccharides in *E.coli* are trehalose [89] and glycogen [90]. As discussed above, trehalose was a big intracellular pool, but did not change over time and was therefore ruled out as a buffer compound. Glycogen is the most well-known storage polysaccharide in *E.coli*. When the substrate is in excess, some of the glycolytic flux is diverted in the production of glycogen by G1P. The cells can then use this storage to grow under substrate limitation [91]. An attempt to quantify intracellular glycogen was performed, leading only to the conclusion that glycogen levels were increased during feast-famine, compared to steady-state. However, the measurements were not accurate enough to conclude if there was production and consumption during the dynamic cycle and therefore data are not shown.

Looking at the rest of the intracellular intermediates, the total accumulation, in terms of carbon, during the feast phase was calculated to be 256  $\mu\text{Cmol/g}_{\text{CDW}}$ , which is 1.6  $\text{mCmol/L}_{\text{EC}}$  (Figure 3.7-top). This amount represented 34% of the total glucose (4.7  $\text{mCmol/L}_{\text{EC}}$ ) consumed by the cells in the first 100 s of the feast-famine cycle. In terms of electrons, this accumulation in the feast phase was 6.4  $\text{mEmol/L}_{\text{EC}}$ . If all the electrons were used during the famine phase, the maximum oxygen consumption observed would be 1.6  $\text{mmol}_{\text{O}_2/\text{L}_{\text{EC}}}$ . In fact, we estimated, from the calculated  $q_{\text{O}_2}$ , that indeed around 1.6  $\text{mmol}_{\text{O}_2/\text{L}_{\text{EC}}}$  were consumed during the famine phase. Therefore, all of the accumulated intracellular metabolites could have been used as electron donors and could explain the  $\text{O}_2$  uptake, while the substrate was depleted. Taymaz-Nikerel H, *et al.* [52] reached to similar conclusions. In their case, 50% of the intracellular metabolites were catabolised in the famine phase, after a single glucose pulse, with glutamate being the most abundant pool.

### 3.4 Discussion

*E.coli* cultured under dynamic substrate conditions exhibited a different physiology compared to conditions supplying the same amount of substrate steadily. Namely, the average biomass specific consumption (glucose, O<sub>2</sub>) and production rates (CO<sub>2</sub>) increased under the feast-famine regime, compared to the steady-state, while by-product synthesis remained unaffected. Consequently, biomass formation was adversely disturbed with 30% decrease in yield.

These observations suggest that during the intermittent feeding, more glucose was used for respiration than biomass production. This would mean that either the excess of ATP produced was used in other cellular processes or the activity of the proton translocating ATPase showed a reduced efficiency, leading to a decrease of ATP synthesis. If the energy-spilling scenario is correct, it would imply an increase in maintenance or the presence of futile cycles.

Alternatively, this change in physiology could be attributed to an increase in competitiveness. Fast consumption of the substrate generates an advantage compared to slow competitors, as an increasing share of the substrate will go to the faster consuming cells [92].

#### ***Maintenance***

Maintenance is defined as the energy-consuming processes “for functions other than production of new cell material” [93]. In *E.coli*, the most important maintenance processes described in literature, are protein turnover (synthesis and degradation), switches in metabolic pathways, proteome and RNA repair and cell motility [92, 94-96]. Any of these parameters can, therefore, provide an explanation of the decrease in biomass yield. Protein turnover rate is an important characteristic of the cell. Energetically, a majority of ATP is used for protein synthesis and degradation. It is well-known that the cell uses its proteasome to degrade misfolded proteins or proteins with other abnormalities. Therefore, the change from a steady-state to a dynamic environment may have resulted in accumulation of proteins which have to be rapidly eliminated by the cell [97]. The ATP demands for protein turnover could have thus increased, causing the loss in biomass yield. The cost of protein degradation by the proteasome has been estimated to be minimum two ATP molecules per peptide bond [98, 99]. Protein turnover rates can be quantified with dynamic <sup>13</sup>C labelling of the amino acids pools and proteasome activity essays [100, 101], which were not performed in this study.

#### ***Futile cycles***

Futile cycles may also explain the ATP-spilling during the feast-famine regime. Some potential futile cycles, already described in literature, are:

- 1) The reconversion of oxaloacetate to phosphoenolpyruvate by the gluconeogenic PEP carboxykinase [102]. This ATP-dissipating futile cycle has been identified for low dilution rates in glucose-limited chemostats of a pyruvate kinase deficient *E.coli* strain [103], as well as, for the wild-type under very low glucose availability [104]. The induction of this futile cycle showed stimulation of glucose and oxygen uptake rates, decrease of growth yield on glucose and increase of fermentation products [105]. Yang C, *et al.* [106] demonstrated that ATP dissipation, by the PEP carboxykinase futile cycle, increased with the decrease of the growth rate, reaching 8.2% of the total ATP produced, at a dilution rate of 0.01 h<sup>-1</sup>.
- 2) The reconversion of fructose-1,6-biphosphate to fructose-6-phosphate by fructose 1,6-bisphosphatase. Usually this futile cycle is tightly regulated by the cells and is therefore minimal under both glycolytic and gluconeogenic conditions [107, 108].
- 3) The reconversion of pyruvate to phosphoenolpyruvate by phosphoenolpyruvate synthase, with the involvement of Enzyme I of the PTS [109, 110]. 10% of PEP was found to be produced by pyruvate during growth of *E.coli* wild-type on glucose [109].
- 4) The reconversion of acetate to acetyl-coA by acetyl-coA synthetase [111]. Valgepea K, *et al.* [112] claimed that bacteria may use this futile cycle under low nutrient availability, for chemotaxis, fighting other organisms, biofilm formation and other functions.
- 5) Glycogen formation and re-consumption. The formation of glycogen, by glycogen synthetase, requires one ATP per glucose, while its consumption does not form any ATP [92, 113].

All of the above-mentioned futile cycles could be active in *E.coli* during the feast-famine conditions. It is well possible that the cells up-regulate the enzymes of these futile cycles, in order to rapidly switch the direction of the fluxes, when shifting from feast to famine conditions. The reasons behind this metabolic strategy can be the rapid re-initiation of growth and the tight regulation of the ATP levels in the cell. We indeed observed a constant energy cellular status over the intermittent regime, which enhances the hypothesis of this role of futile cycles. However, the identification and interpretation of these energy-spilling reactions, under alternating feast-famine conditions, has not been studied in literature. Measurements of the enzyme expression and <sup>13</sup>C flux determination will be needed to confirm our hypotheses. In addition, knocking out some of the enzymes causing these futile cycles and growing the engineered strains under the same conditions would be a strategy to verify if they are key elements of the ATP homeostasis.

**Proton translocation**

If the less effective proton-translocation ATP synthase scenario is correct (reduced P/O ratio), that would mean that the cells would need to compensate for more ATP by (1) substrate-level phosphorylation and/or (2) increased respiration. Since the glucose uptake was higher under the feast-famine conditions, compared to the reference steady-state, more redox equivalents were produced over time, developing the need for higher respiration rates, which was also verified by our experimental data. In this case respiration is not totally coupled to ATP synthesis, as has been observed before [114]. Noda S, *et al.* [115] and Jensen PR, *et al.* [116] observed significantly decreased growth yield and increased specific rates of both glucose and oxygen consumption in different mutant *E.coli* strains, lacking F<sub>1</sub>-ATPase, under steady-state and batch growth, which shows how the microorganism behaves when oxidative phosphorylation is impaired. Koebmann BJ, *et al.* [117] also demonstrated similar results by manipulating the expression of the F1 subunits from the H<sup>+</sup>-ATP synthase, enhancing uncoupled ATP hydrolysis in *E.coli*.

However, it is still surprising that, in our experimental work, the rise in substrate-level phosphorylation did not lead to an increase in acetate formation, contrary to all the above mentioned studies. Yet, the reason behind the potential less efficient function of ATP synthase is, however, unknown. A hypothesis could be the need of the cells to translocate more protons outside of the cytosol, compared to the amount imported, in order to maintain the intracellular pH homeostasis. Due to the high metabolic rates, many acidic compounds were produced, acidifying the cytoplasmic space. Therefore, decreasing the expression of ATP synthase that brings protons into the cell, can be an advantageous strategy for the intracellular pH to remain constant and close to neutral values. This strategy has been observed for growth under highly acidic environments [118, 119]. However, the decrease in ATP synthase efficiency has not been studied for feast-famine conditions in literature, therefore a proteome study on this complex would be necessary to support this hypothesis. Another approach would be to identify the P/O ratio during steady-state and feast-famine by cultivating the cells under different substrates and growth rates as in [120-122]. More methods have also been used in literature, such as ADP pulses combined with oxygen electrode measurements (for review see [123]).

**Short-term uptake dynamics**

Based on high time resolution, extracellular glucose concentration measurements and PWA rate approximations, the glucose uptake rate was calculated over cycle time and showed an immediate increase after the feeding was switched on. This rate reached a maximum value, higher than batch maximum rates, and decreased before the concentration decreased. The fact that glucose was still in excess, but the uptake rate could not follow up, indicates the

existence of an intracellular metabolic limitation. From our intracellular metabolic analysis, we showed that there was enough PEP during the whole cycle to drive glucose transport in the cell through the PTS, therefore, the import of substrate was not the limiting step. One hypothesis which could explain the switch in the uptake rate is the phenomenon of macromolecular crowding. Macromolecular crowding is occurring in all living organisms, as a large part of the volume of the cell is occupied by high concentrations of macromolecules, such as proteins. Thus, there is limited intracellular volume available for other molecules. This volume exclusion affects various enzymatic reactions, either by increasing or decreasing their rates, depending on the change in size of the reactants [124-127]. While it has been shown that macromolecular crowding demonstrates mostly advantageous effects on cell metabolism [124, 127-129], it can also function as a constraint for cells which exhibit high metabolic rates [130]. Beg QK, *et al.* [131] developed a flux balance model of *E.coli* (FBAwMC), including a constraint for the enzyme concentrations, considering the macromolecular crowding. With this model they predicted the maximum growth both in single-substrate, but also in mixed substrate media, accurately representing experimental observations, showing that the growth rate was influenced by the solvent availability in the cytoplasm. In a following study, Vazquez A, *et al.* [132] applied the same modelling framework to changes from low to high growth rates. Their results demonstrated, among others, that under high metabolic rates the limitation in substrate uptake and growth rate is highly related to the crowding of the intracellular space. Therefore, the high metabolic rates observed in our study, during the feast-famine regime, may have caused the limitation observed in the glucose uptake rate after 18 s, as the cytosol space may have been unable to handle further increase of macromolecules produced. It was, however, challenging to identify if this source of regulation is indeed the cause for the change in the uptake rate, with the current dataset. More reasons could involve membrane integrity, as there is a minimal lipid to transporter proteins ratio [133] or enzyme kinetic constraints [130].

Furthermore, we observed the high capacity of intracellular metabolism facing the substrate gradients applied. There was a rapid response in intracellular metabolite concentrations and fluxes, which generally deviated significantly from the steady-state. The dynamics observed were less pronounced moving downstream, from glycolysis to TCA and then to amino acid synthesis, with more modest changes over time. One of our most interesting observations, was the impressive capability of the cells to maintain the adenylate energy charge homeostasis, over the whole time of the substrate perturbations. One potential mechanism, which could explain this balance between ATP production and consumption, is the production of inorganic polyphosphate, a long-chain polymer, as an energy buffer [134]. The enzyme polyphosphate kinase (Ppk) has been identified and characterized in *E.coli* [135-137]. This enzyme is responsible for the polymerization of the terminal phosphate of ATP towards

polyphosphate ( $n\text{ATP} \leftrightarrow n\text{ADP} + \text{polyP}_n$ ). It also catalyses the reversible reaction of ADP phosphorylation [138]. Many functions of polyphosphate have been described in literature, including ATP substitute, energy recycling, and environmental stress regulation [139-142]. It is therefore highly possible that the cells can balance the ATP production and consumption during the feast-famine regime, by synthesizing inorganic polyphosphate when ATP is produced in excess and consume it when the demand for ATP is increasing. Proteomics or enzymatic assays are necessary steps to prove the existence of polyphosphate kinase and the potential polyphosphate accumulation under these dynamic conditions.

In addition, during the highly dynamic conditions, applied in this study, we demonstrated the ability of the cells to store an amount of carbon and electrons intracellularly during the feast phase, which were then used when substrate was depleted, therefore, explaining oxygen consumption during the famine phase. This strategy proves to be important for the survival and robustness of *E.coli* under nutrient-limited conditions.

### ***Industrial relevance***

These observations are highly relevant in an industrial context, where *E.coli* is aerobically cultivated in large-scale bioreactors, facing long-term substrate gradients. Fed-batch regimes are often preferred, since the substrate concentration or the specific growth rate can be controlled in such a way to avoid overflow metabolism [143, 144]. Therefore fed-batch cultivations facilitate higher biomass and product yields than batch or chemostat cultivations [145]. However, with the present study, we have shown that the circulation of cells around zones of substrate excess and limitation can lead to significant biomass yield losses, decreasing the profitability of the process. In addition, the immediate response of the microorganism to the excess of substrate, observed by the increased capacity of uptake rate, also leads to higher oxygen consumption. Therefore, oxygen limitation will be observed in these zones, or more oxygen should be supplemented in the process, which is not economically favourable. Moreover, several modelling approaches, which have been used to predict the behaviour of the cells in the scale-up, assume biomass yield as the optimization target. However, yields from steady-state cannot be transferred to dynamic conditions. Additional energy is required for processes like maintaining the energy charge homeostasis. Also, if these dynamic conditions affect severely the endogenous pathways of a wild-type strain, we would expect that artificial metabolic pathways would be even more sensitive, as their regulation in an engineered strain has not evolved over various environmental conditions [146].

### 3.5 Conclusions

Studying the physiological and metabolic responses of an adapted *Escherichia coli* culture to substrate perturbations, highlights parameters to take into account for metabolic engineering and process design in relation to large-scale reactor operation.

(1) Cells responded immediately to an excess of substrate, by increasing their uptake rate and consequently the intracellular fluxes in tens of seconds. Carbon was stored in intracellular intermediates, during substrate feast and was consumed during a famine phase.

(2) Despite, the highly changing dynamics, energy charge homeostasis was observed, as a remarkable fitness characteristic of the response to perturbations, indicating rapid metabolic regulation.

(3) More important and highly relevant to industrial fermentations, was the 30% decrease of the biomass yield, occurring during the intermittent feeding, compared to a reference steady-state. Energy-spilling, was therefore, a trade-off for the adaptation of the microorganism in the dynamic environment, seeking for robust growth.

The obtained results revealed some reasons for the reduced performance of cell factories during scale-up. *E.coli* responds to stress, induced by substrate gradients, by launching a specific metabolic strategy. In order to improve productivity cost-effectively in large-scale bioprocesses, we need to further identify the mechanisms behind stress adaptation, limitations in substrate uptake and respiration, potential energy-spilling pathways and optimal growth targets of the cells, combining multi-omics approaches.



## References

1. Choi S, Song CW, Shin JH, Lee SY: **Biorefineries for the production of top building block chemicals and their derivatives.** *Metab Eng* 2015, **28**:223-239.
2. Gavrilescu M, Chisti Y: **Biotechnology-a sustainable alternative for chemical industry.** *Biotechnol Adv* 2005, **23**:471-499.
3. Lee JW, Kim HU, Choi S, Yi J, Lee SY: **Microbial production of building block chemicals and polymers.** *Curr Opin Biotechnol* 2011, **22**:758-767.
4. Straathof AJJ, Wahl SA, Benjamin KR, Takors R, Wierckx N, Noorman HJ: **Grand Research Challenges for Sustainable Industrial Biotechnology.** *Trends Biotechnol* 2019, **37**:1042-1050.
5. Humphrey A: **Shake flask to fermentor: What have we learned?** *Biotechnology Progress* 1998, **14**:3-7.
6. Schmidt FR: **Optimization and scale up of industrial fermentation processes.** *Appl Microbiol Biotechnol* 2005, **68**:425-435.
7. Junker BH: **Scale-up methodologies for Escherichia coli and yeast fermentation processes.** *Journal of Bioscience and Bioengineering* 2004, **97**:347-364.
8. Bylund F, Collet E, Enfors SO, Larsson G: **Substrate gradient formation in the large-scale bioreactor lowers cell yield and increases by-product formation.** *Bioprocess Engineering* 1998, **18**:171-180.
9. Lapin A, Schmid J, Reuss M: **Modeling the dynamics of E-coli populations in the three-dimensional turbulent field of a stirred-tank bioreactor - A structured-segregated approach.** *Chemical Engineering Science* 2006, **61**:4783-4797.
10. Takors R: **Scale-up of microbial processes: Impacts, tools and open questions.** *Journal of Biotechnology* 2012, **160**:3-9.
11. Noorman H: **An industrial perspective on bioreactor scale-down: What we can learn from combined large-scale bioprocess and model fluid studies.** *Biotechnology Journal* 2011, **6**:934-943.
12. Lara AR, Galindo E, Ramirez OT, Palomares LA: **Living with heterogeneities in bioreactors: understanding the effects of environmental gradients on cells.** *Mol Biotechnol* 2006, **34**:355-381.
13. Wehrs M, Tanjore D, Eng T, Lievens J, Pray TR, Mukhopadhyay A: **Engineering Robust Production Microbes for Large-Scale Cultivation.** *Trends Microbiol* 2019, **27**:524-537.
14. Farmer IS, Jones CW: **The energetics of Escherichia coli during aerobic growth in continuous culture.** *Eur J Biochem* 1976, **67**:115-122.
15. Postma E, Verduyn C, Scheffers WA, Van Dijken JP: **Enzymic analysis of the crabtree effect in glucose-limited chemostat cultures of Saccharomyces cerevisiae.** *Appl Environ Microbiol* 1989, **55**:468-477.
16. Valgepea K, Adamberg K, Vilu R: **Decrease of energy spilling in Escherichia coli continuous cultures with rising specific growth rate and carbon wasting.** *BMC Syst Biol* 2011, **5**:106.
17. Vemuri GN, Altman E, Sangurdekar DP, Khodursky AB, Eiteman MA: **Overflow metabolism in Escherichia coli during steady-state growth: transcriptional regulation and effect of the redox ratio.** *Appl Environ Microbiol* 2006, **72**:3653-3661.
18. Enfors SO, Jahic M, Rozkov A, Xu B, Hecker M, Jurgen B, Kruger E, Schweder T, Hamer G, O'Beirne D, et al: **Physiological responses to mixing in large scale bioreactors.** *J Biotechnol* 2001, **85**:175-185.
19. Larsson G, Tornkvist M, Wernersson ES, Tragardh C, Noorman H, Enfors SO: **Substrate gradients in bioreactors: Origin and consequences.** *Bioprocess Engineering* 1996, **14**:281-289.
20. Larsson G, Tornkvist M: **Rapid sampling, cell inactivation and evaluation of low extracellular glucose concentrations during fed-batch cultivation.** *J Biotechnol* 1996, **49**:69-82.

21. Haringa C, Tang W, Deshmukh AT, Xia J, Reuss M, Heijnen JJ, Mudde RF, Noorman HJ: **Euler-Lagrange computational fluid dynamics for (bio)reactor scale down: An analysis of organism lifelines.** *Eng Life Sci* 2016, **16**:652-663.
22. Lapin A, Muller D, Reuss M: **Dynamic behavior of microbial populations in stirred bioreactors simulated with Euler-Lagrange methods: Traveling along the lifelines of single cells.** *Industrial & Engineering Chemistry Research* 2004, **43**:4647-4656.
23. McClure DD, Kavanagh JM, Fletcher DF, Barton GW: **Characterizing bubble column bioreactor performance using computational fluid dynamics.** *Chemical Engineering Science* 2016, **144**:58-74.
24. Bylund F, Castan A, Mikkola R, Veide A, Larsson G: **Influence of scale-up on the quality of recombinant human growth hormone.** *Biotechnol Bioeng* 2000, **69**:119-128.
25. Xu B, Jahic M, Blomsten G, Enfors SO: **Glucose overflow metabolism and mixed-acid fermentation in aerobic large-scale fed-batch processes with *Escherichia coli*.** *Appl Microbiol Biotechnol* 1999, **51**:564-571.
26. Castan A, Enfors SO: **Formate accumulation due to DNA release in aerobic cultivations of *Escherichia coli*.** *Biotechnol Bioeng* 2002, **77**:324-328.
27. Savageau MA: ***Escherichia-Coli* Habitats, Cell-Types, and Molecular Mechanisms of Gene-Control.** *American Naturalist* 1983, **122**:732-744.
28. Neubauer P, Junne S: **Scale-down simulators for metabolic analysis of large-scale bioprocesses.** *Current Opinion in Biotechnology* 2010, **21**:114-121.
29. Spadiut O, Rittmann S, Dietzsch C, Herwig C: **Dynamic process conditions in bioprocess development.** *Engineering in Life Sciences* 2013, **13**:88-101.
30. Brand E, Junne S, Anane E, Cruz-Bournazou MN, Neubauer P: **Importance of the cultivation history for the response of *Escherichia coli* to oscillations in scale-down experiments.** *Bioprocess and Biosystems Engineering* 2018, **41**:1305-1313.
31. Ferenci T: **Adaptation to life at micromolar nutrient levels: the regulation of *Escherichia coli* glucose transport by endoinduction and cAMP.** *FEMS Microbiol Rev* 1996, **18**:301-317.
32. Lambert G, Kussell E: **Memory and fitness optimization of bacteria under fluctuating environments.** *PLoS Genet* 2014, **10**:e1004556.
33. Schweder T, Kruger E, Xu B, Jurgen B, Blomsten G, Enfors SO, Hecker M: **Monitoring of genes that respond to process-related stress in large-scale bioprocesses.** *Biotechnol Bioeng* 1999, **65**:151-159.
34. Loffler M, Simen JD, Jager G, Schaferhoff K, Freund A, Takors R: **Engineering *E. coli* for large-scale production - Strategies considering ATP expenses and transcriptional responses.** *Metab Eng* 2016, **38**:73-85.
35. Suarez-Mendez CA, Sousa A, Heijnen JJ, Wahl A: **Fast "Feast/Famine" Cycles for Studying Microbial Physiology Under Dynamic Conditions: A Case Study with *Saccharomyces cerevisiae*.** *Metabolites* 2014, **4**:347-372.
36. Somsen OJ, Hoeben MA, Esgalhado E, Snoep JL, Visser D, van der Heijden RT, Heijnen JJ, Westerhoff HV: **Glucose and the ATP paradox in yeast.** *Biochem J* 2000, **352 Pt 2**:593-599.
37. de Jonge L, Buijs NA, Heijnen JJ, van Gulik WM, Abate A, Wahl SA: **Flux response of glycolysis and storage metabolism during rapid feast/famine conditions in *Penicillium chrysogenum* using dynamic (<sup>13</sup>C) labeling.** *Biotechnol J* 2014, **9**:372-385.
38. Pickett AM, Bazin MJ, Topiwala HH: **Growth and Composition of *Escherichia-Coli* Subjected to Square-Wave Perturbations in Nutrient Supply - Effect of Varying Amplitudes.** *Biotechnology and Bioengineering* 1980, **22**:1213-1224.
39. Sunya S, Bideaux C, Molina-Jouve C, Gorret N: **Short-term dynamic behavior of *Escherichia coli* in response to successive glucose pulses on glucose-limited chemostat cultures.** *J Biotechnol* 2013, **164**:531-542.

40. Verduyn C, Postma E, Scheffers WA, Van Dijken JP: **Effect of benzoic acid on metabolic fluxes in yeasts: a continuous-culture study on the regulation of respiration and alcoholic fermentation.** *Yeast* 1992, **8**:501-517.
41. Taymaz-Nikerel H, de Mey M, Ras C, ten Pierick A, Seifar RM, van Dam JC, Heijnen JJ, van Gulik WM: **Development and application of a differential method for reliable metabolome analysis in Escherichia coli.** *Anal Biochem* 2009, **386**:9-19.
42. Wu L, Mashego MR, van Dam JC, Proell AM, Vinke JL, Ras C, van Winden WA, van Gulik WM, Heijnen JJ: **Quantitative analysis of the microbial metabolome by isotope dilution mass spectrometry using uniformly C-13-labeled cell extracts as internal standards.** *Analytical Biochemistry* 2005, **336**:164-171.
43. Niedenfuhr S, ten Pierick A, van Dam PT, Suarez-Mendez CA, Noh K, Wahl SA: **Natural isotope correction of MS/MS measurements for metabolomics and (13)C fluxomics.** *Biotechnol Bioeng* 2016, **113**:1137-1147.
44. Canelas AB, ten Pierick A, Ras C, Seifar RM, van Dam JC, van Gulik WM, Heijnen JJ: **Quantitative Evaluation of Intracellular Metabolite Extraction Techniques for Yeast Metabolomics.** *Analytical Chemistry* 2009, **81**:7379-7389.
45. de Jonge LP, Buijs NA, ten Pierick A, Deshmukh A, Zhao Z, Kiel JA, Heijnen JJ, van Gulik WM: **Scale-down of penicillin production in Penicillium chrysogenum.** *Biotechnol J* 2011, **6**:944-958.
46. Seifar RM, Ras C, van Dam JC, van Gulik WM, Heijnen JJ, van Winden WA: **Simultaneous quantification of free nucleotides in complex biological samples using ion pair reversed phase liquid chromatography isotope dilution tandem mass spectrometry.** *Analytical Biochemistry* 2009, **388**:213-219.
47. Mashego MR, Wu L, Van Dam JC, Ras C, Vinke JL, Van Winden WA, Van Gulik WM, Heijnen JJ: **MIRACLE: mass isotopomer ratio analysis of U-C-13-labeled extracts. A new method for accurate quantification of changes in concentrations of intracellular metabolites.** *Biotechnology and Bioengineering* 2004, **85**:620-628.
48. Stock JB, Waygood EB, Meadow ND, Postma PW, Roseman S: **Sugar transport by the bacterial phosphotransferase system. The glucose receptors of the Salmonella typhimurium phosphotransferase system.** *J Biol Chem* 1982, **257**:14543-14552.
49. Wu L, Lange HC, van Gulik WM, Heijnen JJ: **Determination of in vivo oxygen uptake and carbon dioxide evolution rates from off-gas measurements under highly dynamic conditions.** *Biotechnology and Bioengineering* 2003, **81**:448-458.
50. De Mey M, Taymaz-Nikerel H, Baart G, Waegeman H, Maertens J, Heijnen JJ, van Gulik WM: **Catching prompt metabolite dynamics in Escherichia coli with the BioScope at oxygen rich conditions.** *Metab Eng* 2010, **12**:477-487.
51. Hua Q, Yang C, Baba T, Mori H, Shimizu K: **Responses of the central metabolism in Escherichia coli to phosphoglucose isomerase and glucose-6-phosphate dehydrogenase knockouts.** *Journal of Bacteriology* 2003, **185**:7053-7067.
52. Taymaz-Nikerel H, van Gulik WM, Heijnen JJ: **Escherichia coli responds with a rapid and large change in growth rate upon a shift from glucose-limited to glucose-excess conditions.** *Metab Eng* 2011, **13**:307-318.
53. Kayser A, Weber J, Hecht V, Rinas U: **Metabolic flux analysis of Escherichia coli in glucose-limited continuous culture. I. Growth-rate-dependent metabolic efficiency at steady state.** *Microbiology* 2005, **151**:693-706.
54. Renilla S, Bernal V, Fuhrer T, Castano-Cerezo S, Pastor JM, Iborra JL, Sauer U, Canovas M: **Acetate scavenging activity in Escherichia coli: interplay of acetyl-CoA synthetase and the PEP-glyoxylate cycle in chemostat cultures.** *Applied Microbiology and Biotechnology* 2012, **93**:2109-2124.
55. Holms H: **Flux analysis and control of the central metabolic pathways in Escherichia coli.** *FEMS Microbiol Rev* 1996, **19**:85-116.

56. Luli GW, Strohl WR: **Comparison of Growth, Acetate Production, and Acetate Inhibition of Escherichia-Coli Strains in Batch and Fed-Batch Fermentations.** *Applied and Environmental Microbiology* 1990, **56**:1004-1011.
57. Xu B, Jahic M, Enfors SO: **Modeling of overflow metabolism in batch and fed-batch cultures of Escherichia coli.** *Biotechnol Prog* 1999, **15**:81-90.
58. Verheijen PJT: **Data Reconciliation and Error Detection.** *Metabolic Pathway Engineering Handbook: Fundamentals* 2010.
59. Taymaz-Nikerel H, Borujeni AE, Verheijen PJT, Heijnen JJ, van Gulik WM: **Genome-Derived Minimal Metabolic Models for Escherichia coli MG1655 With Estimated In Vivo Respiratory ATP Stoichiometry.** *Biotechnology and Bioengineering* 2010, **107**:369-381.
60. Lara AR, Taymaz-Nikerel H, Mashego MR, van Gulik WM, Heijnen JJ, Ramirez OT, van Winden WA: **Fast dynamic response of the fermentative metabolism of Escherichia coli to aerobic and anaerobic glucose pulses.** *Biotechnol Bioeng* 2009, **104**:1153-1161.
61. Sunya S, Delvigne F, Uribelarrea JL, Molina-Jouve C, Gorret N: **Comparison of the transient responses of Escherichia coli to a glucose pulse of various intensities.** *Applied Microbiology and Biotechnology* 2012, **95**:1021-1034.
62. Neubauer P, Haggstrom L, Enfors SO: **Influence of substrate oscillations on acetate formation and growth yield in Escherichia coli glucose limited fed-batch cultivations.** *Biotechnol Bioeng* 1995, **47**:139-146.
63. van Kleeff BH, Kuenen JG, Heijnen JJ: **Heat flux measurements for the fast monitoring of dynamic responses to glucose additions by yeasts that were subjected to different feeding regimes in continuous culture.** *Biotechnol Prog* 1996, **12**:510-518.
64. Vieth E: **Fitting piecewise linear regression functions to biological responses.** *J Appl Physiol (1985)* 1989, **67**:390-396.
65. Schumacher R, Wahl SA: **Effective Estimation of Dynamic Metabolic Fluxes Using (13)C Labeling and Piecewise Affine Approximation: From Theory to Practical Applicability.** *Metabolites* 2015, **5**:697-719.
66. Kundig W, Roseman S, Ghosh S: **Phosphate Bound to Histidine in Protein as Intermediate in Novel Phospho-Transferase System.** *Proceedings of the National Academy of Sciences of the United States of America* 1964, **52**:1067-&.
67. Misset O, Blaauw M, Postma PW, Robillard GT: **Bacterial phosphoenolpyruvate-dependent phosphotransferase system. Mechanism of the transmembrane sugar translocation and phosphorylation.** *Biochemistry* 1983, **22**:6163-6170.
68. Fischer E, Zamboni N, Sauer U: **High-throughput metabolic flux analysis based on gas chromatography-mass spectrometry derived 13C constraints.** *Anal Biochem* 2004, **325**:308-316.
69. Nanchen A, Schicker A, Sauer U: **Nonlinear dependency of intracellular fluxes on growth rate in miniaturized continuous cultures of Escherichia coli.** *Applied and Environmental Microbiology* 2006, **72**:1164-1172.
70. Siddiquee KA, Arauzo-Bravo MJ, Shimizu K: **Metabolic flux analysis of pykF gene knockout Escherichia coli based on C-13-labeling experiments together with measurements of enzyme activities and intracellular metabolite concentrations.** *Applied Microbiology and Biotechnology* 2004, **63**:407-417.
71. Zhao J, Shimizu K: **Metabolic flux analysis of Escherichia coli K12 grown on C-13-labeled acetate and glucose using GG-MS and powerful flux calculation method.** *Journal of Biotechnology* 2003, **101**:101-117.
72. Segre D, Vitkup D, Church GM: **Analysis of optimality in natural and perturbed metabolic networks.** *Proceedings of the National Academy of Sciences of the United States of America* 2002, **99**:15112-15117.

73. Willemsen AM, Hendrickx DM, Hoefsloot HCJ, Hendriks MMWB, Wahl SA, Teusink B, Smilde AK, van Kampen AHC: **MetDFBA: incorporating time-resolved metabolomics measurements into dynamic flux balance analysis.** *Molecular Biosystems* 2015, **11**:137-145.
74. Ren SG, Zeng B, Qian XN: **Adaptive bi-level programming for optimal gene knockouts for targeted overproduction under phenotypic constraints.** *Bmc Bioinformatics* 2013, **14**.
75. Buchholz A, Hurllebaus J, Wandrey C, Takors R: **Metabolomics: quantification of intracellular metabolite dynamics.** *Biomolecular Engineering* 2002, **19**:5-15.
76. Hoque MA, Ushiyama H, Tomita M, Shimizu K: **Dynamic responses of the intracellular metabolite concentrations of the wild type and pykA mutant Escherichia coli against pulse addition of glucose or NH<sub>3</sub> under those limiting continuous cultures.** *Biochemical Engineering Journal* 2005, **26**:38-49.
77. Schaub J, Reuss M: **In vivo dynamics of glycolysis in Escherichia coli shows need for growth-rate dependent metabolome analysis.** *Biotechnol Prog* 2008, **24**:1402-1407.
78. Christodoulou D, Link H, Fuhrer T, Kochanowski K, Gerosa L, Sauer U: **Reserve Flux Capacity in the Pentose Phosphate Pathway Enables Escherichia coli's Rapid Response to Oxidative Stress.** *Cell Syst* 2018, **6**:569-578 e567.
79. Rui B, Shen T, Zhou H, Liu J, Chen J, Pan X, Liu H, Wu J, Zheng H, Shi Y: **A systematic investigation of Escherichia coli central carbon metabolism in response to superoxide stress.** *BMC Syst Biol* 2010, **4**:122.
80. Anastasiou D, Poulogiannis G, Asara JM, Boxer MB, Jiang JK, Shen M, Bellinger G, Sasaki AT, Locasale JW, Auld DS, et al: **Inhibition of pyruvate kinase M2 by reactive oxygen species contributes to cellular antioxidant responses.** *Science* 2011, **334**:1278-1283.
81. Ralser M, Wamelink MM, Kowald A, Gerisch B, Heeren G, Struys EA, Klipp E, Jakobs C, Breitenbach M, Lehrach H, Krobitsch S: **Dynamic rerouting of the carbohydrate flux is key to counteracting oxidative stress.** *J Biol* 2007, **6**:10.
82. Atkinson DE, Walton GM: **Adenosine triphosphate conservation in metabolic regulation. Rat liver citrate cleavage enzyme.** *J Biol Chem* 1967, **242**:3239-3241.
83. Hardiman T, Lemuth K, Keller MA, Reuss M, Siemann-Herzberg M: **Topology of the global regulatory network of carbon limitation in Escherichia coli.** *J Biotechnol* 2007, **132**:359-374.
84. De la Fuente IM, Cortes JM, Valero E, Desroches M, Rodrigues S, Malaina I, Martinez L: **On the dynamics of the adenylate energy system: homeorhesis vs homeostasis.** *PLoS One* 2014, **9**:e108676.
85. Chapman AG, Fall L, Atkinson DE: **Adenylate energy charge in Escherichia coli during growth and starvation.** *J Bacteriol* 1971, **108**:1072-1086.
86. Walker-Simmons M, Atkinson DE: **Functional capacities and the adenylate energy charge in Escherichia coli under conditions of nutritional stress.** *J Bacteriol* 1977, **130**:676-683.
87. Taymaz-Nikerel H, De Mey M, Baart G, Maertens J, Heijnen JJ, van Gulik W: **Changes in substrate availability in Escherichia coli lead to rapid metabolite, flux and growth rate responses.** *Metabolic Engineering* 2013, **16**:115-129.
88. Link H, Anselment B, Weuster-Botz D: **Rapid media transition: an experimental approach for steady state analysis of metabolic pathways.** *Biotechnol Prog* 2010, **26**:1-10.
89. Ruhel R, Kataria R, Choudhury B: **Trends in bacterial trehalose metabolism and significant nodes of metabolic pathway in the direction of trehalose accumulation.** *Microbial Biotechnology* 2013, **6**:493-502.
90. Preiss J: **Bacterial Glycogen-Synthesis and Its Regulation.** *Annual Review of Microbiology* 1984, **38**:419-458.
91. Morin M, Ropers D, Cinquemani E, Portais JC, Enjalbert B, Coccagn-Bousquet M: **The Csr System Regulates Escherichia coli Fitness by Controlling Glycogen Accumulation and Energy Levels.** *MBio* 2017, **8**.
92. Russell JB, Cook GM: **Energetics of bacterial growth: balance of anabolic and catabolic reactions.** *Microbiol Rev* 1995, **59**:48-62.

93. Pirt SJ: **The maintenance energy of bacteria in growing cultures.** *Proc R Soc Lond B Biol Sci* 1965, **163**:224-231.
94. Kempes CP, van Bodegom PM, Wolpert D, Libby E, Amend J, Hoehler T: **Drivers of Bacterial Maintenance and Minimal Energy Requirements.** *Front Microbiol* 2017, **8**:31.
95. van Bodegom P: **Microbial maintenance: a critical review on its quantification.** *Microb Ecol* 2007, **53**:513-523.
96. Tempest DW, Neijssel OM: **The status of YATP and maintenance energy as biologically interpretable phenomena.** *Annu Rev Microbiol* 1984, **38**:459-486.
97. Gottesman S: **Proteases and their targets in Escherichia coli.** *Annu Rev Genet* 1996, **30**:465-506.
98. Burton RE, Siddiqui SM, Kim YI, Baker TA, Sauer RT: **Effects of protein stability and structure on substrate processing by the ClpXP unfolding and degradation machine.** *EMBO J* 2001, **20**:3092-3100.
99. Menon AS, Goldberg AL: **Binding of nucleotides to the ATP-dependent protease La from Escherichia coli.** *J Biol Chem* 1987, **262**:14921-14928.
100. Hong KK, Hou J, Shoaie S, Nielsen J, Bordel S: **Dynamic <sup>13</sup>C-labeling experiments prove important differences in protein turnover rate between two Saccharomyces cerevisiae strains.** *FEMS Yeast Res* 2012, **12**:741-747.
101. Pratt JM, Petty J, Riba-Garcia I, Robertson DH, Gaskell SJ, Oliver SG, Beynon RJ: **Dynamics of protein turnover, a missing dimension in proteomics.** *Mol Cell Proteomics* 2002, **1**:579-591.
102. Sauer U, Eikmanns BJ: **The PEP-pyruvate-oxaloacetate node as the switch point for carbon flux distribution in bacteria.** *FEMS Microbiol Rev* 2005, **29**:765-794.
103. Emmerling M, Dauner M, Ponti A, Fiaux J, Hochuli M, Szyperski T, Wuthrich K, Bailey JE, Sauer U: **Metabolic flux responses to pyruvate kinase knockout in Escherichia coli.** *J Bacteriol* 2002, **184**:152-164.
104. Sauer U, Lasko DR, Fiaux J, Hochuli M, Glaser R, Szyperski T, Wuthrich K, Bailey JE: **Metabolic flux ratio analysis of genetic and environmental modulations of Escherichia coli central carbon metabolism.** *J Bacteriol* 1999, **181**:6679-6688.
105. Chao YP, Liao JC: **Metabolic responses to substrate futile cycling in Escherichia coli.** *J Biol Chem* 1994, **269**:5122-5126.
106. Yang C, Hua Q, Baba T, Mori H, Shimizu K: **Analysis of Escherichia coli anaplerotic metabolism and its regulation mechanisms from the metabolic responses to altered dilution rates and phosphoenolpyruvate carboxykinase knockout.** *Biotechnol Bioeng* 2003, **84**:129-144.
107. Chambost J-P, Fraenkel DG: **The Use of 6-Labeled Glucose to Assess Futile Cycling in Escherichia coli.** *The Journal of Biological Chemistry* 1980, **255**:2867-2869.
108. Daldal F, Fraenkel DG: **Assessment of a futile cycle involving reconversion of fructose 6-phosphate to fructose 1,6-bisphosphate during gluconeogenic growth of Escherichia coli.** *J Bacteriol* 1983, **153**:390-394.
109. Long CP, Au J, Sandoval NR, Gebreselassie NA, Antoniewicz MR: **Enzyme I facilitates reverse flux from pyruvate to phosphoenolpyruvate in Escherichia coli.** *Nat Commun* 2017, **8**:14316.
110. Patnaik R, Roof WD, Young RF, Liao JC: **Stimulation of glucose catabolism in Escherichia coli by a potential futile cycle.** *J Bacteriol* 1992, **174**:7527-7532.
111. Irague R, Massou S, Moulis C, Saurel O, Milon A, Monsan P, Remaud-Simeon M, Portais JC, Potocki-Veronese G: **NMR-based structural glycomics for high-throughput screening of carbohydrate-active enzyme specificity.** *Anal Chem* 2011, **83**:1202-1206.
112. Valgepea K, Adamberg K, Nahku R, Lahtvee PJ, Arike L, Vilu R: **Systems biology approach reveals that overflow metabolism of acetate in Escherichia coli is triggered by carbon catabolite repression of acetyl-CoA synthetase.** *BMC Syst Biol* 2010, **4**:166.
113. Portais JC, Delort AM: **Carbohydrate cycling in micro-organisms: what can (<sup>13</sup>)C-NMR tell us?** *FEMS Microbiol Rev* 2002, **26**:375-402.

114. Bekker M, de Vries S, Ter Beek A, Hellingwerf KJ, de Mattos MJT: **Respiration of Escherichia coli Can Be Fully Uncoupled via the Nonelectrogenic Terminal Cytochrome bd-II Oxidase.** *Journal of Bacteriology* 2009, **191**:5510-5517.
115. Noda S, Takezawa Y, Mizutani T, Asakura T, Nishiumi E, Onoe K, Wada M, Tomita F, Matsushita K, Yokota A: **Alterations of cellular physiology in Escherichia coli in response to oxidative phosphorylation impaired by defective F-1-ATPase.** *Journal of Bacteriology* 2006, **188**:6869-6876.
116. Jensen PR, Michelsen O: **Carbon and energy metabolism of atp mutants of Escherichia coli.** *J Bacteriol* 1992, **174**:7635-7641.
117. Koebmann BJ, Westerhoff HV, Snoep JL, Nilsson D, Jensen PR: **The glycolytic flux in Escherichia coli is controlled by the demand for ATP.** *J Bacteriol* 2002, **184**:3909-3916.
118. Slonczewski JL, Fujisawa M, Dopson M, Krulwich TA: **Cytoplasmic pH measurement and homeostasis in bacteria and archaea.** *Adv Microb Physiol* 2009, **55**:1-79, 317.
119. Lund P, Tramonti A, De Biase D: **Coping with low pH: molecular strategies in neutralophilic bacteria.** *FEMS Microbiol Rev* 2014, **38**:1091-1125.
120. vanGulik WM, Antoniewicz MR, deLaat WT, Vinke JL, Heijnen JJ: **Energetics of growth and penicillin production in a high-producing strain of Penicillium chrysogenum.** *Biotechnol Bioeng* 2001, **72**:185-193.
121. van Gulik WM, Heijnen JJ: **A metabolic network stoichiometry analysis of microbial growth and product formation.** *Biotechnol Bioeng* 1995, **48**:681-698.
122. Vanrolleghem PA, de Jong-Gubbels P, van Gulik WM, Pronk JT, van Dijken JP, Heijnen S: **Validation of a metabolic network for Saccharomyces cerevisiae using mixed substrate studies.** *Biotechnol Prog* 1996, **12**:434-448.
123. Hinkle PC: **P/O ratios of mitochondrial oxidative phosphorylation.** *Biochim Biophys Acta* 2005, **1706**:1-11.
124. Ellis RJ: **Macromolecular crowding: obvious but underappreciated.** *Trends Biochem Sci* 2001, **26**:597-604.
125. Minton AP, Colclasure GC, Parker JC: **Model for the role of macromolecular crowding in regulation of cellular volume.** *Proc Natl Acad Sci U S A* 1992, **89**:10504-10506.
126. Minton AP: **The influence of macromolecular crowding and macromolecular confinement on biochemical reactions in physiological media.** *J Biol Chem* 2001, **276**:10577-10580.
127. Chung S, Lerner E, Jin Y, Kim S, Alhadid Y, Grimaud LW, Zhang IX, Knobler CM, Gelbart WM, Weiss S: **The effect of macromolecular crowding on single-round transcription by Escherichia coli RNA polymerase.** *Nucleic Acids Res* 2019, **47**:1440-1450.
128. Golkaram M, Hellander S, Drawert B, Petzold LR: **Macromolecular Crowding Regulates the Gene Expression Profile by Limiting Diffusion.** *PLoS Comput Biol* 2016, **12**:e1005122.
129. Al-Habori M: **Macromolecular crowding and its role as intracellular signalling of cell volume regulation.** *Int J Biochem Cell Biol* 2001, **33**:844-864.
130. Goel A, Wortel MT, Molenaar D, Teusink B: **Metabolic shifts: a fitness perspective for microbial cell factories.** *Biotechnol Lett* 2012, **34**:2147-2160.
131. Beg QK, Vazquez A, Ernst J, de Menezes MA, Bar-Joseph Z, Barabasi AL, Oltvai ZN: **Intracellular crowding defines the mode and sequence of substrate uptake by Escherichia coli and constrains its metabolic activity.** *Proceedings of the National Academy of Sciences of the United States of America* 2007, **104**:12663-12668.
132. Vazquez A, Beg QK, Demenezes MA, Ernst J, Bar-Joseph Z, Barabasi AL, Boros LG, Oltvai ZN: **Impact of the solvent capacity constraint on E. coli metabolism.** *BMC Syst Biol* 2008, **2**:7.
133. Molenaar D, van Berlo R, de Ridder D, Teusink B: **Shifts in growth strategies reflect tradeoffs in cellular economics.** *Mol Syst Biol* 2009, **5**:323.
134. Murata K, Uchida T, Kato J, Chibata I: **Polyphosphate Kinase - Distribution, Some Properties and Its Application as an Atp Regeneration System.** *Agricultural and Biological Chemistry* 1988, **52**:1471-1477.

135. Akiyama M, Crooke E, Kornberg A: **The polyphosphate kinase gene of *Escherichia coli*. Isolation and sequence of the *ppk* gene and membrane location of the protein.** *J Biol Chem* 1992, **267**:22556-22561.
136. Zhu Y, Huang WJ, Lee SSK, Xu WQ: **Crystal structure of a polyphosphate kinase and its implications for polyphosphate synthesis.** *Embo Reports* 2005, **6**:681-687.
137. Kornberg A, Kornberg SR, Simms ES: **Metaphosphate synthesis by an enzyme from *Escherichia coli*.** *Biochim Biophys Acta* 1956, **20**:215-227.
138. Kornberg SR: **Adenosine triphosphate synthesis from polyphosphate by an enzyme from *Escherichia coli*.** *Biochim Biophys Acta* 1957, **26**:294-300.
139. Kornberg A: **Inorganic Polyphosphate - toward Making a Forgotten Polymer Unforgettable.** *Journal of Bacteriology* 1995, **177**:491-496.
140. Brown MRW, Kornberg A: **The long and short of it - polyphosphate, PPK and bacterial survival.** *Trends in Biochemical Sciences* 2008, **33**:284-290.
141. Shiba T, Tsutsumi K, Ishige K, Noguchi T: **Inorganic polyphosphate and polyphosphate kinase: Their novel biological functions and applications.** *Biochemistry-Moscow* 2000, **65**:315-323.
142. Kuroda A, Kornberg A: **Polyphosphate kinase as a nucleoside diphosphate kinase in *Escherichia coli* and *Pseudomonas aeruginosa*.** *Proceedings of the National Academy of Sciences of the United States of America* 1997, **94**:439-442.
143. Habegger L, Crespo KR, Dabros M: **Preventing Overflow Metabolism in Crabtree-Positive Microorganisms through On-Line Monitoring and Control of Fed-Batch Fermentations.** *Fermentation-Basel* 2018, **4**.
144. Henes B, Sonnleitner B: **Controlled fed-batch by tracking the maximal culture capacity.** *Journal of Biotechnology* 2007, **132**:118-126.
145. Hewitt CJ, Nienow AW: **The scale-up of microbial batch and fed-batch fermentation processes.** *Adv Appl Microbiol* 2007, **62**:105-135.
146. Deparis Q, Claes A, Foulquie-Moreno MR, Thevelein JM: **Engineering tolerance to industrially relevant stress factors in yeast cell factories.** *FEMS Yeast Res* 2017, **17**.



## Appendix A

### A.1 Repetitiveness of block-wise feeding cycles

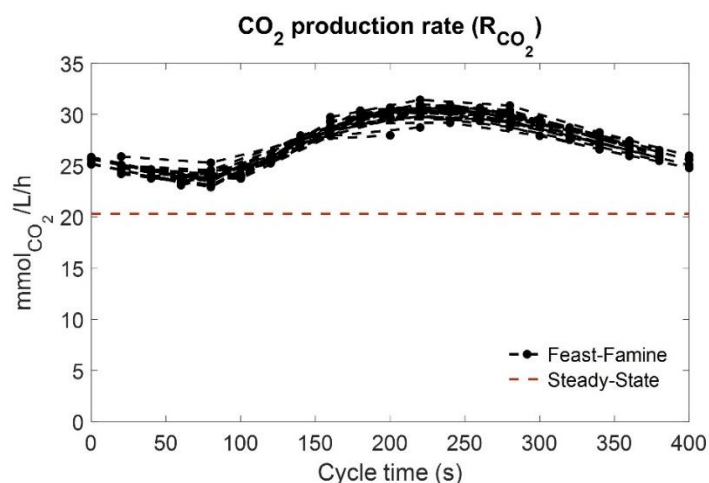


**Figure A-1** In black: Calculated  $\text{CO}_2$  production rate ( $\text{mmol}_{\text{CO}_2} \cdot \text{L}^{-1} \cdot \text{h}^{-1}$ ) based on the raw offgas  $\text{CO}_2$  data, over the feast-famine cycle time (s). Data of 30 successive cycles, after at least 8 residence times, are overlapped. These rates are not corrected for delays expected due to headspace, tubing and bicarbonate in the broth. In red:  $\text{CO}_2$  production rate (non-reconciled) during the reference steady-state.

### A.2 Dissolved oxygen

The dissolved oxygen sensor used in this work was a polarographic ADI probe (Applisens, Applikon, Delft, The Netherlands) submerged into the broth. At a polarographic electrode, oxygen is reduced to water (cathode) and the electrons produced generate current, which transmits the signal. These types of probes are known to show some response delays, as a result of many factors, such as the membrane thickness etc. [1]. Because of the short-term behaviour of our experiment (seconds), the time delay of the probe should be taken into account, in order to estimate the real respiration rates. We will describe the oxygen probe dynamics with the following first order model [2]:

$$\frac{dC_{O_2,L}}{dt} = \frac{(\widehat{C}_{O_2,L} - C_{O_2,L})}{\tau_{\text{probe}}} \quad (1)$$

where  $C_{O_2,L}$  is the dissolved oxygen measured by the sensor (%),  $\widehat{C}_{O_2,L}$  is the estimated real dissolved oxygen in the broth (%),  $t$  is the cycle time (s) and  $\tau_{\text{probe}}$  is the time (s) needed for the sensor to reach 63.7 % of the ultimate response in a step exchange experiment [3]. The  $\tau_{\text{probe}}$  of our sensor was measured to be 16.65 s. Therefore, the estimated dissolved oxygen in the broth during the feast-famine regime was calculated as follows:

$$\widehat{C}_{O_2,L} = C_{O_2,L} + \tau_{\text{probe}} \frac{dC_{O_2,L}}{dt} \quad (2)$$

### A.3 Calculation of O<sub>2</sub> uptake and CO<sub>2</sub> production rates

In order to calculate the O<sub>2</sub> uptake and CO<sub>2</sub> production rates over one cycle time, the rates were first estimated by applying the respective mass balances over time.

The offgas in our system consisted of oxygen, carbon dioxide and nitrogen. Nitrogen gas was not produced or consumed during the cultivation. Therefore the sum of fractions of gases entering and exiting the reactor was 1:

$$y_{N_2,G,in} + y_{O_2,G,in} + y_{CO_2,G,in} = 1 \quad (3)$$

$$y_{N_2,G,out} + y_{O_2,G,out} + y_{CO_2,G,out} = 1 \quad (4)$$

where  $y_{x,G,in}$  and  $y_{x,G,out}$  are the fractions of the respective x gases (N<sub>2</sub>, O<sub>2</sub> and CO<sub>2</sub>) entering and exiting the reactor, respectively. The fractions of O<sub>2</sub> and CO<sub>2</sub> were measured by the offgas analyzer every minute and values for every second were obtained with interpolation.

Applying the nitrogen gas balance:

$$F_{G,in} \cdot y_{N_2,G,in} = F_{G,out} \cdot y_{N_2,G,out} \quad (5)$$

where  $F_{G,out}$  and  $F_{G,in}$  are the flow rates (mmol<sub>air</sub> h<sup>-1</sup>) of air exiting and entering the reactor, respectively. In our experimental setup air was provided with a flow rate of 1.875 mmol<sub>air</sub>h<sup>-1</sup>.

From (3), (4) and (5), the gas outflow leaving the reactor was calculated, every second of the cycle:

$$F_{G,out} = \frac{F_{G,in} \cdot (1 - y_{O_2,G,in} - y_{CO_2,G,in})}{1 - y_{O_2,G,out} - y_{CO_2,G,out}} \quad (6)$$

From the mass balances of O<sub>2</sub> and CO<sub>2</sub>, the rates of consumption and production were then estimated respectively:

$$R_{O_2} = F_{G,out} \cdot y_{O_2,G,out} - F_{G,in} \cdot y_{O_2,G,in} \quad (7)$$

$$R_{CO_2} = F_{G,out} \cdot y_{CO_2,G,out} - F_{G,in} \cdot y_{CO_2,G,in} \quad (8)$$

where  $R_{O_2}$  (mmol<sub>O<sub>2</sub></sub> h<sup>-1</sup>) and  $R_{CO_2}$  (mmol<sub>CO<sub>2</sub></sub> h<sup>-1</sup>) are the O<sub>2</sub> consumption and CO<sub>2</sub> production rates, respectively, for every timepoint in the feast-famine cycle.

The biomass specific rates were then calculated:

$$q_{O_2} = \frac{R_{O_2}}{C_{BM} \cdot V}, \quad q_{CO_2} = \frac{R_{CO_2}}{C_{BM} \cdot V} \quad (9)$$

where  $C_{BM}$  is the biomass concentration in the broth ( $g_{CDW} L^{-1}$ ) and  $V$  is the broth volume (L).

We performed the above calculations for 16 successive feast-famine cycles and then used the average of all cycles for every second of the cycle.

We then added a pure time delay in both rates, which was assumed to be 46 seconds for  $O_2$  and 72 seconds for  $CO_2$ , based on the time it took for the offgas  $O_2$  concentration to decrease and  $CO_2$  concentration to increase (offgas analyzer) after the beginning of the feeding.

For both rates, a piecewise affine (PWA) rate approximation [4] was calculated. The breakpoints used were timepoints of 0, 20, 50, 80, 135, 262 and 400 s. These breakpoints were chosen, as they exhibited the highest goodness of fit ( $R^2$  was used), among various combinations [5]. The rates between the breakpoints followed a first order linear function.

Using the measured  $y_{O_2,G,out}$  and  $y_{CO_2,G,out}$  ratios and the calculated  $q_{O_2}$  and  $q_{CO_2}$  rates, an optimization was performed (Matlab R2018a, The MathWorks, Inc.) by minimizing the sum of squares between the initial measurements and the predicted.

The following differential equations were used for the optimization:

For oxygen:

$$\frac{d[O_2]_{out}}{dt} = F_{G,in} \cdot [O_2]_{in} - F_{G,out} \cdot [O_2]_{out} - R_{O_2} \quad (10)$$

where  $[O_2]$  is the concentration of oxygen in the gas phase.

For carbon dioxide:

At pH 7.0 there is significant interconversion of dissolved  $CO_2$  and bicarbonate in the broth [6], which was taken into account in our model. Using the system described in [7], the following differential equations for  $CO_2$  and  $HCO_3^-$  were derived:

$$\begin{aligned} \frac{d[CO_2]_{out}}{dt} = & F_{G,in} \cdot [CO_2]_{in} - F_{G,out} \cdot [CO_2]_{out} + R_{CO_2} - (k_1 + k_2 \cdot 10^{pH-14}) \\ & \cdot [CO_2]_{out} + (k_{-2} + k_{-1} \cdot 10^{-pH}) \cdot [HCO_3^-] \end{aligned} \quad (11)$$

$$\frac{d[\text{HCO}_3^-]}{dt} = (k_1 + k_2 \cdot 10^{\text{pH}-14}) \cdot [\text{CO}_2]_{\text{out}} - (k_{-2} + k_{-1} \cdot 10^{-\text{pH}}) \cdot [\text{HCO}_3^-] \quad (12)$$

where  $[\text{CO}_2]$  is the concentration of  $\text{CO}_2$  in the gas phase and  $[\text{HCO}_3^-]$  is the concentration of bicarbonate in the broth.  $k_1$ ,  $k_{-1}$ ,  $k_2$  and  $k_{-2}$  are the reaction constants, as described in [7]. For our calculations we used values from the literature for  $37^\circ\text{C}$ , as follows:

$$k_{-1} = 60 \text{ in } \text{s}^{-1} [6]$$

$$k_1 = e^{-11.582 - \frac{918.9}{T}} \cdot k_{-1} \text{ in } \text{M}^{-1}\text{s}^{-1} [8], \text{ where } T = 310.15 \text{ K}$$

$$k_{-2} = 107 \cdot 10^{-5} \text{ in } \text{s}^{-1} [6]$$

$$k_2 = \frac{e^{-11.582 - \frac{918.9}{T}}}{k_{\text{wf}}} \cdot k_{-2} \text{ in } \text{M}^{-1}\text{s}^{-1}, \text{ where } k_{\text{wf}} = e^{148.9802 - \frac{13847.26}{T} - 23.6521 \cdot \ln T} \text{ is the water dissociation equilibrium constant [9].}$$

## A.4 Extracellular by-products

**Table A-1** Extracellular by-product concentration measurements in mM for steady-state (3 replicates) and feast-famine (over time).

	Lactate	Formate	Acetate	Ethanol
<b>Steady-state</b>				
<b>Sample 1</b>	4.42	0.33	1.11	9.27
<b>Sample 2</b>	4.53	0.33	1.12	8.62
<b>Sample 3</b>	4.97	0.37	1.17	7.90
<b>Feast-famine</b>				
<b>Timepoints (s)</b>				
0	1.52	1.66	2.13	-
2.5	1.56	1.61	1.99	0.59
5	1.54	1.62	2.01	2.15
7.5	1.56	1.64	2.00	1.38
10	1.57	1.52	2.21	1.13
12.5	1.60	1.76	2.47	1.85
15	1.54	1.75	2.39	6.58
17.5	1.75	1.89	2.45	3.82
20	1.80	1.94	2.44	4.21
25	1.93	2.07	2.40	3.27
30	1.50	1.74	2.11	4.99
40	1.51	1.74	2.45	3.34
50	1.67	1.77	2.33	4.74
60	1.66	1.89	2.46	2.64
70	1.64	1.87	2.55	2.60
80	1.81	1.95	2.37	2.98
90	1.56	1.63	2.07	2.52
95	1.64	1.88	2.40	4.89
100	1.54	1.63	2.06	-
110	1.50	1.74	1.93	3.91
120	1.96	2.14	2.46	3.73
135	1.56	1.66	2.13	-
150	1.58	1.67	2.04	5.03
185	1.58	1.79	2.30	5.88
220	1.55	1.64	2.07	2.68
260	1.56	1.63	2.06	-
330	1.54	1.63	2.08	-
360	1.61	1.71	2.06	4.69
400	1.52	1.66	2.13	-

## A.5 Biomass specific rates (raw data)

**Table A-2** Raw data of steady-state and average feast-famine biomass specific rates with their associated standard deviations. The third column shows data from the test experiments with the 13 s feeding.

	Steady-state		Feast-famine (cycle average)		
			20 s feeding	13 s feeding	
	Raw	Reconciled	Raw	Reconciled	
<b>Working volume (L)</b>	0.947 ± 0.001		0.947 ± 0.001		0.883 ± 0.001
<b>Biomass concentration</b> (g L <sup>-1</sup> )	9.71 ± 0.63		6.57 ± 0.15		6.57 ± 0.23
<b>Biomass growth <math>\mu</math></b> (g g <sub>CDW</sub> <sup>-1</sup> h <sup>-1</sup> )	0.044 ± 0.004		0.048 ± 0.009		0.05 ± 0.003
<b>q<sub>Glucose</sub></b> (mmol <sub>glc</sub> g <sub>CDW</sub> <sup>-1</sup> h <sup>-1</sup> )	-0.70 ± 0.05		-1.07 ± 0.03		-1.16 ± 0.05
<b>q<sub>O<sub>2</sub></sub></b> (mmol <sub>O<sub>2</sub></sub> g <sub>CDW</sub> <sup>-1</sup> h <sup>-1</sup> )	-2.16 ± 0.16		-4.22 ± 0.19		-4.17 ± 0.08
<b>q<sub>CO<sub>2</sub></sub></b> (mmol <sub>CO<sub>2</sub></sub> g <sub>CDW</sub> <sup>-1</sup> h <sup>-1</sup> )	2.21 ± 0.15		4.35 ± 0.12		4.50 ± 0.08
<b>Respiratory Quotient</b>	1.02 ± 0.10		1.03 ± 0.04		1.08 ± 0.01
	<b>Raw</b>	<b>Reconciled</b>	<b>Raw</b>	<b>Reconciled</b>	
<b>q<sub>acetate</sub></b> (mmol <sub>ace</sub> g <sub>CDW</sub> <sup>-1</sup> h <sup>-1</sup> )	0.005 ± 0.0004	0.005 ± 0.0002	0.016 ± 0.003	0.016 ± 0.003	N.A. <sup>1</sup>
<b>q<sub>ethanol</sub></b> (mmol <sub>eth</sub> g <sub>CDW</sub> <sup>-1</sup> h <sup>-1</sup> )	0.039 ± 0.004	0.041 ± 0.003	0.028 ± 0.012	0.029 ± 0.012	N.A.
<b>q<sub>formate</sub></b> (mmol <sub>form</sub> g <sub>CDW</sub> <sup>-1</sup> h <sup>-1</sup> )	0.002 ± 0.0001	0.002 ± 0.0001	0.012 ± 0.003	0.013 ± 0.003	N.A.
<b>q<sub>lactate</sub></b> (mmol <sub>lac</sub> g <sub>CDW</sub> <sup>-1</sup> h <sup>-1</sup> )	0.021 ± 0.002	0.022 ± 0.001	0.011 ± 0.002	0.013 ± 0.002	N.A.
<b>Biomass Yield</b> (g <sub>CDW</sub> g <sub>glc</sub> <sup>-1</sup> )	0.32 ± 0.04		0.22 ± 0.04		0.22 ± 0.01
<b>Oxygen Yield</b> (mmol <sub>O<sub>2</sub></sub> mmol <sub>glc</sub> <sup>-1</sup> )	3.09 ± 0.31		3.94 ± 0.15		3.59 ± 0.16
<b>Carbon recovery</b> (%)	101.8		101.6		N.A.
<b>Electron recovery</b> (%)	112.3		108.7		N.A.

<sup>1</sup> N.A.: Not available

## A.6 Elemental analysis and microscopy

For the elemental analysis performed, carbon (C), hydrogen (H) and nitrogen (N) were quantified with a CHN-Analyzer, phosphorus (P) was quantified with UV/VIS and sulphur (S) with ion chromatography. The measurements were performed by Mikroanalytisches Laboratorium Kolbe, Oberhausen, Germany. The oxygen content was calculated, assuming that biomass was composed only by C, H, N, P, S, O and 3% metals.

**Table A.1** Elemental composition of dried biomass in steady-state and feast-famine regime. The values represent grams of elements per 100 grams of dried biomass. Standard errors were derived by duplicate samples of each regime.

Composition	Carbon C (%)	Hydrogen H (%)	Nitrogen N (%)	Phosphorus P (%)	Sulphur S (%)	Oxygen O (%)
Steady-state	48.88 ± 0.01	7.56 ± 0.01	15.23 ± 0.01	5.03 ± 0.02	1.33 ± 0.01	18.99 ± 0.03
Feast-famine	48.69 ± 0.01	7.48 ± 0.01	15.53 ± 0.01	5.17 ± 0.02	1.25 ± 0.01	18.89 ± 0.03
Change (%)	-0.39 ± 0.03	-1.06 ± 0.19	+1.97 ± 0.09	+2.78 ± 0.56	-6.02 ± 1.07	-0.53 ± 0.22

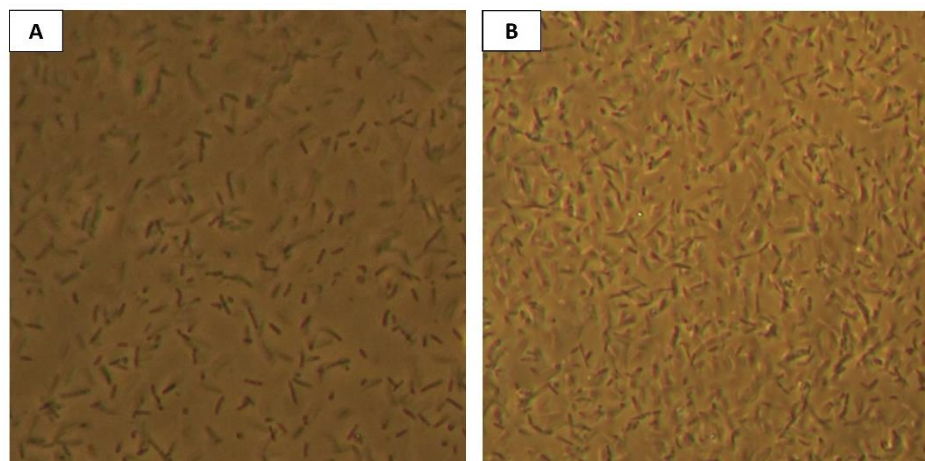


**Figure A-2** Optical microscope (Zeiss Axiostar Plus) images from *E.coli* cells during (A) reference steady-state growth and (B) feast-famine growth. 1000x zoom was used and the dilution of the samples was not the same.

## A.7 Reaction list used in FBA

Flux Abbreviations	Enzymes	Reactions
1. PTS	Phosphotransferase system enzymes	Glucose + PEP $\rightarrow$ G6P + PEP <sub>out</sub>
2. G6PDH	Glucose-6-phosphate dehydrogenase	G6P $\rightarrow$ 6PG
3. PGI	Glucose-6-phosphate isomerase	G6P $\leftrightarrow$ F6P
4. PFK	Phosphofructokinase	F6P $\leftrightarrow$ FBP
5. FBA	Fructose-biphosphate aldolase	FBP $\leftrightarrow$ DHAP + GAP
6. TPI	Triose-phosphate isomerase	DHAP $\leftrightarrow$ GAP
7. GAPD/PGK	Glyceraldehyde-3-phosphate/ Phosphoglycerate kinase	GAP $\leftrightarrow$ 3PG
8. PGM	Phosphoglycerate mutase	3PG $\leftrightarrow$ 2PG
9. ENO	Enolase	2PG $\leftrightarrow$ PEP
10. PYK	Pyruvate kinase	PEP $\rightarrow$ PEP <sub>out</sub>
11. GND/RPE	6-phosphogluconate dehydrogenase/ Ribulose-phosphate 3-epimerase	6PG $\leftrightarrow$ Xyl5P
12. GND/RPI	6-phosphogluconate dehydrogenase/ Ribose-5-phosphate isomerase	6PG $\leftrightarrow$ Rib5P
13. TKT1	Transketolase 1	Xyl5P + Rib5P $\leftrightarrow$ GAP + S7P
14. TKT2	Transketolase 2	Xyl5P + E4P $\leftrightarrow$ F6P + GAP
15. TALA	Transaldolase A	GAP + S7P $\leftrightarrow$ F6P + E4P

Metabolites with the subscript “out” are products outside of the balancing space. We assume that pyruvate is the product of the PYK reaction.

## A.8 Flux balance analysis – Derived fluxes

**Table A.2** FBA estimated fluxes in  $\mu\text{mol}_{\text{substrate}}/\text{g}_{\text{CDW}}/\text{s}$ .

Fluxes (Glycolysis)										
Time (s)	PTS	G6PDH	PGI	PFK	FBA	TPI	GAPD/PGK	PGM	ENO	PYK
0	0.005	0.000	0.017	0.022	0.034	0.042	0.076	0.069	0.067	0.050
2	4.676	2.681	2.920	4.905	4.932	4.990	10.810	10.243	10.192	5.149
15	4.404	1.885	2.123	3.448	4.019	4.211	8.908	8.975	8.981	4.676
18	1.042	0.382	0.620	0.854	0.800	0.784	1.706	1.742	1.745	0.717
110	0.022	0.000	0.018	0.021	0.008	0.000	0.000	0.003	0.005	0.000
400	0.005	0.000	0.017	0.022	0.034	0.042	0.076	0.069	0.067	0.050
Fluxes (Pentose phosphate pathway)										
	GND/RPE	GND/RPI	TKT1	TKT2	TALA					
0	0.001	0.0002	0.0002	0.001	0.001					
2	1.823	0.874	0.890	0.924	0.924					
15	1.302	0.658	0.671	0.674	0.673					
18	0.248	0.122	0.123	0.121	0.121					
110	0.006	0.000	0.000	0.010	0.000					
400	0.014	0.0002	0.0002	0.001	0.001					



## A.9 Amino acids

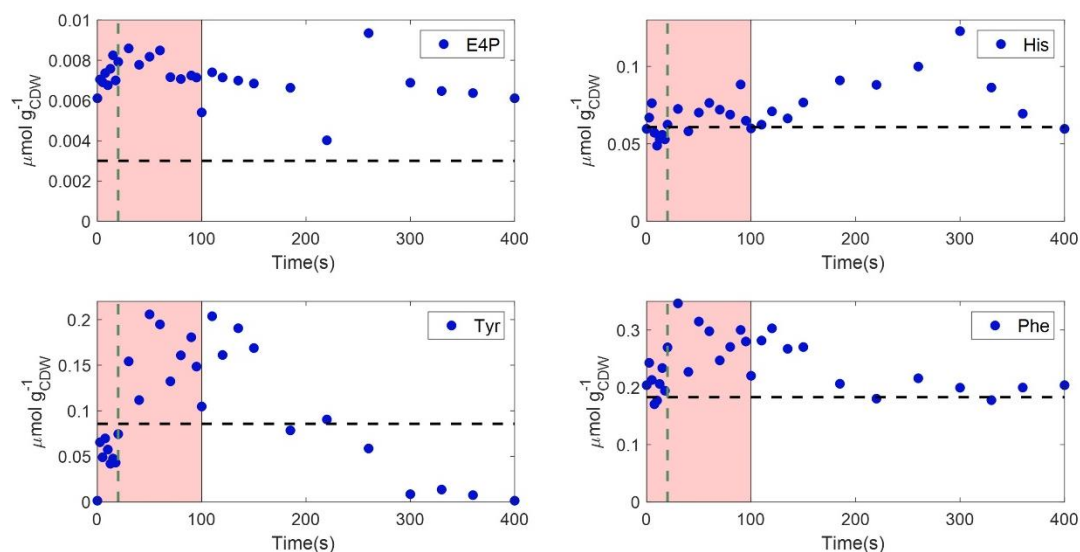


**Figure A-3** Intracellular concentrations ( $\mu\text{mol/g}_{\text{CDW}}$ ) of amino acids (histidine, tyrosine and phenylalanine) with E4P as a precursor, over a feast-famine cycle (s). Black horizontal dashed lines represent the average steady-state levels. Green vertical dashed lines show the end of the feeding (20 s). The pink area represents the substrate feast phase.

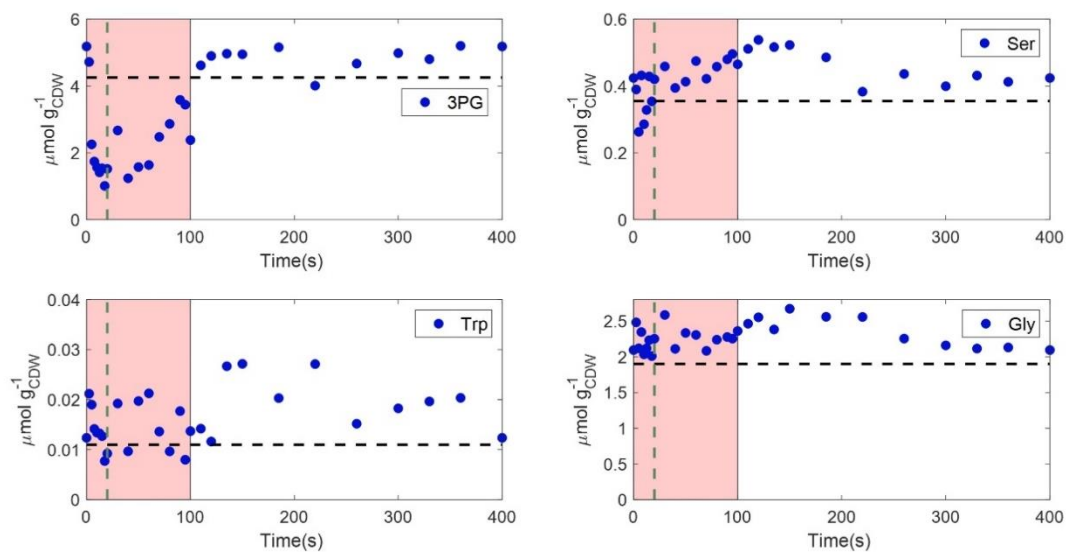


**Figure A-4** Intracellular concentrations ( $\mu\text{mol/g}_{\text{CDW}}$ ) of amino acids (serine, tryptophan and glycine) with 3PG as a precursor, over a feast-famine cycle (s). Black horizontal dashed lines represent the average steady-state levels. Green vertical dashed lines show the end of the feeding (20 s). The pink area represents the substrate feast phase.

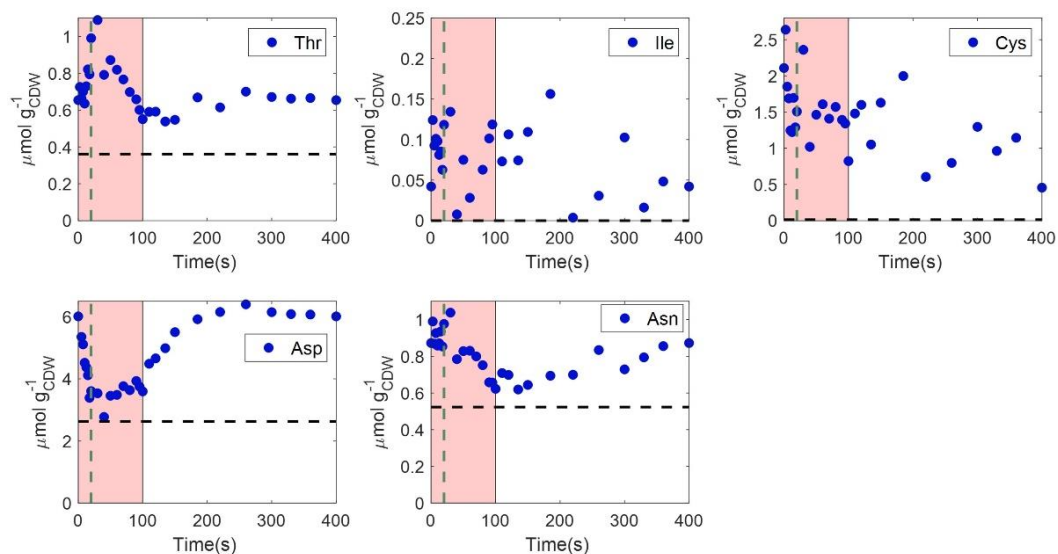


**Figure A-5** Intracellular concentrations ( $\mu\text{mol}/g_{\text{CDW}}$ ) of amino acids (threonine, isoleucine, cysteine, aspartate and asparagine) with oxaloacetate as a precursor, over a feast-famine cycle (s). Black horizontal dashed lines represent the average steady-state levels. Green vertical dashed lines show the end of the feeding (20 s). The pink area represents the substrate feast phase.

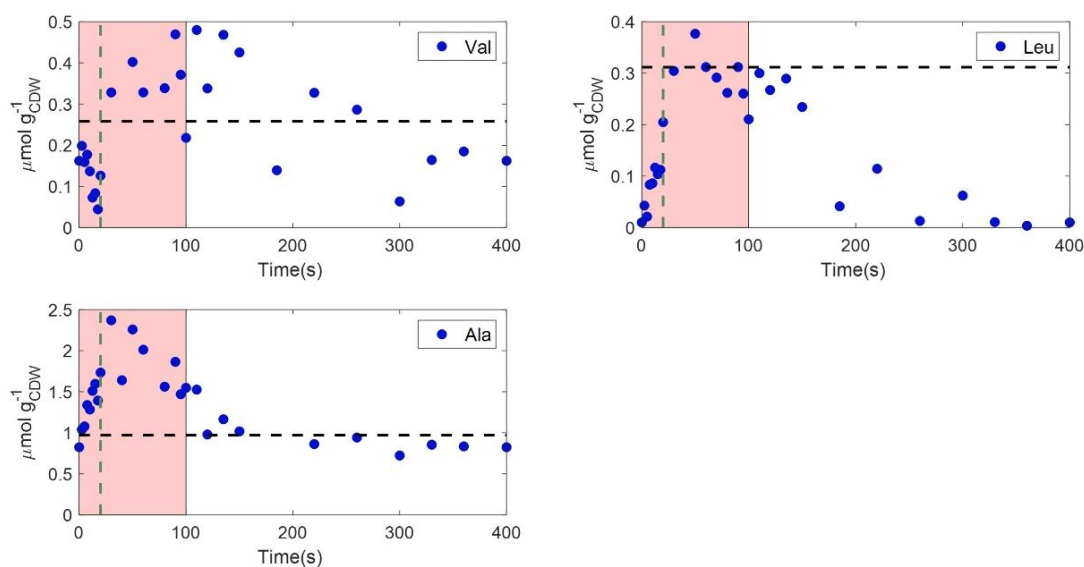


**Figure A-6** Intracellular concentrations ( $\mu\text{mol}/g_{\text{CDW}}$ ) of amino acids (valine, leucine and alanine) with pyruvate as a precursor, over a feast-famine cycle (s). Black horizontal dashed lines represent the average steady-state levels. Green vertical dashed lines show the end of the feeding (20 s). The pink area represents the substrate feast phase.

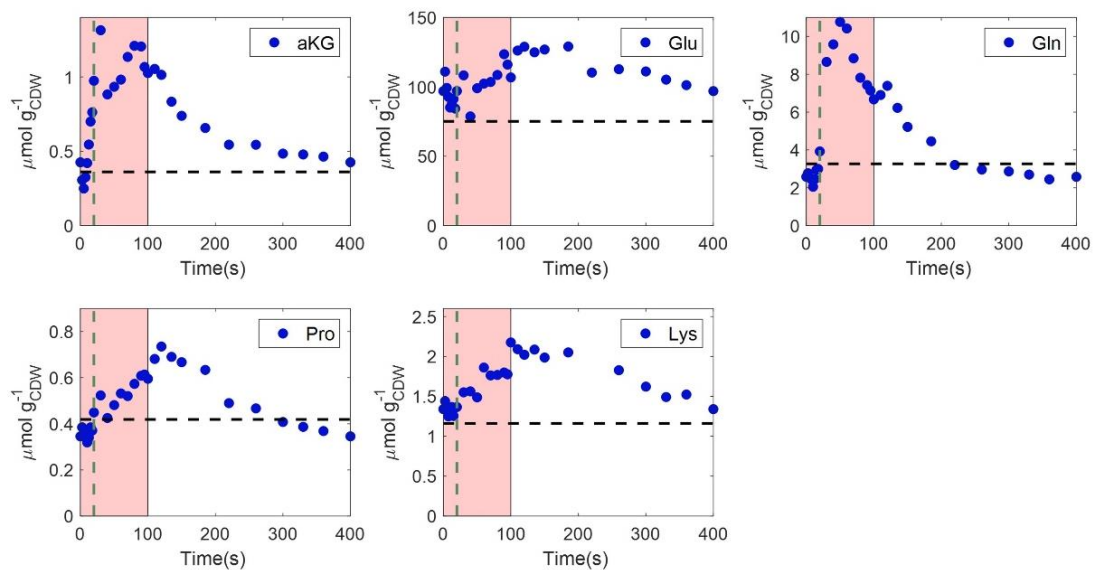


**Figure A-7** Intracellular concentrations ( $\mu\text{mol}/\text{g}_{\text{CDW}}$ ) of amino acids (glutamate, glutamine, proline and lysine) with aKG as a precursor, over a feast-famine cycle (s). Black horizontal dashed lines represent the average steady-state levels. Green vertical dashed lines show the end of the feeding (20 s). The pink area represents the substrate feast phase.

## A.10 Total metabolome

**Table A-3** List of metabolites quantified in this chapter.

Central Carbon	Amino acids	Nucleotides	Rest
Fumarate (Fum)	Alanine (Ala)	Adenosine diphosphate (ADP)	Trehalose (Tre)
Malate (Mal)	Glycine (Gly)	Adenosine triphosphate (ATP)	Trehalose-6-phosphate (T6P)
alpha-ketoglutarate (aKG)	Valine (Val)	Uridine triphosphate (UTP)	Mannose-6-phosphate (M6P)
Glyceraldehydophosphate (GAP)	Leucine (Leu)	Uridine diphosphate (UDP)	Uridine diphosphate glucose (UDP-glucose)
Citrate (Cit)	Isoleucine (Ile)	Guanosine diphosphate (GDP)	Mannitol-1-phosphate (M1P)
Isocitrate (iCit)	Proline (Pro)	Guanosine triphosphate (GTP)	Glucose-1-phosphate (G1P)
2-phosphoglycerate (2PG)	Serine (Ser)		
3-phosphoglycerate (3PG)	Threonine (Thr)		
Dihydroacetonephosphate (DHAP)	Methionine (Meth)		
Erythrose-4-phosphate (E4P)	Aspartate (Asp)		
Ribose-5-phosphate (Rib5P)	Phenylalanine (Phe)		
Xylose-5-phosphate (Xyl5P)	Glutamate (Glu)		
Fructose-6-phosphate (F6P)	Lysine (Lys)		
Glucose-6-phosphate (G6P)	Asparagine (Asn)		
Sedoheptulose-7-phosphate (S7P)	Glutamine (Gln)		
Fructobiphosphate (FBP)	Tyrosine (Tyr)		
Phosphoenolpyruvate (PEP)	Histidine (His)		
Succinate (Suc)	Cysteine (Cys)		
6-phosphogluconate (6PG)	Tryptophan (Trp)		

## References

1. Philichi TL, Stenstrom MK: **Effects of Dissolved-Oxygen Probe Lag on Oxygen-Transfer Parameter-Estimation.** *Journal Water Pollution Control Federation* 1989, **61**:83-86.
2. Vanrolleghem PA, Spanjers H: **A hybrid respirometric method for more reliable assessment of activated sludge model parameter.** *Water Science and Technology* 1998, **37**:237-246.
3. Smith CA, Corripio AB: *Principles and practice of automatic process control.* Hoboken, NJ: Wiley; 2006.
4. Vieth E: **Fitting piecewise linear regression functions to biological responses.** *J Appl Physiol (1985)* 1989, **67**:390-396.
5. Schumacher R, Wahl SA: **Effective Estimation of Dynamic Metabolic Fluxes Using (13)C Labeling and Piecewise Affine Approximation: From Theory to Practical Applicability.** *Metabolites* 2015, **5**:697-719.
6. Wang X, Conway W, Burns R, McCann N, Maeder M: **Comprehensive study of the hydration and dehydration reactions of carbon dioxide in aqueous solution.** *J Phys Chem A* 2010, **114**:1734-1740.
7. Sperandio M, Paul E: **Determination of carbon dioxide evolution rate using on-line gas analysis during dynamic biodegradation experiments.** *Biotechnol Bioeng* 1997, **53**:243-252.
8. Minkevich IG, Neubert M: **Influence of Carbon-Dioxide Solubility on the Accuracy of Measurements of Carbon-Dioxide Production-Rate by Gas Balance Technique.** *Acta Biotechnologica* 1985, **5**:137-143.
9. Dickson AG, Millero FJ: **A Comparison of the Equilibrium-Constants for the Dissociation of Carbonic-Acid in Seawater Media.** *Deep-Sea Research Part a-Oceanographic Research Papers* 1987, **34**:1733-1743.





# Chapter



## Model-based identification of cellular mechanisms during the transition of *Escherichia coli* from steady-state to dynamic environments

In collaboration with: L. de Graaf, M.C.M. van Loosdrecht and S.A. Wahl



## Abstract

**Background:** The microbial cell adaptation to dynamic environmental conditions is regulated by complex mechanisms, which determine the physiological and metabolic adjustments for survival and optimal growth. The combination of experimental perturbation studies and kinetic modelling is crucial for revealing these mechanisms and predicting the behaviour of microorganisms transitioning through various growth conditions. However, most of the developed kinetic models have been validated under steady-state growth, resulting in inconsistencies simulating dynamic conditions.

**Results:** In this work, we studied potential cellular strategies of *Escherichia coli* cells, occurring during the transition from steady-state conditions to repetitive substrate gradients. The published kinetic model for central carbon metabolism by Peskov K, *et al.* [1] was used to investigate our experimental observations. Kinetic parameter optimization of the original model, highlighted the significant alterations in the enzymatic kinetics of glycolysis during feast-famine, compared to steady-state growth. Post-transcriptional modifications were assumed to explain the limitation in the substrate uptake rate, observed while glucose was in excess. However, separating the feast-famine cycle into two phases and using the experimental uptake rate as fixed input appeared not to be enough for the model to simulate the experimental observations. Accurate predictions in the glycolytic intermediates were acquired only when glycogen synthesis and assimilation was implemented in the model. Glycogen acted as a storage pool, providing carbon and energy to reinitiate growth during famine conditions. However, only the inclusion of ATP-spilling reaction, initially hypothesised for inorganic polyphosphate production, led to accurate predictions of the experimentally observed adenylate energy homeostasis. The continuous draining of ATP supported the hypothesis of increased maintenance during the feast-famine regime.

**Conclusions:** Alterations in enzyme kinetics, storage metabolism and maintenance compose some of the important features of *E.coli* cellular responses to growth under substrate gradients. The implementation of these strategies in the construction of dynamic kinetic models, generates higher accuracy in the predictability of the model and highlights the potential of using similar approaches to study and predict microbial growth in industrial large-scale bioprocesses.

## 4.1 Introduction

Microbial cells have been long studied for their noteworthy ability to adapt to environmental changes, by modifying their intracellular network in such way to grow optimally under the new conditions [2-6]. Adaptation, which is coordinated by various regulatory mechanisms, can occur on different time scales, depending on the type of microorganism and the nature of the environmental perturbation [7, 8]. These may range from seconds (e.g. flux adjustments), hours (e.g. cell growth) to hundreds of generations (e.g. genetic evolution) [3].

Nutrient availability is one of the most commonly fluctuating environmental variables, in the natural habitat of microbes, as well as, in large-scale industrial bioprocesses [9-14]. Microorganisms respond to short-term substrate gradients by adjusting their metabolism, either by gene expression control or by regulating metabolite-enzyme interactions [15]. As a consequence, enzyme kinetic parameters (e.g. capacity and/or activity) are rapidly changing during environmental perturbations, affecting the rates of metabolic fluxes and resulting in altered phenotypes. Some examples derived from experimental observations for *Escherichia coli*, involve overflow metabolism [13], enhanced uptake rates [16] and energy spilling [10, 17].

The combination of experiments and mathematical modelling is a very powerful approach in order to enhance the understanding of microbial metabolism [18]. Especially, due to the dynamic environments of microbial cultures in industrial biotechnological processes, predicting cell growth under non-stationary conditions using models, is a necessity towards identifying targets for metabolic engineering and optimizing process parameters [19-21]. Kinetic models are particularly appropriate for this goal, as they can better represent the cellular responses to environmental perturbations [19, 22]. These models are mainly based on reaction kinetics and the system behaviour over time is described by mass balance equations. For more extended knowledge on kinetic metabolic modelling the following reviews are recommended: [19, 23-27].

Even though numerous kinetic models have been designed with the aim to capture metabolic responses under dynamic conditions, they have been calibrated and evaluated under stationary growth (steady-state fluxes), which leads to limitations predicting metabolism under different circumstances. Recent studies have evaluated and compared the quality and predictive power of published models, using experimental datasets under various genetic and environmental perturbations for *Escherichia coli* [28-30]. Many inconsistencies were observed between model predictions and experimental observations, especially for simulating dynamic conditions (e.g. batch growth), as well as, discrepancies between the performance of each model. Due to the complexity of cellular networks, the lack of knowledge on biochemical mechanisms and reaction kinetics for many phenotypes is the main cause of

the limited prediction capacity of biological models [31-34]. The increased multi-omics data generation and their integration into kinetic models is one of the current approaches, which paves the way towards better understanding of the complex regulation under dynamic conditions and the construction of more accurate models.

Chassagnole C, *et al.* [35] were the first to construct and validate a dynamic model of *E.coli* central carbon metabolism with kinetic information. Afterwards, many attempts have been made to increase the accuracy in the models of *E.coli* metabolism, by adding more pathways [36], using combination of *in vitro* and *in vivo* data for model evaluation [1], introducing new methods for better kinetic parameter identification [37], integrating gene regulation [38] and adding complexity with more detailed kinetic properties [15]. Lima AP, *et al.* [30] have published a detailed comparison between the main kinetic models for *E.coli* central carbon metabolism, based on their stoichiometric and kinetic differences

In our previous work (Chapter 3 of this thesis), a repetitive feast-famine regime was applied to an aerobic *E.coli* culture and the physiological and metabolic responses of the cells were reported, in time scale of seconds. From the collected experimental data, different hypotheses were derived on the mechanisms of cellular adaptation during the transition of a steady-state to substrate gradients. The potential metabolic strategies were mainly related to changes in the substrate uptake rate, increased capacities of enzymatic reactions, the effect of storage metabolism, energy spilling processes and adenylate energy charge homeostasis. The aim of the current chapter is to unravel significant cellular functions and regulatory mechanisms occurring under substrate dynamic conditions, using kinetic modelling, as a tool to evaluate the hypotheses derived from the experimental observations. The *E.coli* kinetic model, published by Peskov K, *et al.* [1], was chosen for this purpose, for two main reasons:

1. Adenosine nucleotides ATP, ADP and AMP were included in the model as balanced metabolites (involved in metabolic reactions), rather than fixed parameters. This is an important trait for the goal of this chapter, as the mechanisms behind the adenylate energy charge homeostasis, observed in Chapter 3, can be further studied. In addition, the constant energy charge can be used as a factor evaluating the predictability of the model.
2. Comparing the published models [30] which agree with the first requirement, the Peskov model was the least complex (with 48 metabolites and 75 fluxes) and therefore easier to analyse in depth.

## 4.2 Methods

### 4.2.1 Kinetic Model

The kinetic model used for the simulations in this study was published by Peskov K, *et al.* [1], describing the *E. coli* central carbon metabolism. The model was developed for aerobic growth under steady-state conditions, with glucose as the limiting carbon source. The model was retrieved from JWS Online [39] in SBML format (not available online anymore) and was converted to MATLAB (The MathWorks Inc., USA) code, by the Systems Biology Format Converter (SBFC) (<http://sbfc.sourceforge.net>).

Extracellular glucose was implemented as a balanced metabolite, instead of a fixed parameter. Intracellular glucose was eliminated from the model, as extracellular glucose is converted directly to G6P, when entering the intracellular space, by the phosphotransferase system. In addition, there was no intracellular glucose identified experimentally during the feast-famine regime (Chapter 3). This term was included in the model by Peskov and co-workers, in order to describe growth conditions in case a non-PTS system was active; the *mgIBAC* transport system.

Simulations were performed for one dynamic cycle (0-400 s) with a time interval of 1 s. MATLAB was used for all the simulations in this study and MATLAB solver *ode15s* was used for the ordinary differential equation (ODE) system.

### 4.2.2 Parameter optimization

Parameter optimization was performed in the kinetic model, for several different sets of parameters. The MATLAB function *fminsearch* was used in order to minimize the sum of squares of the differences between the experimental and the simulated observations. The objective function was described as:

$$p_{\text{opt}} = \arg \min_p \sum_{i=1}^n (y_i - \hat{y}_i(p))^2$$

where  $p$  is the parameter vector for optimization,  $y_i$  are the experimental observations for every timepoint  $i$ ,  $\hat{y}_i$  are the model simulated results and  $n$  is the amount of observations.

### 4.2.3 Model evaluation criteria

Two different metrics were used to evaluate the performance of each simulation. With these metrics, it was feasible to compare the simulation results with the observed experimental data, as well as, to compare the different simulations with each other.

The first estimation error was given for every metabolite ( $i$ ) by the normalized Euclidean distance, as given in [40]:

$$e_i = \frac{\|y - \hat{y}\|}{\|y\|}$$

where  $\|\dots\|$  is an L2 norm,  $y$  is the vector of experimental observations and  $\hat{y}$  is the vector of the model simulated results for all timepoints. The smaller the normalized error is, the closer to experimental observations the simulated results are.

The second metric, which was used to compare different parameter optimizing strategies, is the Akaike information criterion [41]:

$$\text{AIC} = \ln\left(\frac{s^2}{N}\right) + \frac{2k}{N}$$
$$s^2 = \sum_{i=1}^n \left(\frac{\hat{y}_i - y_i}{y_i}\right)^2$$

where  $N$  denotes the amount of observations and  $k$  is the amount of model parameters used for optimization. The AIC is dependent on the residual sum of squares, as well as, the amount of parameters used for optimization. Therefore, strategies with different number of optimized parameters can be compared. A lower AIC score suggests better goodness-of-fit of the model, avoiding over-fitting [42].

#### 4.2.4 Experimental data

The experimental data from the *E.coli* feast-famine cultivation, described in Chapter 3, were used in this study, to validate the model predictions.

### 4.3 Results

During the transition of the cells from steady-state conditions to growth under substrate gradients (feast-famine regime in Chapter 3), we observed major changes, as a result of cell adaptation. Several regulation mechanisms could be responsible for these changes. Different hypotheses (Figure 4.1) were tested, applying different modifications to a published kinetic model [1].

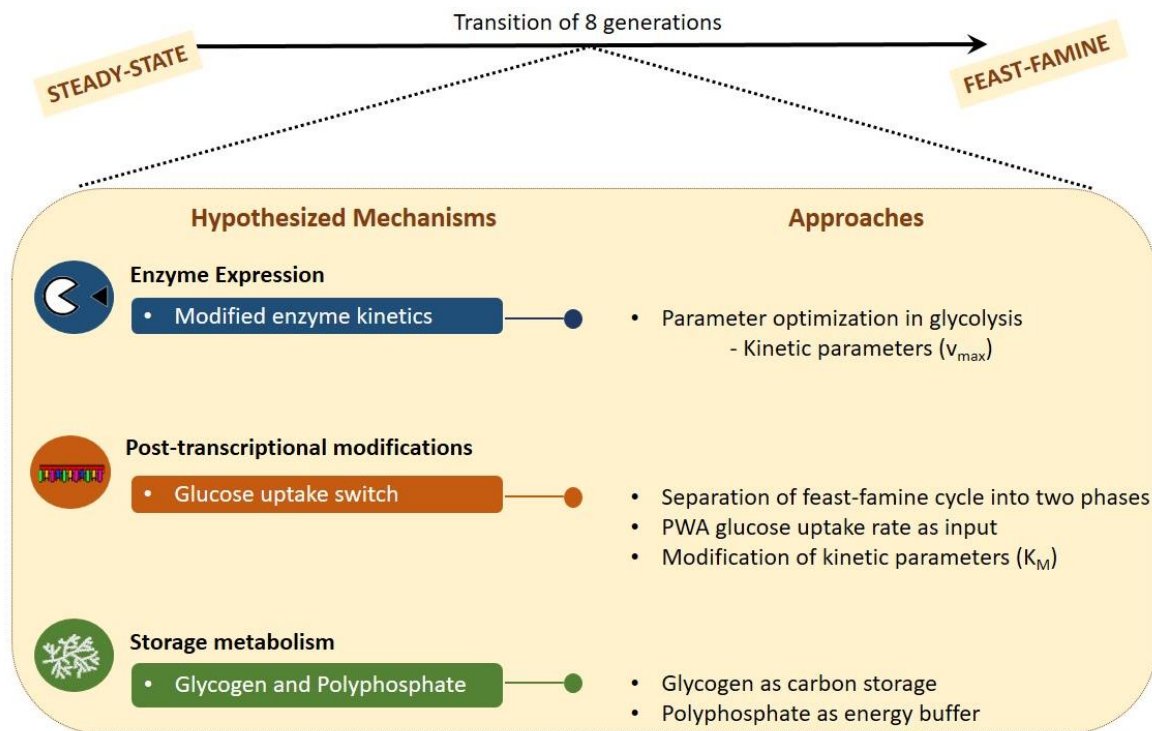


**Figure 4.1** Scheme summarizing potential changes in the cell metabolism, during the transition from steady-state to feast-famine conditions, and the approaches used for their assessment.

### 4.3.1 Application of the kinetic model for feast-famine conditions

The kinetic model was used to study the cellular activity under feast-famine conditions. Therefore, a glucose feeding phase of 20 s, followed by a non-feeding phase of 380 s was implemented. In addition, Table 4.1 shows the experimental culture parameters (from the work in Chapter 3) used as input in the model.

**Table 4.1** Culture parameters (experimental measurements of Chapter 3).

Parameter	Value	Units
pH	7.0	-
Biomass concentration (reconciled)	6.28	$g_{CDW} \cdot L_{EC}^{-1}$
Medium feeding rate	0.88	$L_{medium} \cdot h^{-1}$
Broth volume	0.95	L
Glucose concentration in feed	0.151	$mol_{glucose} \cdot L_{medium}^{-1}$

The metabolite concentrations and fluxes were defined in units of mM and  $mM \cdot min^{-1}$ , respectively, where mM referred to the intracellular volume. In order to ease the comparison between the simulation results and the experimental observations, the experimental measurements ( $\mu mol \cdot g_{CDW}^{-1}$ ) were converted assuming a cytosolic volume of  $1.77 \cdot 10^{-3} L_C \cdot g_{CDW}^{-1}$  [35].

The intracellular metabolite concentrations, quantified in Chapter 3, were used as initial conditions for the simulations. The list of these metabolites, along with their values, can be found in Appendix B.1. For metabolites that were not measured, the initial conditions reported in the article (simulation for  $0.1 \text{ h}^{-1}$  dilution rate) were used [1].

The enzymatic kinetic parameters used in the Peskov model were primarily obtained by *in vitro* literature data, while then *in vivo* experimental metabolite concentrations and fluxes were employed for verification of the complete model. However, in all cases the data used were derived from steady-state glucose-limited cultivations.

*E.coli* exhibited significant physiological and metabolic changes when cultivated under a feast-famine regime, compared to steady-state growth. The glucose uptake rate and subsequently all central carbon metabolic rates increased, in tens of seconds, following the excess of substrate, leading to considerable dynamic changes in most of the metabolite pools. Homeostasis was, however, observed in the concentration of ATP and the adenylate energy charge, indicating tight regulation. In addition, significant biomass yield losses were detected during the feast-famine regime, compared to steady-state (see details in Chapter 3). Due to these enzymatic alterations, the Peskov model was not expected to reproduce metabolism under dynamics, using the published steady-state derived parameters.

This was indeed confirmed by the simulation results (OP1 – ‘Original parameters’), where there was accumulation of glycolytic intermediates (G6P, F6P, FBP and GAP) over time, which led to lower flux towards PEP (Figure 4.2). Therefore, PEP was not produced fast enough in order to support the glucose transport by the PTS system [43], as it depleted immediately after the beginning of the feeding. As a consequence, the simulated substrate uptake was slower than the experimental piecewise affine (PWA) rate approximation (section 3.3.2, Chapter 3). This inconsistency in the glucose consumption prediction resulted in discrepancies in all metabolites (Appendix B.2), compared to the experiments.

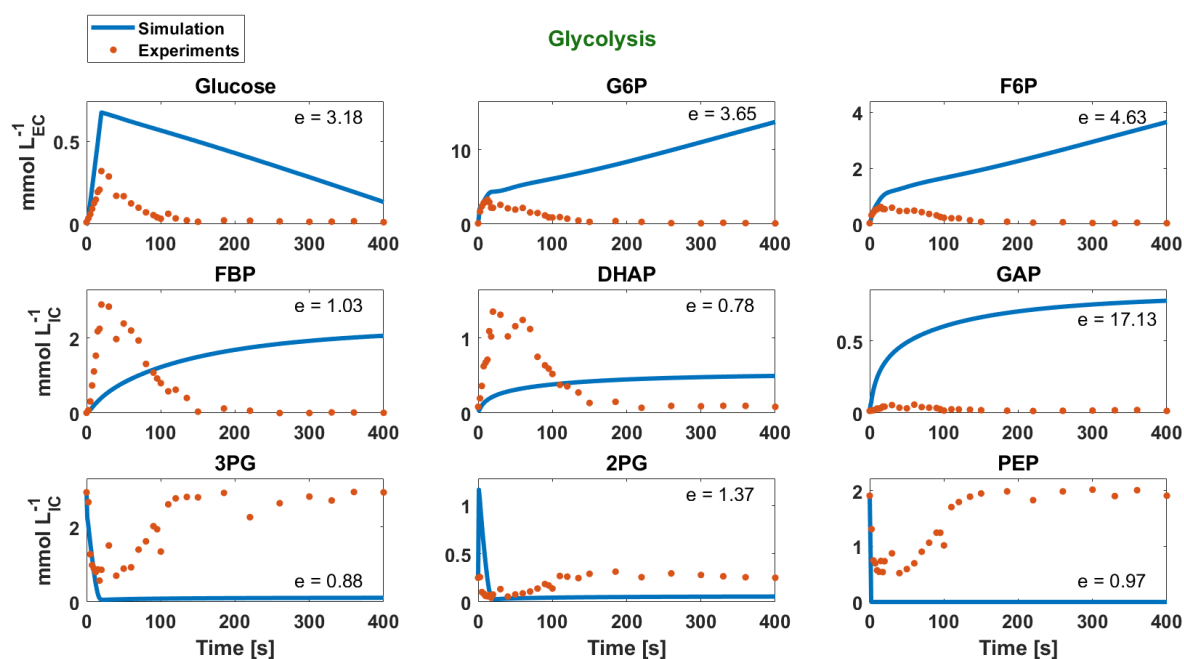


**Figure 4.2** Glycolytic metabolite concentrations over a feast-famine cycle. Orange dots: experimental intracellular measurements. Blue lines: **OP1** - Simulations with the kinetic model using the steady-state-derived parameters. All concentrations are given in mmol per units of intracellular volume (L), while glucose is given per units of extracellular volume. The normalized error  $e$  is given for every metabolite.

### 4.3.2 Enzyme kinetic adaptation in glycolysis

From the initial simulations (OP1), it was observed that the model should predict higher glycolytic fluxes, in order to reproduce the experimental results. In fact, central carbon metabolism was expected to become faster under feast-famine conditions, compared to the steady-state cultivation, as shown by the flux balance analysis performed in Chapter 3 (section 3.3.3). The environmental conditions influence enzyme expression and therefore may lead to changes in the enzymatic kinetic parameters ( $V_{max}$ ), during the feast-famine regime. Post-transcriptional modifications may also affect  $K_M$  values. In order to verify this hypothesis of enzymatic adjustments and study the influence on glycolysis, various attempts to optimize the main glycolytic parameters of the kinetic model were made. In addition, in order to tackle the inconsistency of the model to reproduce the glucose uptake rate, the PWA rate approximation was used as input in some of the optimization strategies.

Different sets of parameters (Appendix B.3) were used for every optimization (MP1-9 'Modified Parameters'), as well as, various optimization targets (summarized in Table 4.2) and the results can be found in Appendix B.4. The AIC was calculated for the glycolytic metabolites in every simulation and was used for comparing the different strategies. In addition, the  $e$  values were plotted in order to visually compare the accuracy of the predictions for every metabolite (Figure B-9, Appendix B.4). However, none of the chosen strategies could sufficiently reproduce all the glycolytic metabolite observations, showing a clear limitation of



the model to predict glycolysis under the studied conditions, even with the adapted kinetic parameters. This limitation was mainly derived by the failure of the model to predict the glucose uptake rate, resulting in discrepancies in the glucose concentration over time and affecting all metabolites in the cascade of glycolysis. Even when the PWA uptake rate was fixed, the performance of the model was still not acceptable.

**Table 4.2** Glycolytic parameter optimization strategies, for the complete feast-famine cycle.

Strategy	Optimization Target Metabolites	Fixed PWA glucose uptake rate	Optimization Parameter List*	AIC**	Comments
MP1	Glucose	No	A	3.90	High simulated glucose uptake in famine phase, G6P and FBP accumulation
MP2	Glucose	No	B	9.57	Unable to predict glucose uptake flux
MP3	ATP, ADP	No	A	1.48	Unable to predict glucose uptake flux, PEP depletion
MP4	PEP	Yes	C	4.48	Lower concentrations of upper glycolysis than experimental
MP5	Glycolytic***	No	A	9.75	Glucose uptake hindered by PEP depletion after 20 s
MP6	Glycolytic***	No	B	10.69	Same as in MP5
MP7, MP8	Glycolytic***	Yes	A, B	-	Optimization failed****
MP9	Glycolytic***	Yes	C	4.47	Not able to reproduce most glycolytic metabolites

\* All the optimization parameter lists of can be found in Appendix B.3.

\*\* AIC was calculated for the glycolytic metabolite concentrations of G6P, F6P, FBP, DHAP, GAP, 3PG, 2PG and PEP.

\*\*\*Glycolytic metabolites are G6P, F6P, FBP, GAP, DHAP, 3PG, 2PG and PEP. Glucose was not included in this list.

\*\*\*\* Optimization failure occurred when no parameters could be found so that PEP concentration was enough to run the import of glucose and therefore the ODE system could not be solved.

### ***Simulation of the non-feeding phase (20-400 s)***

One of the main observations, which the model was unable to predict, was the decrease in the glucose uptake rate, occurring experimentally, while the substrate was still in excess. In the beginning of the cycle, the uptake rate increased immediately and reached a value higher than reported batch maximum rates. However, it significantly decreased (at least 4-fold) after 15 s of feeding (section 3.3.2, Chapter 3). With this observed abrupt change in glucose uptake, the presence of non-kinetic mechanisms, like post-transcriptional modifications could be hypothesized. Therefore, the feast-famine cycle was split in two phases. Phase A (from 0-20 s, during which the uptake rate was the highest) and Phase B (from 20-400 s, where the uptake rate decreased significantly and the glucose feeding was stopped). Due to the weakness of the kinetic model to predict Phase A, Phase B was simulated separately, as an attempt to reproduce this part of the feast-famine cycle and gain more information on the

cellular mechanisms. For these simulations, the measured metabolite concentrations at 20 s (Chapter 3) were used as initial conditions. For the rest of the metabolites, the initial steady-state conditions ( $D=0.1 \text{ h}^{-1}$ ), of the model publication, were used. Optimization of the glycolytic parameters was again performed, for Phase B. The different strategies (MP10-MP18) are presented in Table 4.3 and the detailed results are given in Appendix B.5.

**Table 4.3** Glycolytic parameter optimization strategies, for Phase B.

Strategy	Optimization Target Metabolites	Fixed PWA glucose uptake rate	Optimization Parameter List*	AIC**	Comments
MP10	Glucose	No	A	5.89	PEP depletion, G6P accumulation
MP11	Glycolytic***	No	A	5.74	Glucose uptake hindered by PEP depletion
MP12	Glycolytic***	No	B	10.84	Same as MP11
MP13	Glucose	No	B	5.95	G6P accumulation
MP14	ATP, ADP	No	A	6.38	PEP depletion, accumulation of upper glycolytic intermediates
MP15	G6P, F6P,FBP	No	A	12.46	Same as MP11
MP16	G6P, F6P,FBP	Yes	B	-	Optimization failed****
MP17	Glycolytic***	Yes	B	1.92	F6P, GAP, 2PG not well reproduced
MP18	Glycolytic***	Yes	A	-	Optimization failed****

\* All the optimization parameter lists of can be found in Appendix B.3.

\*\* AIC was calculated for the glycolytic metabolite concentrations of G6P, F6P, FBP, DHAP, GAP, 3PG, 2PG and PEP.

\*\*\*Glycolytic metabolites are G6P, F6P, FBP, GAP, DHAP, 3PG, 2PG and PEP. Glucose was not included in this list.

\*\*\*\* Optimization failure occurred when no parameters could be found so that PEP concentration was enough to run the import of glucose and therefore the ODE system could not be solved.

Despite the adapted kinetic parameters, the separation of the two phases and the input of the PWA substrate uptake rate, the prediction of glycolytic metabolite concentrations was still not possible during Phase B, with the optimization strategies chosen. The best strategy, according to the AIC and the simulated vs. experimental data plot (Figure B-16, Appendix B.5), was MP17, where the  $V_{\max}$  values of the glycolytic reactions were estimated, using the PWA uptake rate as input. Even though it was the only strategy where PEP was simulated close to the experimental values, the predictions of main metabolites, such as F6P, GAP and 2PG, displayed high discrepancies. This behaviour leads to the assumption that there may be other metabolic features during a feast-famine regime, which were not incorporated in the original kinetic model and could justify its inconsistency with the experimental observations. In the following sections, some potential missing metabolic aspects were studied.

### 4.3.3 Storage Metabolism - Glycogen

The hypothesis of an intracellular storage compound, glycogen, was discussed in Chapter 3, to explain oxygen consumption during the famine phase, as well as, the ATP losses observed during the feast-famine regime. In addition, the proteome analysis performed for the same experiment, revealed the concentration increase of enzymes, participating in the production and the consumption of glycogen (detailed results in Chapter 5). Glycogen formation and re-assimilation can be considered as a potential storage pathway in *E.coli* during substrate dynamic conditions. However, this pathway is usually neglected in most dynamic kinetic models, like the Peskov model, as has been previously reviewed by [30]. Glycogen production and subsequent consumption could play a role in the accumulation of G6P observed in all the previous simulations. Therefore, this pathway was incorporated and further evaluated in the kinetic model.

Glycogen was set to be produced by G6P and during its formation and assimilation, one net ATP is consumed (Figure 4.3) [44, 45]. As this pathway is also regulated by the enzymes of the PTS system [46-48], the extracellular glucose concentration had an influence on the fluxes, i.e. production of glycogen was set to occur while glucose was available and glycogen consumption when glucose was absent.

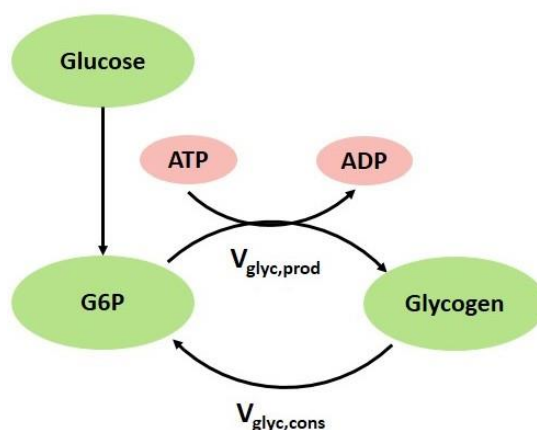


**Figure 4.3** Schematic representation of the glycogen pathway added in the kinetic model.

The reactions between G6P and glycogen, involving metabolites such as G1P and ADP-glucose, were lumped for simplicity. The rate of glycogen consumption was set in such way to ensure that all glycogen produced in the feast phase was then consumed in the famine phase, as the feast-famine cycles were repetitive and there was no indication of glycogen accumulation, according to all the experimental observations (discussed in Chapter 3). The residual glucose threshold, defining the feast and the famine phase, was set to  $10 \mu\text{mol}\cdot\text{L}_{\text{EC}}^{-1}$  (equals to  $0.9 \mu\text{mol}\cdot\text{L}_{\text{IC}}^{-1}$ ), as the reported glucose affinity constant ( $K_M$ ) [49]. One new

balanced metabolite (glycogen) and two new reactions (glycogen production and consumption) were implemented in the model, as follows:

$$V_{\text{glyc,prod}} = \begin{cases} k_{\text{glyc}} \cdot C_{\text{G6P}}, & C_{\text{glucose}} \geq 0.9 \\ 0, & C_{\text{glucose}} < 0.9 \end{cases}$$

$$V_{\text{glyc,cons}} = \begin{cases} 0, & C_{\text{glucose}} \geq 0.9 \\ \frac{C_{\text{glyc}}}{t_{\text{cycle}} - t_{(C_{\text{glucose}}=0)}}, & C_{\text{glucose}} < 0.9 \end{cases}$$

$$\frac{dC_{\text{glyc}}}{dt} = V_{\text{glyc,prod}} - V_{\text{glyc,cons}}$$

where  $k_{\text{glyc}}$  is a kinetic parameter of glycogen formation in  $\text{min}^{-1}$ ,  $t_{\text{cycle}}$  is the total cycle time in min,  $t_{(C_{\text{glucose}}=0)}$  is the timepoint when glucose gets depleted and  $C_{\text{G6P}}$ ,  $C_{\text{glyc}}$  are the concentrations of G6P and glycogen, respectively, in  $\text{mmol} \cdot \text{L}_{\text{IC}}^{-1}$ .

In the implemented pathway, there was one new parameter,  $k_{\text{glyc}}$ , which affected the glycogen production rate and which was estimated using different optimization strategies. Using the model with the implemented glycogen pathway, optimizations (MPG – ‘Modified parameters with glycogen’) were performed in order to define the glycolytic and/or glycogen parameters, which would enable predictions close to the experimental observations for Phase B (Table 4.4).

For this phase, since no experimental data were available, the initial concentration of glycogen (i.e. glycogen produced during the first 20 s of the regime) was hypothesised to be 20% of the total glucose consumed during that period, which was translated in  $14.3 \mu\text{mol}_{\text{glc}} \cdot \text{g}_{\text{CDW}}^{-1}$ . Because of the uncertainty of this assumption, different glycogen initial values ( $10 - 50 \mu\text{mol}_{\text{glc}} \cdot \text{g}_{\text{CDW}}^{-1}$ ) were also tested (data not shown), but all resulted in the same conclusion; the inclusion of glycogen recycling improves the reproduction of the experimental data. More detailed results of the optimizations can be found in Appendix B.6.

Evaluating the simulations with glycogen, it was observed that the concentration of GAP and the concentration of 2PG (during the famine phase) were always overestimated in glycolysis. The deviation of GAP was also observed in the previous simulations and was probably due to the equilibrium constant used for the triose-phosphate isomerase. Usually, the ratio of DHAP over GAP is 20:1 [50]. However, the  $K_{\text{eq,tpi}}$  in the original kinetic model was 1.6. By modifying

this parameter to 1/20, GAP and 2PG were reproduced much better in all the simulations with glycogen. The modified parameter was used for all the subsequent simulations performed in the rest of the study.

**Table 4.4** Glycolytic and glycogen parameter optimization strategies performed using the extended kinetic model, for Phase B.

Strategy	Optimization Target Metabolites	Fixed PWA glucose uptake rate	Optimization Parameter List*	AIC**	Comments
MPG1	Glycolytic***	No	A, $k_{\text{glyc}}$	2.67	Glucose uptake underestimated due to PEP depletion
MPG2	Glycolytic***	Yes	A, $k_{\text{glyc}}$	1.59	Good prediction of most glycolytic metabolites
MPG3	Glycolytic***	No	B, $k_{\text{glyc}}$	6.23	PEP depletion, inconsistencies in lower glycolysis, glycogen accumulation
MPG4	Glycolytic***	Yes	B, $k_{\text{glyc}}$	4.15	Underestimation of G6P and F6P, overestimation of DHAP, GAP, 2PG

\* All the optimization parameter lists of can be found in Appendix B.3.

\*\* AIC was calculated for the glycolytic metabolite concentrations of G6P, F6P, FBP, DHAP, GAP, 3PG, 2PG and PEP.

\*\*\*Glycolytic metabolites are G6P, F6P, FBP, GAP, DHAP, 3PG, 2PG and PEP. Glucose was not included in this list.

We observed that MPG1 and MPG2 simulated the metabolite concentrations closer to the experimental ones, indicating that changes occurred both in  $V_{\text{max}}$  and  $K_M$  values, during dynamic conditions. The best reproduction of glycolysis was derived by the MPG2 strategy (Table 4.4), optimizing the glycolytic and glycogen parameters for Phase B, using the PWA glucose uptake rate as input in the model (AIC = 1.59). The optimized parameters were significantly different than the initial ones (up to 14 fold times change), for all the reactions of glycolysis, emphasizing on the enzymatic adjustments during the feast-famine regime.

The resulting optimized parameters can be found in Table B-5, Appendix B.6 and the glycolytic metabolite concentrations (MPG2 strategy) are shown in Figure 4.4.

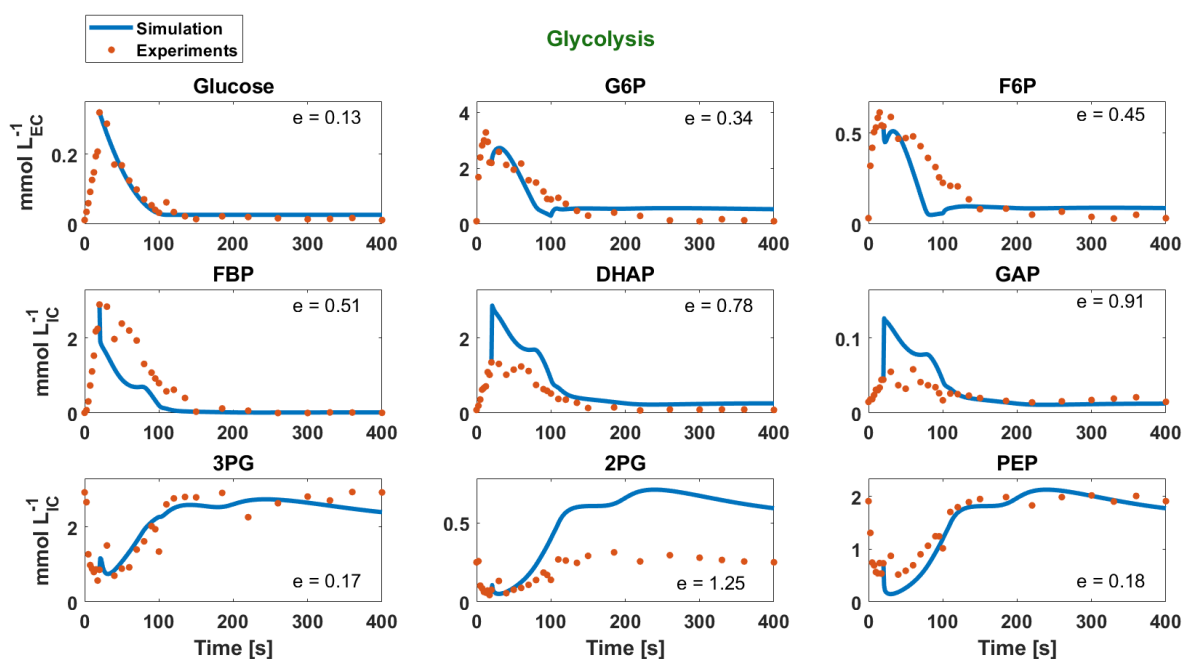


**Figure 4.4** Glycolytic metabolite concentrations over a feast-famine cycle. Orange dots: experimental intracellular measurements. Blue lines: **MPG2** - Simulations with the extended kinetic model for the time interval of 20-400 s, using the optimized glycolytic and glycogen parameters. All concentrations are given in mmol per units of intracellular volume (L), while glucose is given per units of extracellular volume. The normalized error  $e$  is given for every metabolite.

The ability of the model to predict glycolysis, when the glycogen pathway was implemented, directly shows the importance of storage for cell growth under substrate dynamic conditions. Glycogen was predicted to reach a concentration of  $37.2 \mu\text{mol}_{\text{glucose\_equivalents}} \cdot \text{g}_{\text{CDW}}^{-1}$ , which was less than 1% of the biomass dry weight ( $0.007 \text{ g}_{\text{glc}} \cdot \text{g}_{\text{CDW}}^{-1}$ ) and thus biologically feasible [51].

Glycolysis is the pathway functioning as the entrance to central carbon metabolism. Although the simulations were favourable for glycolytic fluxes, this was not the case for the rest of the simulated pathways (TCA cycle, pentose-phosphate pathway and adenine nucleotides). Most of the metabolite concentrations were overestimated (Figure B-19, Appendix B.6), including ATP, specifically during the famine phase. During the feast-famine regime, alterations in the enzymatic activity of these pathways were also expected. Indeed, the concentrations of several enzymes, catalysing reactions of these pathways, were found to alternate during the switch from steady-state to feast-famine (detailed results in Chapter 5). Further optimizations for the rest of the kinetic parameters were not made, as more computational power would be needed and complexity would be added to the interpretation of the results. However, it is undeniable that all kinetic parameters should be estimated for the dynamic conditions, in order to unravel the metabolic response of the whole central carbon metabolism.

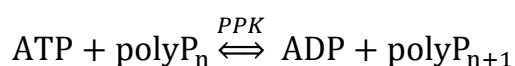
#### 4.3.4 Unravelling the energy homeostasis

Despite the variations observed in the concentrations of the adenosine nucleotides during the feast-famine regime, the energy charge, as well as the ATP/ADP ratio, showed a homeostatic behaviour (Chapter 3). However, in all previous sections, we observed that this homeostasis could not be predicted by the kinetic model, even when the glycolytic parameters were optimized and the glycogen storage pathway was implemented.

One of the hypotheses for the ATP balance in the cells, already mentioned in Chapter 3, was the formation and consumption of inorganic polyphosphate (PolyP). Indeed, the levels of the polyphosphate kinase (*PPK*) increased during the transition from steady-state to feast-famine (detailed results in Chapter 5), suggesting that there could be ATP/PolyP cycling. It is known that polyphosphate synthesis is a reversible reaction [52] and it seems that ATP levels are maintained by the shift between the forward and the reverse rate. Adenylate kinase (catalysing the interconversion of adenosine nucleotides) and *PPK* have been proposed to catalyse these reactions [53]. However, the molecular mechanisms that control this function are not yet studied in detail.

Polyphosphate synthesis and degradation are not included in current *E. coli* kinetic models of central carbon metabolism. There is one exception, where Van Dien SJ, *et al.* [54] improved a previously developed dynamic model, by including the kinetics of polyphosphate metabolism, in order to study the effects of phosphate-starvation response in *E.coli*. Even though the authors included simplified differential equations for ATP and polyphosphate, with a constant sum of ATP and ADP, the improved simulation results showed a better agreement with the experimental observations.

In order to test the hypothesis of polyphosphate pool functioning as an energy regulator, we implemented the synthesis and degradation of polyphosphate in the kinetic model and studied the effects of this addition to the performance of the simulations under feast-famine conditions. Polyphosphate is synthesised (and degraded) via the following reversible reaction:



The net rate was simulated with the following kinetic expression, based on reversible Michaelis-Menten kinetics, as formed in [54] and considering the enzymatic measurements from [55, 56]:

$$V_{\text{PolyP}} = v_{\text{max},f} \frac{[\text{ATP}]}{K_{M1} + [\text{ATP}]} - v_{\text{max},r} \frac{[\text{ADP}]}{K_{M2} + [\text{ADP}]}$$

where  $V_{\text{PolyP}}$  is the rate of formation (or degradation if negative) of polyphosphate,  $v_{\text{max},f}$  and  $v_{\text{max},r}$  are the forward and reverse maximum rates, respectively,  $[\text{ATP}]$  and  $[\text{ADP}]$  are

the intracellular concentrations of ATP and ADP and  $K_{M1}$  and  $K_{M2}$  are the Michaelis-Menten constants for ATP and ADP, respectively.

It is assumed that the ATP and ADP concentrations are the main drivers of the reaction and that the change of polyphosphate in chain length does not contribute significantly to the thermodynamic driving force and is therefore neglected in the kinetic expression.

The balance for polyphosphate was also added in the model:

$$\frac{d\text{PolyP}}{dt} = V_{\text{PolyP}}$$

With the two pathways of glycogen and polyphosphate added to the model, optimization of the glycolytic, glycogen and polyphosphate kinetic parameters was performed (MPGP – ‘Modified parameters with glycogen and polyphosphate’) for Phase B of the feast-famine regime. A polyphosphate concentration of  $0.03 \text{ mmol} \cdot \text{g}_{\text{CDW}}^{-1}$  was assumed as initial value, as no experimental data were available for the intracellular polyphosphate content. It should be noted that the initial concentration has no impact on the flux estimation (PolyP has no influence on the rate). With the aim to reproduce the energy homeostasis, minimizing the difference between experimental and simulated observations for ATP and ADP was used as optimization target (Table 4.5). Detailed results can be found in Appendix B.7.

**Table 4.5** Glycolytic, glycogen and polyphosphate parameter optimization strategy using the extended kinetic model, for Phase B.

Strategy	Optimization Target Metabolites	Fixed PWA glucose uptake rate	Optimization Parameter List*	AIC**	Comments
MPGP1	Glycolytic***, ATP, ADP	Yes	A, $k_{\text{glyc}}$ , $V_{\text{max},f}$ , $V_{\text{max},r}$ , $K_{M1}$ , $K_{M2}$	4.93	Glycolytic metabolites and ATP are well reproduced

\* All the optimization parameter lists of can be found in Appendix B.3.

\*\* AIC was calculated for the glycolytic metabolite concentrations of G6P, F6P, FBP, DHAP, GAP, 3PG, 2PG and PEP.

\*\*\*Glycolytic metabolites are G6P, F6P, FBP, GAP, DHAP, 3PG, 2PG and PEP. Glucose was not included in this list.

The implementation of the polyphosphate pathway resulted in an improved reproduction of all glycolytic metabolites, as well as the concentration of ATP (Figure 4.5). In comparison with the glycogen simulation (MPG2), the predicted ATP/ADP ratio was much closer to the experimental observations. Additionally, the concentrations of GAP and DHAP matched the measured values.



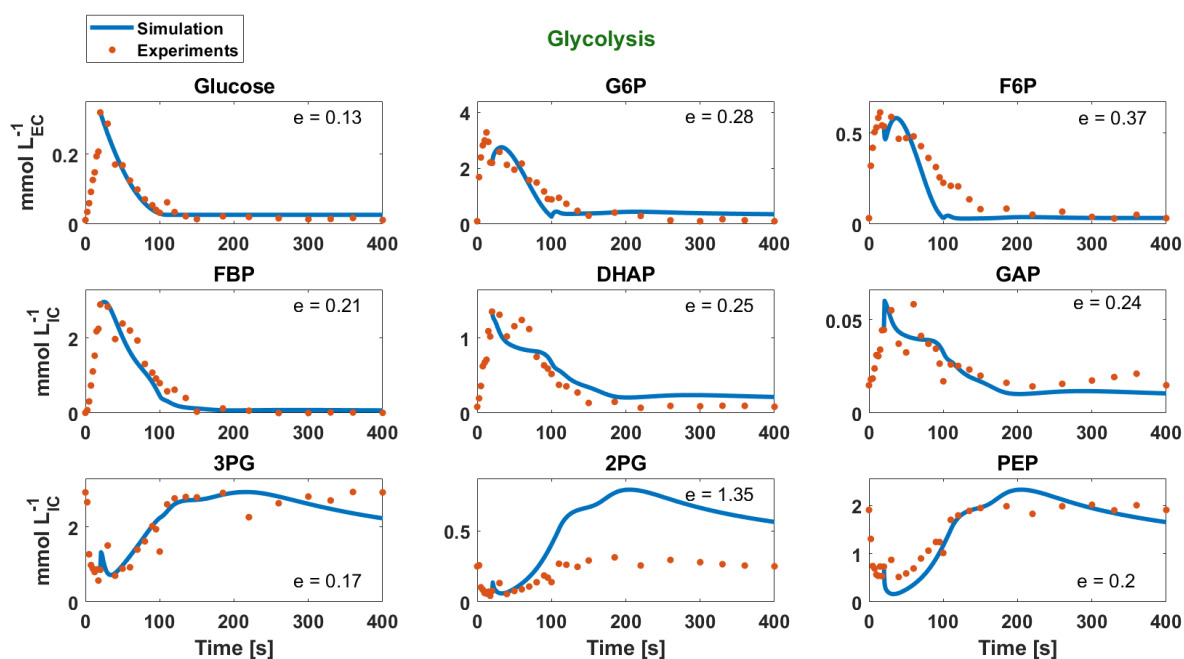


**Figure 4.5** Glycolytic metabolite concentrations over a feast-famine cycle. Orange dots: experimental intracellular measurements. Blue lines: **MPGP1** - Simulations with the extended kinetic model for the time interval of 20-400 s, using the optimized glycolytic, glycogen and polyphosphate parameters. All concentrations are given in mmol per units of intracellular volume (L), while glucose is given per units of extracellular volume. The normalized error  $e$  is given for every metabolite.

The average polyphosphate production rate over the cycle was simulated to be  $0.14 \text{ mmol}_P \cdot \text{L}_{IC}^{-1} \cdot \text{s}^{-1}$ . Due to the definition of the applied feast-famine cycles, the concentration of polyphosphate must be the same at the beginning and at the end of the cycle. Thus, the accumulation of intracellular polyphosphate can be explained by either a consuming reaction, during the feast phase, or wash-out as part of the biomass. In case of growth-related washout, the intracellular concentration would increase to  $10.3 \text{ mol}_P \cdot \text{L}_{IC}^{-1}$  (derived by the polyphosphate mass balance over a cycle using the average growth rate of  $0.048 \text{ h}^{-1}$  for washout), which is a huge and not realistic amount.

Such high phosphorus content should be detectable by biomass elemental analysis. However, the content of phosphorus was elevated by only  $2.8 \pm 0.6\%$  (Appendix A.6, Chapter 3), compared to the steady-state composition. Hence, the PolyP synthesis, predicted by the model, should be interpreted more as generic ATP sink than ‘real’ PolyP accumulation.

Maintenance is an example of such energy-consuming processes. Increased maintenance during feast-famine conditions was, also, suggested in order to explain the significant decrease in the biomass yield, compared to steady-state growth (Chapter 3). Thus, the extension of the Peskov kinetic model further supports this proposition of ATP losses through maintenance, preserving the cellular energy homeostasis.

In addition, numerous dynamic kinetic parameters estimated in the MPGP1 optimization strategy were significantly different than the ones from the MPG2 strategy (Table B-6 and Table B-5 respectively, Appendix B), showing that the ATP homeostasis affected the rest of the glycolytic metabolites, which was expected due to the various ATP-dependent reactions occurring in glycolysis. In general, we observed that almost all (except for the *fba* reaction) the  $V_{\max}$  values were estimated to be higher than the steady-state, as hypothesised earlier from the rapid increase in the substrate uptake rate. The highest changes were spotted for the maximum velocities of the GAP dehydrogenase (23 fold times increase) ( $\text{GAP} + \text{NAD}^+ \rightarrow \text{BPG} + \text{NADH}$ ) and the enolase (15 fold times increase) ( $2\text{PG} \rightarrow \text{PEP}$ ) enzymes, again revealing the remarkable ability of enzymatic adaptation to the changing environments.

#### 4.4 Discussion and Future Directions

Metabolic kinetic models are beneficial for industrial biotechnology, because they can be used for:

- i. understanding cellular mechanisms and regulation
- ii. predicting microbial growth under various conditions
- iii. optimizing the use of cell factories

In this study a published kinetic model of *E.coli* (steady-state) metabolism [1] was extended and modified to identify the cellular mechanisms, which enable the survival and growth of the microorganism under dynamic conditions, more precisely when a feast-famine regime was applied in repetitive cycles of 400 s each.

##### ***Enzymatic alterations under feast-famine conditions***

The original model was formulated, using steady-state derived enzymatic kinetic parameters, which proved to be inadequate for simulating growth under a repetitive dynamic environment. The repetitive transition of the cells from substrate excess to substrate limitation was expected to lead to considerable changes in protein expression. The increased rates of central carbon metabolic fluxes and the extensive proteome changes (Chapters 3 and 5 of this thesis), compared to steady-state growth, suggested modifications in the enzyme functions, which were confirmed by our efforts on optimizing various kinetic parameters of glycolysis, in order to better predict the experimental observations. In all the different scenarios tested, these parameters exhibited a variety of changes up to thousands fold times compared to the steady-state values. These alterations referred to maximum enzyme capacities ( $V_{\max}$ ) and Michaelis-Menten constants ( $K_M$ ). Therefore, metabolic fluxes were regulated by enzymatic changes occurred through alterations in gene expression. The type

and extent of these modifications should be taken into consideration when using metabolic modelling, in order to ensure correct representation of the metabolic network under dynamic environments. There are several ways to determine kinetic parameters, such as the use of existing enzymatic databases, *in vivo* measurements, model fitting with experimental data etc. [19, 57]. In addition, the switch observed experimentally in the glucose uptake rate, during the feast phase, could not be predicted by the kinetic model, implying the presence of post-transcriptional modifications, which were not implemented in the model. The details for this mechanism have still not been identified.

Nevertheless, the consideration of this so-called ‘hierarchical’ regulation mechanism was not sufficient for the model to predict the experimentally observed metabolic behaviour, under feast-famine conditions. Indeed, several studies have shown that this type of regulation is not always the main controller of flux adjustments, in *Escherichia coli* [15, 58], as well as, *Saccharomyces cerevisiae* [59, 60] and *Bacillus subtilis* [61]. In addition, enzyme-metabolite interactions play a critical role in flux regulation.

### ***Glycogen metabolism as a carbon storage mechanism***

The production and re-consumption of glycogen during feast-famine growth, as a storage polysaccharide, was assumed based on experimental evidence. The combination of estimating the dynamic kinetic parameters and implementing the glycogen pathway in the kinetic model resulted in sufficient model predictions for all glycolytic metabolites. Glycogen functioned as a carbon buffer and controlled the glycolytic fluxes in such way that no metabolite accumulation was observed. Even assuming simplistic kinetics, glycogen storage appeared to be an indispensable mechanism for the cell to handle the sudden variations in glycolytic fluxes, occurring under substrate dynamics. The essence of glycogen for environmental survival and energy supply under nutrient limitation, has been proved using metabolomics approaches [51] and has been linked to CsrA-mediated post-transcriptional control [62]. Recently, Sekar K, *et al.* [63] experimentally demonstrated the crucial role of glycogen under various short-term (time-scale of minutes) nutrient fluctuations, by comparing wild-type with glycogen-deficient cells of *E.coli*. Their results indicated enhanced growth and higher uptake rates for the cells with an active glycogen pathway in all transitions from substrate excess to starvation. It is, therefore, surprising that no significant effort has been done to include this pathway in kinetic models, except, for example from Morin M, *et al.* [51], who demonstrated the glycogen function, using a genome-scale model, during the transition from glycolysis to gluconeogenesis. Thus, our current results highlighted:

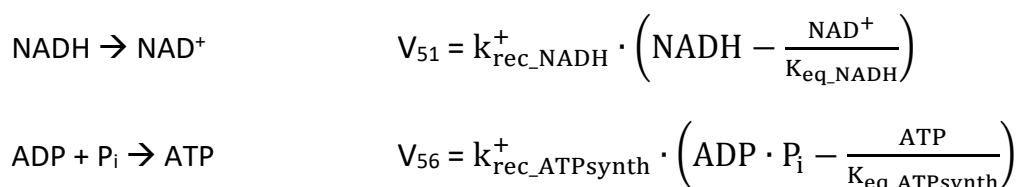
- i. The importance of glycogen pathway for metabolic adaptation of *E.coli* under short-term feast-famine conditions.

- ii. The need for accurate intracellular glycogen measurements during growth under dynamic conditions.
- iii. The need for better characterization of the glycogen synthesis and degradation kinetics and their inclusion in kinetic metabolic modelling approaches.

***Adenosine nucleotide homeostasis affected by increased maintenance***

One of the most interesting observations of metabolic behaviour under the feast-famine regime (Chapter 3), was the energy homeostasis achieved (i.e. constant ATP/ADP ratio). Due to this, a hypothesis of inorganic polyphosphate production and degradation was introduced as a potential energy buffer, supported by the measured increased levels of *PPK* enzyme under these conditions (Chapter 5). The implementation of polyphosphate pathway led to a satisfying reproduction of the ATP and the energy charge homeostasis and improved the prediction of all glycolytic intermediates. However, the forward reaction was simulated to be more active than the reverse, leading to a high unrealistic intracellular polyphosphate concentration during the feast-famine cycles. Due to the unfeasibility of this observation, maintenance (e.g. protein synthesis and degradation) was considered to be a more probable mechanism representing this ATP spilling.

Furthermore, the adenosine nucleotides are produced and consumed in various reactions and therefore the use of incorrect (or simplified) kinetics in the model, or the absence of unknown regulatory mechanisms can be a bottleneck for the prediction of the constant ATP/ADP ratio. Especially, for the Peskov model, used in this study, we express our scepticism on the way oxidative phosphorylation was modelled. In aerobic respiration, a membrane potential is formed across the cytoplasmic membrane when electrons are transferred from the substrate (i.e. glucose) to oxygen and NADH is converted to NAD<sup>+</sup> (electron transport chain). This potential drives the ATP synthesis, catalysed by the ATP synthase. Therefore, these two reactions involving NADH and ADP as substrates, are biologically coupled. However, in the original Peskov model, the following separate reactions (oxygen was not included as metabolite in the model and phosphate P<sub>i</sub> was included as a fixed parameter) were used:



Thus, the absence of coupling of the two reactions may result to considerable deviations of the model predictions from reality.

Taking all of the above-mentioned points into consideration, there is evidence that maintenance is one of the main controllers of cellular energy homeostasis and decrease of biomass yield, under feast-famine conditions. The existence of inorganic polyphosphate, as an energy buffer, cannot be completely excluded, taking into consideration the experimental proteomic evidence. Thus, measurements of the intracellular polyphosphate content would be required. In addition, maintenance should not be ignored in dynamic kinetic models and further knowledge on its individual processes, active under these conditions, would undoubtedly improve the modeling performance.

### ***Improvement of kinetic modelling and industrial bioprocesses***

With the increased generation of experimental data, under various dynamic environmental conditions, researchers are more extensively using kinetic models to reproduce these observations. While, most of the models can provide accurate predictions of steady-state growth, they regularly fail in dynamic simulations, such as pulse perturbations, shifts in dilution rates or different phases of batch cultivations [29, 30]. A step towards their improvement would, thus, be the identification and implementation of cellular mechanisms, which prove to be vital for stress-induced metabolic behaviour. For example, Kurata H, *et al.* [64] constructed a kinetic model, which was able to predict the dynamic behaviour of wild-type *E.coli* and several mutants, under not only steady-state, but also batch growth. They achieved this by improving an older model [38], adding missing regulatory mechanisms.

The ultimate ambition of kinetic modelling is to be of beneficial use to industrial biotechnology. As industrial large-scale bioprocesses are characterized by microbial growth under dynamic environmental conditions, such as substrate gradients, it is crucial to develop dynamic tools. These tools can be used for maximizing productivity and support the economic viability of bioprocesses. This study demonstrated that mechanisms, such as modified enzyme expression, storage metabolism and energy homeostasis are significant parts of the dynamic microbial responses and should always be taken into consideration when modelling and studying large-scale cultivations.

## References

1. Peskov K, Mogilevskaya E, Demin O: **Kinetic modelling of central carbon metabolism in *Escherichia coli***. *FEBS J* 2012, **279**:3374-3385.
2. Ferenci T: **'Growth of bacterial cultures' 50 years on: towards an uncertainty principle instead of constants in bacterial growth kinetics**. *Res Microbiol* 1999, **150**:431-438.
3. Sonnleitner B: **Dynamic adaptation of microbes**. *J Biotechnol* 1998, **65**:47-60.
4. Wirtz KW: **A generic model for changes in microbial kinetic coefficients**. *J Biotechnol* 2002, **97**:147-162.
5. Brooks AN, Turkarslan S, Beer KD, Lo FY, Baliga NS: **Adaptation of cells to new environments**. *Wiley Interdisciplinary Reviews-Systems Biology and Medicine* 2011, **3**:544-561.
6. Mitchell A, Romano GH, Groisman B, Yona A, Dekel E, Kupiec M, Dahan O, Pilpel Y: **Adaptive prediction of environmental changes by microorganisms**. *Nature* 2009, **460**:220-U280.
7. Chubukov V, Gerosa L, Kochanowski K, Sauer U: **Coordination of microbial metabolism**. *Nat Rev Microbiol* 2014, **12**:327-340.
8. Gerosa L, Sauer U: **Regulation and control of metabolic fluxes in microbes**. *Curr Opin Biotechnol* 2011, **22**:566-575.
9. Larsson G, Tornkvist M, Wernersson ES, Tragardh C, Noorman H, Enfors SO: **Substrate gradients in bioreactors: Origin and consequences**. *Bioprocess Engineering* 1996, **14**:281-289.
10. Bylund F, Collet E, Enfors SO, Larsson G: **Substrate gradient formation in the large-scale bioreactor lowers cell yield and increases by-product formation**. *Bioprocess Engineering* 1998, **18**:171-180.
11. Enfors SO, Jahic M, Rozkov A, Xu B, Hecker M, Jurgen B, Kruger E, Schweder T, Hamer G, O'Beirne D, et al: **Physiological responses to mixing in large scale bioreactors**. *J Biotechnol* 2001, **85**:175-185.
12. Takors R: **Scale-up of microbial processes: Impacts, tools and open questions**. *Journal of Biotechnology* 2012, **160**:3-9.
13. Lara AR, Galindo E, Ramirez OT, Palomares LA: **Living with heterogeneities in bioreactors: understanding the effects of environmental gradients on cells**. *Mol Biotechnol* 2006, **34**:355-381.
14. Noorman H: **An industrial perspective on bioreactor scale-down: What we can learn from combined large-scale bioprocess and model fluid studies**. *Biotechnology Journal* 2011, **6**:934-943.
15. Millard P, Smallbone K, Mendes P: **Metabolic regulation is sufficient for global and robust coordination of glucose uptake, catabolism, energy production and growth in *Escherichia coli***. *Plos Computational Biology* 2017, **13**.
16. Sunya S, Bideaux C, Molina-Jouve C, Gorret N: **Short-term dynamic behavior of *Escherichia coli* in response to successive glucose pulses on glucose-limited chemostat cultures**. *J Biotechnol* 2013, **164**:531-542.
17. Larsson G, Tornkvist M: **Rapid sampling, cell inactivation and evaluation of low extracellular glucose concentrations during fed-batch cultivation**. *J Biotechnol* 1996, **49**:69-82.
18. Vasilakou E, Machado D, Theorell A, Rocha I, Noh K, Oldiges M, Wahl SA: **Current state and challenges for dynamic metabolic modeling**. *Curr Opin Microbiol* 2016, **33**:97-104.
19. Almquist J, Cvijovic M, Hatzimanikatis V, Nielsen J, Jirstrand M: **Kinetic models in industrial biotechnology - Improving cell factory performance**. *Metab Eng* 2014, **24**:38-60.
20. Patil KR, Akesson M, Nielsen J: **Use of genome-scale microbial models for metabolic engineering**. *Current Opinion in Biotechnology* 2004, **15**:64-69.
21. Wiechert W, Noack S: **Mechanistic pathway modeling for industrial biotechnology: challenging but worthwhile**. *Current Opinion in Biotechnology* 2011, **22**:604-610.
22. Gabor A, Villaverde AF, Banga JR: **Parameter identifiability analysis and visualization in large-scale kinetic models of biosystems**. *Bmc Systems Biology* 2017, **11**.

23. Kim OD, Rocha M, Maia P: **A Review of Dynamic Modeling Approaches and Their Application in Computational Strain Optimization for Metabolic Engineering.** *Frontiers in Microbiology* 2018, **9**.
24. Link H, Christodoulou D, Sauer U: **Advancing metabolic models with kinetic information.** *Current Opinion in Biotechnology* 2014, **29**:8-14.
25. Miskovic L, Tokic M, Fengos G, Hatzimanikatis V: **Rites of passage: requirements and standards for building kinetic models of metabolic phenotypes.** *Current Opinion in Biotechnology* 2015, **36**:146-153.
26. Saa PA, Nielsen LK: **Formulation, construction and analysis of kinetic models of metabolism: A review of modelling frameworks.** *Biotechnology Advances* 2017, **35**:981-1003.
27. Song HS, DeVilbiss F, Ramkrishna D: **Modeling metabolic systems: the need for dynamics.** *Current Opinion in Chemical Engineering* 2013, **2**:373-382.
28. Costa RS, Vinga S: **Assessing Escherichia coli metabolism models and simulation approaches in phenotype predictions: Validation against experimental data.** *Biotechnol Prog* 2018, **34**:1344-1354.
29. Shepelin D, Machado D, Nielsen LK, Herrgård MJ: **Benchmarking kinetic models of Escherichia coli metabolism.** *bioRxiv* 2020:2020.2001.2016.908921.
30. Lima AP, Baixinho V, Machado D, Rocha I: **A Comparative Analysis of Dynamic Models of the Central Carbon Metabolism of Escherichia coli.** *Ifac Papersonline* 2016, **49**:270-276.
31. Schaber J, Liebermeister W, Klipp E: **Nested uncertainties in biochemical models.** *IET Syst Biol* 2009, **3**:1-9.
32. Kaltenbach HM, Dimopoulos S, Stelling J: **Systems analysis of cellular networks under uncertainty.** *FEBS Lett* 2009, **583**:3923-3930.
33. Chowdhury A, Khodayari A, Maranas CD: **Improving prediction fidelity of cellular metabolism with kinetic descriptions.** *Current Opinion in Biotechnology* 2015, **36**:57-64.
34. Tummler K, Klipp E: **The discrepancy between data for and expectations on metabolic models: How to match experiments and computational efforts to arrive at quantitative predictions?** *Current Opinion in Systems Biology* 2018, **8**:1-6.
35. Chassagnole C, Noisommit-Rizzi N, Schmid JW, Mauch K, Reuss M: **Dynamic modeling of the central carbon metabolism of Escherichia coli.** *Biotechnol Bioeng* 2002, **79**:53-73.
36. Kadir TA, Mannan AA, Kierzek AM, McFadden J, Shimizu K: **Modeling and simulation of the main metabolism in Escherichia coli and its several single-gene knockout mutants with experimental verification.** *Microb Cell Fact* 2010, **9**:88.
37. Khodayari A, Zomorodi AR, Liao JC, Maranas CD: **A kinetic model of Escherichia coli core metabolism satisfying multiple sets of mutant flux data.** *Metab Eng* 2014, **25**:50-62.
38. Jahan N, Maeda K, Matsuoka Y, Sugimoto Y, Kurata H: **Development of an accurate kinetic model for the central carbon metabolism of Escherichia coli.** *Microb Cell Fact* 2016, **15**:112.
39. Olivier BG, Snoep JL: **Web-based kinetic modelling using JWS Online.** *Bioinformatics* 2004, **20**:2143-2144.
40. Machado D, Herrgard M: **Systematic evaluation of methods for integration of transcriptomic data into constraint-based models of metabolism.** *PLoS Comput Biol* 2014, **10**:e1003580.
41. Akaike H: **A new look at the statistical model identification.** *IEEE Transactions on Automatic Control* 1974, **19**:716-723.
42. Burnham KP, Anderson DR: **Multimodel inference - understanding AIC and BIC in model selection.** *Sociological Methods & Research* 2004, **33**:261-304.
43. Misset O, Blaauw M, Postma PW, Robillard GT: **Bacterial phosphoenolpyruvate-dependent phosphotransferase system. Mechanism of the transmembrane sugar translocation and phosphorylation.** *Biochemistry* 1983, **22**:6163-6170.
44. Portais JC, Delort AM: **Carbohydrate cycling in micro-organisms: what can (13)C-NMR tell us?** *FEMS Microbiol Rev* 2002, **26**:375-402.

45. Russell JB, Cook GM: **Energetics of bacterial growth: balance of anabolic and catabolic reactions.** *Microbiol Rev* 1995, **59**:48-62.
46. Seok YJ, Koo BM, Sondej M, Peterkofsky A: **Regulation of E. coli glycogen phosphorylase activity by HPr.** *J Mol Microbiol Biotechnol* 2001, **3**:385-393.
47. Deutscher J, Francke C, Postma PW: **How phosphotransferase system-related protein phosphorylation regulates carbohydrate metabolism in bacteria.** *Microbiology and Molecular Biology Reviews* 2006, **70**:939-+.
48. Wilson WA, Roach PJ, Montero M, Baroja-Fernandez E, Munoz FJ, Eydallin G, Viale AM, Pozueta-Romero J: **Regulation of glycogen metabolism in yeast and bacteria.** *Fems Microbiology Reviews* 2010, **34**:952-985.
49. Stock JB, Waygood EB, Meadow ND, Postma PW, Roseman S: **Sugar transport by the bacterial phosphotransferase system. The glucose receptors of the Salmonella typhimurium phosphotransferase system.** *J Biol Chem* 1982, **257**:14543-14552.
50. Harris TK, Cole RN, Comer FI, Mildvan AS: **Proton transfer in the mechanism of triosephosphate isomerase.** *Biochemistry* 1998, **37**:16828-16838.
51. Morin M, Ropers D, Cinquemani E, Portais JC, Enjalbert B, Coccagn-Bousquet M: **The Csr System Regulates Escherichia coli Fitness by Controlling Glycogen Accumulation and Energy Levels.** *MBio* 2017, **8**.
52. Kornberg SR: **Adenosine triphosphate synthesis from polyphosphate by an enzyme from Escherichia coli.** *Biochim Biophys Acta* 1957, **26**:294-300.
53. Shiba T, Tsutsumi K, Ishige K, Noguchi T: **Inorganic polyphosphate and polyphosphate kinase: Their novel biological functions and applications.** *Biochemistry-Moscow* 2000, **65**:315-323.
54. Van Dien SJ, Keasling JD: **Effect of polyphosphate metabolism on the Escherichia coli phosphate-starvation response.** *Biotechnology Progress* 1999, **15**:587-593.
55. Ahn K, Kornberg A: **Polyphosphate kinase from Escherichia coli. Purification and demonstration of a phosphoenzyme intermediate.** *J Biol Chem* 1990, **265**:11734-11739.
56. Kuroda A, Kornberg A: **Polyphosphate kinase as a nucleoside diphosphate kinase in Escherichia coli and Pseudomonas aeruginosa.** *Proceedings of the National Academy of Sciences of the United States of America* 1997, **94**:439-442.
57. Davidi D, Milo R: **Lessons on enzyme kinetics from quantitative proteomics.** *Curr Opin Biotechnol* 2017, **46**:81-89.
58. Haverkorn van Rijsewijk BR, Nanchen A, Nallet S, Kleijn RJ, Sauer U: **Large-scale 13C-flux analysis reveals distinct transcriptional control of respiratory and fermentative metabolism in Escherichia coli.** *Mol Syst Biol* 2011, **7**:477.
59. Fendt SM, Oliveira AP, Christen S, Picotti P, Dechant RC, Sauer U: **Unraveling condition-dependent networks of transcription factors that control metabolic pathway activity in yeast.** *Mol Syst Biol* 2010, **6**:432.
60. Rossell S, van der Weijden CC, Lindenbergh A, van Tuijl A, Francke C, Bakker BM, Westerhoff HV: **Unraveling the complexity of flux regulation: A new method demonstrated for nutrient starvation in Saccharomyces cerevisiae.** *Proceedings of the National Academy of Sciences of the United States of America* 2006, **103**:2166-2171.
61. Chubukov V, Uhr M, Le Chat L, Kleijn RJ, Jules M, Link H, Aymerich S, Stelling J, Sauer U: **Transcriptional regulation is insufficient to explain substrate-induced flux changes in Bacillus subtilis.** *Molecular Systems Biology* 2013, **9**.
62. Timmermans J, Van Melder L: **Conditional Essentiality of the csrA Gene in Escherichia coli.** *Journal of Bacteriology* 2009, **191**:1722-1724.
63. Sekar K, Linker SM, Nguyen J, Grünhagen A, Stocker R, Sauer U: **Bacterial glycogen provides short-term benefits in changing environments.** *bioRxiv* 2019:841718.
64. Kurata H, Sugimoto Y: **Improved kinetic model of Escherichia coli central carbon metabolism in batch and continuous cultures.** *J Biosci Bioeng* 2018, **125**:251-257.



## Appendix B

## B.1 Initial metabolite concentrations

**Table B-1** Intracellular metabolite concentrations, quantified in Chapter 3, used as initial conditions in the model for the beginning of the feast-famine cycle ( $t=0$  s).

Metabolites	Initial conditions ( $\mu\text{mol g}_{\text{CDW}}^{-1}$ )	Metabolites	Initial conditions ( $\mu\text{mol g}_{\text{CDW}}^{-1}$ )
Glucose	1.84	6PG	0.40
G6P	0.18	Xyl5P	0.01
F6P	0.06	Rib5P	0.01
FBP	0.01	E4P	0.01
DHAP	0.15	S7P	0.17
GAP	0.03	Malate	0.28
3PG	5.18	aKG	0.43
2PG	0.44	Fumarate	0.26
PEP	3.38		
ATP	4.06		
ADP	2.44		

## B.2 Model simulation with steady-state derived kinetic parameters (0-400 s)

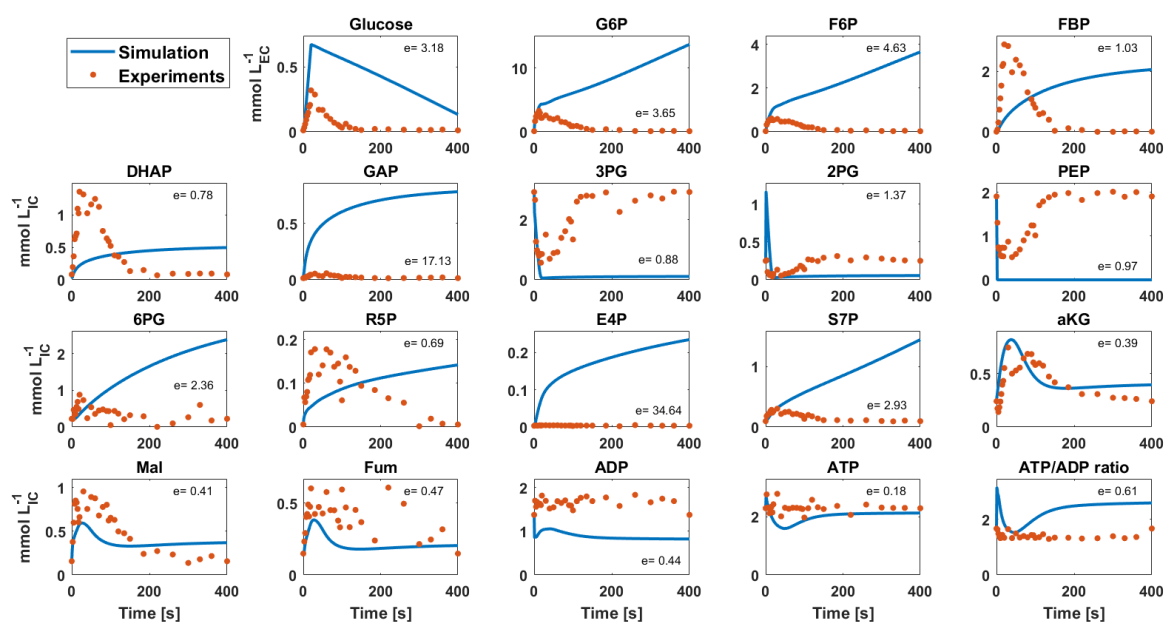


**Figure B-1** Intracellular metabolite concentrations over a feast-famine cycle. Orange dots: experimental measurements. Blue lines: **OP1** - Simulations with the Peskov model using the steady-state derived parameters. All concentrations are given in  $\text{mmol per units of intracellular volume (L)}$ , while glucose is given per units of extracellular volume. The normalized error  $e$  is given for every metabolite.

### B.3 Sets of glycolytic kinetic parameters

Different kinetic parameters, involved in the glycolytic reactions, were chosen for optimization. List A includes  $V_{\max}$  and  $K_M$  parameters of the glycolytic enzymes, List B includes only  $V_{\max}$  values and List C includes only one parameter with which all the glycolytic fluxes are multiplied.

List of reactions from the Peskov model, optimized in this work:

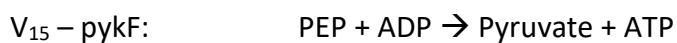


**Table B-2** List of kinetic parameters from glycolytic reactions used for model optimizations performed in this work.

List A	Reactions	List A	Reactions	List B	Reactions	List C	Reactions
$V_{pts}^*$	$V_1$	$V_{f,pgk}$	$V_{11}$	$V_{f,pgi}$	$V_5$	Fixed parameter	$V_5$
$K_{m,PEP,pts}^*$	$V_1$	$K_{m,ADP,Mg,pgk}$	$V_{11}$	$V_{mr,pfk1}$	$V_6$	-/-	$V_6$
$K_{m,Glc,pts}^*$	$V_1$	$K_{m,BPG,pgk}$	$V_{11}$	$V_{mr,pfk2}$	$V_7$	-/-	$V_8$
$V_{f,pgi}$	$V_5$	$K_{m,ATP,Mg,pgk}$	$V_{11}$	$V_{f,fba}$	$V_8$	-/-	$V_9$
$K_{m,G6P,pgi}$	$V_5$	$K_{m,PGA3,pgk}$	$V_{11}$	$V_{f,tpi}$	$V_9$	-/-	$V_{10}$
$K_{m,F6P,pgi}$	$V_5$	$V_{f,pgm}$	$V_{12}$	$V_{f,gap}$	$V_{10}$	-/-	$V_{11}$
$V_{mr,pfk1}$	$V_6$	$K_{m,PGA3,pgm}$	$V_{12}$	$V_{f,pgk}$	$V_{11}$	-/-	$V_{12}$
$K_{mr,ATP,Mg,pfk1}$	$V_6$	$K_{m,PGA2,pgm}$	$V_{12}$	$V_{f,pgm}$	$V_{12}$	-/-	$V_{13}$
$K_{mr,ADP,pfk1}$	$V_6$	$V_{f,eno}$	$V_{13}$	$V_{f,eno}$	$V_{13}$	-/-	$V_{15}$
$K_{mr,FbP,pfk1}$	$V_6$	$K_{m,PGA2,eno}$	$V_{13}$	$V_{mr,pyk1}$	$V_{15}$		
$V_{f,fba}$	$V_8$	$K_{m,PEP,eno}$	$V_{13}$				
$K_{m,FbP,fba}$	$V_8$	$V_{mr,pyk1}$	$V_{15}$				
$K_{m,GAP,fba}$	$V_8$	$K_{mr,ADP,Mg,pyk1}$	$V_{15}$				
$K_{m,DAP,fba}$	$V_8$	$K_{mr,PEP,pyk1}$	$V_{15}$				
$V_{f,tpi}$	$V_9$						
$K_{m,DAP,tpi}$	$V_9$						
$K_{m,GAP,tpi}$	$V_9$						
$V_{f,gap}$	$V_{10}$						
$K_{m,GAP,gap}$	$V_{10}$						
$K_{m,NAD,gap}$	$V_{10}$						
$K_{m,BPG,gap}$	$V_{10}$						
$K_{m,NADH,gap}$	$V_{10}$						

\* When the PWA uptake rate was used as input in the model, it replaced  $V_1$  and therefore these parameters were not part of the simulations.

## B.4 Optimization strategies MP1 – MP9

**Table B-3** Initial (steady-state derived) and optimized glycolytic kinetic parameters. All rates  $V$  are given in  $\text{mmol}\cdot\text{Lic}^{-1}\cdot\text{min}^{-1}$  and  $K$  values are given in  $\text{mmol}\cdot\text{Lic}^{-1}$ . Values shown in **blue** are higher than their steady-state value, while the ones in **red** are lower.

Parameters	Initial	MP1	MP2	MP3	MP4	MP5	MP6	MP9
$V_{\text{pts}}$	22.0	10.9		10.4		14.1		
$K_{\text{m,PEP,pts}}$	$10^{-5}$	$1.6\cdot 10^{-6}$		$3.2\cdot 10^{-6}$		$1.5\cdot 10^{-5}$		
$K_{\text{m,Glc,pts}}$	0.18	$2.8\cdot 10^{-5}$		0.58		0.14		
$V_{\text{f,pgi}}$	57.0	93.9	501	62.4		93.8	43.1	
$K_{\text{m,G6P,pgi}}$	1.0	0.42		0.94		0.33		
$K_{\text{m,F6P,pgi}}$	0.15	0.16		0.04		0.22		
$V_{\text{mr,pfk1}}$	2.6	30.7	27.5	3.4		0.70	0.37	
$K_{\text{mr,ATP,Mg,pfk1}}$	$8\cdot 10^{-5}$	$6.6\cdot 10^{-8}$		$8.2\cdot 10^{-5}$		$1.2\cdot 10^{-4}$		
$K_{\text{mr,ADP,pfk1}}$	0.69	2.1		0.75		0.71		
$K_{\text{mr,FbP,pfk1}}$	10.0	1.4		8.8		9.4		
$V_{\text{f,fba}}$	437	76.6	18.1	454		235	542	
$K_{\text{m,FbP,fba}}$	0.06	0.02		0.07		0.06		
$K_{\text{m,GAP,fba}}$	0.13	0.05		0.01		0.15		
$K_{\text{m,DAP,fba}}$	0.13	0.02		0.06		0.13		
$V_{\text{f,tpi}}$	510	1486	248	454		562	1288	
$K_{\text{m,DAP,tpi}}$	0.01	0.02		0.01		0.01		
$K_{\text{m,GAP,tpi}}$	0.01	$8.2\cdot 10^{-4}$		0.01		0.01		
$V_{\text{f,gap}}$	50.0	557	825	101		9.1	0.02	
$K_{\text{m,GAP,gap}}$	0.89	0.17		0.27		1.3		
$K_{\text{m,NAD,gap}}$	0.05	0.02		0.05		0.03		
$K_{\text{m,BPG,gap}}$	0.20	0.32		0.18		0.24		
$K_{\text{m,NADH,gap}}$	0.01	$5.4\cdot 10^{-4}$		0.01		0.01		
$V_{\text{f,pgk}}$	111	74.3	478	70.3		111	208	
$K_{\text{m,ADP,Mg,pgk}}$	0.20	$5.6\cdot 10^{-4}$		0.27		0.21		
$K_{\text{m,BPG,pgk}}$	0.02	$2.5\cdot 10^{-3}$		0.02		0.02		
$K_{\text{m,ATP,Mg,pgk}}$	0.48	0.38		0.60		0.44		
$K_{\text{m,PGA3,pgk}}$	1.3	2.2		0.47		1.4		
$V_{\text{f,pgm}}$	309	236	7013	401		555	621	
$K_{\text{m,PGA3,pgm}}$	0.19	0.37		0.25		0.27		
$K_{\text{m,PGA2,pgm}}$	0.20	0.09		$5.3\cdot 10^{-6}$		0.11		
$V_{\text{f,eno}}$	23.0	109	99.0	8.3		$2.8\cdot 10^{-7}$	4.3	
$K_{\text{m,PGA2,eno}}$	0.10	$2.7\cdot 10^{-4}$		0.13		0.10		
$K_{\text{m,PEP,eno}}$	0.10	0.01		0.11		0.13		
$V_{\text{mr,pyk1}}$	563	534	6314	859		535	1434	
$K_{\text{mr,ADP,Mg,pyk1}}$	2.8	0.14		3.4		2.7		
$K_{\text{mr,PEP,pyk1}}$	$10^{-6}$	$1.6\cdot 10^{-6}$		$1.4\cdot 10^{-5}$		$1.3\cdot 10^{-5}$		
$V_{\text{mr,pfk2}}$	500		808				971	
Parameter (List C)	1				3530			3945

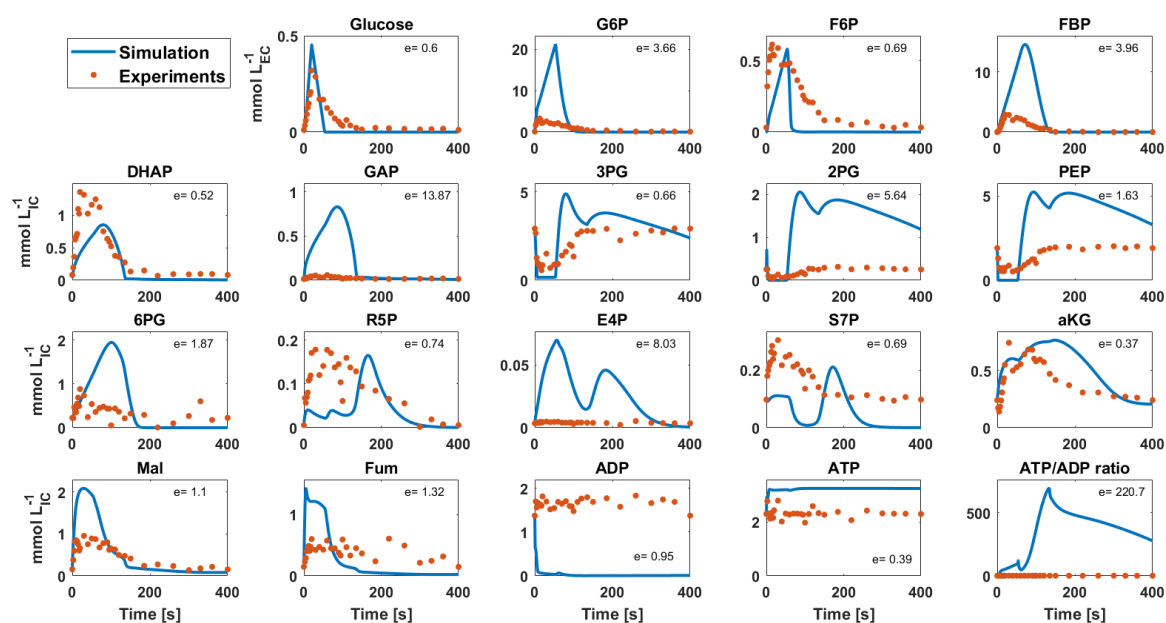


**Figure B-2** Optimization strategy **MP1**: Intracellular metabolite concentrations over a feast-famine cycle. Orange dots: experimental measurements. Blue lines: Simulations with the Peskov model. All concentrations are given in mmol per units of intracellular volume (L), while glucose is given per units of extracellular volume. The normalized error  $e$  is given for every metabolite.

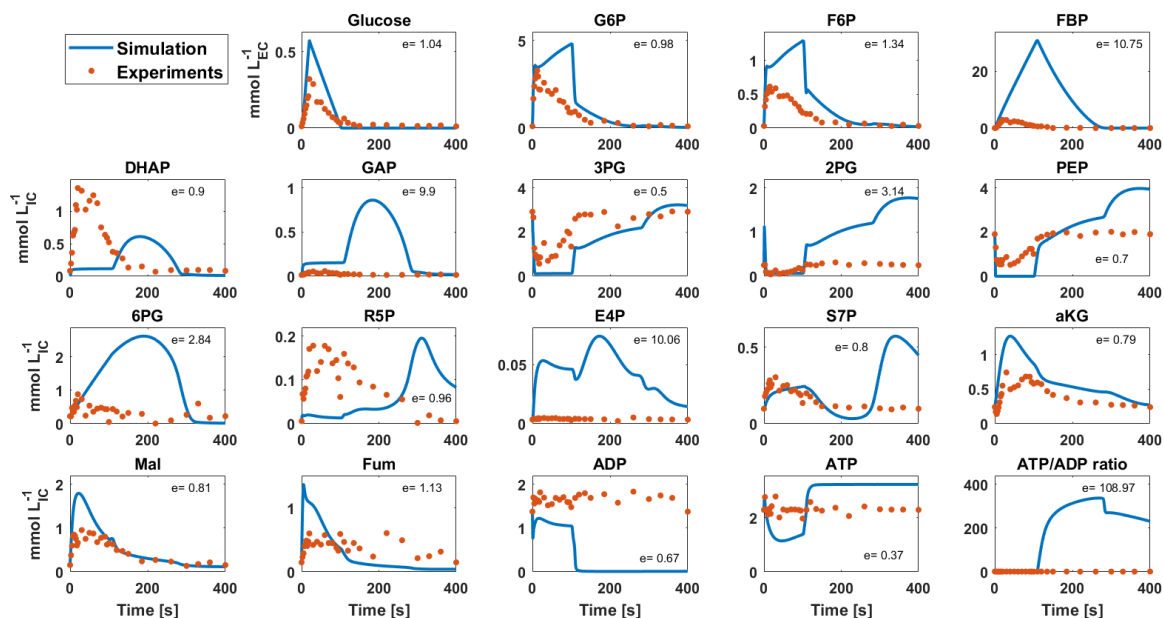


**Figure B-3** Optimization strategy **MP2**: Intracellular metabolite concentrations over a feast-famine cycle. Orange dots: experimental measurements. Blue lines: Simulations with the Peskov model. All concentrations are given in mmol per units of intracellular volume (L), while glucose is given per units of extracellular volume. The normalized error  $e$  is given for every metabolite.

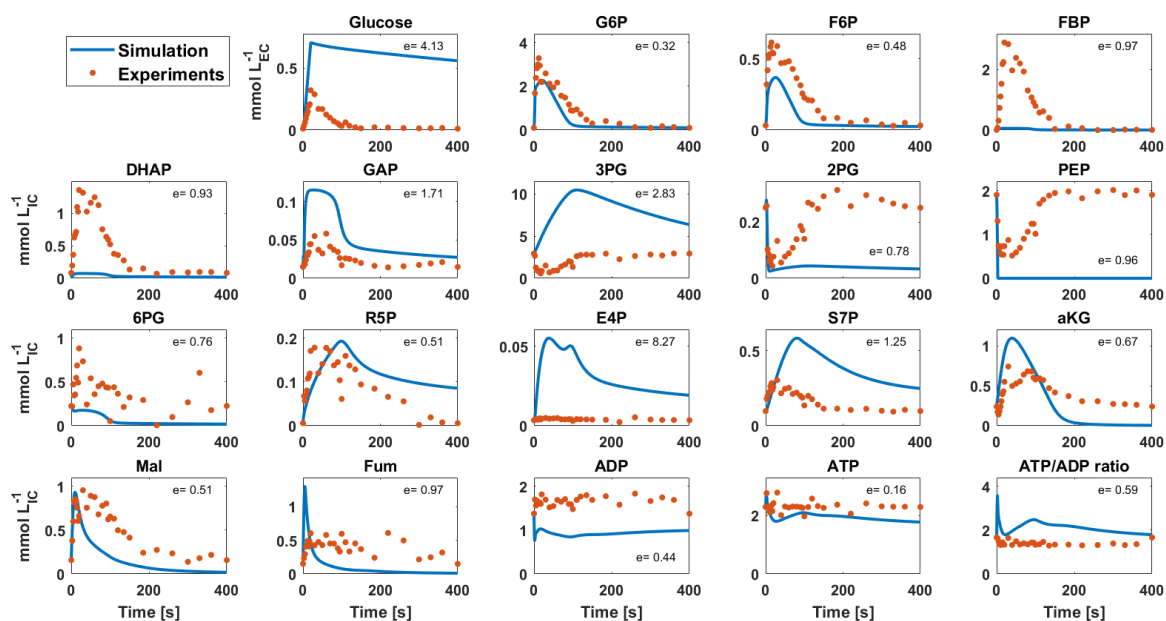


**Figure B-4** Optimization strategy **MP3**: Intracellular metabolite concentrations over a feast-famine cycle. Orange dots: experimental measurements. Blue lines: Simulations with the Peskov model. All concentrations are given in  $\text{mmol}$  per units of intracellular volume ( $L$ ), while glucose is given per units of extracellular volume. The normalized error  $e$  is given for every metabolite.

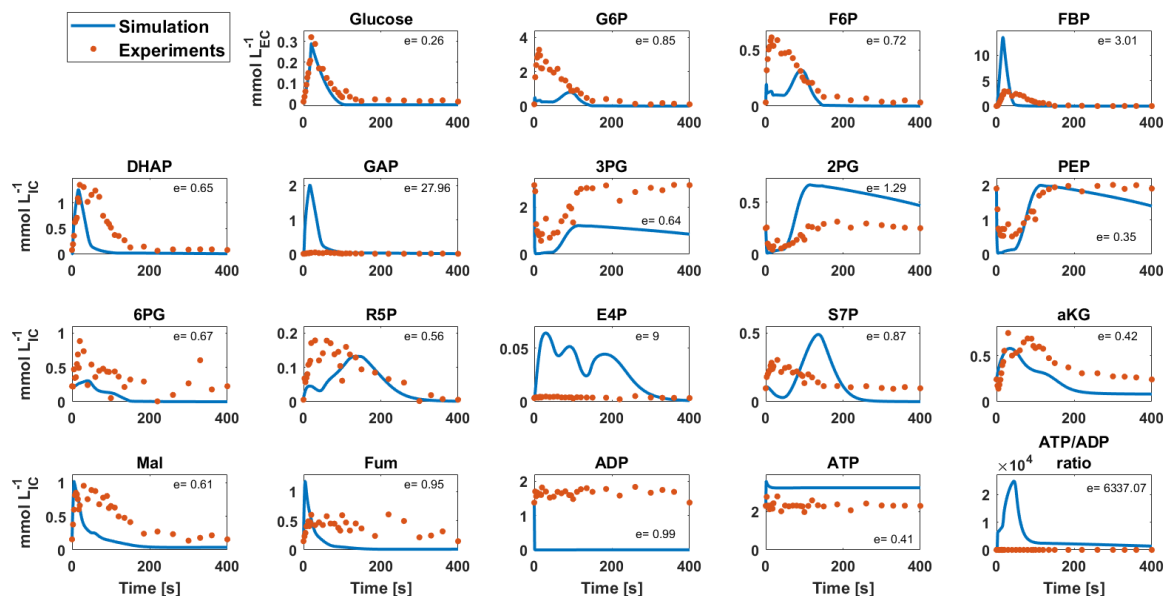


**Figure B-5** Optimization strategy **MP4**: Intracellular metabolite concentrations over a feast-famine cycle. Orange dots: experimental measurements. Blue lines: Simulations with the Peskov model. All concentrations are given in  $\text{mmol}$  per units of intracellular volume ( $L$ ), while glucose is given per units of extracellular volume. The normalized error  $e$  is given for every metabolite.

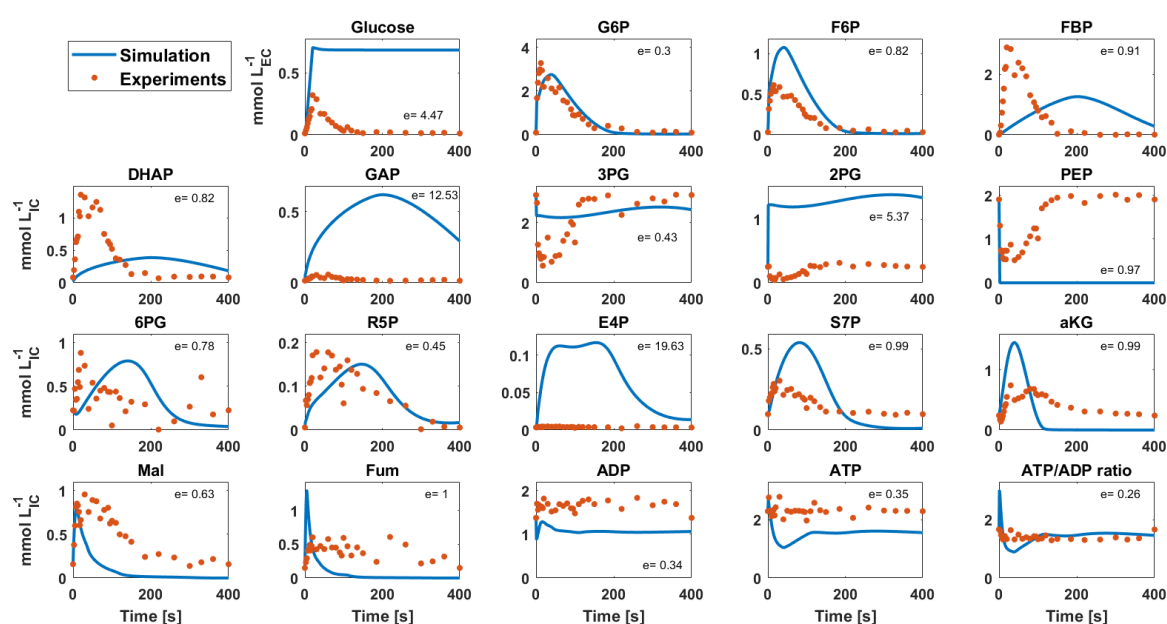


**Figure B-6** Optimization strategy **MP5**: Intracellular metabolite concentrations over a feast-famine cycle. Orange dots: experimental measurements. Blue lines: Simulations with the Peskov model. All concentrations are given in mmol per units of intracellular volume (L), while glucose is given per units of extracellular volume. The normalized error  $e$  is given for every metabolite.

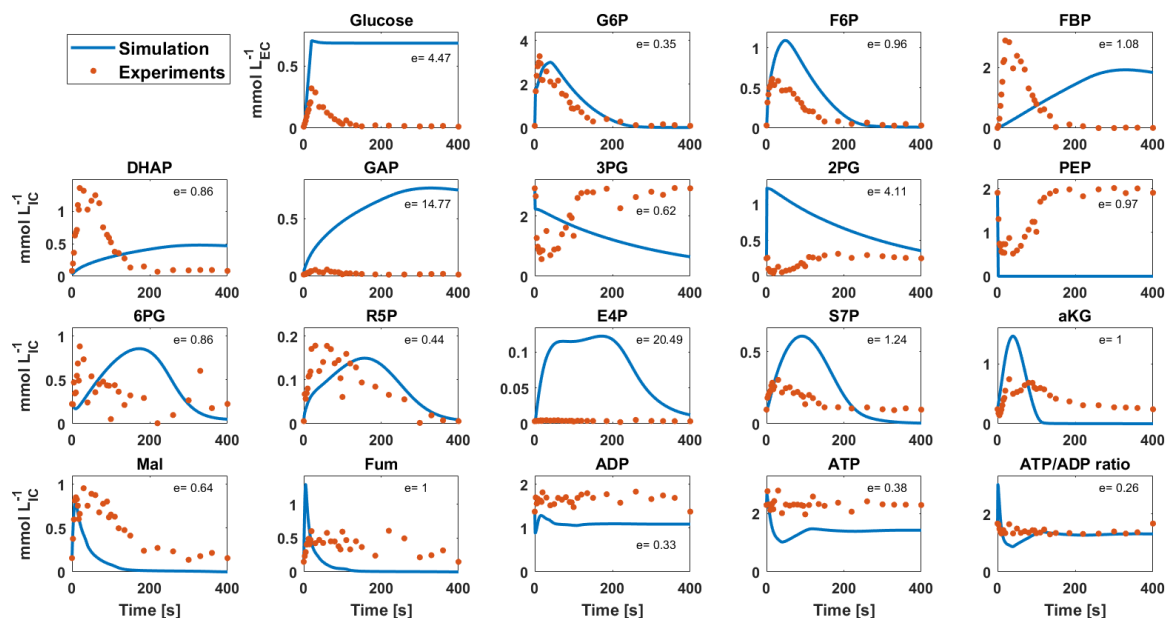


**Figure B-7** Optimization strategy **MP6**: Intracellular metabolite concentrations over a feast-famine cycle. Orange dots: experimental measurements. Blue lines: Simulations with the Peskov model. All concentrations are given in mmol per units of intracellular volume (L), while glucose is given per units of extracellular volume. The normalized error  $e$  is given for every metabolite.

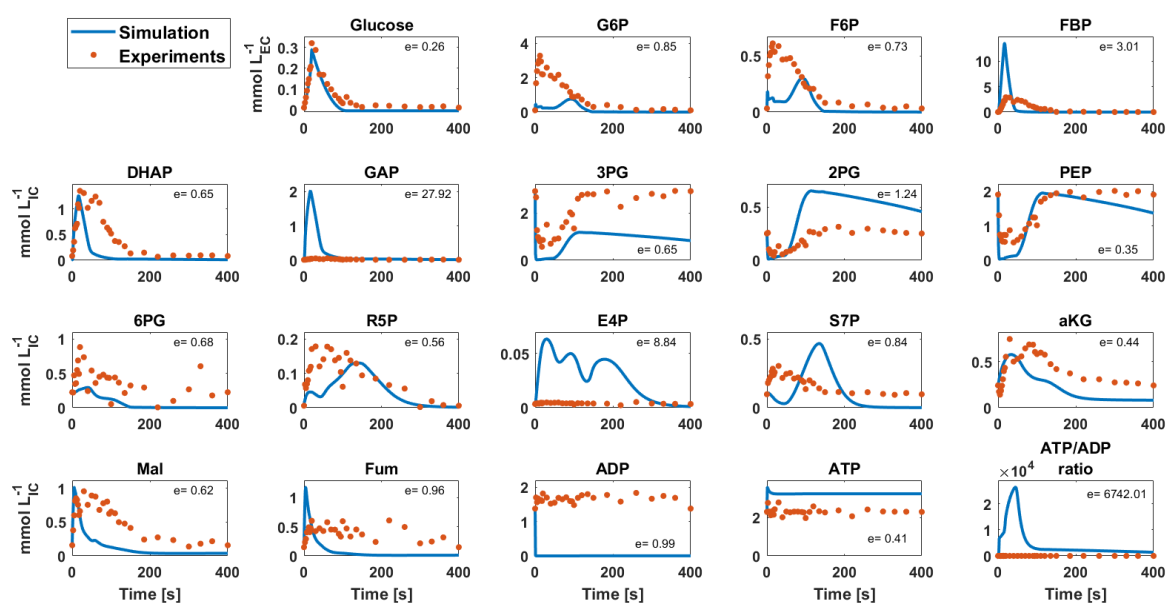


**Figure B-8** Optimization strategy **MP9**: Intracellular metabolite concentrations over a feast-famine cycle. Orange dots: experimental measurements. Blue lines: Simulations with the Peskov model. All concentrations are given in mmol per units of intracellular volume (L), while glucose is given per units of extracellular volume. The normalized error  $e$  is given for every metabolite.

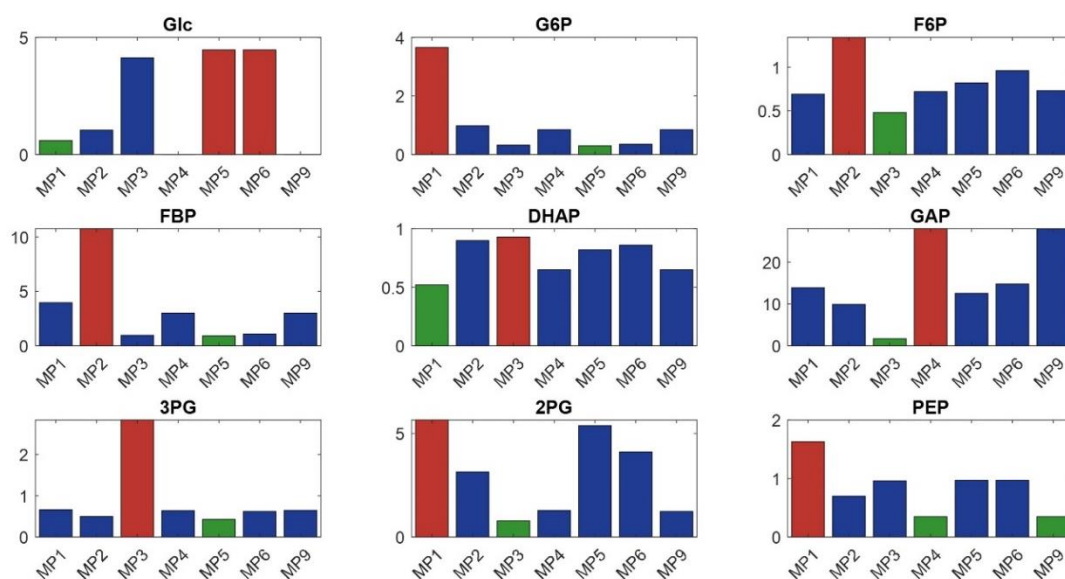


**Figure B-9** Normalized error ( $e$ ) values plotted for every glycolytic metabolite, as calculated in the optimization strategies MP1 – MP9. The green bars represent the lower values for the respective metabolite (i.e. the best reproduction of experimental observations), while the red bars represent the maximum values (i.e. least accurate reproduction). For glucose the PWA uptake rate was used as input for the strategies MP4 and MP9, so the respective  $e$  values are not included in the comparison.



## B.5 Optimization strategies MP10-MP18

**Table B-4** Initial (steady-state derived) and optimized glycolytic kinetic parameters. All rates  $V$  are given in  $\text{mmol}\cdot\text{Lic}^{-1}\cdot\text{min}^{-1}$  and  $K$  values are given in  $\text{mmol}\cdot\text{Lic}^{-1}$ . Values shown in **blue** are higher than their steady-state value, while the ones in **red** are lower.

Parameters	Initial	MP10	MP11	MP12	MP13	MP14	MP15	MP17
$V_{\text{pts}}$	22.0	1.8	11.2			58.4	23.0	
$K_{\text{m,PEP,pts}}$	$10^{-5}$	$2.3\cdot 10^{-5}$	$1.2\cdot 10^{-5}$			$2.7\cdot 10^{-5}$	$9.8\cdot 10^{-6}$	
$K_{\text{m,Glc,pts}}$	0.18	1.03	0.23			0.53	0.18	
$V_{\text{f,pgi}}$	57.0	3.4	70.8	331	2.4	528	77.9	68.9
$K_{\text{m,G6P,pgi}}$	1.0	0.41	0.15			1.6	1.4	
$K_{\text{m,F6P,pgi}}$	0.15	0.36	0.13			0.09	0.22	
$V_{\text{mr,pfk1}}$	2.6	1.7	1.9	0.30	1.7	$2.6\cdot 10^{-4}$	$8.7\cdot 10^{-7}$	36.3
$K_{\text{mr,ATP,Mg,pfk1}}$	$8\cdot 10^{-5}$	$2.6\cdot 10^{-4}$	$1.1\cdot 10^{-4}$			$9.9\cdot 10^{-5}$	$8.0\cdot 10^{-5}$	
$K_{\text{mr,ADP,pfk1}}$	0.69	0.53	1.5			1.1	0.78	
$K_{\text{mr,FbP,pfk1}}$	10.0	12.5	13.5			26.9	9.6	
$V_{\text{f,fba}}$	437	147	552	1340	115	219	379	2206
$K_{\text{m,FbP,fba}}$	0.06	$2.4\cdot 10^{-6}$	0.12			0.13	0.06	
$K_{\text{m,GAP,fba}}$	0.13	0.09	0.12			0.12	0.14	
$K_{\text{m,DAP,fba}}$	0.13	$2.6\cdot 10^{-3}$	0.28			0.02	0.16	
$V_{\text{f,tpi}}$	510	3569	547	1876	228	530	536	58.1
$K_{\text{m,DAP,tpi}}$	0.01	0.01	$1.5\cdot 10^{-4}$			0.05	0.01	
$K_{\text{m,GAP,tpi}}$	0.01	$5.4\cdot 10^{-4}$	$5.3\cdot 10^{-4}$			0.02	0.01	
$V_{\text{f,gap}}$	50.0	402	152	11.5	664	39.2	$4.7\cdot 10^{-6}$	3731
$K_{\text{m,GAP,gap}}$	0.89	0.01	1.3			0.32	1.3	
$K_{\text{m,NAD,gap}}$	0.05	$9.9\cdot 10^{-4}$	0.04			0.03	0.05	
$K_{\text{m,BPG,gap}}$	0.20	$6.6\cdot 10^{-4}$	0.12			0.03	0.22	
$K_{\text{m,NADH,gap}}$	0.01	$5.2\cdot 10^{-3}$	0.01			$3.9\cdot 10^{-4}$	0.01	
$V_{\text{f,pgk}}$	111	24.2	73.3	208	110	108	114	29.8
$K_{\text{m,ADP,Mg,pgk}}$	0.20	0.07	0.20			0.10	0.23	
$K_{\text{m,BPG,pgk}}$	0.02	$2.7\cdot 10^{-3}$	0.02			$2.0\cdot 10^{-3}$	0.02	
$K_{\text{m,ATP,Mg,pgk}}$	0.48	0.36	0.40			0.21	0.48	
$K_{\text{m,PGA3,pgk}}$	1.3	0.87	$6.1\cdot 10^{-5}$			1.3	1.2	
$V_{\text{f,pgm}}$	309	197	221	673	40.9	8.2	289	32.2
$K_{\text{m,PGA3,pgm}}$	0.19	0.01	0.24			0.08	0.17	
$K_{\text{m,PGA2,pgm}}$	0.20	0.02	0.12			0.13	0.21	
$V_{\text{f,eno}}$	23.0	25.9	$3.6\cdot 10^{-6}$	$1.8\cdot 10^{-7}$	52.1	5.0	16.6	72.1
$K_{\text{m,PGA2,eno}}$	0.10	$2.2\cdot 10^{-3}$	0.04			$1.7\cdot 10^{-7}$	0.09	
$K_{\text{m,PEP,eno}}$	0.10	$4.5\cdot 10^{-3}$	0.15			0.21	0.11	
$V_{\text{mr,pyk1}}$	563	147	416	132	3910	350	578	4200
$K_{\text{mr,ADP,Mg,pyk1}}$	2.8	15.1	1.8			0.13	2.9	
$K_{\text{mr,PEP,pyk1}}$	$10^{-6}$	$1.1\cdot 10^{-5}$	$1.3\cdot 10^{-5}$			$5.4\cdot 10^{-6}$	$1.1\cdot 10^{-5}$	
$V_{\text{mr,pfk2}}$	500			455	1609			1375

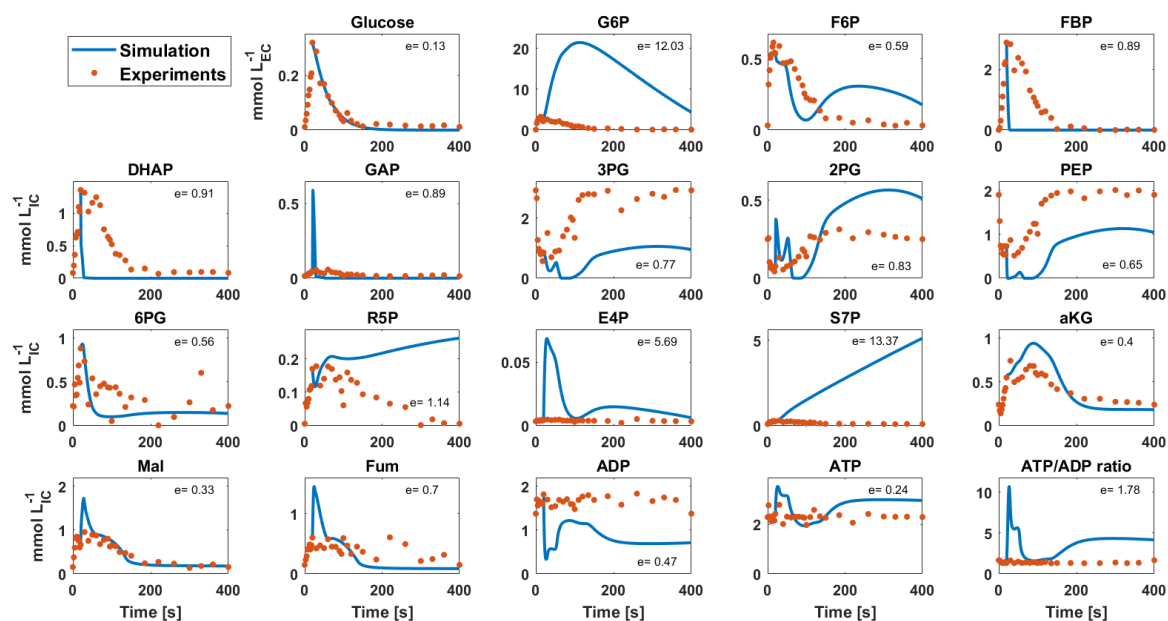


**Figure B-10** Optimization strategy **MP10**: Intracellular metabolite concentrations over a feast-famine cycle. Orange dots: experimental measurements. Blue lines: Simulations with the Peskov model. All concentrations are given in mmol per units of intracellular volume (L), while glucose is given per units of extracellular volume. The normalized error  $e$  is given for every metabolite.

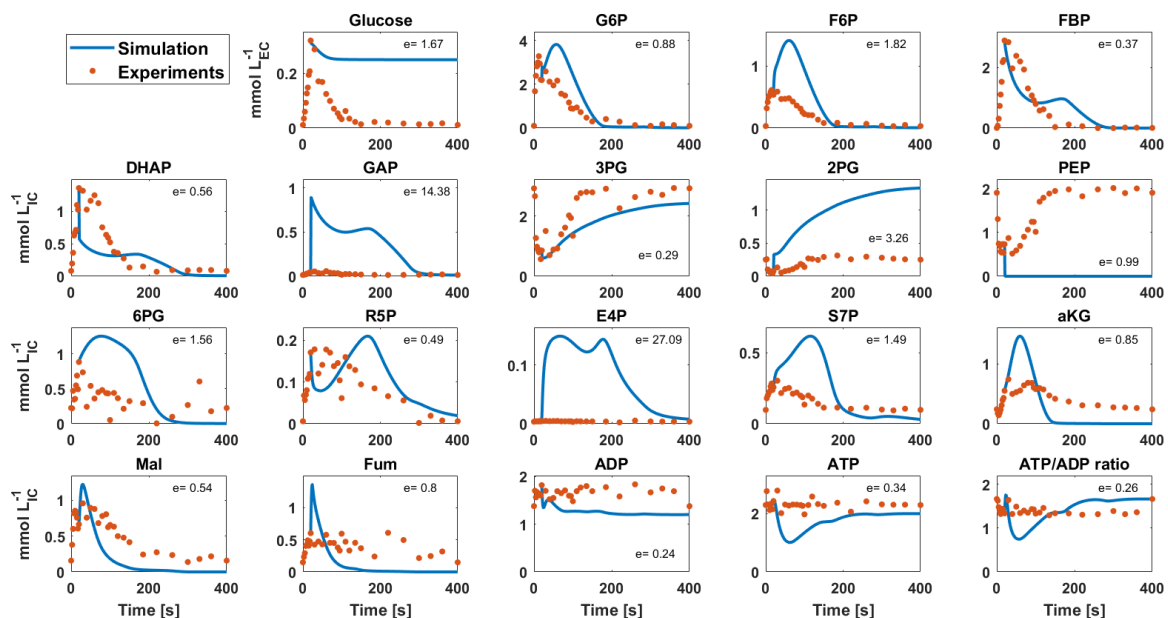


**Figure B-11** Optimization strategy **MP11**: Intracellular metabolite concentrations over a feast-famine cycle. Orange dots: experimental measurements. Blue lines: Simulations with the Peskov model. All concentrations are given in mmol per units of intracellular volume (L), while glucose is given per units of extracellular volume. The normalized error  $e$  is given for every metabolite.

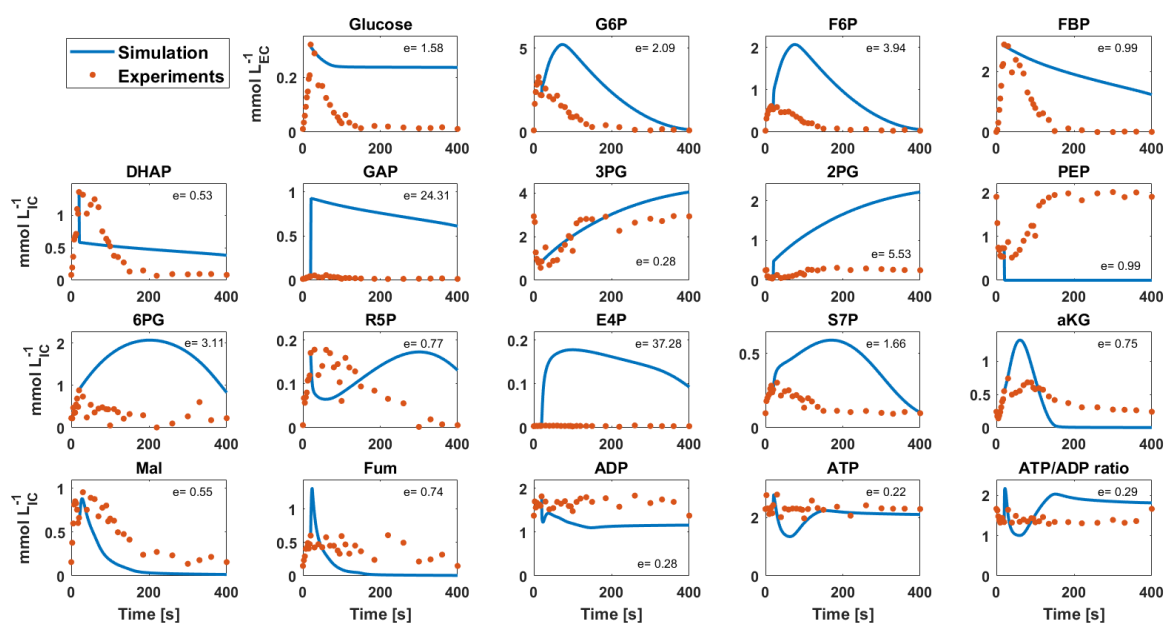


**Figure B-12** Optimization strategy **MP12**: Intracellular metabolite concentrations over a feast-famine cycle. Orange dots: experimental measurements. Blue lines: Simulations with the Peskov model. All concentrations are given in mmol per units of intracellular volume (L), while glucose is given per units of extracellular volume. The normalized error  $e$  is given for every metabolite.

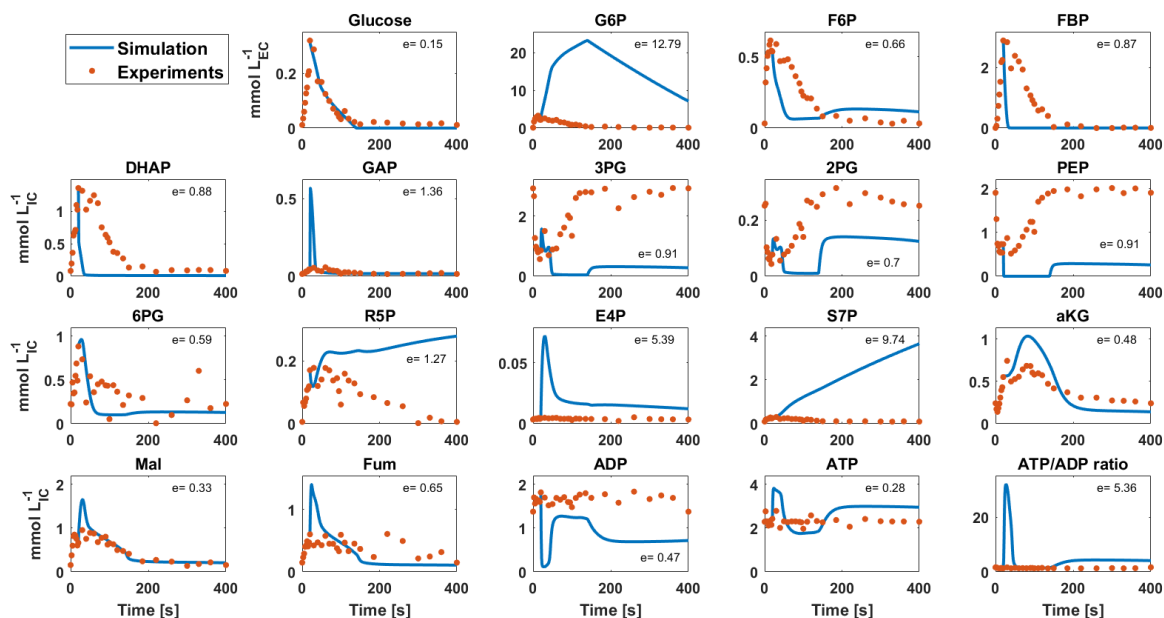


**Figure B-13** Optimization strategy **MP13**: Intracellular metabolite concentrations over a feast-famine cycle. Orange dots: experimental measurements. Blue lines: Simulations with the Peskov model. All concentrations are given in mmol per units of intracellular volume (L), while glucose is given per units of extracellular volume. The normalized error  $e$  is given for every metabolite.

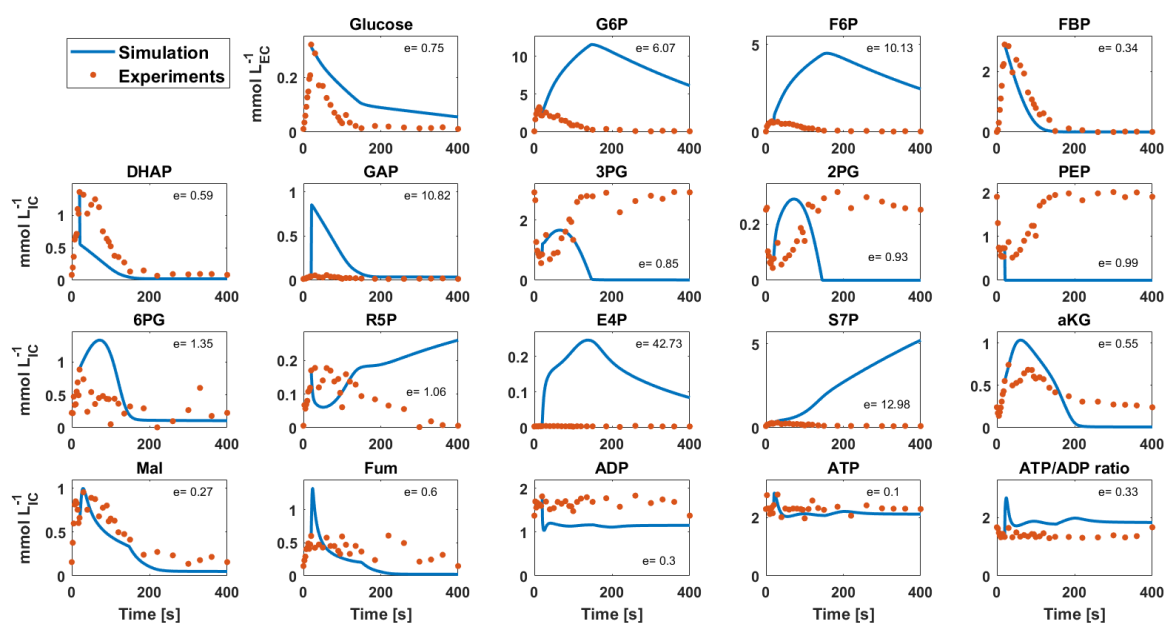


**Figure B-14** Optimization strategy **MP14**: Intracellular metabolite concentrations over a feast-famine cycle. Orange dots: experimental measurements. Blue lines: Simulations with the Peskov model. All concentrations are given in mmol per units of intracellular volume (L), while glucose is given per units of extracellular volume. The normalized error  $e$  is given for every metabolite.

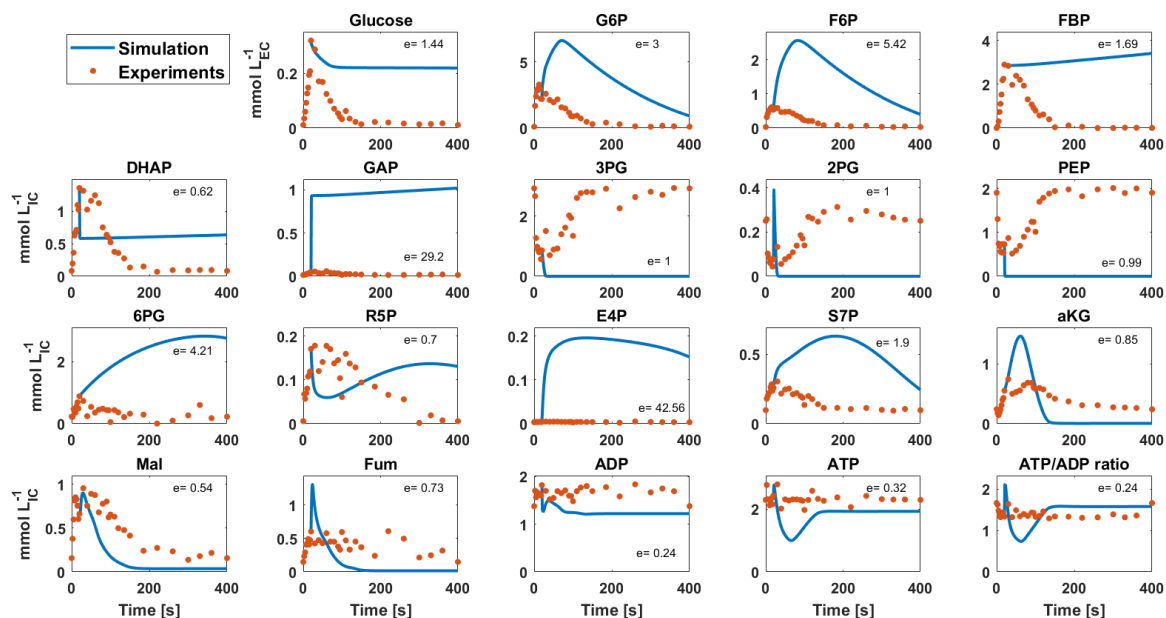


**Figure B-15** Optimization strategy **MP15**: Intracellular metabolite concentrations over a feast-famine cycle. Orange dots: experimental measurements. Blue lines: Simulations with the Peskov model. All concentrations are given in mmol per units of intracellular volume (L), while glucose is given per units of extracellular volume. The normalized error  $e$  is given for every metabolite.

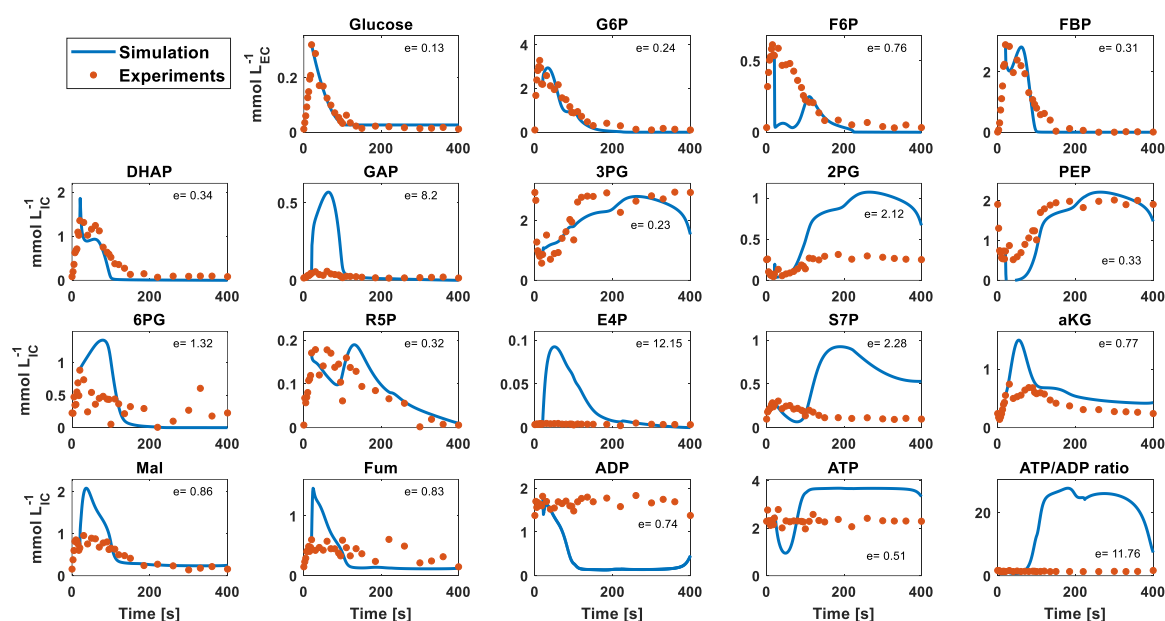


**Figure B-16** Optimization strategy **MP17**: Intracellular metabolite concentrations over a feast-famine cycle. Orange dots: experimental measurements. Blue lines: Simulations with the Peskov model. All concentrations are given in mmol per units of intracellular volume (L), while glucose is given per units of extracellular volume. The normalized error  $e$  is given for every metabolite.

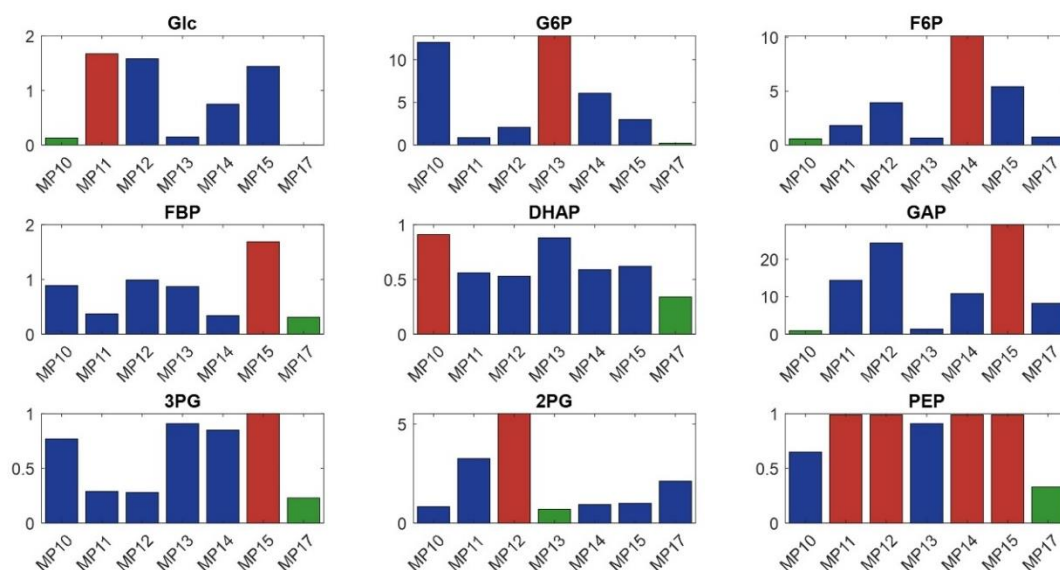


**Figure B-17** Normalized error ( $e$ ) values plotted for every glycolytic metabolite, as calculated in the optimization strategies MP10 – MP17. The green bars represent the lower values for the respective metabolite (i.e. the best reproduction of experimental observations), while the red bars represent the maximum values (i.e. least accurate reproduction). For glucose the PWA uptake rate was used as input for the MP17 strategy, so the respective  $e$  value is not included in the comparison.

## B.6 Optimization strategies MPG1-MPG4

**Table B-5** Initial (steady-state derived) and optimized glycolytic and glycogen kinetic parameters. All rates  $V$  are given in  $\text{mmol}\cdot\text{Lic}^{-1}\cdot\text{min}^{-1}$ ,  $K$  values are given in  $\text{mmol}\cdot\text{Lic}^{-1}$  and  $k_{\text{glyc}}$  in  $\text{min}^{-1}$ . Values shown in **blue** are higher than their steady-state value, while the ones in **red** are lower.

Parameters	Initial	MPG1	MPG2	MPG3	MPG4
$V_{\text{pts}}$	22.0	0.50			
$K_{\text{m,PEP,pts}}$	$10^{-5}$	$1.8\cdot 10^{-7}$			
$K_{\text{m,Glc,pts}}$	0.18	2.0			
$V_{\text{f,pgi}}$	57.0	2.0	178	122	$1.8\cdot 10^4$
$K_{\text{m,G6P,pgi}}$	1.0	0.13	1.2		
$K_{\text{m,F6P,pgi}}$	0.15	0.11	0.07		
$V_{\text{mr,pfk1}}$	2.6	0.42	7.6	1.3	217
$K_{\text{mr,ATP,Mg,pfk1}}$	$8\cdot 10^{-5}$	$1.4\cdot 10^{-6}$	$1.5\cdot 10^{-5}$		
$K_{\text{mr,ADP,pfk1}}$	0.69	0.08	0.17		
$K_{\text{mr,FbP,pfk1}}$	10.0	2.1	4.8		
$V_{\text{f,fba}}$	437	4.4	8333	571	$1.3\cdot 10^5$
$K_{\text{m,FbP,fba}}$	0.06	$9.9\cdot 10^{-7}$	0.04		
$K_{\text{m,GAP,fba}}$	0.13	$1.1\cdot 10^{-3}$	0.14		
$K_{\text{m,DAP,fba}}$	0.13	$1.9\cdot 10^{-5}$	0.35		
$V_{\text{f,tpi}}$	510	14097	162	83.2	$1.1\cdot 10^5$
$K_{\text{m,DAP,tpi}}$	0.01	$2.7\cdot 10^{-3}$	0.06		
$K_{\text{m,GAP,tpi}}$	0.01	$1.8\cdot 10^{-8}$	0.02		
$V_{\text{f,gap}}$	50.0	583	510	380	909
$K_{\text{m,GAP,gap}}$	0.89	0.01	0.07		
$K_{\text{m,NAD,gap}}$	0.05	$5.8\cdot 10^{-4}$	0.05		
$K_{\text{m,BPG,gap}}$	0.20	$4.0\cdot 10^{-5}$	0.05		
$K_{\text{m,NADH,gap}}$	0.01	$1.6\cdot 10^{-3}$	$1.8\cdot 10^{-3}$		
$V_{\text{f,pgk}}$	111	4.4	87	10.1	$2.4\cdot 10^4$
$K_{\text{m,ADP,Mg,pgk}}$	0.20	0.11	0.17		
$K_{\text{m,BPG,pgk}}$	0.02	$3.8\cdot 10^{-3}$	0.01		
$K_{\text{m,ATP,Mg,pgk}}$	0.48	$1.1\cdot 10^{-3}$	0.04		
$K_{\text{m,PGA3,pgk}}$	1.3	1.8	0.39		
$V_{\text{f,pgm}}$	309	418	234	223	$9.9\cdot 10^4$
$K_{\text{m,PGA3,pgm}}$	0.19	$4.4\cdot 10^{-3}$	0.22		
$K_{\text{m,PGA2,pgm}}$	0.20	$1.6\cdot 10^{-6}$	$3.2\cdot 10^{-3}$		
$V_{\text{f,eno}}$	23.0	1.3	1460	13.2	1613
$K_{\text{m,PGA2,eno}}$	0.10	$1.3\cdot 10^{-4}$	$5.2\cdot 10^{-6}$		
$K_{\text{m,PEP,eno}}$	0.10	0.02	$3.7\cdot 10^{-3}$		
$V_{\text{mr,pyk1}}$	563	1615	3450	769	3533
$K_{\text{mr,ADP,Mg,pyk1}}$	2.8	$3.7\cdot 10^{-4}$	2.5		
$K_{\text{mr,PEP,pyk1}}$	$10^{-6}$	$1.5\cdot 10^{-4}$	$5.6\cdot 10^{-6}$		
$V_{\text{mr,pfk2}}$	500			131	$2.4\cdot 10^5$
$k_{\text{glyc}}$	-	1.7	6.3	5.3	44

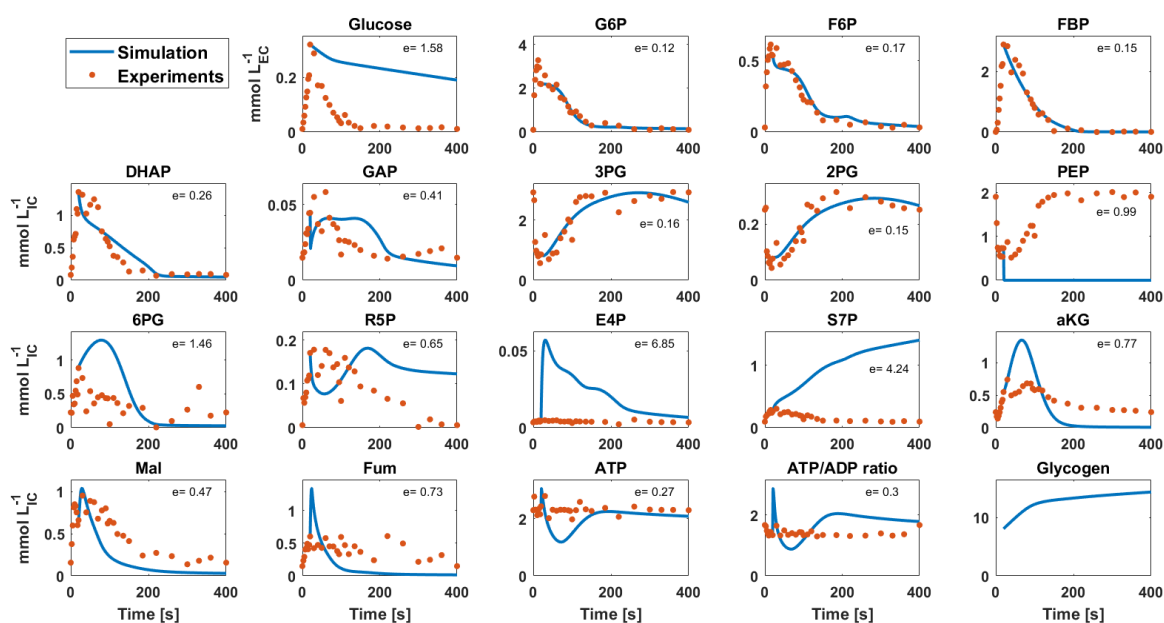


**Figure B-18** Optimization strategy **MPG1**: Intracellular metabolite concentrations over a feast-famine cycle. Orange dots: experimental measurements. Blue lines: Simulations with the extended Peskov model. All concentrations are given in mmol per units of intracellular volume (L), while glucose is given per units of extracellular volume. The normalized error  $e$  is given for every metabolite.

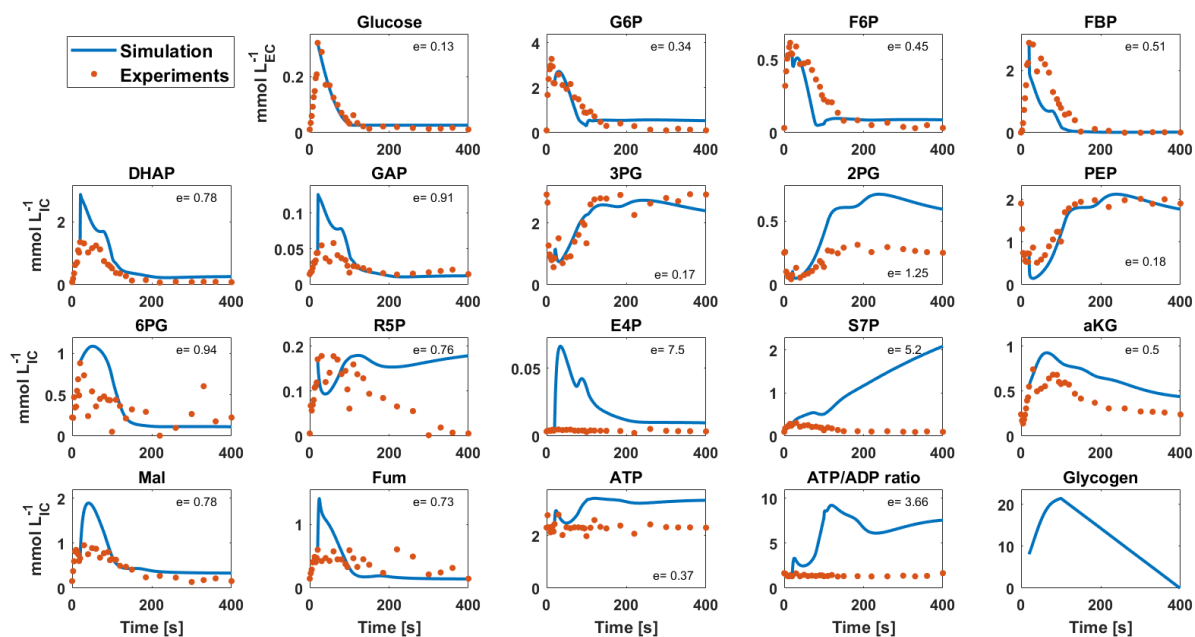


**Figure B-19** Optimization strategy **MPG2**: Intracellular metabolite concentrations over a feast-famine cycle. Orange dots: experimental measurements. Blue lines: Simulations with the extended Peskov model. All concentrations are given in mmol per units of intracellular volume (L), while glucose is given per units of extracellular volume. The normalized error  $e$  is given for every metabolite.

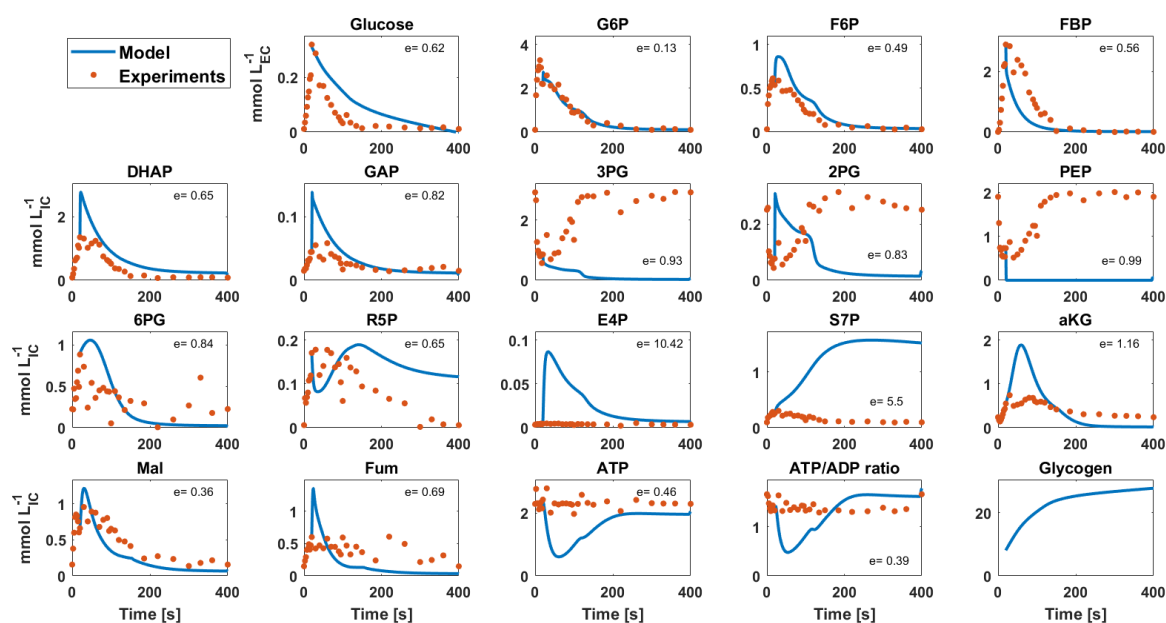


**Figure B-20** Optimization strategy **MPG3**: Intracellular metabolite concentrations over a feast-famine cycle. Orange dots: experimental measurements. Blue lines: Simulations with the extended Peskov model. All concentrations are given in mmol per units of intracellular volume (L), while glucose is given per units of extracellular volume. The normalized error  $e$  is given for every metabolite.

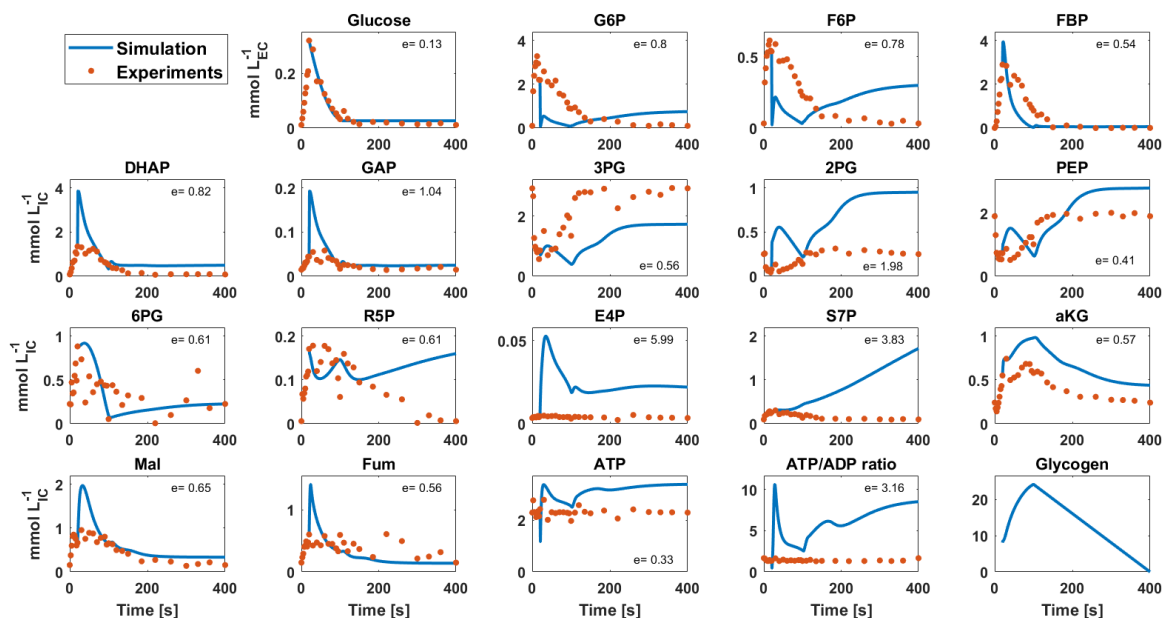


**Figure B-21** Optimization strategy **MPG4**: Intracellular metabolite concentrations over a feast-famine cycle. Orange dots: experimental measurements. Blue lines: Simulations with the extended Peskov model. All concentrations are given in mmol per units of intracellular volume (L), while glucose is given per units of extracellular volume. The normalized error  $e$  is given for every metabolite.



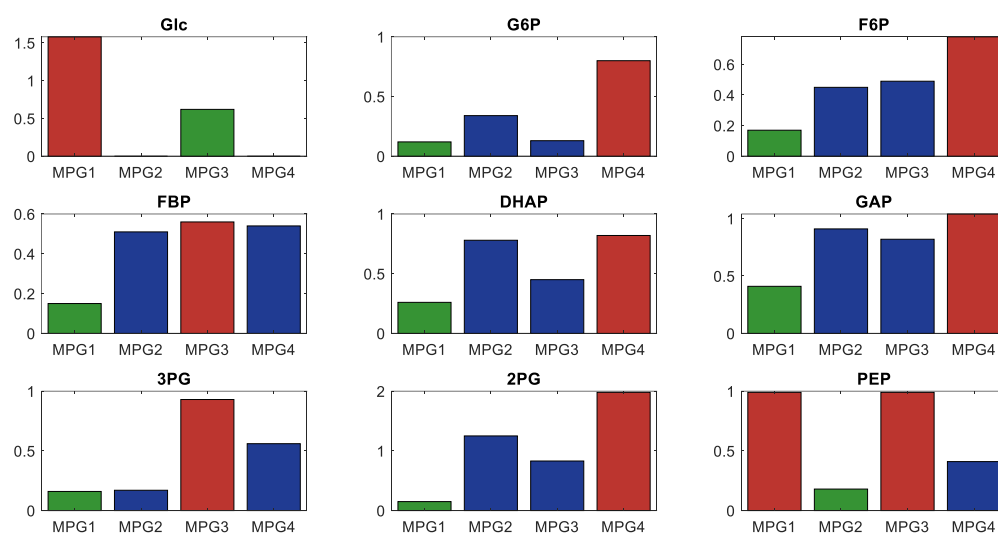


**Figure B-22** Normalized error ( $e$ ) values plotted for every glycolytic metabolite, as calculated in the optimization strategies MPG1 – MPG4. The green bars represent the lower values for the respective metabolite (i.e. the best reproduction of experimental observations), while the red bars represent the maximum values (i.e. least accurate reproduction). For glucose the PWA uptake rate was used as input for the strategies MPG2 and MPG4, so the respective  $e$  values are not included in the comparison.

## B.7 Optimization strategy MPPG1

**Table B-6** Initial (steady-state derived) and optimized glycolytic, glycogen and polyphosphate kinetic parameters. All rates  $V$  are given in  $\text{mmol}\cdot\text{L}^{-1}\cdot\text{min}^{-1}$ ,  $K$  values are given in  $\text{mmol}\cdot\text{L}^{-1}$  and  $k_{\text{glyc}}$  in  $\text{min}^{-1}$ . Values shown in **blue** are higher than their steady-state value, while the ones in **red** are lower.

Parameters	Initial	MPPG1
$V_{f,\text{pgi}}$	57.0	362
$K_{m,\text{G6P},\text{pgi}}$	1.0	2.4
$K_{m,\text{F6P},\text{pgi}}$	0.15	0.08
$V_{m,r,\text{pfk1}}$	2.6	10.9
$K_{m,r,\text{ATP},\text{Mg},\text{pfk1}}$	$8\cdot 10^{-5}$	$1.1\cdot 10^{-5}$
$K_{m,r,\text{ADP},\text{pfk1}}$	0.69	0.02
$K_{m,r,\text{FbP},\text{pfk1}}$	10.0	23.2
$V_{f,\text{fba}}$	437	26.7
$K_{m,\text{FbP},\text{fba}}$	0.06	0.11
$K_{m,\text{GAP},\text{fba}}$	0.13	0.02
$K_{m,\text{DAP},\text{fba}}$	0.13	0.24
$V_{f,\text{tpi}}$	510	630
$K_{m,\text{DAP},\text{tpi}}$	0.01	0.03
$K_{m,\text{GAP},\text{tpi}}$	0.01	$6.8\cdot 10^{-4}$
$V_{f,\text{gap}}$	50.0	1151
$K_{m,\text{GAP},\text{gap}}$	0.89	0.05
$K_{m,\text{NAD},\text{gap}}$	0.05	0.02
$K_{m,\text{BPG},\text{gap}}$	0.20	0.01
$K_{m,\text{NADH},\text{gap}}$	0.01	$2.5\cdot 10^{-4}$
$V_{f,\text{pgk}}$	111	198
$K_{m,\text{ADP},\text{Mg},\text{pgk}}$	0.20	0.05
$K_{m,\text{BPG},\text{pgk}}$	0.02	0.01
$K_{m,\text{ATP},\text{Mg},\text{pgk}}$	0.48	0.08
$K_{m,\text{PGA3},\text{pgk}}$	1.3	0.35
$V_{f,\text{pgm}}$	309	377
$K_{m,\text{PGA3},\text{pgm}}$	0.19	0.20
$K_{m,\text{PGA2},\text{pgm}}$	0.20	$2.0\cdot 10^{-3}$
$V_{f,\text{eno}}$	23.0	355
$K_{m,\text{PGA2},\text{eno}}$	0.10	$2.9\cdot 10^{-6}$
$K_{m,\text{PEP},\text{eno}}$	0.10	$2.1\cdot 10^{-3}$
$V_{m,r,\text{pyk1}}$	563	2569
$K_{m,r,\text{ADP},\text{Mg},\text{pyk1}}$	2.8	2.6
$K_{m,r,\text{PEP},\text{pyk1}}$	$10^{-6}$	$5.0\cdot 10^{-6}$
$k_{\text{glyc}}$	-	5.8
$V_{\text{max},f,\text{PolyP}}$	-	8.3
$V_{\text{max},r,\text{PolyP}}$	-	0.03
$K_{M1,\text{PolyP}}$	-	$2.0\cdot 10^{-4}$
$K_{M2,\text{PolyP}}$	-	0.02

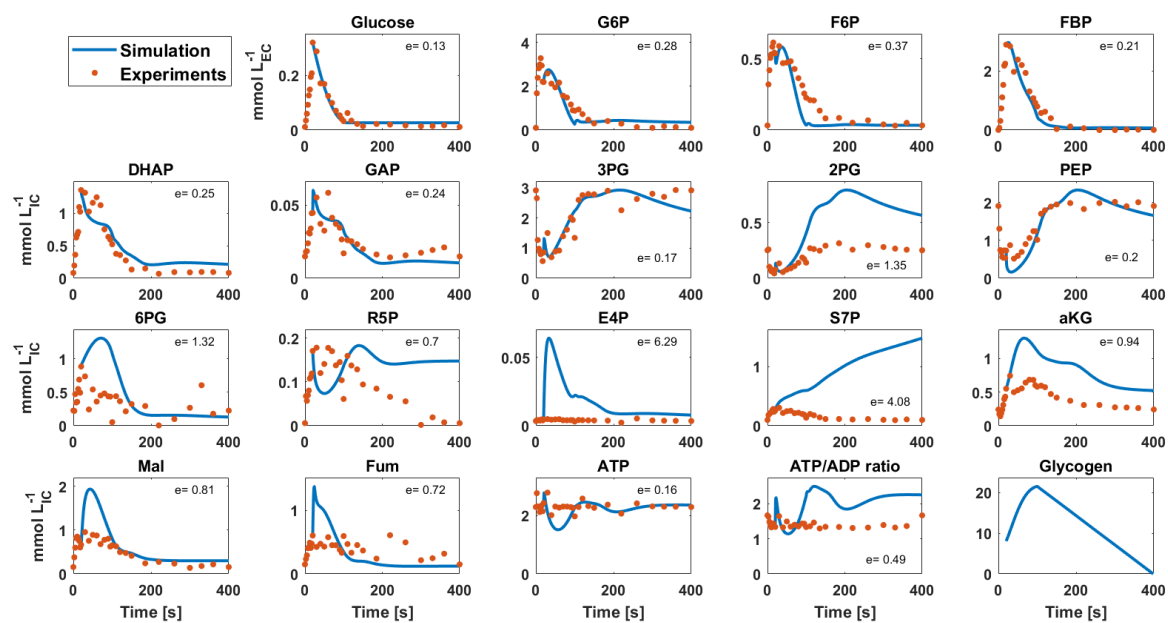


**Figure B-23** Optimization strategy **MPGP1**: Intracellular metabolite concentrations over a feast-famine cycle. Orange dots: experimental measurements. Blue lines: Simulations with the extended Peskov model. All concentrations are given in  $\text{mmol per units of intracellular volume (L)}$ , while glucose is given per units of extracellular volume. The normalized error  $e$  is given for every metabolite.





# Chapter



## Proteomic and metabolomic analysis of *Escherichia coli* adaptation strategies to substrate fluctuations

In collaboration with: M. Pabst, M.C.M. van Loosdrecht and S.A. Wahl

**Abstract**

**Background:** Microbes use intricate cellular mechanisms in order to adapt to changing extracellular environments. Physiological and metabolic analysis of the transition of *Escherichia coli* cells from reference constant feeding to block-wise feeding, combined with kinetic modelling, unveiled several potential traits of cellular adaptation (this work). Increased uptake rates, biomass yield losses, storage cycling and adenylate energy homeostasis were observed responses during the repetitive substrate gradients. To identify the origin of the cellular adaptations, a multi-omics analysis is crucial.

**Results:** In this work, shotgun cellular proteomics and  $^{13}\text{C}$ -labelled metabolomics were performed, generating new insights on cellular regulatory mechanisms when cells are subjected to fluctuations in substrate availability. The extracellular dynamics were expected to trigger global stress responses, in line with the observed reduced biomass yield. Surprisingly, a lack of significant response in stress-related proteins was observed, while the proteome adjusted for specific functional categories, including biosynthesis and translation processes (ribosomes). This can be due to either increased protein production to support the rapid growth changes, during the short time of substrate availability, or ribosome stalling due to amino acid limitation during the famine phase. During substrate-limited growth (constant feeding) cells have an overcapacity of metabolic enzymes (involved in central carbon pathways), which is used under nutrient up-shift to handle rapid increase in metabolic fluxes. The down-regulation of several enzymes in glycolysis, TCA cycle and pentose phosphate pathway, as well as, transporter proteins, revealed that cells respond more to the substrate excess period than the starvation period, during the block-wise feeding regime. This is also in accordance with the observed down-regulation of the glyoxylate-shunt enzymes. Moreover, the increased levels of polyphosphate kinase indicated the use of a polyphosphate pool as a putative buffer for energy homeostasis. Glycogen production and degradation was verified by the proteomic and  $^{13}\text{C}$  tracing analysis and is suggested to contribute to the ATP spilling (biomass yield losses), along with the increased protein turnover, which was identified by an increased section of the cellular proteasome.

**Conclusions:** Dynamic conditions caused several adjustments of cellular physiology, including increased storage and protein turnover, leading to robustness, but also reduced biomass yield. For a comprehensive description of metabolism and engineering of cells for large-scale conditions, metabolic pathways, outside the classical central carbon metabolism, have to be taken into account.

## 5.1 Introduction

Microbial adaptation to environmental changes constitutes an extensively studied topic of microbiology (for reviews see [1, 2]). The cellular responses require the coordination of various regulatory mechanisms, which control different layers of metabolism; from gene and protein expression to fluxes and cell morphology [3-9]. When an environmental perturbation is applied, the cells sense the extracellular and intracellular environment, process the signals and initiate the suitable mechanisms, which will allow them to efficiently adapt to the specific stimuli [10, 11]. Depending on the environmental change, cells have certain flux distribution requirements to ensure survival and growth. We can therefore consider that the goal of their adaptation strategies is based on providing the necessary proteins to meet these requirements [12].

In case of nutrient perturbations, occurring in bacterial natural habitats or in large-scale cultivations, cells have to regulate gene expression to achieve maximum specific growth rates, by inducing either specific catabolic operons, or global adaptation regulons [13-15]. For example, under nutrient excess the cells need to allocate their proteome in a way that high uptake and protein synthesis rates can be achieved. On the contrary, under carbon and energy limitation, the cell priority is to scavenge nutrients from alternative sources without a detrimental delay in the biomass synthesis. The increase in protein abundance comes with the cost of higher resource consumption, ribosome occupation, misfolding etc. [16, 17]. Hence, a critical challenge for the cells is the regulation of protein distribution between metabolic enzymes, ribosomes and other proteins, while maintaining proteome homeostasis [18].

The regulatory network that controls adaptation, is based on complex interactions between molecular components, such as proteins and metabolites [19]. Metabolic fluxes are the end result of the integrated multi-level (transcriptional, post-transcriptional, translational and post-translational) cellular response [20, 21]. The faster response systems consist of allosteric regulations and post-translational modifications [22], enabling short-term adaptations, while transcriptional regulation responds slower and is used for longer-term adaptation to environmental perturbations [23]. Schweder T, *et al.* [24] experimentally showed that stress gene expression in *E.coli* was induced (elevated mRNA levels) within seconds of substrate perturbations (<54 s) in a scaled-down (STR-PFR) cultivation, proving the rapid cellular capacity of gradient sensing. They also showed that mRNA levels were changing when sampling at different zones of a large-scale (30 m<sup>3</sup>) fed-batch industrial bioreactor, with mixing time estimated in timescale of seconds, while no changes were observed in the corresponding proteome, as protein translation and folding, following the gene expression



alterations, requires longer time. Thus, the time of the applied dynamics plays a major role in the adaptation strategy and responses of the cells [25].

To identify metabolic adjustments when bacteria are shifted from growth under constant substrate limitation to fluctuating substrate availability, *E.coli* cells were cultivated first under a reference constant feeding (RCF), followed by a block-wise feeding (BWF) (Chapter 3). The duration of each BWF cycle was 400 s (100 s of feast and 300 s of famine) and successive cycles were applied for at least 8 generation times. The average growth rate was  $0.048 \text{ h}^{-1}$  (same as during the RCF), and in combination with the 20 h of average doubling time in *E.coli*, shows that the perturbations were in a much shorter time scale than the generation time. The change in the feeding regime led to significant alterations in cell metabolism. More specifically we observed:

- i. Increased biomass specific substrate and oxygen consumption rates and subsequent reduced biomass yield (30%), pointing to energy spilling processes, such as intracellular recycling and/or increased maintenance (inorganic polyphosphate and glycogen as carbon storage pool / protein production and degradation). (Chapter 3 and 4)
- ii. ATP homeostasis during the BWF, potentially derived by inorganic polyphosphate synthesis and assimilation (Chapters 3 and 4)

The drastic changes observed in the cell metabolism could not be explained by enzyme kinetic mechanisms only and thus are expected to at least partially originate from proteome adjustments (Chapter 4). Two alternative scenarios may characterize the proteomic adaptation after the switch from constant to fluctuating substrate availability:

- i. No change in ribosome usage (same growth rate): Cells grow much slower than the applied perturbations (doubling time is 20 h, while the cycle length is 400 s), no large changes are expected in the average protein synthesis (ribosomes). ATP, an important substrate for protein synthesis, was constant over the whole cycle.
- ii. Peaks in growth during a cycle: The rapid changes in the metabolite pools (including amino acids), observed during every BWF cycle, influence the protein synthesis rate, i.e. protein synthesis is dynamic during the cycle and higher maximal capacities are needed (higher ribosome content).

The goal of this chapter is to identify the origins of the BWF metabolic adaptation, using cellular proteomics analysis. The putative mechanisms and the expected proteome alterations, studied in this work, are schematically presented in Figure 5.1.

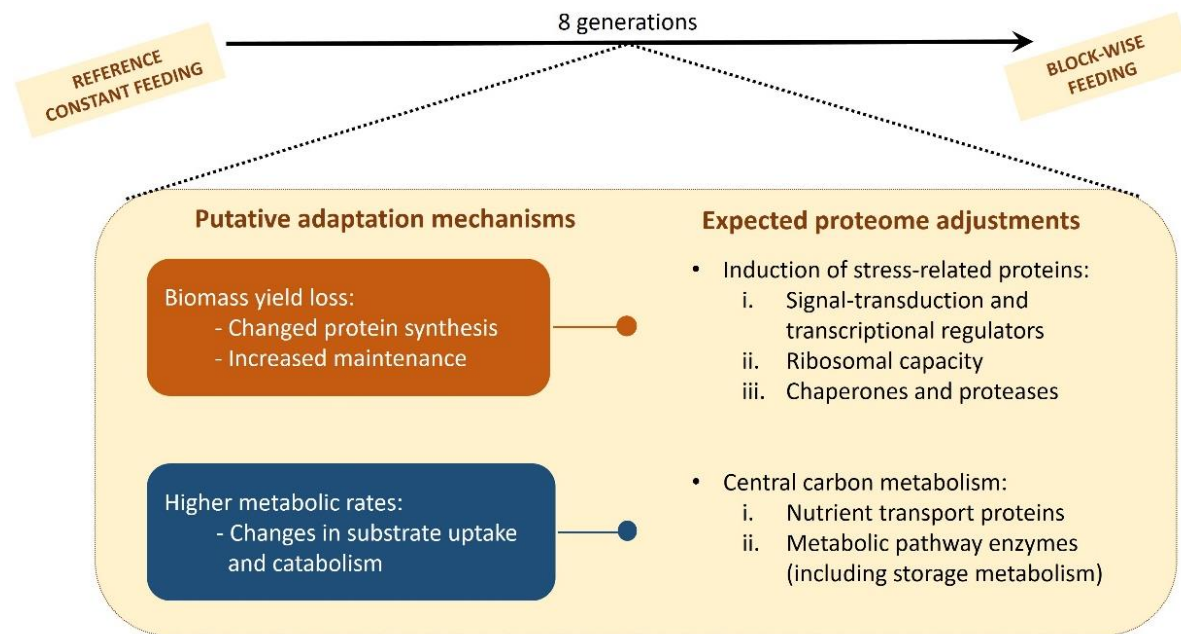


**Figure 5.1** Overview of hypotheses for cell adaptation mechanisms, during the transition from RCF to BWF and the expected responsible proteome alterations.

## 5.2 Materials and Methods

### 5.2.1 Strain and growth conditions

Samples from the experiment described in Chapter 3 were subjected to shotgun cellular proteomic analysis. The strain and all used cultivation conditions are described in sections 3.2.1-3.2.4 of Chapter 3.

Due to technical reasons, the cultivation was re-started with exactly the same conditions. Figure 5.2 shows an overlap (of several successive BWF cycles) of the CO<sub>2</sub> production rate over time, indicating the reproducibility of the cultivations. The Pearson correlation coefficient of these rates, between the two cultivations, was calculated to be 0.99 with p-value of  $6.1 \cdot 10^{-7}$ . Note that the exact value can be an overestimation due to data dependencies within the time-series [26, 27].

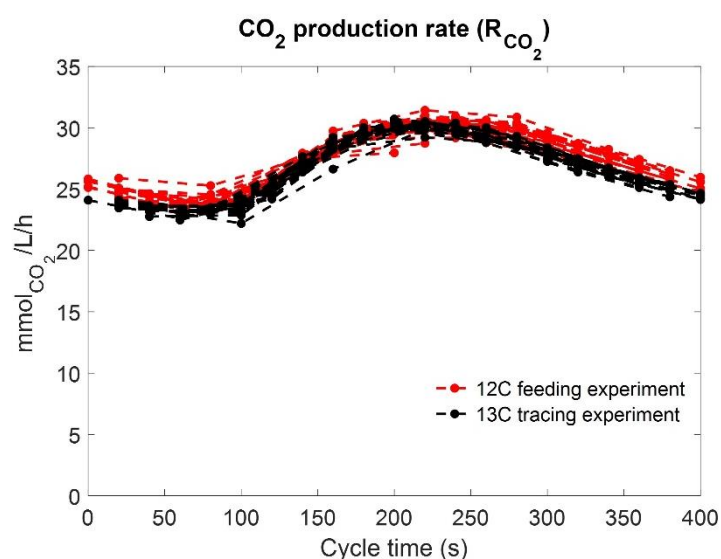


**Figure 5.2**  $\text{CO}_2$  production rate ( $\text{mmol}_{\text{CO}_2} \cdot \text{L}^{-1} \cdot \text{h}^{-1}$ ) calculated from the offgas  $\text{CO}_2$  data, over the BWF cycle time (s) for the  $^{12}\text{C}$  (red) and the  $^{13}\text{C}$  cultivations (black). Data of 10 successive cycles, after around 180 hours of the BWF, are overlapped. These rates are not corrected for delays expected due to headspace, tubing and bicarbonate in the broth.

After more than 8 generations of the BWF, the feed was switched to a medium containing U- $^{13}\text{C}$ -labelled glucose with the same concentration. The labelled medium was supplied for two consecutive BWF cycles and then switched back to the unlabelled glucose.

## 5.2.2 Proteomic analysis

### **Sampling**

For each sample, 2 mL of broth were withdrawn into a tube (eppendorf) and immediately centrifuged (Heraeus Biofuge Stratos centrifuge) at 15000 g for 5 min at  $4^\circ\text{C}$ . The supernatant was discarded and the pellet was resuspended in 1 mL of phosphate buffer (solution previously stored at  $4^\circ\text{C}$ ) and centrifuged again under the same conditions. The supernatant was discarded using a pipette and the pellet was stored at  $-80^\circ\text{C}$  until further analysis. Duplicate samples were withdrawn for every cultivation sampling time.

### **Protein extraction and digestion**

The following solutions (A-D) were used:

- A. 100 mM TEAB (triethylammonium bicarbonate buffer) (Sigma-Aldrich, St. Louis, Missouri, USA) diluted in water
- B. 50 mM TEAB (diluted in water)

- C. Lysis buffer: 200  $\mu$ L of 10% SDS denaturing agent (Sigma-Aldrich) were mixed with 1.8 mL of 100 mM TEAB. A protease inhibitor cocktail (DMSO solution, Sigma-Aldrich) was also added to the mixture (10  $\mu$ L for every 1 mL of lysis buffer).
- D. 600 mM DTT: Dithiothreitol DTT (99.5% BioUltra, Sigma-Aldrich) diluted in the 100 mM TEAB dissolution buffer.
- E. 375 mM iodoacetamide: 9 mg of iodoacetamide (Sigma-Aldrich) were dissolved in 132  $\mu$ L of 100 mM TEAB, protected from light (solution made just before use).

Lysis buffer (solution C) was added to the pellet samples (1:5 pellet to buffer volume ratio) to lyse the cells. 0.2 g of glass beads (100  $\mu$ m diameter, Sigma-Aldrich) were added, samples were vortexed and put into ice for 2 seconds. Vortexing and ice was repeated 2 more times and samples were then stored at  $-80^{\circ}\text{C}$  for 30 minutes. After freezing, samples were incubated at  $40^{\circ}\text{C}$  for 20 min to thaw and centrifuged at 14000 g for 10 min at  $4^{\circ}\text{C}$  (Heraeus Biofuge Stratos centrifuge). 100  $\mu$ L of each sample were transferred to new tubes, 5  $\mu$ L of solution D were added and samples were incubated at  $55^{\circ}\text{C}$  for 1 hour at 300 rpm. 5  $\mu$ L of solution E were added to each tube and incubated for 30 min at room temperature (protected from light). The samples were mixed with acetone (Sigma-Aldrich) ( $-20^{\circ}\text{C}$ ) (1:6 sample to acetone volume ratio) and stored at  $-20^{\circ}\text{C}$  for at least half hour (for the precipitation to proceed), followed by centrifugation at 8000 g for 10 min at  $4^{\circ}\text{C}$ . The supernatant was carefully discarded without disturbing the pellet. Samples were resuspended in 600  $\mu$ L acetone, thoroughly vortexed, centrifuged again and the supernatant was discarded. The pellets were stored at  $-20^{\circ}\text{C}$  until further analysis.

400  $\mu$ L of solution B were added to the precipitated protein pellets. Samples were incubated at  $55^{\circ}\text{C}$  (low shaking) and vortexed until the pellet was completely dissolved. 100  $\mu$ L of sample were transferred in a new eppendorf tube. Trypsin (Promega) was added (5  $\mu$ L per 100  $\mu$ g protein) and the samples were incubated overnight at  $37^{\circ}\text{C}$  and 300 rpm for digestion.

#### ***Label-free quantification (LFQ) by shotgun proteomics***

Solvents:

- A.  $\text{H}_2\text{O}$  containing 0.1% formic acid (Thermo Scientific/Fisher Chemical, Optima LC-MS grade, A117-60)
- B. 80% acetonitrile (Thermo Scientific/Fisher Chemical, Optima LC-MS grade, A955-1) in  $\text{H}_2\text{O}$  and 0.1% formic acid

An aliquot corresponding to approx. 250 ng protein digest was analysed in duplicates using an one dimensional shotgun proteomics approach [28]. The samples were analysed using a

nano-liquid-chromatography system consisting of an ESAY nano LC 1200, equipped with an Acclaim PepMap RSLC RP C18 separation column (50  $\mu\text{m}$  x 150 mm, 2 $\mu\text{m}$ ), and an QE plus Orbitrap mass spectrometer (ThermoFischer Scientific). The flow rate was maintained at 350 nL/min. Following sample loading and a wash step at 5% solvent B, a linear gradient was performed, first to 25% over 50 minutes, and further to 60% solvent B over additional 20 minutes. Finally, the separation column was equilibrated back to starting conditions. The Orbitrap acquired data from 1 to 90, using a data depended acquisition mode, thereby acquiring peptide signals from 385-1250 m/z at 70K resolution, 3e6 AGC target and 100 ms max IT. The top 10 signals were isolated at a window of 2.0 m/z and fragmented using a NCE of 28. Fragments were acquired at 17K resolution, at an AGC target of 2e5 and 75 ms max IT.

### ***Database search, label-free quantification and visualisation***

Data were mapped using the proteome database from *Escherichia coli* (downloaded from Uniprot, *E.coli* K12, July 2018) using PEAKS Studio 8.5 (Bioinformatics Solutions Inc.) [29], allowing for 20 ppm parent ion and 0.02 m/z fragment ion mass error, 2 missed cleavages, carbamidomethylation as fixed and methionine oxidation and N/Q deamidation as variable modifications. Peptide spectrum matches were filtered against 1% false discovery rate (FDR) and protein identifications with  $\geq 2$  unique peptides were accepted. Changes in protein abundances between conditions were further evaluated using the label free quantification (LFQ) option provided by the PEAKS Q software tool (Bioinformatics Solutions Inc.). A pairwise comparison of the above mentioned conditions was performed on identified peptide spectra filtered against 1% FDR, a mass error equal or less 12.5 ppm and a maximum RT shift between runs of 2.5 minutes. Peptides with variable modifications were excluded. The significance method was set to ANOVA with a significance level threshold of  $\geq 15$  (significance level =  $-10\log(p)$ ), 1.5 fold change and 2 unique peptides per protein.

### **5.2.3 Metabolomic isotopologue analysis**

#### ***Sampling***

For intracellular mass isotopomer enrichment quantification, rapid sampling over three consecutive feast-famine cycles was performed. 1.5 mL of broth was withdrawn from the reactor into a tube filled with 7.5 mL aqueous methanol quenching solution (60% v/v) at -40°C, to rapidly stop metabolic activity. The sample was immediately vortexed to ensure homogeneity, centrifuged for 5 min, at 1500 g, at -19°C (Heraeus Biofuge Stratos centrifuge) and the supernatant was discarded. For the extraction of metabolites from the pellet, 7.5 mL of aqueous ethanol solution (75% v/v), preheated at 70°C, were added to the sample and the tube was then placed into a water bath at 95°C for 4 minutes. After the boiling extraction, the sample was immediately cooled down to -40°C in a cryostat.

The ethanol-water mixture in all samples was then evaporated in a Rapid-Vap (Labconco, MO, USA) at 30°C, under vacuum. The dried sediment was resuspended in 600 µL Milli-Q water, vortexed and transferred to eppendorf tubes. The samples were centrifuged at 15000 g for 5 minutes at 1°C (Heraeus Biofuge Stratos centrifuge). The supernatants were transferred to new empty tubes and centrifuged again under the same conditions. The supernatant was stored in screw-cap vials, at -80°C, until further analysis.

### Analytical methods

The metabolite mass isotopomer samples were then analysed by GC-MS/MS, GC-MS and LC-MS/MS. The techniques are described in section 3.2.5 (Chapter 3), for metabolites of central carbon pathways and amino acids. The data were corrected for the natural stable mass isotopes, using the MS correction tool, as established by Wahl SA, *et al.* [30].

## 5.3 Results

The physiological changes of *Escherichia coli* cells switched from a RCF to a BWF regime were characterized by an increase in the biomass specific uptake rates and a lower biomass yield (Table 5.1).

**Table 5.1** Steady-state and average feast-famine biomass specific rates and substrate yields with their associated standard deviations (data from Chapter 3). All the results were calculated using data reconciliation. The total biomass yield also includes the lysed biomass.

	RCF	BWF (cycle average)	Fold change
<b>Biomass Growth <math>\mu</math></b> ( $\text{g g}_{\text{CDW}}^{-1} \text{h}^{-1}$ )	0.044 ± 0.002	0.048 ± 0.003	+ 1.09
<b>Lysis rate</b> ( $\text{g g}_{\text{CDW}}^{-1} \text{h}^{-1}$ )	-	0.008 ± 0.006	-
<b><math>q_{\text{Glucose}}</math></b> ( $\text{mmol}_{\text{glc}} \text{g}_{\text{CDW}}^{-1} \text{h}^{-1}$ )	-0.73 ± 0.01	-1.12 ± 0.02	+ 1.53
<b>O<sub>2</sub> to Substrate ratio</b> ( $\text{mmol}_{\text{O}_2} \text{mmol}_{\text{glc}}^{-1}$ )	2.85 ± 0.05	3.94 ± 0.08	+ 1.38
<b>CO<sub>2</sub> to Substrate ratio</b> ( $\text{mmol}_{\text{CO}_2} \text{mmol}_{\text{glc}}^{-1}$ )	3.16 ± 0.05	4.05 ± 0.08	+ 1.28
<b>Total Biomass Yield</b> ( $\text{g}_{\text{CDW}} \text{g}_{\text{glc}}^{-1}$ )	0.31 ± 0.01	0.21 ± 0.01	- 1.48

Protein abundances of *Escherichia coli* under RCF and BWF were measured using untargeted shotgun proteomics. For this, samples were withdrawn in duplicates from the reactor at the switch from the continuous to the block-wise feeding regime (t=0) and 172 h later (Figure 5.3), where cycles showed identical on-line measured CO<sub>2</sub> offgas patterns (Appendix A.1, Chapter 3). In addition, samples were also withdrawn 24 hours before the switch, in order to confirm that proteome was constant during the RCF. For every sample, double injections were

performed in the chromatographic system. The results discussed in this work are the average of biological and analytical replicates for every timepoint.

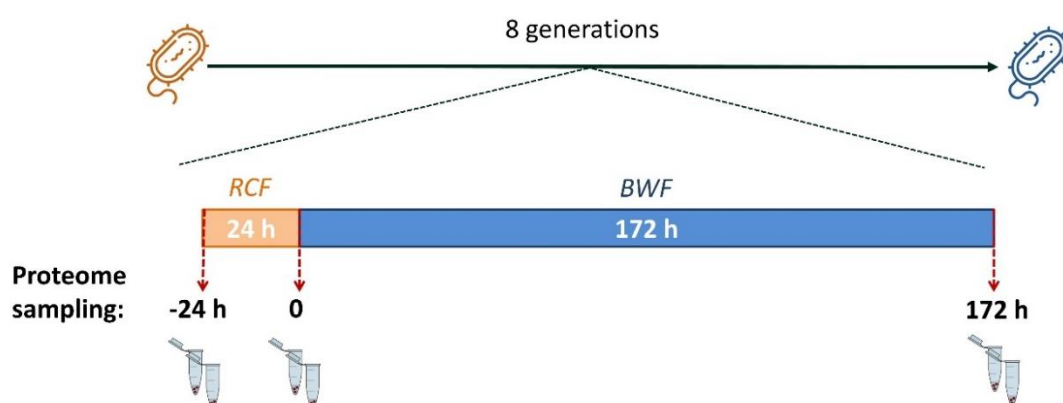


**Figure 5.3** Sampling timepoints before and after the switch of cultivation conditions from RCF to BWF. Duplicate samples were collected for every timepoint.

In the following sections:

- 1) Proteomic results will be compared between the RCF (t=0) and the BWF (t=172 h after the switch of regimes).
- 2) A functional analysis of metabolism, based on isotope tracing from fully  $^{13}\text{C}$ -labeled glucose BWF cultivation, will be discussed.

### 5.3.1 Global proteome response to feast-famine conditions

A total of 1711 proteins were detected, out of which 1232 could be quantitatively accessed (significance score >15). The number of proteins with a significant abundance change (> 1.5 fold), between the RCF and the BWF, were 402, the majority of which exhibited changes up to 2 fold. 285 proteins significantly increased after 8 generation times of the BWF, while 117 decreased. The altered proteins belong to various categories with numerous biological functions (Figure 5.4). KEGG pathway maps were used to assign proteins to their functions [31].

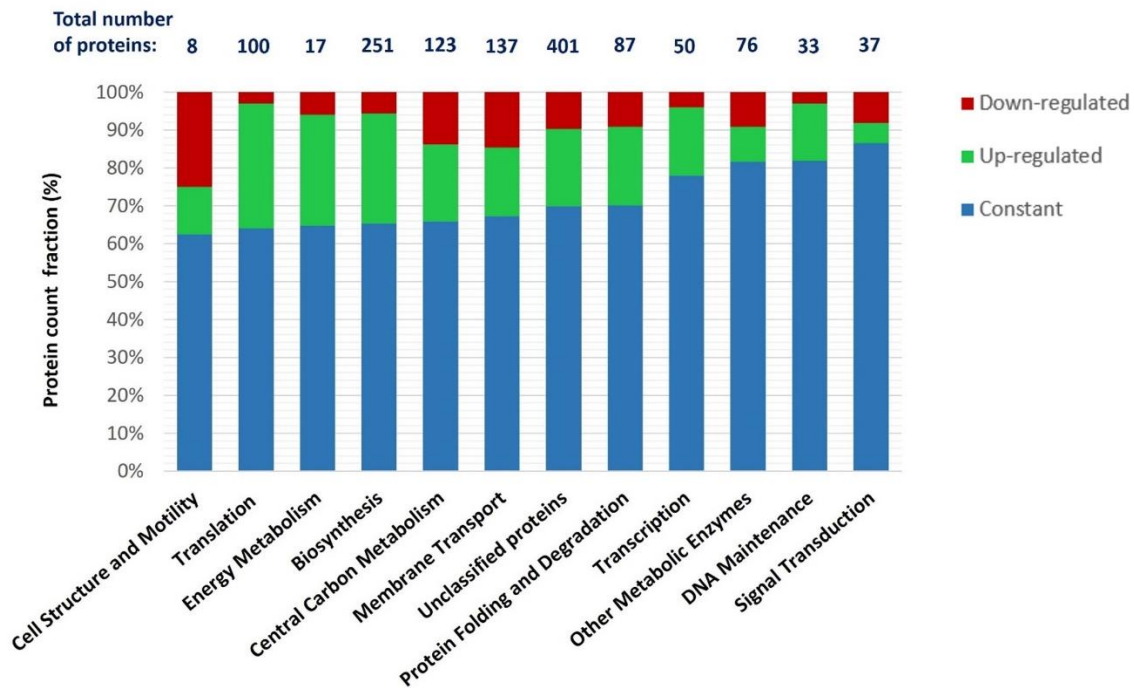


**Figure 5.4** Fractions of quantitatively assessed proteins in the block-wise feeding regime, which are constant, up-regulated (>1.5 fold) or down-regulated (<1.5 fold), as compared to the constant feeding regime. Proteins are grouped into functional (KEGG) categories. The total number of proteins for every category is given above each bar. Detailed data can be found in Appendix C.1.

The largest functional category, with regards to the identified proteins, was related to biosynthesis, followed by membrane transport and central carbon metabolism. In all categories, the number of up-regulated proteins was higher than the down-regulated ones, with the exception of signal transduction and cell structure, where however only a few proteins were identified. The highest fraction of up-regulated proteins was found for translation (33%), which includes ribosome structure and biogenesis, tRNA biogenesis and loading, translation elongation and translation factors. Nevertheless, there was no category with more than 37.5% changed proteins, showing some degree of homeostasis, even though the extracellular conditions changed. The most significant changes were observed for proteins linked to cell structure, translation, energy metabolism, biosynthesis and central carbon metabolism, while signal transduction proteins exhibited the smallest changes. In the following sections the main categories and observed changes are discussed in detail.

### 5.3.2 Proteome reflecting the genetic and environmental information processing

#### ***Transcription and signal transduction***

Receptors in the cells sense environmental conditions and thereby give signals that influence the transcription by various mechanisms. Two-component signal transduction systems, consisting of a sensor protein (histidine kinase) and a response regulator [32, 33], are commonly found. Some of the main global regulatory proteins and sigma factors in *E.coli* are



Cra (catabolite repression), CsrA (carbon storage regulator), Crp (cyclic AMP receptor), RpoS (sigma factor  $\sigma^{38}$ ) and RpoD (sigma factor  $\sigma^{70}$ ), which induce changes in a transcriptional level [34, 35]. In addition, universal stress proteins (Usp) have been found to also control gene expression following an external stimulus [36, 37]. Table 5.2 shows a summary of the proteins, related to signal-transduction and transcriptional regulation, which were significantly up- and down-regulated during the BWF.

**Table 5.2** Significant changes of protein abundances related to signal-transduction and transcriptional regulation during the BWF, compared to the RCF.

Protein	Accession Number	Fold change	Function	Reference
<b>Up-regulated</b>				
Phage shock protein C ( <b>PspC</b> )	POAFN2	5.0	The <i>pspABCDE</i> operon may play a significant role in the competition for survival under nutrient- or energy-limited conditions.	[38, 39]
Periplasmic protein <b>CpxP</b>	POAE85	2.5	Involved in resistance to extracytoplasmic stresses and may also act as a chaperone. It is a negative regulator of the Cpx pathway; an envelope stress response system.	[40, 41]
Universal stress protein G ( <b>UspG</b> )	P39177	2.4	Increases in response to stresses including heat, stationary phase, carbon or phosphate starvation.	[37, 42]
Phosphate signalling protein <b>PhoU</b>	POA9K7	2.2	It is a negative regulator of the phosphate regulon PhoU and modulates the activity of the PstSCAB transporter.	[43-45]
<b>NrdR</b> transcriptional repressor	POA8D0	1.9	Regulates the expression of several operons that encode ribonucleotide reductases (RNRs), according to the abundance of deoxyribonucleoside triphosphates (dNTPs) generated from ribonucleotides.	[46, 47]
RNA polymerase-binding ATPase and RNAP recycling factor ( <b>RapA</b> )	P60240	1.9	Activates transcription by stimulating RNA polymerase (RNAP) recycling in case of stress conditions such as supercoiled DNA or high salt concentrations.	[48]
Stringent starvation protein A ( <b>SspA</b> )	POACA3	1.8	Induced under glucose, nitrogen, phosphate or amino acid starvation and it increases with decreasing growth rate.	[49]
DNA-binding transcriptional dual regulator <b>ArgR</b>	POA6D0	1.8	Represses the transcription of several genes involved in arginine biosynthesis and transport, histidine transport and activates genes for arginine catabolism.	[50-53]
DNA-binding transcriptional activator <b>BaeR</b>	P69228	1.8	Activated in response to exogenous or endogenous stimulation.	[54]
DUF179 domain-containing protein <b>YqgE</b>	POA8W5	1.7	It belongs to a network of genes which facilitate stress-induced mutagenesis.	[55]

Protein	Accession Number	Fold change	Function	Reference
Transcription antitermination protein <b>NusB</b>	POA780	1.7	Involved in transcription antitermination and required for transcription of rRNA genes.	[56, 57]
Sensor lipoprotein <b>NlpE</b>	P40710	1.6	Activates the Cpx signalling pathway to provide a protective response when lipoprotein transport to the outer membrane is disturbed or when oxidative folding is impaired.	[58]
RNA polymerase sigma 24 factor ( <b>RpoE</b> )	POAGB6	1.6	A minor sigma factor, specializing in response to the effects of heat shock and other stresses on membrane and periplasmic proteins.	[59-61]
Integration host factor subunit $\alpha$ ( <b>IhfA</b> )	POA6X7	1.6	Functions in genetic recombination as well as in transcriptional and translational control.	[62]
Sensor lipoprotein <b>RscF</b>	P69411	1.6	A surface exposed outer membrane lipoprotein which detects perturbations or defects in the cell envelope and activates the Rcs signal transduction system. This system functions as a global regulator controlling cell surface composition.	[63, 64]
<b>Dps</b> stationary phase nucleoid component	POABT2	1.5	Highly abundant in stationary-phase and is required for the normal starvation response.	[65, 66]
Universal stress protein D ( <b>UspD</b> )	POAAB8	1.5	Expressed during starvation and certain other stresses, requiring ppGpp.	[67]
DNA-binding transcriptional dual regulator <b>Lrp</b>	POACJ0	1.5	Regulator for genes involved in amino acid biosynthesis and catabolism, nutrient transport and other cellular functions	[68-71]
<b>Down-regulated</b>				
Cold shock protein <b>CspA</b>	POA9X9	4.5	A major cold shock protein detected only during early-log-phase growth at 37°C.	[72, 73]
DNA-binding transcriptional activator <b>MhpR</b>	P77569	2.0	Activator of the mhpABCDFE operon involved in the 3-hydroxyphenylpropionate degradation pathway.	[74]
DNA-binding transcriptional regulator <b>RstA</b>	P52108	1.6	Member of the two-component regulatory system RstB/RstA, related to acid tolerance, among others.	[75, 76]
DNA-binding transcriptional repressor <b>NikR</b>	POA6Z6	1.6	Active in the presence of excessive concentrations of intracellular nickel.	[77]
Carbon starvation protein A ( <b>CstA</b> )	P15078	1.5	Induced during carbon starvation or upon entry into stationary phase; expression is dependent on $\sigma^{70}$ and positively regulated by cAMP-CRP.	[78, 79]

Only one sigma-factor (RpoE  $\sigma^{24}$ ), increased in abundance under the BWF conditions, compared to the RCF, which is an envelope-stress protein. However, RpoS ( $\sigma^{38}$ ) which is considered to act as a master regulator of the general stress response in *E.coli*, regulating sugar and nucleotide metabolism, remained constant under both conditions. The same was observed for RpoD ( $\sigma^{70}$ ), the primary sigma factor during exponential growth. Two universal proteins (UspG and UspD) also increased and are known to be induced during carbon starvation [37]. CpxP protein, which is part of the two-component system increased 2.5 fold and functions as a negative regulator of the stress response Cpx pathway [80]. This was also consistent with the increase in the sensor lipoprotein NlpE, which is an activator of the same signalling pathway. However, CpxP may also act as a chaperone, which could be another explanation for its up-regulation [41].

Interestingly, no significant change was observed in the Cra and Crp proteins, which play a major role in carbon catabolite repression [81-83]. No change was also observed for the CsrA protein, which is mainly induced under carbon starvation and is known to control a variety of cell physiological processes, including glycolysis, but also negative regulation of glycogen synthesis [84, 85].

A usual bacterial response to nutrient starvation is the stringent response, characterized by the accumulation of (p)ppGpp, which aims at the repression of rRNA and tRNA and the overexpression of genes involved in amino acid biosynthesis [86-88]. Two main enzymes play an important role in this response; the ribosome-bound ppGpp synthetase (RelA) and the bifunctional (p)ppGpp synthase/hydrolase (SpoT), which regulate the intracellular levels of (p)ppGpp [89, 90]. Both enzymes were identified under both conditions, but no changes were observed, indicating that this cellular response was not differentially regulated during the fluctuating substrate availability. Also, ribosomal protein L11 (RplK), which regulates the RelA activity [91], and DksA transcription factor, which aids ppGpp binding in RNA polymerase [92], were constant under both conditions.

### **Translation**

Protein synthesis, occurring in ribosomes, is directly related to cell growth [93, 94]. Biosynthetic proteins are located further away from the primary perturbation source, the glucose availability. Especially, the important energy source for polymerization, ATP, was quasi homeostatic (Chapter 3). Thus, ribosomal proteins could be much less affected by the environmental conditions, as metabolism buffers the short-term perturbation. On the contrary, if the biosynthetic proteins could sense the environment, the biomass synthesis rate would vary during the cycle, and a higher ribosomal capacity, compared to the RCF, would be needed. The following data are used to evaluate these hypotheses.

**Table 5.3** Significant changes of translation (ribosome structure, function and biogenesis) protein abundances during the BWF, compared to the RCF.

Protein	Accession Number	Fold change	Reference
<b>Up-regulated</b>			
16S rRNA m <sup>7</sup> G527 methyltransferase ( <b>RsmG</b> )	P0A6U5	6.5	[95]
16S rRNA m <sup>4</sup> C1402 methyltransferase ( <b>RsmH</b> )	P60390	2.5	[96]
Peptide chain release factor RF1 ( <b>PrfA</b> )	P0A7I0	2.4	[97-100]
16S rRNA pseudouridine <sup>516</sup> synthase ( <b>RsuA</b> )	P0AA43	2.2	[101]
Methyltransferase for 50S ribosomal subunit protein L11 ( <b>PrmA</b> )	P0A8T1	2.2	[102]
30S ribosomal subunit protein S3 ( <b>RpsC</b> )	P0A7V3	2.0	[103]
Stationary phase translation inhibitor and ribosome stability factor ( <b>RaiA</b> )	P0AD49	2.0	[104]
30S ribosomal subunit protein S6 ( <b>RpsF</b> )	P02358	1.9	[105, 106]
30S ribosomal subunit protein S21 ( <b>RpsU</b> )	P68679	1.9	[107]
50S ribosomal subunit protein L10 ( <b>RplJ</b> )	P0A7J3	1.8	[108]
50S ribosomal subunit protein L7 ( <b>RplL</b> )	P0A7K2	1.8	[108]
50S ribosomal subunit protein L32 ( <b>RpmF</b> )	P0A7N4	1.7	[109]
23S rRNA 2'-O-ribose U2552 methyltransferase ( <b>RlmE</b> )	P0C0R7	1.7	[110]
30S ribosomal subunit protein S13 ( <b>RpsM</b> )	P0A7S9	1.7	[111]
30S ribosomal subunit protein S20 ( <b>RpsT</b> )	P0A7U7	1.7	[112]
50S ribosomal subunit protein L31 ( <b>RpmE</b> )	P0A7M9	1.7	[113]
Peptide chain release factor RF3 ( <b>PrfC</b> )	P0A7I4	1.7	[114, 115]
50S ribosomal subunit protein L33 ( <b>RpmG</b> )	P0A7N9	1.7	[116]
16S rRNA m <sup>3</sup> U1498 methyltransferase ( <b>RsmE</b> )	P0AGL7	1.6	[117]
50S ribosomal subunit protein L17 ( <b>RplQ</b> )	P0AG44	1.6	[118]
23S rRNA m <sup>5</sup> C1962 methyltransferase ( <b>RlmI</b> )	P75864	1.5	[119]
50S ribosomal subunit protein L5 ( <b>RplE</b> )	P62399	1.5	[120]
<b>Down-regulated</b>			
Peptide chain release factor RF2 ( <b>PrfB</b> )	P07012	2.4	[97, 98]
50S ribosomal subunit protein L13 ( <b>RplM</b> )	P0AA10	2.0	[121]

Bacterial ribosomes consist of two components; a small (30S) subunit, which decodes mRNA, and a large (50S) subunit, which forms a polypeptide chain, linking amino acids together. Each subunit consists of both rRNA and proteins [122]. The levels of 8 50S ribosomal proteins were altered up to 1.8 fold times during the BWF (7 up-regulated and 1 down-regulated, Table 5.3). Regarding the 30S ribosomal subunit, the abundance of 5 proteins was significantly increased (Table 5.3). In *E.coli* ribosomes, the small subunit consists of 21 proteins, while 31 proteins form the large one [120]. Hence, this change observed represents 25% of the total ribosomal proteome, with the majority of it being up-regulated.

In addition to the ribosomal components, increase (up to 6.5 fold) in the abundance of several proteins involved in ribosome biogenesis, such as methyltransferases, responsible for the modification of rRNA [123], was also observed. Finally, two peptide chain release factors (PrfA and PrfC) increased, while the third (PrfB) decreased. PrfA and PrfB facilitate the release of the polypeptide chain synthesized in ribosomes at stop codons and PrfC stimulates the release of the former two factors from the ribosome after synthesis termination [97, 98]. PrfA also contributes to the rescue of stalled ribosomes [99, 100].

Different hypotheses to explain the high abundance of ribosomes will follow in the Discussion section.

### ***Protein folding and degradation***

The higher ribosomal capacity during the substrate fluctuations, compared to the RCF conditions, indicates increase in the protein turnover (simultaneous protein synthesis and degradation). Various conditions, such as intracellular pH variations, molecular crowding or incomplete protein synthesis in ribosomes, can induce protein misfolding in the cells [124, 125]. In case of growth under the BWF, the increased production of charged metabolites can lead to acidification of the cytosol. Lower intracellular pH usually results in aggregated proteins, which have to be rapidly degraded [124, 126]. Furthermore, it is highly possible that amino acid depletion or energy limitation lead to pauses in the function of ribosomes and thus abortion of useless proteins [127]. We experimentally observed depletion of two amino acids, tyrosine and leucine, at the end of the famine phase (300-400 s), while the other amino acids were always available in the cell (Appendix A.9, Chapter 3). Previous studies have shown that ribosome pausing can indeed occur in *E.coli* under single amino acid (serine or leucine) depletion [128, 129]. Therefore, chaperones and proteases are expected to be more abundant under the BWF, as they play a significant role in restoring the cellular proteome homeostasis. Chaperones contribute to protein folding, while proteases degrade the misfolded proteins [130, 131].

**Table 5.4** Significant changes of protein abundances related to protein folding and degradation during the BWF, compared to the RCF.

Protein	Accession Number	Fold change	Function	Reference
<b>Up-regulated</b>				
[Fe-S] cluster biosynthesis co-chaperone <b>HscB</b>	P0A6L9	2.6	HscA together with HscB comprises a chaperone/cochaperone.	[132, 133]
Metalloprotease <b>LoiP</b>	P25894	2.5	Induced in response to stress (e.g. heat shock, UV irradiation, low osmolarity).	[134, 135]
Aminopeptidase B ( <b>PepB</b> )	P37095	2.3	Belongs to the M17 family of metallopeptidases.	[136]
[Fe-S] cluster biosynthesis chaperone <b>HscA</b>	P0A6Z1	2.2	HscA together with HscB comprises a chaperone/cochaperone.	[132, 133]
<b>SecB</b> chaperone	P0AG86	2.0	Assists the folding of cytosolic proteins and its synthesis may be related to the cAMP-cAMP receptor protein complex-mediated activation.	[137, 138]
Protein disulphide isomerase <b>DsbC</b>	P0AEG6	2.0	DsbC has chaperone activity independent from its isomerase activity.	[139, 140]
Redox enzyme maturation protein <b>DmsD</b>	P69853	2.0	DmsD interacts with the molecular chaperones DnaK, DnaJ, GrpE, GroEL, TF and Ef-Tu.	[141]
RNase R ( <b>Rnr</b> )	P21499	1.9	Ribonuclease involved in the maturation of tmRNA, a small RNA involved in rescue of stalled ribosomes, and in the tmRNA-mediated degradation of non-stop mRNAs.	[142-144]
Protein/nucleic acid deglycase 3 ( <b>YajL</b> )	Q46948	1.9	Functions as a chaperone in response to oxidative stress.	[145]
Peptidase T ( <b>PepT</b> )	P29745	1.8	Its expression is up-regulated during biofilm development and anaerobic growth.	[146, 147]
Peptidyl-prolyl cis-trans isomerase A ( <b>PpiA</b> )	P0AFL3	1.7	Facilitates proper protein folding and is regulated by cAMP-CRP, CytR, and the Cpx two-component system.	[148-150]
Aminopeptidase A/I ( <b>PepA</b> )	P68767	1.7	Peptidase	[151]
D-alanyl-D-alanine carboxypeptidase <b>DacA</b>	P0AEB2	1.7	Contributes to normal cell morphology and is implicated in the stationary phase stress response.	[152]
Periplasmic serine endoprotease <b>DegP</b>	P0C0V0	1.7	Functions as a protease degrading unfolded outer membrane proteins under stress conditions and also has an independent chaperone activity.	[153-156]
<b>HslV</b> hexamer	P0A7B8	1.7	Component of the ATP-stimulated HslVU protease	[157, 158]
Nucleotide exchange factor <b>GrpE</b>	P09372	1.5	Part of the DnaK-DnaJ-GrpE chaperone system. Regulates the release of ADP from DnaK, providing further stimulation for the ATP turnover.	[159, 160]

Protein	Accession Number	Fold change	Function	Reference
<b>Down-regulated</b>				
Periplasmic chaperone <b>OsmY</b>	P0AFH8	5.4	Induced by stresses known to cause protein misfolding such as hyperosmotic stress and upon entry into stationary phase.	[161, 162]
Periplasmic acid stress chaperone <b>HdeB</b>	P0AET2	3.3	Both HdeB and HdeA are required for optimal protection against acid stress.	[163]
Putative zinc peptidase ( <b>Pqql</b> )	P31828	2.6	Peptidase	[164]
Protease 7 ( <b>OmpT</b> )	P09169	2.5	Outer membrane protease	[165]
Peptidase E ( <b>PepE</b> )	P0A7C6	1.6	Peptidase	[166]

In total 16 proteins, related to protein folding and degradation, were up-regulated, while 5 exhibited decreased abundance compared to the RCF (Table 5.4). Many of those are connected to stress response, such as the entry of the cells in the stationary phase (e.g. DacA). No change was observed for major *E. coli* chaperones such as DnaK, DnaJ, ClpAX and GroEL. It is important to note that these were present in both conditions, but not significantly changed. The highest up-regulation for chaperones was found for the HscA/HscB system. The specific function of this system has not yet been clarified, but it was suggested to respond to mechanical stress [167]. Nevertheless, knock-out studies have shown that it is not an essential system for cell viability [168, 169].

Regarding proteolysis, the main energy-dependent proteases known for *E. coli*, belonging in the AAA+ family, are Lon, ClpXP, ClpAP, HflB, HslV and HslU [170], out of which HslV was the only one changed (1.65 fold increase).

### 5.3.3 Proteome reflecting metabolism

#### **Nutrient Transport**

Nutrient availability was the main difference between the two feeding regimes. Especially, instead of constant limiting substrate concentration, the microorganism experienced rapid, repetitive gradients in glucose during the BWF.

In *E. coli* cells, glucose is first transported in the periplasm via the outer membrane porins OmpC, OmpF, and LamB (protein facilitated diffusion) [171] and is then transported into the cytosol by the glucose-specific phosphotransferase system (PTS with  $K_m$  in the range of 3-10  $\mu\text{M}$ ) [172-174]. Since a 50% increase in the (average) glucose uptake rate (Table 5.1) was observed during the BWF, compared to the RCF, changes in the related transport proteins were expected.

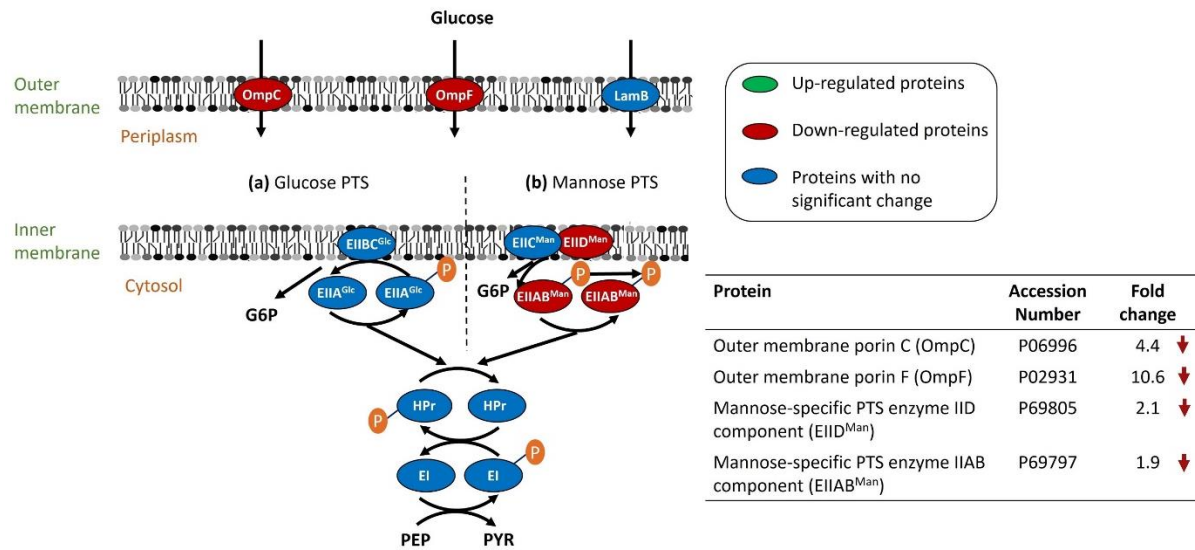


**Figure 5.5** Glucose transport in the cell, involving the outer membrane proteins and two alternative glucose transport systems: (a) Glucose-specific PTS and (b) Mannose-specific PTS. Proteins are shown in oval shapes, coloured based on the fold change observed in their abundance during the BWF, compared to the RCF.

The two main outer membrane proteins OmpC and OmpF were considerably down-regulated (Figure 5.5). This suggests that the temporary excess of glucose during the feast phase of the BWF, dominated the expression regulation, while the constantly low concentration, during the RCF, triggered increased porin production [175, 176]. On the other hand, LamB, a porin that is reported to contribute to glucose transport under low concentrations (sub-micromolar) [177, 178], did not show any significant changes in its abundance (Figure 5.5), indicating a different regulation signal.

During the BWF, the extracellular concentration of glucose ranged from 12 to 320  $\mu\text{M}$  (time integrated average of  $49 \pm 0.31 \mu\text{M}$ ). The concentration measured during the RCF was  $15 \pm 0.31 \mu\text{M}$  (Chapter 3).

Regarding the transport of glucose into the cytosol by the PTS, none of the related protein components was found to change between the two conditions. However, *E. coli* is known to have various transporters with low and high affinity for the same sugar, in order to cope with both feast and famine conditions. For example, similar to the glucose PTS, the mannose PTS can also contribute to glucose import with lower affinity (affinity constant of 1.3 mM) [179]. In addition, the galactose and the maltose ABC transporters can also translocate glucose in the cytosol, during glucose-limitation conditions [176, 178, 180-183].

The proteins EIIB<sup>Man</sup> and EIID<sup>Man</sup> of the mannose PTS were down-regulated (Figure 5.5). The maltose (MalEFG) and galactose (MglABC) ABC transporters showed no changes. Hence, there was no overexpression of any of the potential glucose uptake systems under the BWF,



indicating that the glucose-specific PTS had the capacity to accommodate higher fluxes, without adjusting these proteins.

### **Central carbon metabolism**

The higher metabolic rates compared to the RCF, observed during the BWF (Chapter 3), are expected to have been induced by significant changes in the central carbon metabolic pathways, such as glycolysis, TCA cycle and pentose-phosphate pathway (Chapter 4).

**Table 5.5** Significant changes in enzyme abundances of the central carbon metabolic pathways during the BWF, compared to the RCF.

Protein	Accession Number	Fold change	Function	Reference
<b>Up-regulated</b>				
<b>GLYCOLYSIS</b>				
2,3-bisphosphoglycerate-independent phosphoglycerate mutase ( <b>GpmM</b> )	P37689	2.4	Catalyses the interconversion: 2PG $\leftrightarrow$ 3PG	[184, 185]
6-phosphofruktokinase I ( <b>PfkA</b> )	P0A796	1.8	Catalyses the reaction: F6P + ATP $\rightarrow$ FBP + ADP + H <sup>+</sup>	[186]
<b>PENTOSE PHOSPHATE PATHWAY</b>				
Ribulose-phosphate 3-epimerase ( <b>Rpe</b> )	P0AG07	1.7	Catalyses the reaction: Ribulose 5-phosphate $\leftrightarrow$ Xylulose 5-phosphate	[187]
NADP <sup>+</sup> -dependent glucose-6-phosphate dehydrogenase ( <b>Zwf</b> )	P0AC53	1.7	Catalyses the first reaction of the PPP: G6P + NADP <sup>+</sup> $\rightarrow$ 6PG + NADPH + H <sup>+</sup>	[188]
<b>Down-regulated</b>				
<b>GLUCONEOGENESIS</b>				
Phosphoenolpyruvate synthetase ( <b>PpsA</b> )	P23538	1.6	Catalyses the gluconeogenic reaction: Pyruvate + ATP + H <sub>2</sub> O $\rightarrow$ PEP + AMP + P <sub>i</sub> + 2H <sup>+</sup>	[189]

#### 1) Glycolysis and gluconeogenesis

Looking at the glycolytic and gluconeogenic enzymes, hardly any changes were observed (Table 5.5). Even though all the known enzymes were identified, only two glycolytic ones, phosphofruktokinase I (PfkA) and phosphoglycerate mutase (GpmM) were up-regulated. PfkA catalyses the phosphorylation F6P to FBP by ATP and is a key enzyme regulating the glycolytic pathway [190-192]. GpmM is one of the two phosphoglycerate mutases (GpmA is the other one), which catalyse the interconversion of 2PG and 3PG in lower glycolysis. The difference between the two enzymes is that the cofactor 2,3-bisphosphoglycerate (2,3-BPGA) is required for the activity of GpmA, while GpmM is independent of it.

The observation of small changes, contradicts our kinetic modelling approaches (Chapter 4), which required an increased amount of all glycolytic enzymes (except fructose-bisphosphate aldolase), compared to the RCF, to reproduce the metabolome measurements. More specifically, the  $v_{\max}$  of PfkA was increased 4 fold in the model, but only 1.8 fold experimentally and the  $v_{\max}$  of Gpm was increased 1.2 fold times, in contrast to its 2.4 fold experimental increase. However, changes such as the 6.4 fold increase in the  $v_{\max}$  of glucose-6-phosphate isomerase (Pgi) or the 23 fold in glyceraldehyde-3-phosphate dehydrogenase (GapA), were not evident in the proteome measurements, raising doubts about the accuracy of the kinetic model.

The levels of PpsA enzyme, which generates PEP from pyruvate during gluconeogenesis, decreased (1.6 fold) after the switch to the BWF. Hence, glycolysis and gluconeogenesis seem to be robust against changes in the nutrient availability and higher fluxes can be achieved without overexpression of the enzymes catalysing the reactions of these pathways.

## 2) Pentose phosphate pathway

Minor abundance changes were observed for the pentose phosphate pathway proteins. Two enzymes were up-regulated (approx. 1.7 fold) (Table 5.5); a) the G6P dehydrogenase which catalyses the first reaction of the pentose phosphate pathway, providing a large fraction of NADPH needed for anabolism and b) the ribulose-phosphate epimerase (Rpe), enzyme of the non-oxidative branch of the pathway.

Upon perturbations, the expression of the genes encoding for these two enzymes (*zwf* and *rpe* respectively) is correlated with the metabolic flux alterations, as has been shown for shifts in the dilution rate of chemostat cultivations [193]. Our metabolic flux analysis (performed in Chapter 3) indicated an increase of 1.4 and 1.5 fold times in the fluxes of Zwf and Gnd/Rpe reactions, respectively, comparing the RCF with the BWF, which was indeed reflected in their proteomic changes. However, this was not the case for the rest of the pentose phosphate fluxes.

## 3) TCA cycle, glyoxylate bypass and acetate formation

The enzymes of the TCA cycle, the glyoxylate shunt and the acetate synthesis and assimilation, which changed after the switch to the BWF are shown in Figure 5.6. Only two enzymes of the TCA cycle showed differences in their abundance. The SdhD subunit of the succinate dehydrogenase enzyme complex, catalysing the reduction of succinate to fumarate, which connects the TCA cycle with the respiratory electron transport chain, was up-regulated. One (AcnB) of the two enzymes, catalysing the reversible isomerization of iso-citrate from citrate, was down-regulated. AcnB is the major enzyme of this reaction, whereas AcnA is specifically induced by iron and redox-stress [194]. In addition, the levels of the NAD<sup>+</sup>-dependent malate

dehydrogenase enzyme (MaeA), which catalyses the decarboxylation of malate to form pyruvate (also part of gluconeogenesis), decreased.

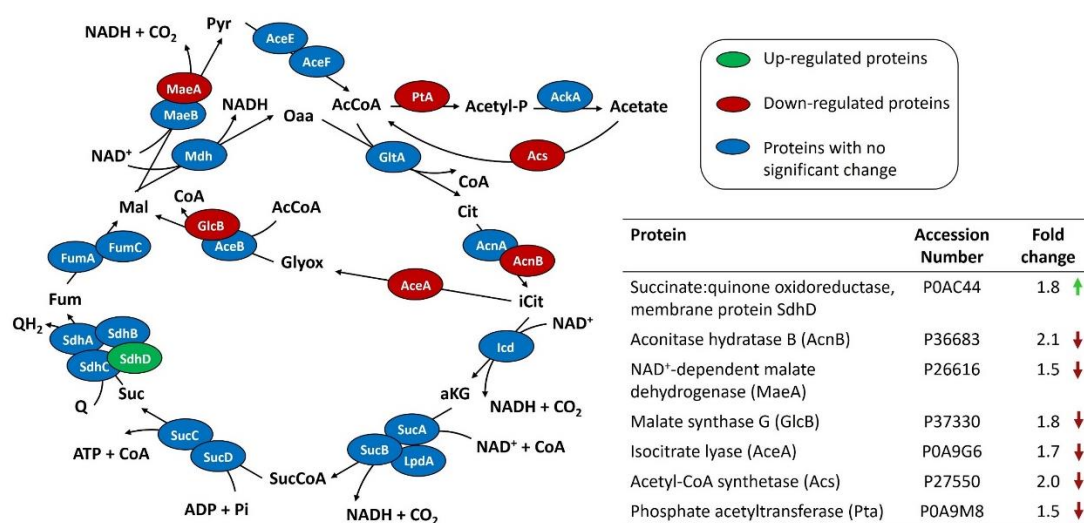


**Figure 5.6** TCA cycle, the glyoxylate bypass. Proteins are shown in oval shapes, coloured based on the fold change observed in their abundance during the BWF, compared to the RCF.

Regarding the glyoxylate shunt, 2 out of the 3 enzymes of this pathway were down-regulated, indicating that this pathway might be less utilized during substrate fluctuations.

Moreover, the levels of phosphate acetyltransferase (Pta) and acetyl-coA synthetase (Acs) decreased. These enzymes catalyse acetate synthesis from acetyl-coA and assimilation, respectively. Acs is known to be repressed by the presence of glucose [195, 196], therefore its down-regulation could be expected due to the glucose excess conditions applied during the feast phase of the BWF cycles. The fact that increase in overflow metabolism was not observed during the BWF, based on the acetate measurements (Chapter 3) was indeed verified by the proteomic results.

### 5.3.4 Storage metabolism

#### Glycogen

Glycogen synthesis and re-consumption was discussed in the previous chapters, as an intracellular carbon and energy storage pool, used by the cells to balance the substrate uptake flux and the anabolic processes during the BWF. The proteomic analysis verified the expression of this pathway, as not only all the related enzymes were present in the cell, but the main ones were also up-regulated (Figure 5.7).

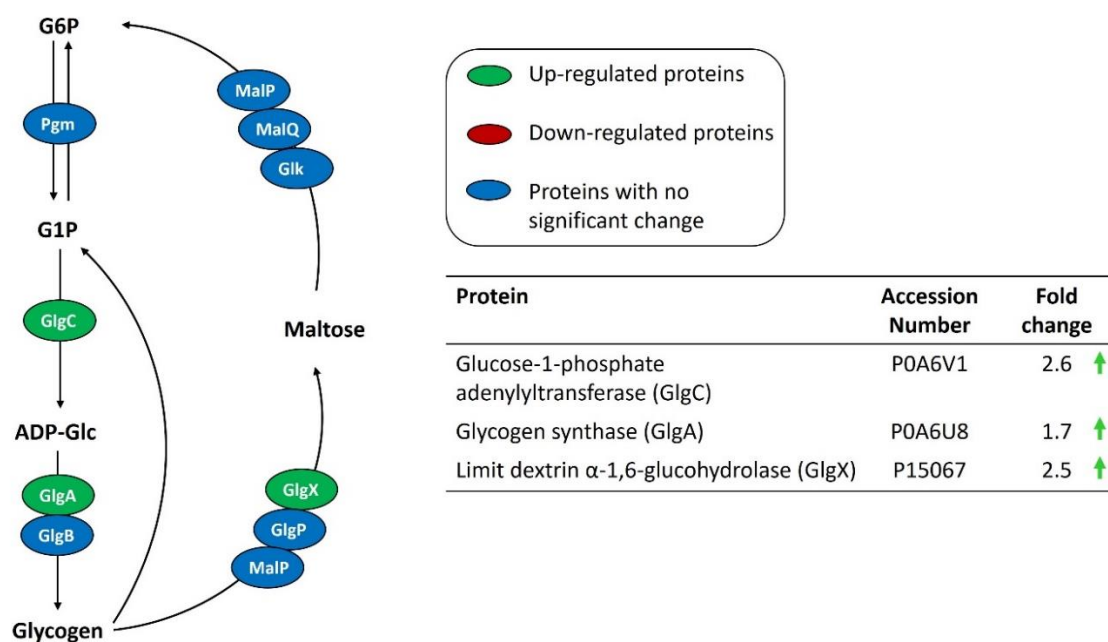


**Figure 5.7** Glycogen synthesis and degradation pathway. Proteins are shown in oval shapes, coloured based on the fold change observed in their abundance during the BWF, compared to the RCF.

### ***Inorganic Polyphosphate***

Moreover, the hypothesis of the formation and re-assimilation of inorganic polyphosphate, which could partly explain the ATP homeostasis observed during the BWF (Chapter 3), was verified by the 1.8 fold increase in the levels of polyphosphate kinase (Ppk), the enzyme catalysing the reversible reaction of polyphosphate synthesis and degradation.

#### **5.3.5 Functional analysis of metabolism using <sup>13</sup>C tracing**

The metabolome was tested by adding fully <sup>13</sup>C-labelled glucose for two consecutive cycles during the BWF, followed by a cycle where the feed was switched back to <sup>12</sup>C glucose and the isotope enrichment in the metabolites was measured. For glycolysis, accurate data could be derived only for three metabolites; FBP, 3PG and 2PG (all <sup>13</sup>C enrichment data can be found in Appendix C.2). From these data, we observed an immediate increase of the <sup>13</sup>C enrichment of FBP during the first cycle, which decreased after the end of the feeding, reaching low values (around 10%) during the famine phase (Figure 5.8). The same behaviour was observed during the second cycle where the total enrichment reached, however, slightly higher values. Furthermore, in the last cycle, where <sup>12</sup>C glucose was fed, the enrichment initially decreased as expected but then increased during the famine phase. This increase was, also, observed in the lower glycolytic metabolites 3PG and 2PG. These data indicate the presence of a storage pool upstream of FBP (like glycogen), which assimilated labelled carbon during the two labelling cycles and then acted as a source of <sup>13</sup>C enrichment (while being degraded) in the upper glycolytic metabolites, during the famine phase of the second and the third cycle.

Higher enrichment (80-90%) than observed would be expected for the upper glycolytic metabolites, which may be explained by cell lysis, which was predicted during the BWF (Chapter 3). In case inactive cells (not yet lysed) were present in the broth as a subpopulation, then the presence of unlabelled metabolites contributes to the lower enrichment. In addition,  $^{13}\text{C}$  enrichment of glucose and G6P, which could unfortunately not be detected, would enforce the hypotheses of glycogen storage. The inconsistency of the 3PG and 2PG labelling patterns with the FBP profile cannot be currently explained. The lower glycolytic metabolites were expected to follow the pattern of FBP and thus immediately increase their enrichment when  $^{13}\text{C}$  glucose is fed, also based on their pool concentration measurements (Chapter 3).

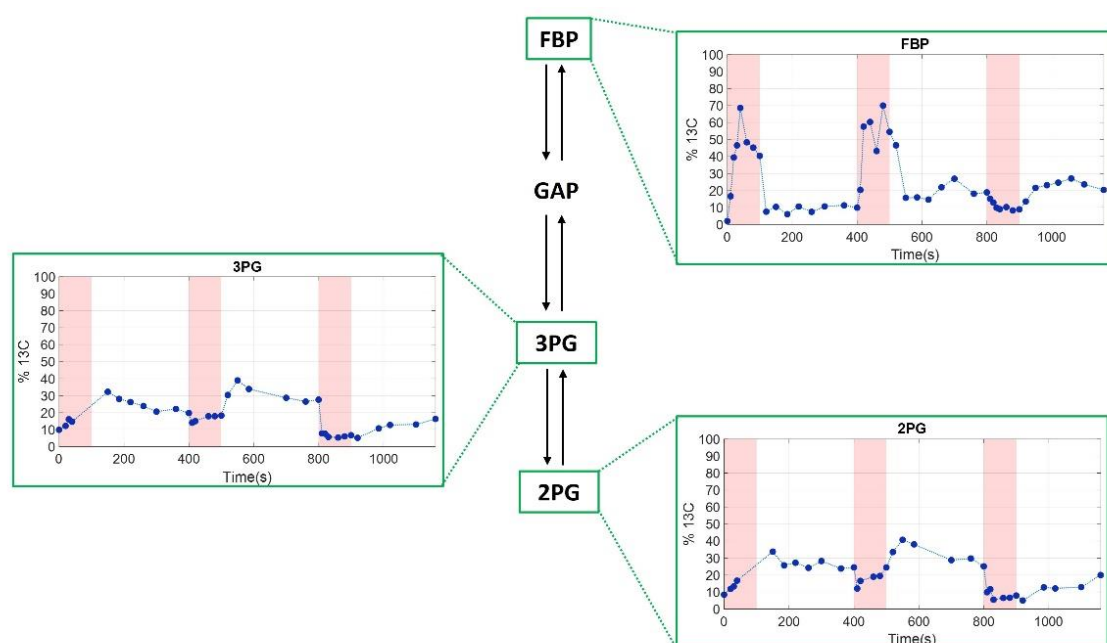


**Figure 5.8** Total  $^{13}\text{C}$  enrichment (%) over time for glycolytic intermediates during the BWF. The plots show results from three successive cycles. In the two first cycles  $^{13}\text{C}$  labelled glucose was fed in the culture, while in the third cycle the medium was switched to  $^{12}\text{C}$  glucose. The pink area represents the substrate feast phase.

## 5.4 Discussion

In the present study, the behaviour of *Escherichia coli* growing under BWF, compared to RCF, was investigated as a way to decipher growth under the highly dynamic environment of large-scale cultivations. The study focused on the proteome-level adjustments following the switch of feeding conditions, investigated by label-free cellular shotgun proteomics. The analysis resulted in the identification of 1711 proteins, of which 23.5% showed significant changes between the RCF and the BWF. However, the ability of screening such a wide range of proteins comes at the expense of accuracy and sensibility. Hence, we separated the identified proteins in functional groups and analysed their behaviour in categories, in order to link the

physiological and metabolic responses of the cells to substrate gradients with their proteome rearrangements.

### ***Global regulation mechanisms as response to substrate perturbations***

When bacteria face drastic changes in the nutrient availability, they may activate global regulatory proteins, which control gene expression in response to the environmental stimuli. During the transition from the RCF to the BWF, we observed several changes in the abundance of global response proteins and transcriptional regulators, specifically related to nutrient stress. It has been known that seven proteins (ArcA, Crp, Fis, Fnr, Ihf, Lrp, and NarL) can directly control the expression of 50% of the *E.coli* genes [34]. Only IhfA (1.6 fold decrease) and Lrp (1.5 fold increase) were found to significantly change under the tested substrate perturbations. Fnr was not detected and Fis could not be quantitatively accessed. The rest remained unchanged. Sigma factors and universal stress proteins displayed no major changes. The carbon catabolite repression (CCR) mechanism was expected to be activated under substrate excess, as has been previously reported to be the case after glucose pulses [197]; the concentration of cAMP receptor protein (Crp) is known to decrease at high glucose conditions [198]. However, no changes were observed in the Cra and Crp proteins, involved in catabolite repression, between the two feeding conditions. In addition, no proof of the stringent response was found in the related proteins, even though its activation was expected as response to nutrient starvation during the famine phase. These results may lead to the conclusion that under these conditions *E.coli* triggers specific cellular responses, rather than global. However, currently, we cannot exclude lower fold changes which were not considered under chosen statistical thresholds.

### ***Ribosomes and Protein turnover***

The maximum growth rate is dependent on the proteome investment on catabolism and polymerization. The optimal scenario for the cell is to maintain a balance between metabolic reactions, which produce precursors and energy, and biosynthetic reactions, which utilize these products for growth. However, this balance is less obvious for non-constant substrate feeding. In these cases, ribosomes are some of the most important cellular components controlling protein synthesis. During the BWF, approximately 20-25% of the total ribosomal proteins present in *E.coli*, were observed being up-regulated in comparison to the RCF (at the chosen statistical thresholds). Several studies have shown that cells of various bacteria (*Wautersia eutropha*, *Escherichia coli* ML30 and heterotrophic bacterial strain HIS 53) accumulated more rRNA during block-wise substrate perturbations (cycles of at least 1 hour), than when cultivated in chemostats [199-201]. Several hypotheses could explain the ribosomal increase observed:

- 1) Increased ribosomal capacity to accommodate a high growth rate during the feast phase: Assuming that the growth rate is not constant during the BWF, i.e. higher values are reached during high substrate conditions, compared to the reference (RCF) growth rate. Such change in the growth rate cannot be measured (very small change in the biomass concentration), nevertheless, the majority of amino acids reached higher intracellular concentrations during the BWF (Chapter 3). Therefore, high abundance of ribosomes is expected for higher protein synthesis during rapid growth, requiring higher capacity.
- 2) Increased ribosomal proteins to compensate for higher protein turnover: Although the average growth rate during the BWF remained the same as under the RCF, the overall protein synthesis rate was increased due to increased turnover. If this hypothesis holds true, then the 30% biomass yield loss (Chapter 3) can be partially explained by ATP spilling on protein synthesis. Several chaperones and proteases were up-regulated, showing potential increase in folding activity and proteolysis. In these conditions misfolded and aggregated proteins could be formed by acidification of the cytoplasm due to the accumulation of acidic metabolites. However, no protein related to pH homeostasis was found to change and the same was observed for the ATPase, which transports protons through the membrane. A more feasible explanation could then be ribosome stalling. Due to the rapid nutrient dynamics, ribosomes may suffer loss of energy or depletion of amino acids, during proteins synthesis. This translational pausing or arrest is thus the source of incomplete, misfolded and toxic proteins, which the cell needs to fold properly or destroy [127]. Specific quality control systems, such as the SsrA or tmRNA system, tackle ribosome stalling by adding a degradation tag on the polypeptide chain [202]. The levels of SmpB binding protein, which is required by the SsrA RNA, were not altered after the switch of regimes. In addition, no changes were observed for the ClpP, Tsp and HflB proteases, which are known to be involved in the degradation of the SsrA-tagged chains [202-204]. However, increase of two out of the three peptide chain release factors may indicate that ribosome stalling was indeed occurring during the BWF.
- 3) Ribosomal overcapacity as an adaptation strategy: Koch AL [205], [206] were the first to demonstrate that cells accumulate extra inactive ribosomes, especially under substrate-limited conditions, which can be immediately used for rapid growth acceleration during a potential nutrient upshift. More studies, suggesting the same adaptation strategy, followed [207, 208]. If that holds true then we would expect that during the RCF, the cells would have an overcapacity of ribosomes and would be ready to face the switch to the BWF. Increase of this established overcapacity would indicate

potential incorrect deciphering of the environmental signals, leading to the production of more proteins than needed for the actual growth under the BWF.

### ***Nutrient transport and central carbon metabolism***

The first step in substrate uptake is characterized by the mechanisms of importing nutrients inside the cytosol. Cells make choices on the expression of transport systems based on extracellular and intracellular signals, in such way to efficiently regulate occupation of membrane space and energy consumption [2]. During the BWF, the cells decreased the abundance of two main outer membrane porins (OmpC and OmpF), used for glucose import into the periplasm. Regarding the subsequent transport into the cytosol, the main system (glucose-PTS) remained unaffected by the changing conditions and only a decrease in the EIIBD components of the low affinity mannose-specific PTS was observed, compared to the RCF conditions. No increase occurred in the expression of higher affinity transport systems, such as ABC transporters, which are known to increase with the decrease in growth rates [209]. The minimum extracellular glucose concentration during the BWF was comparable to the RCF levels, while the average was measured to be higher (Chapter 3). Thus, the cells likely decreased the porin abundance, as a proteome allocation strategy; increased membrane permeability was not necessary for high glucose availability and decrease of these proteins saves resources and serves for keeping the cellular protein concentration homeostasis.

More transport proteins were up-regulated but their specific functions could not be identified. In addition, no changes were observed for proteins related to transport of alternative sugars, such as fructose, lactose, arabinose etc., indicating that the cellular capacity for their consumption, if needed, remained the same as during the RCF.

During the BWF, significantly higher than the RCF macroscopic and metabolic rates were observed (Chapter 3). In addition, using modelling approaches we demonstrated that alterations in maximum enzyme capacities ( $V_{max}$ ) must have occurred during the BWF (Chapter 4).

Only slight changes occurred in glycolysis, gluconeogenesis, pentose phosphate pathway and TCA cycle, which were not sufficient to explain the increased flux variations between the two regimes. In glycolysis, only the PfkA and the GpmM enzymes were found to increase, which catalyse the reactions from F6P to FBP and from 2PG to 3PG, respectively. Koebmann BJ, *et al.* [210] showed that the ATP demand controls the flux through glycolysis to a greater extent than the levels of the glycolytic enzymes. With their study they demonstrated why previous attempts to increase the glycolytic flux, by overexpressing the levels of these enzymes or the PTS-related proteins, did not succeed [211]. However, ATP levels remained constant during the BWF in our experimental setup. Another hypothesis for the robustness of the main central



carbon metabolic enzymes is that the enzyme levels were already increased during the RCF, but not used in full capacity, as a mechanism to rapidly accommodate higher fluxes after nutritional shifts [212]. The same mechanism was already described before for the ribosomes. Proteomic studies have shown that glycolytic enzymes are some of the higher abundant proteins, accounting for 3.5-7 % of total *E.coli* proteome [213]. Valgepea K, *et al.* [214] integrated multi-omics data, for *E.coli* cultivated under different growth rates, and showed that cells achieved higher metabolic fluxes (for faster growth) by mainly increasing the enzyme catalytic rates, while the enzyme abundances (mainly for glycolysis, TCA cycle and PPP) were already overexpressed under nutrient limitation. The same adaptation strategy was supported by the extremely rapid (40 s) increase in growth rate observed after glucose-pulses [215].

Moreover, the glyoxylate bypass enzymes were down-regulated during the BWF. The importance of the glyoxylate shunt in growth efficiency has been shown for glucose-limited conditions [25, 216, 217] and could also be the case for the RCF conditions. With the transition to the BWF it seems that it was no longer an essential part in central carbon metabolism. Two enzymes, involved in acetate formation and re-assimilation, were down-regulated, indicating decrease of the overflow metabolism, despite the glucose excess phases during the BWF.

Therefore, we argue that, during substrate limitation, cells have an enzymatic reserve for pathways carrying high fluxes, such as glycolysis and TCA cycle, while the catalytic rates do not function under saturation. With this strategy, they can then rapidly respond to the nutrient availability perturbations, by mainly modifying the catalytic rates and not the enzyme levels. Post-transcriptional regulation, thus, plays a significant role in these pathways.

Our results are in accordance with the work of Borirak O, *et al.* [218], who performed transcriptomic and proteomic analysis after a glucose pulse addition to a steady-state culture. Their main observations indicated increase in ribosomal and biosynthetic proteins, while enzymes involved in glycolysis, pentose phosphate pathway, glyoxylate shunt and TCA cycle were down-regulated after the switch to substrate excess.

### ***Storage pathways***

The role of storage polymers is very important for the survival of bacteria during growth with changing substrate availability. One of these polymers is glycogen and the importance of its synthesis and degradation was verified by the overexpression of several enzymes catalysing these reactions during the BWF, as well as, <sup>13</sup>C labelling patterns. In addition to our kinetic modelling work (Chapter 4) we assume that glycogen was used to store the extra carbon flux that could not be immediately processed in the anabolic pathways and as a potential mechanism to ensure high substrate uptake rates. The glycogen was subsequently used in the

famine phase for growth and maintenance purposes. Glycogen synthesis and assimilation consumes 1 net ATP, highlighting its role in ATP spilling.

Furthermore, we proved the up-regulation of the inorganic polyphosphate storage pathway, by showing that polyphosphate kinase (Ppk) levels increased 1.8 fold times compared to the RCF. This pathway is thus most likely to be used as a control of the ATP homeostasis, which we observed experimentally (Chapter 3).

### ***Industrial relevance***

The proteome adjustment observed proves that cells circulating in different zones of substrate availability will undergo changes and an altered performance in large-scale bioprocesses has to be expected. We observed that *E.coli* wild-type cells were robust in the face of environmental perturbations regarding central carbon metabolism, as higher fluxes were achieved without overexpression of catalytic enzymes. Energy metabolism seem to play the major role under these conditions, by the induction of inorganic polyphosphate kinase pathway, glycogen storage and increased protein synthesis and proteolysis and is probably the limited factor for biomass yield. Despite the active response of the wild-type towards the substrate gradients, problems could arise with the use of high-producing strains in industry. These strains are usually forced to perform at their metabolic limits and their growth could thus become severely ATP limited under dynamic conditions in the bioreactor.

## **5.5 Conclusions**

The proteome rearrangement in *E.coli* cells, after the switch from constant to block-wise glucose feeding, was extensively studied in this work. The adaptation was characterized by lack of significant changes in global stress regulators, the absence of carbon catabolite repression, stringent response and overflow metabolism, in addition to increased ribosomal activity and hardly changed central carbon metabolic enzymes. The identified cellular response strategies can serve as guidelines for the metabolic engineering of *E.coli* strains, with less losses under large-scale cultivations. In addition, our study enhances the view that *E.coli* metabolism under dynamic conditions is still not well explored and goes beyond our expectations, reshaping the definitions of robustness and metabolic stress.

## References

1. Gerosa L, Sauer U: **Regulation and control of metabolic fluxes in microbes.** *Curr Opin Biotechnol* 2011, **22**:566-575.
2. Chubukov V, Gerosa L, Kochanowski K, Sauer U: **Coordination of microbial metabolism.** *Nat Rev Microbiol* 2014, **12**:327-340.
3. Nahku R, Valgepea K, Lahtvee PJ, Erm S, Abner K, Adamberg K, Vilu R: **Specific growth rate dependent transcriptome profiling of Escherichia coli K12 MG1655 in accelerostat cultures.** *J Biotechnol* 2010, **145**:60-65.
4. Volkmer B, Heinemann M: **Condition-dependent cell volume and concentration of Escherichia coli to facilitate data conversion for systems biology modeling.** *PLoS One* 2011, **6**:e23126.
5. Valgepea K, Adamberg K, Nahku R, Lahtvee PJ, Arike L, Vilu R: **Systems biology approach reveals that overflow metabolism of acetate in Escherichia coli is triggered by carbon catabolite repression of acetyl-CoA synthetase.** *BMC Syst Biol* 2010, **4**:166.
6. Ishii N, Nakahigashi K, Baba T, Robert M, Soga T, Kanai A, Hirasawa T, Naba M, Hirai K, Hoque A, et al: **Multiple high-throughput analyses monitor the response of E. coli to perturbations.** *Science* 2007, **316**:593-597.
7. Kayser A, Weber J, Hecht V, Rinas U: **Metabolic flux analysis of Escherichia coli in glucose-limited continuous culture. I. Growth-rate-dependent metabolic efficiency at steady state.** *Microbiology* 2005, **151**:693-706.
8. Cheng C, O'Brien EJ, McCloskey D, Utrilla J, Olson C, LaCroix RA, Sandberg TE, Feist AM, Palsson BO, King ZA: **Laboratory evolution reveals a two-dimensional rate-yield tradeoff in microbial metabolism.** *PLoS Comput Biol* 2019, **15**:e1007066.
9. Yao R, Hirose Y, Sarkar D, Nakahigashi K, Ye Q, Shimizu K: **Catabolic regulation analysis of Escherichia coli and its crp, mlc, mgsA, pgi and ptsG mutants.** *Microb Cell Fact* 2011, **10**:67.
10. Zhao Q, Stettner AI, Reznik E, Paschalidis I, Segre D: **Mapping the landscape of metabolic goals of a cell.** *Genome Biol* 2016, **17**:109.
11. Stock JB, Ninfa AJ, Stock AM: **Protein phosphorylation and regulation of adaptive responses in bacteria.** *Microbiol Rev* 1989, **53**:450-490.
12. Litsios A, Ortega AD, Wit EC, Heinemann M: **Metabolic-flux dependent regulation of microbial physiology.** *Curr Opin Microbiol* 2018, **42**:71-78.
13. Bruckner R, Titgemeyer F: **Carbon catabolite repression in bacteria: choice of the carbon source and autoregulatory limitation of sugar utilization.** *FEMS Microbiol Lett* 2002, **209**:141-148.
14. Browning DF, Busby SJ: **The regulation of bacterial transcription initiation.** *Nat Rev Microbiol* 2004, **2**:57-65.
15. Vemuri GN, Aristidou AA: **Metabolic engineering in the -omics era: elucidating and modulating regulatory networks.** *Microbiol Mol Biol Rev* 2005, **69**:197-216.
16. Dekel E, Alon U: **Optimality and evolutionary tuning of the expression level of a protein.** *Nature* 2005, **436**:588-592.
17. Scott M, Gunderson CW, Mateescu EM, Zhang Z, Hwa T: **Interdependence of cell growth and gene expression: origins and consequences.** *Science* 2010, **330**:1099-1102.
18. Basan M: **Resource allocation and metabolism: the search for governing principles.** *Curr Opin Microbiol* 2018, **45**:77-83.
19. Shimizu K: **Metabolic Regulation of a Bacterial Cell System with Emphasis on Escherichia coli Metabolism.** *ISRN Biochem* 2013, **2013**:645983.
20. Sauer U: **Metabolic networks in motion: 13C-based flux analysis.** *Mol Syst Biol* 2006, **2**:62.
21. Bervoets I, Charlier D: **Diversity, versatility and complexity of bacterial gene regulation mechanisms: opportunities and drawbacks for applications in synthetic biology.** *FEMS Microbiol Rev* 2019, **43**:304-339.

22. Beltrao P, Bork P, Krogan NJ, van Noort V: **Evolution and functional cross-talk of protein post-translational modifications.** *Mol Syst Biol* 2013, **9**:714.
23. Shimizu K: **Regulation Systems of Bacteria such as Escherichia coli in Response to Nutrient Limitation and Environmental Stresses.** *Metabolites* 2014, **4**:1-35.
24. Schweder T, Kruger E, Xu B, Jurgen B, Blomsten G, Enfors SO, Hecker M: **Monitoring of genes that respond to process-related stress in large-scale bioprocesses.** *Biotechnol Bioeng* 1999, **65**:151-159.
25. Franchini AG, Egli T: **Global gene expression in Escherichia coli K-12 during short-term and long-term adaptation to glucose-limited continuous culture conditions.** *Microbiology* 2006, **152**:2111-2127.
26. Pasanen L, Holmström L: **Scale space multiresolution correlation analysis for time series data.** *Computational Statistics* 2017, **32**:197-218.
27. Brett MT: **When is a correlation between non-independent variables “spurious”?** *Oikos* 2004, **105**:647-656.
28. Kocher T, Pichler P, Swart R, Mechtler K: **Analysis of protein mixtures from whole-cell extracts by single-run nanoLC-MS/MS using ultralong gradients.** *Nat Protoc* 2012, **7**:882-890.
29. Valikangas T, Suomi T, Elo LL: **A comprehensive evaluation of popular proteomics software workflows for label-free proteome quantification and imputation.** *Brief Bioinform* 2018, **19**:1344-1355.
30. Wahl SA, Dauner M, Wiechert W: **New tools for mass isotopomer data evaluation in (13)C flux analysis: mass isotope correction, data consistency checking, and precursor relationships.** *Biotechnol Bioeng* 2004, **85**:259-268.
31. Kanehisa M, Goto S: **KEGG: kyoto encyclopedia of genes and genomes.** *Nucleic Acids Res* 2000, **28**:27-30.
32. Cheung J, Hendrickson WA: **Sensor domains of two-component regulatory systems.** *Curr Opin Microbiol* 2010, **13**:116-123.
33. Groisman EA: **Feedback Control of Two-Component Regulatory Systems.** *Annu Rev Microbiol* 2016, **70**:103-124.
34. Martinez-Antonio A, Collado-Vides J: **Identifying global regulators in transcriptional regulatory networks in bacteria.** *Curr Opin Microbiol* 2003, **6**:482-489.
35. Maeda H, Fujita N, Ishihama A: **Competition among seven Escherichia coli sigma subunits: relative binding affinities to the core RNA polymerase.** *Nucleic Acids Research* 2000, **28**:3497-3503.
36. Nachin L, Nannmark U, Nystrom T: **Differential roles of the universal stress proteins of Escherichia coli in oxidative stress resistance, adhesion, and motility.** *Journal of Bacteriology* 2005, **187**:6265-6272.
37. Kvint K, Nachin L, Diez A, Nystrom T: **The bacterial universal stress protein: function and regulation.** *Current Opinion in Microbiology* 2003, **6**:140-145.
38. Brissette JL, Weiner L, Ripmaster TL, Model P: **Characterization and sequence of the Escherichia coli stress-induced psp operon.** *J Mol Biol* 1991, **220**:35-48.
39. Weiner L, Model P: **Role of an Escherichia coli stress-response operon in stationary-phase survival.** *Proc Natl Acad Sci U S A* 1994, **91**:2191-2195.
40. Danese PN, Silhavy TJ: **CpxP, a stress-combative member of the Cpx regulon.** *J Bacteriol* 1998, **180**:831-839.
41. DiGiuseppe PA, Silhavy TJ: **Signal detection and target gene induction by the CpxRA two-component system.** *J Bacteriol* 2003, **185**:2432-2440.
42. Bochkareva ES, Girshovich AS, Bibi E: **Identification and characterization of the Escherichia coli stress protein UP12, a putative in vivo substrate of GroEL.** *Eur J Biochem* 2002, **269**:3032-3040.

43. Shinagawa H, Makino K, Nakata A: **Regulation of the pho regulon in Escherichia coli K-12. Genetic and physiological regulation of the positive regulatory gene phoB.** *J Mol Biol* 1983, **168**:477-488.
44. Steed PM, Wanner BL: **Use of the rep technique for allele replacement to construct mutants with deletions of the pstSCAB-phoU operon: evidence of a new role for the PhoU protein in the phosphate regulon.** *J Bacteriol* 1993, **175**:6797-6809.
45. Rice CD, Pollard JE, Lewis ZT, McCleary WR: **Employment of a promoter-swapping technique shows that PhoU modulates the activity of the PstSCAB2 ABC transporter in Escherichia coli.** *Appl Environ Microbiol* 2009, **75**:573-582.
46. Rodionov DA, Gelfand MS: **Identification of a bacterial regulatory system for ribonucleotide reductases by phylogenetic profiling.** *Trends Genet* 2005, **21**:385-389.
47. McKethan BL, Spiro S: **Cooperative and allosterically controlled nucleotide binding regulates the DNA binding activity of NrdR.** *Mol Microbiol* 2013, **90**:278-289.
48. Sukhodolets MV, Cabrera JE, Zhi H, Jin DJ: **RapA, a bacterial homolog of SWI2/SNF2, stimulates RNA polymerase recycling in transcription.** *Genes Dev* 2001, **15**:3330-3341.
49. Williams MD, Ouyang TX, Flickinger MC: **Starvation-induced expression of SspA and SspB: the effects of a null mutation in sspA on Escherichia coli protein synthesis and survival during growth and prolonged starvation.** *Mol Microbiol* 1994, **11**:1029-1043.
50. Caldara M, Charlier D, Cunin R: **The arginine regulon of Escherichia coli: whole-system transcriptome analysis discovers new genes and provides an integrated view of arginine regulation.** *Microbiology* 2006, **152**:3343-3354.
51. Lim DB, Oppenheim JD, Eckhardt T, Maas WK: **Nucleotide sequence of the argR gene of Escherichia coli K-12 and isolation of its product, the arginine repressor.** *Proc Natl Acad Sci U S A* 1987, **84**:6697-6701.
52. Charlier D, Roovers M, Van Vliet F, Boyen A, Cunin R, Nakamura Y, Glansdorff N, Pierard A: **Arginine regulon of Escherichia coli K-12. A study of repressor-operator interactions and of in vitro binding affinities versus in vivo repression.** *J Mol Biol* 1992, **226**:367-386.
53. Kiupakis AK, Reitzer L: **ArgR-independent induction and ArgR-dependent superinduction of the astCADBE operon in Escherichia coli.** *J Bacteriol* 2002, **184**:2940-2950.
54. Bury-Mone S, Nomane Y, Reymond N, Barbet R, Jacquet E, Imbeaud S, Jacq A, Bouloc P: **Global analysis of extracytoplasmic stress signaling in Escherichia coli.** *PLoS Genet* 2009, **5**:e1000651.
55. Al Mamun AA, Lombardo MJ, Shee C, Lisewski AM, Gonzalez C, Lin D, Nehring RB, Saint-Ruf C, Gibson JL, Frisch RL, et al: **Identity and function of a large gene network underlying mutagenic repair of DNA breaks.** *Science* 2012, **338**:1344-1348.
56. Luttgen H, Robelek R, Muhlberger R, Diercks T, Schuster SC, Kohler P, Kessler H, Bacher A, Richter G: **Transcriptional regulation by antitermination. Interaction of RNA with NusB protein and NusB/NusE protein complex of Escherichia coli.** *J Mol Biol* 2002, **316**:875-885.
57. Torres M, Balada JM, Zellars M, Squires C, Squires CL: **In vivo effect of NusB and NusG on rRNA transcription antitermination.** *J Bacteriol* 2004, **186**:1304-1310.
58. Delhay A, Laloux G, Collet JF: **The Lipoprotein NlpE Is a Cpx Sensor That Serves as a Sentinel for Protein Sorting and Folding Defects in the Escherichia coli Envelope.** *J Bacteriol* 2019, **201**.
59. Mecsas J, Rouviere PE, Erickson JW, Donohue TJ, Gross CA: **The activity of sigma E, an Escherichia coli heat-inducible sigma-factor, is modulated by expression of outer membrane proteins.** *Genes Dev* 1993, **7**:2618-2628.
60. Rouviere PE, De Las Penas A, Mecsas J, Lu CZ, Rudd KE, Gross CA: **rpoE, the gene encoding the second heat-shock sigma factor, sigma E, in Escherichia coli.** *EMBO J* 1995, **14**:1032-1042.
61. Raina S, Missiakas D, Georgopoulos C: **The rpoE gene encoding the sigma E (sigma 24) heat shock sigma factor of Escherichia coli.** *EMBO J* 1995, **14**:1043-1055.

62. Grainger DC, Hurd D, Goldberg MD, Busby SJ: **Association of nucleoid proteins with coding and non-coding segments of the *Escherichia coli* genome.** *Nucleic Acids Res* 2006, **34**:4642-4652.
63. Majdalani N, Heck M, Stout V, Gottesman S: **Role of RcsF in signaling to the Rcs phosphorelay pathway in *Escherichia coli*.** *J Bacteriol* 2005, **187**:6770-6778.
64. Clarke DJ: **The Rcs phosphorelay: more than just a two-component pathway.** *Future Microbiol* 2010, **5**:1173-1184.
65. Almiron M, Link AJ, Furlong D, Kolter R: **A novel DNA-binding protein with regulatory and protective roles in starved *Escherichia coli*.** *Genes Dev* 1992, **6**:2646-2654.
66. Nair S, Finkel SE: **Dps protects cells against multiple stresses during stationary phase.** *J Bacteriol* 2004, **186**:4192-4198.
67. Gustavsson N, Diez A, Nystrom T: **The universal stress protein paralogues of *Escherichia coli* are co-ordinately regulated and co-operate in the defence against DNA damage.** *Mol Microbiol* 2002, **43**:107-117.
68. Calvo JM, Matthews RG: **The leucine-responsive regulatory protein, a global regulator of metabolism in *Escherichia coli*.** *Microbiol Rev* 1994, **58**:466-490.
69. Tani TH, Khodursky A, Blumenthal RM, Brown PO, Matthews RG: **Adaptation to famine: A family of stationary-phase genes revealed by microarray analysis.** *Proceedings of the National Academy of Sciences of the United States of America* 2002, **99**:13471-13476.
70. Ernsting BR, Atkinson MR, Ninfa AJ, Matthews RG: **Characterization of the regulon controlled by the leucine-responsive regulatory protein in *Escherichia coli*.** *J Bacteriol* 1992, **174**:1109-1118.
71. Brinkman AB, Ettema TJ, de Vos WM, van der Oost J: **The Lrp family of transcriptional regulators.** *Mol Microbiol* 2003, **48**:287-294.
72. Jones PG, VanBogelen RA, Neidhardt FC: **Induction of proteins in response to low temperature in *Escherichia coli*.** *J Bacteriol* 1987, **169**:2092-2095.
73. Goldstein J, Pollitt NS, Inouye M: **Major cold shock protein of *Escherichia coli*.** *Proc Natl Acad Sci U S A* 1990, **87**:283-287.
74. Torres B, Porras G, Garcia JL, Diaz E: **Regulation of the mhp cluster responsible for 3-(3-hydroxyphenyl)propionic acid degradation in *Escherichia coli*.** *J Biol Chem* 2003, **278**:27575-27585.
75. Ogasawara H, Hasegawa A, Kanda E, Miki T, Yamamoto K, Ishihama A: **Genomic SELEX search for target promoters under the control of the PhoQP-RstBA signal relay cascade.** *J Bacteriol* 2007, **189**:4791-4799.
76. Yamamoto K, Hirao K, Oshima T, Aiba H, Utsumi R, Ishihama A: **Functional characterization in vitro of all two-component signal transduction systems from *Escherichia coli*.** *J Biol Chem* 2005, **280**:1448-1456.
77. De Pina K, Desjardin V, Mandrand-Berthelot MA, Giordano G, Wu LF: **Isolation and characterization of the nikR gene encoding a nickel-responsive regulator in *Escherichia coli*.** *J Bacteriol* 1999, **181**:670-674.
78. Schultz JE, Matin A: **Molecular and functional characterization of a carbon starvation gene of *Escherichia coli*.** *J Mol Biol* 1991, **218**:129-140.
79. Blum PH, Jovanovich SB, McCann MP, Schultz JE, Lesley SA, Burgess RR, Matin A: **Cloning and in vivo and in vitro regulation of cyclic AMP-dependent carbon starvation genes from *Escherichia coli*.** *J Bacteriol* 1990, **172**:3813-3820.
80. Raivio TL, Popkin DL, Silhavy TJ: **The Cpx envelope stress response is controlled by amplification and feedback inhibition.** *Journal of Bacteriology* 1999, **181**:5263-5272.
81. Saier MH, Ramseier TM: **The catabolite repressor/activator (Cra) protein of enteric bacteria.** *Journal of Bacteriology* 1996, **178**:3411-3417.
82. Ramseier TM: **Cra and the control of carbon flux via metabolic pathways.** *Research in Microbiology* 1996, **147**:489-493.

83. Zhang ZG, Aboulwafa M, Saier MH: **Regulation of crp Gene Expression by the Catabolite Repressor/Activator, Cra, in Escherichia coli.** *Journal of Molecular Microbiology and Biotechnology* 2014, **24**:135-141.
84. Timmermans J, Van Melderen L: **Post-transcriptional global regulation by CsrA in bacteria.** *Cellular and Molecular Life Sciences* 2010, **67**:2897-2908.
85. Sabnis NA, Yang H, Romeo T: **Pleiotropic regulation of central carbohydrate metabolism in Escherichia coli via the gene csrA.** *J Biol Chem* 1995, **270**:29096-29104.
86. Jain V, Kumar M, Chatterji D: **ppGpp: stringent response and survival.** *J Microbiol* 2006, **44**:1-10.
87. Magnusson LU, Farewell A, Nystrom T: **ppGpp: a global regulator in Escherichia coli.** *Trends Microbiol* 2005, **13**:236-242.
88. Baracchini E, Bremer H: **Stringent and growth control of rRNA synthesis in Escherichia coli are both mediated by ppGpp.** *J Biol Chem* 1988, **263**:2597-2602.
89. Torok I, Kari C: **Accumulation of ppGpp in a relA mutant of Escherichia coli during amino acid starvation.** *J Biol Chem* 1980, **255**:3838-3840.
90. Johnson GS, Adler CR, Collins JJ, Court D: **Role of the spoT gene product and manganese ion in the metabolism of guanosine 5'-diphosphate 3'-diphosphate in Escherichia coli.** *J Biol Chem* 1979, **254**:5483-5487.
91. Parker J, Watson RJ, Friesen JD: **A relaxed mutant with an altered ribosomal protein L11.** *Mol Gen Genet* 1976, **144**:111-114.
92. Artsimovitch I, Patlan V, Sekine S, Vassilyeva MN, Hosaka T, Ochi K, Yokoyama S, Vassilyev DG: **Structural basis for transcription regulation by alarmone ppGpp.** *Cell* 2004, **117**:299-310.
93. Bosdriesz E, Molenaar D, Teusink B, Bruggeman FJ: **How fast-growing bacteria robustly tune their ribosome concentration to approximate growth-rate maximization.** *FEBS J* 2015, **282**:2029-2044.
94. Neidhardt FC, Magasanik B: **Studies on the role of ribonucleic acid in the growth of bacteria.** *Biochim Biophys Acta* 1960, **42**:99-116.
95. Okamoto S, Tamaru A, Nakajima C, Nishimura K, Tanaka Y, Tokuyama S, Suzuki Y, Ochi K: **Loss of a conserved 7-methylguanosine modification in 16S rRNA confers low-level streptomycin resistance in bacteria.** *Mol Microbiol* 2007, **63**:1096-1106.
96. Kimura S, Suzuki T: **Fine-tuning of the ribosomal decoding center by conserved methyl-modifications in the Escherichia coli 16S rRNA.** *Nucleic Acids Res* 2010, **38**:1341-1352.
97. Capecchi MR: **Polypeptide chain termination in vitro: isolation of a release factor.** *Proc Natl Acad Sci U S A* 1967, **58**:1144-1151.
98. Scolnick E, Tompkins R, Caskey T, Nirenberg M: **Release factors differing in specificity for terminator codons.** *Proc Natl Acad Sci U S A* 1968, **61**:768-774.
99. Janssen BD, Hayes CS: **Kinetics of paused ribosome recycling in Escherichia coli.** *J Mol Biol* 2009, **394**:251-267.
100. Vivanco-Dominguez S, Bueno-Martinez J, Leon-Avila G, Iwakura N, Kaji A, Kaji H, Guarneros G: **Protein synthesis factors (RF1, RF2, RF3, RRF, and tmRNA) and peptidyl-tRNA hydrolase rescue stalled ribosomes at sense codons.** *J Mol Biol* 2012, **417**:425-439.
101. Wrzesinski J, Bakin A, Nurse K, Lane BG, Ofengand J: **Purification, cloning, and properties of the 16S RNA pseudouridine 516 synthase from Escherichia coli.** *Biochemistry* 1995, **34**:8904-8913.
102. Vanet A, Plumbridge JA, Alix JH: **Cotranscription of two genes necessary for ribosomal protein L11 methylation (prmA) and pantothenate transport (panF) in Escherichia coli K-12.** *J Bacteriol* 1993, **175**:7178-7188.
103. Zurawski G, Zurawski SM: **Structure of the Escherichia coli S10 ribosomal protein operon.** *Nucleic Acids Res* 1985, **13**:4521-4526.
104. Maki Y, Yoshida H, Wada A: **Two proteins, YfiA and YhbH, associated with resting ribosomes in stationary phase Escherichia coli.** *Genes Cells* 2000, **5**:965-974.

105. Gregory RJ, Zeller ML, Thurlow DL, Gourse RL, Stark MJ, Dahlberg AE, Zimmermann RA: **Interaction of ribosomal proteins S6, S8, S15 and S18 with the central domain of 16 S ribosomal RNA from *Escherichia coli*.** *J Mol Biol* 1984, **178**:287-302.
106. Stern S, Powers T, Changchien LM, Noller HF: **Interaction of ribosomal proteins S5, S6, S11, S12, S18 and S21 with 16 S rRNA.** *J Mol Biol* 1988, **201**:683-695.
107. Odom OW, Deng HY, Dabbs ER, Hardesty B: **Binding of S21 to the 50S subunit and the effect of the 50S subunit on nonradiative energy transfer between the 3' end of 16S RNA and S21.** *Biochemistry* 1984, **23**:5069-5076.
108. Steward KL, Linn T: **In vivo analysis of overlapping transcription units in the rplKALrpoBC ribosomal protein-RNA polymerase gene cluster of *Escherichia coli*.** *J Mol Biol* 1991, **218**:23-31.
109. Wittmann-Liebold B, Greuer B, Pannenbecker R: **The primary structure of protein L32 from the 50S subunit of *Escherichia coli* ribosomes.** *Hoppe Seylers Z Physiol Chem* 1975, **356**:1977-1979.
110. Caldas T, Binet E, Bouloc P, Costa A, Desgres J, Richarme G: **The FtsJ/RrmJ heat shock protein of *Escherichia coli* is a 23 S ribosomal RNA methyltransferase.** *J Biol Chem* 2000, **275**:16414-16419.
111. Montesano-Roditis L, McWilliams R, Glitz DG, Olah TV, Perrault AR, Cooperman BS: **Placement of dinitrophenyl-modified ribosomal proteins in totally reconstituted *Escherichia coli* 30 S subunits. Localization of proteins S6, S13, S16, and S18 by immune electron microscopy.** *J Biol Chem* 1993, **268**:18701-18709.
112. Gotz F, Dabbs ER, Gualerzi CO: ***Escherichia coli* 30S mutants lacking protein S20 are defective in translation initiation.** *Biochim Biophys Acta* 1990, **1050**:93-97.
113. Fischer N, Neumann P, Konevega AL, Bock LV, Ficner R, Rodnina MV, Stark H: **Structure of the *E. coli* ribosome-EF-Tu complex at <3 Å resolution by Cs-corrected cryo-EM.** *Nature* 2015, **520**:567-570.
114. Mikuni O, Ito K, Moffat J, Matsumura K, McCaughan K, Nobukuni T, Tate W, Nakamura Y: **Identification of the prfC gene, which encodes peptide-chain-release factor 3 of *Escherichia coli*.** *Proc Natl Acad Sci U S A* 1994, **91**:5798-5802.
115. McCaughan KK, Ward CD, Trotman CN, Tate WP: **The ribosomal binding domain for the bacterial release factors RF-1, RF-2 and RF-3.** *FEBS Lett* 1984, **175**:90-94.
116. Maguire BA, Wild DG: **The roles of proteins L28 and L33 in the assembly and function of *Escherichia coli* ribosomes in vivo.** *Mol Microbiol* 1997, **23**:237-245.
117. Basturea GN, Rudd KE, Deutscher MP: **Identification and characterization of RsmE, the founding member of a new RNA base methyltransferase family.** *RNA* 2006, **12**:426-434.
118. Meek DW, Hayward RS: **Nucleotide sequence of the rpoA-rplQ DNA of *Escherichia coli*: a second regulatory binding site for protein S4?** *Nucleic Acids Res* 1984, **12**:5813-5821.
119. Purta E, O'Connor M, Bujnicki JM, Douthwaite S: **YccW is the m5C methyltransferase specific for 23S rRNA nucleotide 1962.** *J Mol Biol* 2008, **383**:641-651.
120. Schuwirth BS, Borovinskaya MA, Hau CW, Zhang W, Vila-Sanjurjo A, Holton JM, Cate JH: **Structures of the bacterial ribosome at 3.5 Å resolution.** *Science* 2005, **310**:827-834.
121. Kakegawa T, Sato E, Hirose S, Igarashi K: **Polyamine binding sites on *Escherichia coli* ribosomes.** *Arch Biochem Biophys* 1986, **251**:413-420.
122. Cate JH, Yusupov MM, Yusupova GZ, Earnest TN, Noller HF: **X-ray crystal structures of 70S ribosome functional complexes.** *Science* 1999, **285**:2095-2104.
123. Kaczanowska M, Ryden-Aulin M: **Ribosome biogenesis and the translation process in *Escherichia coli*.** *Microbiol Mol Biol Rev* 2007, **71**:477-494.
124. Anfinsen CB, Scheraga HA: **Experimental and theoretical aspects of protein folding.** *Adv Protein Chem* 1975, **29**:205-300.
125. Gottesman S: **Proteases and their targets in *Escherichia coli*.** *Annu Rev Genet* 1996, **30**:465-506.



126. Cohen RD, Guseman AJ, Pielak GJ: **Intracellular pH modulates quinary structure.** *Protein Sci* 2015, **24**:1748-1755.
127. Buskirk AR, Green R: **Ribosome pausing, arrest and rescue in bacteria and eukaryotes.** *Philos Trans R Soc Lond B Biol Sci* 2017, **372**.
128. Subramaniam AR, Zid BM, O'Shea EK: **An integrated approach reveals regulatory controls on bacterial translation elongation.** *Cell* 2014, **159**:1200-1211.
129. Subramaniam AR, Pan T, Cluzel P: **Environmental perturbations lift the degeneracy of the genetic code to regulate protein levels in bacteria.** *Proc Natl Acad Sci U S A* 2013, **110**:2419-2424.
130. Maurizi MR: **Proteases and protein degradation in Escherichia coli.** *Experientia* 1992, **48**:178-201.
131. Hartl FU, Bracher A, Hayer-Hartl M: **Molecular chaperones in protein folding and proteostasis.** *Nature* 2011, **475**:324-332.
132. Vickery LE, Silberg JJ, Ta DT: **Hsc66 and Hsc20, a new heat shock cognate molecular chaperone system from Escherichia coli.** *Protein Sci* 1997, **6**:1047-1056.
133. Silberg JJ, Hoff KG, Vickery LE: **The Hsc66-Hsc20 chaperone system in Escherichia coli: chaperone activity and interactions with the DnaK-DnaJ-grpE system.** *J Bacteriol* 1998, **180**:6617-6624.
134. Lutticke C, Hauske P, Lewandrowski U, Sickmann A, Kaiser M, Ehrmann M: **E. coli LoiP (YggG), a metalloprotease hydrolyzing Phe-Phe bonds.** *Mol Biosyst* 2012, **8**:1775-1782.
135. Huang Y, Dong K, Zhang X, Zhang B, Hou L, Chen N, Chen S: **Expression and regulation of the yggG gene of Escherichia coli.** *Curr Microbiol* 2008, **56**:14-20.
136. Suzuki H, Kamatani S, Kim ES, Kumagai H: **Aminopeptidases A, B, and N and dipeptidase D are the four cysteinylglycinases of Escherichia coli K-12.** *J Bacteriol* 2001, **183**:1489-1490.
137. Ullers RS, Luirink J, Harms N, Schwager F, Georgopoulos C, Genevaux P: **SecB is a bona fide generalized chaperone in Escherichia coli.** *Proc Natl Acad Sci U S A* 2004, **101**:7583-7588.
138. Seoh HK, Tai PC: **Carbon source-dependent synthesis of SecB, a cytosolic chaperone involved in protein translocation across Escherichia coli membranes.** *J Bacteriol* 1997, **179**:1077-1081.
139. Vertommen D, Depuydt M, Pan J, Leverrier P, Knoop L, Szikora JP, Messens J, Bardwell JC, Collet JF: **The disulphide isomerase DsbC cooperates with the oxidase DsbA in a DsbD-independent manner.** *Mol Microbiol* 2008, **67**:336-349.
140. Chen J, Song JL, Zhang S, Wang Y, Cui DF, Wang CC: **Chaperone activity of DsbC.** *J Biol Chem* 1999, **274**:19601-19605.
141. Li H, Chang L, Howell JM, Turner RJ: **DmsD, a Tat system specific chaperone, interacts with other general chaperones and proteins involved in the molybdenum cofactor biosynthesis.** *Biochim Biophys Acta* 2010, **1804**:1301-1309.
142. Cheng ZF, Deutscher MP: **Purification and characterization of the Escherichia coli exoribonuclease RNase R. Comparison with RNase II.** *J Biol Chem* 2002, **277**:21624-21629.
143. Cairrao F, Cruz A, Mori H, Arraiano CM: **Cold shock induction of RNase R and its role in the maturation of the quality control mediator SsrA/tmRNA.** *Mol Microbiol* 2003, **50**:1349-1360.
144. Richards J, Mehta P, Karzai AW: **RNase R degrades non-stop mRNAs selectively in an SmpB-tmRNA-dependent manner.** *Mol Microbiol* 2006, **62**:1700-1712.
145. Le HT, Gautier V, Kthiri F, Malki A, Messaoudi N, Mihoub M, Landoulsi A, An YJ, Cha SS, Richarme G: **YajL, prokaryotic homolog of parkinsonism-associated protein DJ-1, functions as a covalent chaperone for thiol proteome.** *J Biol Chem* 2012, **287**:5861-5870.
146. Sussman AJ, Gilvarg C: **Peptidases in Escherichia coli K-12 capable of cleaving lysine homopeptides.** *J Biol Chem* 1970, **245**:6518-6524.
147. Simmonds S, Szeto KS, Fletterick CG: **Soluble tri- and dipeptidases in Escherichia coli K-12+.** *Biochemistry* 1976, **15**:261-271.
148. Norregaard-Madsen M, Mygind B, Pedersen R, Valentin-Hansen P, Sogaard-Andersen L: **The gene encoding the periplasmic cyclophilin homologue, PPlase A, in Escherichia coli, is**

- expressed from four promoters, three of which are activated by the cAMP-CRP complex and negatively regulated by the CytR repressor. *Mol Microbiol* 1994, **14**:989-997.
149. Pogliano J, Lynch AS, Belin D, Lin EC, Beckwith J: **Regulation of Escherichia coli cell envelope proteins involved in protein folding and degradation by the Cpx two-component system.** *Genes Dev* 1997, **11**:1169-1182.
150. Liu J, Walsh CT: **Peptidyl-prolyl cis-trans-isomerase from Escherichia coli: a periplasmic homolog of cyclophilin that is not inhibited by cyclosporin A.** *Proc Natl Acad Sci U S A* 1990, **87**:4028-4032.
151. Devroede N, Huysveld N, Charlier D: **Mutational analysis of intervening sequences connecting the binding sites for integration host factor, PepA, PurR, and RNA polymerase in the control region of the Escherichia coli carAB operon, encoding carbamoylphosphate synthase.** *J Bacteriol* 2006, **188**:3236-3245.
152. Mitchell AM, Wang W, Silhavy TJ: **Novel RpoS-Dependent Mechanisms Strengthen the Envelope Permeability Barrier during Stationary Phase.** *J Bacteriol* 2017, **199**.
153. Strauch KL, Beckwith J: **An Escherichia coli mutation preventing degradation of abnormal periplasmic proteins.** *Proc Natl Acad Sci U S A* 1988, **85**:1576-1580.
154. Strauch KL, Johnson K, Beckwith J: **Characterization of degP, a gene required for proteolysis in the cell envelope and essential for growth of Escherichia coli at high temperature.** *J Bacteriol* 1989, **171**:2689-2696.
155. Costello SM, Plummer AM, Fleming PJ, Fleming KG: **Dynamic periplasmic chaperone reservoir facilitates biogenesis of outer membrane proteins.** *Proc Natl Acad Sci U S A* 2016, **113**:E4794-4800.
156. Spiess C, Beil A, Ehrmann M: **A temperature-dependent switch from chaperone to protease in a widely conserved heat shock protein.** *Cell* 1999, **97**:339-347.
157. Wu WF, Zhou Y, Gottesman S: **Redundant in vivo proteolytic activities of Escherichia coli Lon and the ClpYQ (HslUV) protease.** *J Bacteriol* 1999, **181**:3681-3687.
158. Rohrwild M, Coux O, Huang HC, Moerschell RP, Yoo SJ, Seol JH, Chung CH, Goldberg AL: **HslV-HslU: A novel ATP-dependent protease complex in Escherichia coli related to the eukaryotic proteasome.** *Proc Natl Acad Sci U S A* 1996, **93**:5808-5813.
159. Liberek K, Marszalek J, Ang D, Georgopoulos C, Zylicz M: **Escherichia coli DnaJ and GrpE heat shock proteins jointly stimulate ATPase activity of DnaK.** *Proc Natl Acad Sci U S A* 1991, **88**:2874-2878.
160. Gamer J, Multhaup G, Tomoyasu T, McCarty JS, Rudiger S, Schonfeld HJ, Schirra C, Bujard H, Bukau B: **A cycle of binding and release of the DnaK, DnaJ and GrpE chaperones regulates activity of the Escherichia coli heat shock transcription factor sigma32.** *EMBO J* 1996, **15**:607-617.
161. Lennon CW, Thamsen M, Friman ET, Cacciaglia A, Sachsenhauser V, Sorgenfrei FA, Wasik MA, Bardwell JC: **Folding Optimization In Vivo Uncovers New Chaperones.** *J Mol Biol* 2015, **427**:2983-2994.
162. Weichart D, Lange R, Henneberg N, Hengge-Aronis R: **Identification and characterization of stationary phase inducible genes in Escherichia coli.** *Mol Microbiol* 1993, **10**:407-420.
163. Kern R, Malki A, Abdallah J, Tagourt J, Richarme G: **Escherichia coli HdeB is an acid stress chaperone.** *J Bacteriol* 2007, **189**:603-610.
164. Turlin E, Gasser F, Biville F: **Sequence and functional analysis of an Escherichia coli DNA fragment able to complement pqqE and pqqF mutants from Methylobacterium organophilum.** *Biochimie* 1996, **78**:823-831.
165. Sugimura K, Nishihara T: **Purification, characterization, and primary structure of Escherichia coli protease VII with specificity for paired basic residues: identity of protease VII and OmpT.** *J Bacteriol* 1988, **170**:5625-5632.
166. Zhang H, Zhang J, Wang X, Yang W, Lu J: **Biochemical characterization of alpha-aspartyl dipeptidase. Cloning and expression of its gene.** *Ann N Y Acad Sci* 1998, **864**:621-625.

167. Okutani S, Iwai T, Iwatani S, Matsuno K, Takahashi Y, Hase T: **Response of Fe-S cluster assembly machinery of Escherichia coli to mechanical stress in a model of amino-acid crystal fermentation.** *J Biosci Bioeng* 2015, **120**:287-293.
168. Kluck CJ, Patzelt H, Genevaux P, Brehmer D, Rist W, Schneider-Mergener J, Bukau B, Mayer MP: **Structure-function analysis of HscC, the Escherichia coli member of a novel subfamily of specialized Hsp70 chaperones.** *J Biol Chem* 2002, **277**:41060-41069.
169. Hesterkamp T, Bukau B: **Role of the DnaK and HscA homologs of Hsp70 chaperones in protein folding in E.coli.** *EMBO J* 1998, **17**:4818-4828.
170. Gottesman S: **Proteolysis in bacterial regulatory circuits.** *Annu Rev Cell Dev Biol* 2003, **19**:565-587.
171. Nikaïdo H, Nakae T: **The outer membrane of Gram-negative bacteria.** *Adv Microb Physiol* 1979, **20**:163-250.
172. Stock JB, Waygood EB, Meadow ND, Postma PW, Roseman S: **Sugar transport by the bacterial phosphotransferase system. The glucose receptors of the Salmonella typhimurium phosphotransferase system.** *J Biol Chem* 1982, **257**:14543-14552.
173. Misset O, Blaauw M, Postma PW, Robillard GT: **Bacterial phosphoenolpyruvate-dependent phosphotransferase system. Mechanism of the transmembrane sugar translocation and phosphorylation.** *Biochemistry* 1983, **22**:6163-6170.
174. Kundig W, Roseman S, Ghosh S: **Phosphate Bound to Histidine in Protein as Intermediate in Novel Phospho-Transferase System.** *Proceedings of the National Academy of Sciences of the United States of America* 1964, **52**:1067-&.
175. Liu X, Ferenci T: **Regulation of porin-mediated outer membrane permeability by nutrient limitation in Escherichia coli.** *J Bacteriol* 1998, **180**:3917-3922.
176. Ferenci T: **Adaptation to life at micromolar nutrient levels: the regulation of Escherichia coli glucose transport by endoinduction and cAMP.** *FEMS Microbiol Rev* 1996, **18**:301-317.
177. Death A, Notley L, Ferenci T: **Derepression of LamB protein facilitates outer membrane permeation of carbohydrates into Escherichia coli under conditions of nutrient stress.** *J Bacteriol* 1993, **175**:1475-1483.
178. Hua Q, Yang C, Oshima T, Mori H, Shimizu K: **Analysis of gene expression in Escherichia coli in response to changes of growth-limiting nutrient in chemostat cultures.** *Appl Environ Microbiol* 2004, **70**:2354-2366.
179. Hunter IS, Kornberg HL: **Glucose transport of Escherichia coli growing in glucose-limited continuous culture.** *Biochem J* 1979, **178**:97-101.
180. Death A, Ferenci T: **The Importance of the Binding-Protein-Dependent Mgi System to the Transport of Glucose in Escherichia-Coli Growing on Low Sugar Concentrations.** *Research in Microbiology* 1993, **144**:529-537.
181. Boos W, Shuman H: **Maltose/maltodextrin system of Escherichia coli: transport, metabolism, and regulation.** *Microbiol Mol Biol Rev* 1998, **62**:204-229.
182. Notley L, Ferenci T: **Differential expression of mal genes under cAMP and endogenous inducer control in nutrient-stressed Escherichia coli.** *Mol Microbiol* 1995, **16**:121-129.
183. Steinsiek S, Bettenbrock K: **Glucose Transport in Escherichia coli Mutant Strains with Defects in Sugar Transport Systems.** *Journal of Bacteriology* 2012, **194**:5897-5908.
184. Fraser HI, Kvaratskhelia M, White MF: **The two analogous phosphoglycerate mutases of Escherichia coli.** *FEBS Lett* 1999, **455**:344-348.
185. Foster JM, Davis PJ, Raverdy S, Sibley MH, Raleigh EA, Kumar S, Carlow CK: **Evolution of bacterial phosphoglycerate mutases: non-homologous isofunctional enzymes undergoing gene losses, gains and lateral transfers.** *PLoS One* 2010, **5**:e13576.
186. Hellinga HW, Evans PR: **Nucleotide sequence and high-level expression of the major Escherichia coli phosphofructokinase.** *Eur J Biochem* 1985, **149**:363-373.
187. Sprenger GA: **Genetics of pentose-phosphate pathway enzymes of Escherichia coli K-12.** *Arch Microbiol* 1995, **164**:324-330.

188. Olavarria K, Valdes D, Cabrera R: **The cofactor preference of glucose-6-phosphate dehydrogenase from *Escherichia coli*--modeling the physiological production of reduced cofactors.** *FEBS J* 2012, **279**:2296-2309.
189. Cooper RA, Kornberg HL: **The direct synthesis of phosphoenolpyruvate from pyruvate by *Escherichia coli*.** *Proc R Soc Lond B Biol Sci* 1967, **168**:263-280.
190. Berg JM, Tymoczko JL, Stryer L: **The Glycolytic Pathway Is Tightly Controlled.** In *Biochemistry*. 5th edition. Edited by Freeman WH. New York 2002.
191. Hofmann E: **The significance of phosphofructokinase to the regulation of carbohydrate metabolism.** *Rev Physiol Biochem Pharmacol* 1976, **75**:1-68.
192. Fothergill-Gilmore LA, Michels PA: **Evolution of glycolysis.** *Prog Biophys Mol Biol* 1993, **59**:105-235.
193. Kim HU, Kim WJ, Lee SY: **Flux-coupled genes and their use in metabolic flux analysis.** *Biotechnol J* 2013, **8**:1035-1042.
194. Cunningham L, Gruer MJ, Guest JR: **Transcriptional regulation of the aconitase genes (*acnA* and *acnB*) of *Escherichia coli*.** *Microbiology* 1997, **143 ( Pt 12)**:3795-3805.
195. Oh MK, Rohlin L, Kao KC, Liao JC: **Global expression profiling of acetate-grown *Escherichia coli*.** *J Biol Chem* 2002, **277**:13175-13183.
196. Cozzone AJ: **Regulation of acetate metabolism by protein phosphorylation in enteric bacteria.** *Annu Rev Microbiol* 1998, **52**:127-164.
197. Borirak O, Bekker M, Hellingwerf KJ: **Molecular physiology of the dynamic regulation of carbon catabolite repression in *Escherichia coli*.** *Microbiology* 2014, **160**:1214-1223.
198. Ishizuka H, Hanamura A, Kunimura T, Aiba H: **A lowered concentration of cAMP receptor protein caused by glucose is an important determinant for catabolite repression in *Escherichia coli*.** *Mol Microbiol* 1993, **10**:341-350.
199. Frigon D, Muyzer G, van Loosdrecht M, Raskin L: **rRNA and poly-beta-hydroxybutyrate dynamics in bioreactors subjected to feast and famine cycles.** *Appl Environ Microbiol* 2006, **72**:2322-2330.
200. Pickett AM, Bazin MJ, Topiwala HH: **Growth and Composition of *Escherichia-Coli* Subjected to Square-Wave Perturbations in Nutrient Supply - Effect of Varying Amplitudes.** *Biotechnology and Bioengineering* 1980, **22**:1213-1224.
201. Sepers ABJ: **Effect of variable nutrient supply rates on the RNA level of a heterotrophic bacterial strain.** *Current Microbiology* 1986, **13**:333-336.
202. Keiler KC, Waller PR, Sauer RT: **Role of a peptide tagging system in degradation of proteins synthesized from damaged messenger RNA.** *Science* 1996, **271**:990-993.
203. Herman C, Thevenet D, Bouloc P, Walker GC, D'Ari R: **Degradation of carboxy-terminal-tagged cytoplasmic proteins by the *Escherichia coli* protease HflB (FtsH).** *Genes Dev* 1998, **12**:1348-1355.
204. Gottesman S, Roche E, Zhou Y, Sauer RT: **The ClpXP and ClpAP proteases degrade proteins with carboxy-terminal peptide tails added by the SsrA-tagging system.** *Genes Dev* 1998, **12**:1338-1347.
205. Koch AL: **The adaptive responses of *Escherichia coli* to a feast and famine existence.** *Adv Microb Physiol* 1971, **6**:147-217.
206. Koch AL, Deppe CS: **In vivo assay of protein synthesizing capacity of *Escherichia coli* from slowly growing chemostat cultures.** *J Mol Biol* 1971, **55**:549-562.
207. Dai X, Zhu M, Warren M, Balakrishnan R, Patsalo V, Okano H, Williamson JR, Fredrick K, Wang YP, Hwa T: **Reduction of translating ribosomes enables *Escherichia coli* to maintain elongation rates during slow growth.** *Nat Microbiol* 2016, **2**:16231.
208. Li SH, Li Z, Park JO, King CG, Rabinowitz JD, Wingreen NS, Gitai Z: ***Escherichia coli* translation strategies differ across carbon, nitrogen and phosphorus limitation conditions.** *Nat Microbiol* 2018, **3**:939-947.

209. Schmidt A, Kochanowski K, Vedelaar S, Ahrne E, Volkmer B, Callipo L, Knoop K, Bauer M, Aebersold R, Heinemann M: **The quantitative and condition-dependent Escherichia coli proteome.** *Nat Biotechnol* 2016, **34**:104-110.
210. Koebmann BJ, Westerhoff HV, Snoep JL, Nilsson D, Jensen PR: **The glycolytic flux in Escherichia coli is controlled by the demand for ATP.** *J Bacteriol* 2002, **184**:3909-3916.
211. Ruyter GJ, Postma PW, van Dam K: **Control of glucose metabolism by enzyme IIGlc of the phosphoenolpyruvate-dependent phosphotransferase system in Escherichia coli.** *J Bacteriol* 1991, **173**:6184-6191.
212. Scott M, Hwa T: **Bacterial growth laws and their applications.** *Curr Opin Biotechnol* 2011, **22**:559-565.
213. Flamholz A, Noor E, Bar-Even A, Liebermeister W, Milo R: **Glycolytic strategy as a tradeoff between energy yield and protein cost.** *Proc Natl Acad Sci U S A* 2013, **110**:10039-10044.
214. Valgepea K, Adamberg K, Seiman A, Vilu R: **Escherichia coli achieves faster growth by increasing catalytic and translation rates of proteins.** *Mol Biosyst* 2013, **9**:2344-2358.
215. Taymaz-Nikerel H, van Gulik WM, Heijnen JJ: **Escherichia coli responds with a rapid and large change in growth rate upon a shift from glucose-limited to glucose-excess conditions.** *Metab Eng* 2011, **13**:307-318.
216. Fischer E, Sauer U: **A novel metabolic cycle catalyzes glucose oxidation and anaplerosis in hungry Escherichia coli.** *J Biol Chem* 2003, **278**:46446-46451.
217. Wick LM, Quadroni M, Egli T: **Short- and long-term changes in proteome composition and kinetic properties in a culture of Escherichia coli during transition from glucose-excess to glucose-limited growth conditions in continuous culture and vice versa.** *Environ Microbiol* 2001, **3**:588-599.
218. Borirak O, Rolfe MD, de Koning LJ, Hoefsloot HC, Bekker M, Dekker HL, Roseboom W, Green J, de Koster CG, Hellingwerf KJ: **Time-series analysis of the transcriptome and proteome of Escherichia coli upon glucose repression.** *Biochim Biophys Acta* 2015, **1854**:1269-1279.

## Appendix C

### C.1 Protein functional classification

**Table C-1** Functional classification of statistically significant (significance level threshold of  $\geq 15$ ) proteome changes between the RCF and the BWF.

CATEGORIES	Number of significantly changed proteins		Number of unchanged proteins	Percentage of changed proteins over total measured proteome (%)		
	Up-regulated	Down-regulated		Up-regulated	Down-regulated	Total
<b>Energy Metabolism</b>	5	1	11	29.4	5.9	<b>35.3</b>
<b>Membrane Transport</b>	25	20	92	18.2	14.6	<b>32.8</b>
<b>Biosynthesis</b>	73	14	164	29.1	5.6	<b>34.7</b>
<b>Central Carbon Metabolism</b>	25	17	81	20.3	13.8	<b>34.1</b>
<b>Other Metabolic Enzymes</b>	7	7	62	9.2	9.2	<b>18.4</b>
<b>Translation</b>	33	3	64	33.0	3.0	<b>36.0</b>
<b>Protein Folding and Degradation</b>	18	8	61	20.7	9.2	<b>29.9</b>
<b>Transcription</b>	9	2	39	18.0	4.0	<b>22.0</b>
<b>Signal Transduction</b>	2	3	32	5.4	8.1	<b>13.5</b>
<b>DNA Maintenance</b>	5	1	27	15.2	3.0	<b>18.2</b>
<b>Cell Structure and Motility</b>	1	2	5	12.5	25.0	<b>37.5</b>
Unclassified proteins	82	39	280	20.4	9.7	<b>30.1</b>

## C.2 <sup>13</sup>C isotope tracing

The following tables consist of the mass isotopomer measurements of the <sup>13</sup>C tracing experiment for metabolites of glycolysis, TCA cycle, pentose phosphate pathway and amino acids. The analytical methods are described in section 3.2.5 (Chapter 3). The data were corrected for the natural stable mass isotopes, using the MS correction tool, as established by Wahl SA, *et al.* [1]. <sup>13</sup>C-labelled glucose was fed during the first two cycles and the feed was changed to <sup>12</sup>C-labelled glucose at the 3<sup>rd</sup> cycle. N.Q. is used for non-quantified enrichments.

**Table C-2** Percentages of isotope and total <sup>13</sup>C enrichment of metabolites over time.

FBP									
		Isotope enrichment (%)							Total enrichment (%)
	Cycle time (s)	m+0	m+1	m+2	m+3	m+4	m+5	m+6	
1 <sup>st</sup> cycle	0	92.2	6.0	0.9	0.2	0.2	0.4	0.2	2.1
	10	78.5	3.8	0.5	1.8	0.8	1.1	13.6	16.6
	20	55.1	2.9	0.9	3.2	1.1	3.1	33.8	39.4
	30	48.2	2.7	0.6	3.5	0.9	3.3	40.9	46.6
	40	25.9	1.9	N.Q.	4.9	1.8	5.5	60.0	68.6
	60	46.4	2.9	0.8	2.4	1.1	3.9	42.5	48.4
	80	49.9	3.0	1.0	1.9	0.6	2.8	40.6	45.2
	100	54.1	3.4	1.1	2.2	0.9	3.1	35.1	40.4
	120	85.2	6.3	1.9	0.8	0.5	1.1	4.3	7.6
	150	81.0	7.7	1.6	N.Q.	3.1	0.7	6.0	10.4
	185	86.2	6.2	2.3	0.8	0.7	2.0	1.7	6.1
	220	79.0	7.2	3.3	1.6	2.9	3.1	3.0	10.6
	260	82.8	7.1	3.1	1.2	2.4	1.8	1.5	7.5
	300	75.8	9.1	5.4	1.6	2.9	2.7	2.3	10.7
360	76.1	8.6	3.7	2.8	3.1	3.2	2.5	11.3	
2 <sup>nd</sup> cycle	0	77.0	9.5	3.8	2.2	3.6	2.4	1.6	9.9
	10	68.9	7.2	2.8	2.6	3.4	2.6	12.5	20.3
	20	34.7	3.3	2.1	3.3	2.9	5.5	48.2	57.6
	40	33.2	3.6	1.1	1.9	2.2	5.9	52.0	60.3
	60	47.4	5.7	2.4	2.5	3.2	4.2	34.5	43.2
	80	22.9	3.0	1.7	3.1	2.5	6.8	60.0	70.0
	100	38.0	3.2	2.1	2.8	3.3	5.1	45.4	54.5
	120	44.4	4.7	2.4	3.4	3.4	4.1	37.6	46.6
	150	70.9	7.7	4.5	2.9	5.1	5.0	4.0	15.7
	185	70.7	8.1	3.6	3.1	5.1	5.7	3.8	15.9
	220	72.5	8.2	3.9	1.6	4.9	5.7	3.2	14.7
	260	61.6	8.8	5.4	3.6	7.2	8.3	5.1	21.9
	300	53.9	11.0	4.9	5.0	6.7	12.1	6.4	26.9
	360	66.6	8.5	4.7	3.2	6.9	7.1	3.0	18.1

FBP									
		Isotope enrichment (%)							Total enrichment (%)
	Cycle time (s)	m+0	m+1	m+2	m+3	m+4	m+5	m+6	
3 <sup>rd</sup> cycle	0	65.7	8.2	4.8	3.6	7.0	7.1	3.6	18.9
	10	70.0	8.5	4.8	4.1	5.2	4.6	2.8	15.1
	20	74.2	7.4	4.2	3.4	4.4	4.1	2.2	12.9
	30	77.1	8.9	4.0	3.5	2.2	2.6	1.7	9.9
	40	79.1	7.4	4.6	2.8	2.3	2.3	1.5	9.1
	60	78.2	7.3	3.8	2.7	3.4	2.8	1.8	10.2
	80	79.6	9.2	3.7	2.6	1.1	2.1	1.8	8.3
	100	79.4	8.2	3.5	2.5	2.5	2.6	1.3	8.9
	120	72.8	8.1	3.9	3.7	5.3	4.3	1.9	13.5
	150	63.7	5.9	3.6	6.2	9.0	7.6	4.0	21.6
	185	58.9	7.3	6.7	6.5	8.9	7.2	4.5	23.2
	220	59.1	7.2	4.3	6.3	9.0	7.2	6.8	24.6
	260	51.5	9.8	6.4	8.5	9.9	8.5	5.4	27.1
	300	58.0	8.3	5.3	6.9	10.3	6.7	4.6	23.6
360	62.8	7.7	4.8	6.3	9.5	5.6	3.4	20.4	

2,3-BPG						
		Isotope enrichment (%)				Total enrichment (%)
	Cycle time (s)	m+0	m+1	m+2	m+3	
1 <sup>st</sup> cycle	0	84.1	3.9	2.5	9.5	12.5
	10	82.3	3.6	2.6	11.5	14.5
	20	80.4	3.8	3.9	11.9	15.8
	30	81.1	3.3	1.5	14.1	16.2
	40	79.8	3.3	2.7	14.2	17.1
	60	78.7	3.3	2.6	15.4	18.2
	80	78.0	3.1	2.8	16.1	19.0
	100	72.2	3.0	2.8	22.1	24.9
	120	52.8	3.5	5.9	37.8	42.9
	150	59.0	5.0	4.9	31.2	36.1
	185	63.5	5.8	6.6	24.0	30.4
	220	66.1	6.3	7.6	20.0	27.2
	260	69.6	5.8	5.6	19.0	24.7
	300	70.0	6.4	5.9	17.6	23.7
360	69.0	7.1	6.8	17.1	24.0	
2 <sup>nd</sup> cycle	0	70.0	7.1	7.7	15.3	22.8
	10	82.1	3.8	2.2	11.9	14.6
	20	82.6	0.3	3.5	13.6	16.0
	40	75.6	3.4	2.6	18.5	21.3



2,3-BPG						
		Isotope enrichment (%)				Total enrichment (%)
	Cycle time (s)	m+0	m+1	m+2	m+3	
2 <sup>nd</sup> cycle	60	76.8	3.2	2.6	17.4	20.2
	80	76.6	4.2	2.7	16.6	19.7
	100	76.8	4.0	N.Q.	19.2	20.5
	120	64.4	3.4	3.4	28.8	32.3
	150	53.3	3.9	7.0	35.8	41.7
	185	57.4	5.3	7.0	30.4	36.8
	220	58.6	6.1	8.1	27.3	34.7
	260	57.6	7.0	10.2	25.3	34.4
	300	61.4	7.1	9.3	22.1	30.7
	360	62.5	6.7	8.6	22.2	30.2
3 <sup>rd</sup> cycle	0	60.3	8.1	9.2	22.4	31.2
	10	86.1	4.3	4.2	5.3	9.6
	20	90.4	4.1	1.6	4.0	6.4
	30	88.7	5.1	2.8	3.4	6.9
	40	89.0	4.1	3.4	3.4	7.1
	60	89.3	4.0	3.8	2.9	6.7
	80	91.6	3.5	2.9	2.0	5.1
	100	91.6	3.3	2.3	2.7	5.4
	120	90.7	4.0	2.8	2.6	5.7
	150	86.3	6.5	3.6	3.6	8.2
	185	81.2	7.1	5.9	5.8	12.1
	220	80.8	7.7	4.9	6.7	12.5
	260	76.3	9.2	7.0	7.5	15.2
	300	76.1	9.2	6.5	8.2	15.6
360	77.8	8.0	6.0	8.3	14.9	

Citrate									
		Isotope enrichment (%)							Total enrichment (%)
	Cycle time (s)	m+0	m+1	m+2	m+3	m+4	m+5	m+6	
1 <sup>st</sup> cycle	0	90.2	6.3	1.5	0.1	1.9	N.Q.	N.Q.	2.9
	10	90.0	6.1	2.8	0.3	0.6	0.3	N.Q.	2.7
	20	89.6	6.0	3.0	0.5	N.Q.	0.9	N.Q.	3.0
	30	88.7	6.1	2.5	0.7	0.4	1.5	N.Q.	3.8
	40	86.9	6.2	2.7	0.6	N.Q.	2.2	1.3	5.5
	60	88.3	6.1	2.3	0.7	0.1	2.1	0.5	4.4
	80	83.2	5.4	2.7	0.6	1.8	2.2	4.0	9.2
	100	86.8	6.0	2.6	0.6	N.Q.	2.3	1.6	5.7
	120	89.5	6.7	2.5	0.5	N.Q.	0.8	N.Q.	2.9

Citrate									
		Isotope enrichment (%)							Total enrichment (%)
	Cycle time (s)	m+0	m+1	m+2	m+3	m+4	m+5	m+6	
1 <sup>st</sup> cycle	150	90.5	6.3	1.9	0.4	N.Q.	0.9	N.Q.	2.6
	185	90.8	6.0	2.3	0.4	N.Q.	0.6	N.Q.	2.4
	220	90.8	6.2	2.3	0.3	N.Q.	0.5	N.Q.	2.3
	260	89.6	6.1	1.9	0.3	1.8	0.3	N.Q.	3.3
	300	89.8	6.4	2.1	0.3	1.0	0.3	N.Q.	2.9
	360	90.5	5.9	1.6	0.4	0.9	0.7	N.Q.	2.9
2 <sup>nd</sup> cycle	0	91.6	6.1	1.7	0.3	N.Q.	0.2	N.Q.	2.0
	10	89.8	5.5	2.5	0.6	N.Q.	0.7	0.9	3.6
	20	87.5	6.1	2.8	0.7	0.4	1.5	1.1	4.8
	40	86.8	6.2	2.2	0.7	0.5	2.0	1.6	5.7
	60	87.1	5.7	2.1	0.6	N.Q.	2.1	2.3	6.0
	80	84.1	6.1	2.1	0.5	0.4	2.2	4.6	8.7
	100	86.5	6.0	2.2	0.6	N.Q.	2.3	2.4	6.4
	120	85.2	5.6	2.5	0.6	0.4	2.2	3.5	7.7
	150	90.0	5.9	2.1	0.5	N.Q.	0.9	0.5	3.3
	185	88.8	6.2	2.3	0.5	N.Q.	1.0	1.2	4.1
	220	90.3	6.0	1.7	0.4	0.1	0.8	0.5	3.1
	260	90.8	6.3	1.7	0.5	N.Q.	0.8	N.Q.	2.5
	300	89.8	6.0	1.8	0.4	0.2	0.9	0.8	3.5
360	90.3	6.0	1.9	0.4	0.3	0.7	0.4	3.0	
3 <sup>rd</sup> cycle	0	89.8	5.7	2.3	0.3	N.Q.	0.8	1.1	3.6
	10	88.1	6.6	2.9	0.8	0.4	0.8	0.4	3.8
	20	88.1	6.8	2.7	0.8	0.8	0.8	N.Q.	3.6
	30	87.5	7.6	3.1	0.7	0.3	0.8	N.Q.	3.5
	40	87.9	7.5	3.1	0.7	N.Q.	0.8	N.Q.	3.3
	60	88.1	7.5	3.1	0.6	N.Q.	0.7	N.Q.	3.2
	80	87.9	7.8	2.6	0.7	0.3	0.8	N.Q.	3.3
	100	87.7	7.3	2.8	0.6	N.Q.	0.7	0.8	3.8
	120	88.6	7.2	2.6	0.6	0.3	0.7	N.Q.	3.1
	150	89.5	6.5	2.6	0.5	0.2	0.7	N.Q.	2.9
	185	88.6	6.7	2.4	0.5	1.1	0.7	N.Q.	3.5
	220	88.7	6.7	2.3	0.6	N.Q.	0.7	1.0	3.8
	260	89.5	6.7	2.6	0.5	N.Q.	0.6	N.Q.	2.8
	300	89.4	6.9	2.3	0.6	N.Q.	0.8	N.Q.	2.9
360	89.8	6.4	2.2	0.5	N.Q.	0.8	0.4	3.1	

Succinate							
		Isotope enrichment (%)					Total enrichment (%)
	Cycle time (s)	m+0	m+1	m+2	m+3	m+4	
1 <sup>st</sup> cycle	0	93.5	5.5	1.0	N.Q.	N.Q.	1.9
	10	94.7	4.3	1.0	N.Q.	N.Q.	1.6
	20	92.6	4.9	1.7	0.3	0.5	2.8
	30	91.3	5.1	1.9	0.7	1.0	3.8
	40	92.3	4.3	2.0	0.5	0.8	3.3
	60	90.5	5.3	2.0	0.8	1.4	4.3
	80	91.0	4.9	1.9	0.7	1.5	4.2
	100	90.3	4.9	1.8	0.9	2.0	4.9
	120	93.5	5.2	1.0	0.2	0.2	2.1
	150	93.4	4.9	1.0	0.3	0.5	2.4
	185	92.9	5.0	1.4	0.2	0.4	2.6
	220	92.9	5.1	1.4	0.3	0.3	2.5
	260	92.9	5.2	1.2	0.4	0.4	2.6
	300	92.9	4.9	1.2	0.4	0.5	2.7
360	92.7	5.2	1.3	0.3	0.5	2.7	
2 <sup>nd</sup> cycle	0	92.9	4.9	1.3	0.3	0.5	2.6
	10	91.3	5.4	1.9	0.6	0.8	3.6
	20	89.1	5.0	2.6	1.1	2.1	5.5
	40	88.4	5.1	2.5	1.4	2.7	6.3
	60	88.2	5.2	2.3	1.4	3.0	6.4
	80	88.4	4.9	2.3	1.3	3.1	6.4
	100	87.9	5.2	2.2	1.4	3.3	6.7
	120	88.0	4.6	2.7	1.4	3.3	6.9
	150	91.0	5.1	1.7	0.7	1.5	4.2
	185	92.0	4.3	1.9	0.6	1.2	3.7
	220	90.8	5.0	1.9	0.8	1.4	4.2
	260	91.5	5.1	1.4	0.6	1.4	3.9
	300	91.2	4.6	2.0	0.7	1.4	4.1
360	90.9	5.1	1.7	0.8	1.5	4.3	
3 <sup>rd</sup> cycle	0	90.9	4.7	2.1	0.8	1.6	4.4
	10	91.1	4.5	2.1	0.7	1.5	4.2
	20	88.6	5.4	2.8	1.2	2.0	5.7
	30	88.2	5.5	2.8	1.3	2.3	6.0
	40	89.5	5.4	2.4	0.9	1.8	5.0
	60	88.9	5.9	2.3	1.1	1.7	5.2
	80	89.7	5.0	2.4	1.1	1.7	5.0
	100	88.9	5.7	2.5	1.0	1.9	5.3
	120	88.9	5.5	2.9	1.0	1.8	5.3
	150	90.5	5.3	2.0	0.8	1.4	4.3
	185	90.8	5.3	2.0	0.8	1.1	4.0

Succinate							
		Isotope enrichment (%)					Total enrichment (%)
	Cycle time (s)	m+0	m+1	m+2	m+3	m+4	
3 <sup>rd</sup> cycle	220	90.4	5.5	2.0	0.8	1.4	4.3
	260	91.1	5.3	1.5	0.8	1.3	4.0
	300	90.7	5.3	2.0	0.8	1.3	4.2
	360	90.4	5.2	2.3	0.8	1.3	4.3

M6P									
		Isotope enrichment (%)							Total enrichment (%)
	Cycle time (s)	m+0	m+1	m+2	m+3	m+4	m+5	m+6	
1 <sup>st</sup> cycle	0	N.Q.	7.3	39.0	7.0	12.0	25.9	8.7	56.0
	10	10.6	0.7	0.8	1.5	2.1	N.Q.	84.3	86.8
	20	13.7	1.3	N.Q.	N.Q.	1.2	4.8	78.9	84.0
	30	1.4	1.1	0.5	1.0	2.6	7.8	85.6	94.7
	40	N.Q.	N.Q.	N.Q.	1.3	2.1	N.Q.	96.6	98.7
	60	10.6	1.5	N.Q.	N.Q.	1.2	N.Q.	86.7	87.7
	80	7.3	1.7	2.4	3.2	N.Q.	0.8	84.6	88.0
	100	3.8	2.3	1.4	0.9	1.1	0.8	89.8	92.5
	120	33.8	N.Q.	7.7	1.6	N.Q.	5.5	51.5	59.4
	150	N.Q.	11.3	44.8	N.Q.	30.0	13.9	N.Q.	48.4
	185	N.Q.	11.8	N.Q.	6.9	5.0	3.1	73.2	84.6
	220	28.2	N.Q.	40.2	9.4	13.7	8.5	N.Q.	34.3
	260	24.1	7.1	10.2	10.7	7.1	7.3	33.6	54.3
	300	N.Q.	49.9	N.Q.	N.Q.	25.8	24.3	N.Q.	45.8
360	18.5	14.4	13.6	11.2	18.3	3.4	20.6	48.2	
2 <sup>nd</sup> cycle	0	39.6	21.5	14.7	16.3	N.Q.	7.9	N.Q.	23.2
	10	1.4	1.1	3.1	N.Q.	N.Q.	1.9	92.5	95.3
	20	1.1	2.5	1.9	N.Q.	1.0	5.7	87.7	94.2
	40	N.Q.	N.Q.	3.8	1.7	2.6	5.4	86.6	94.9
	60	2.9	1.0	N.Q.	0.8	1.2	1.3	92.8	95.3
	80	3.2	N.Q.	5.8	1.8	1.5	2.6	85.1	91.1
	100	10.7	3.0	1.1	1.0	N.Q.	5.1	79.1	84.7
	120	N.Q.	1.8	6.3	N.Q.	2.1	2.2	87.6	93.2
	150	N.Q.	9.4	5.6	10.9	N.Q.	2.3	71.8	82.6
	185	15.1	N.Q.	1.4	10.9	4.4	4.3	63.8	76.3
	220	2.4	8.6	5.6	15.2	10.7	3.8	53.8	74.9
	260	6.0	22.1	9.4	12.3	4.0	N.Q.	46.2	61.9
	300	N.Q.	5.0	N.Q.	7.7	6.4	N.Q.	81.0	89.9
	360	17.3	N.Q.	10.5	N.Q.	2.7	17.2	52.4	72.0

M6P									
		Isotope enrichment (%)							Total enrichment (%)
	Cycle time (s)	m+0	m+1	m+2	m+3	m+4	m+5	m+6	
3 <sup>rd</sup> cycle	0	36.1	11.0	14.2	N.Q.	14.7	24.0	N.Q.	36.4
	10	92.6	2.1	1.4	N.Q.	1.5	0.4	2.1	4.2
	20	87.3	5.5	2.2	1.8	1.5	1.7	N.Q.	4.9
	30	96.6	N.Q.	0.6	1.8	0.5	0.5	N.Q.	1.8
	40	87.8	N.Q.	0.5	2.7	1.0	0.3	7.7	10.1
	60	85.6	4.8	4.6	2.5	1.8	0.7	N.Q.	5.4
	80	94.0	N.Q.	3.2	0.9	N.Q.	N.Q.	1.9	3.4
	100	94.2	N.Q.	1.6	0.8	N.Q.	0.8	2.6	4.2
	120	94.7	N.Q.	1.9	1.4	1.2	0.3	0.5	2.8
	150	N.Q.	38.3	21.8	16.0	6.6	2.7	14.5	42.9
	185	42.1	11.2	25.8	8.0	4.9	4.6	3.4	25.0
	220	N.Q.	N.Q.	34.7	14.3	51.0	N.Q.	N.Q.	52.7
	260	N.Q.	N.Q.	68.9	N.Q.	22.4	8.7	N.Q.	45.2
	300	N.Q.	30.9	41.3	6.3	15.3	N.Q.	6.2	38.5
360	N.Q.	N.Q.	15.9	20.7	12.4	2.7	48.3	74.5	

2PG						
		Isotope enrichment (%)				Total enrichment (%)
	Cycle time (s)	m+0	m+1	m+2	m+3	
1 <sup>st</sup> cycle	0	89.3	4.3	N.Q.	8.3	8.5
	20	85.5	4.9	N.Q.	11.3	11.8
	30	85.3	2.1	N.Q.	12.8	13.4
	40	81.1	3.3	N.Q.	15.6	16.7
	150	62.3	5.0	1.9	30.9	33.8
	185	69.4	4.8	4.9	20.8	25.7
	220	70.5	2.5	2.0	25.1	27.2
	260	70.1	6.3	4.5	19.1	24.2
	300	63.8	10.2	3.5	22.5	28.3
	360	70.2	6.9	4.1	18.8	23.8
2 <sup>nd</sup> cycle	0	68.5	7.8	5.4	18.4	24.5
	10	84.4	6.6	N.Q.	11.5	12.1
	20	81.9	2.4	N.Q.	15.9	16.5
	60	78.6	3.6	N.Q.	17.8	19.0
	80	77.2	4.6	0.8	17.4	19.5
	100	77.1	N.Q.	N.Q.	25.9	24.5
	120	64.7	2.0	1.0	32.2	33.6
	150	56.0	2.9	4.0	37.1	40.7
	185	55.9	5.5	6.9	31.6	38.1
	300	64.7	6.2	7.1	22.0	28.8
360	63.3	6.5	7.9	22.3	29.7	
3 <sup>rd</sup> cycle	0	70.3	4.0	5.8	19.9	25.1
	10	85.3	5.7	2.9	6.1	9.9
	20	86.8	1.2	2.1	9.9	11.7
	30	90.7	4.6	2.0	2.6	5.5
	60	90.3	4.9	N.Q.	5.1	6.6
	80	88.3	7.1	0.8	3.7	6.6
	100	92.3	N.Q.	N.Q.	8.2	7.9
	120	91.5	4.8	0.7	2.9	5.0
	185	79.4	9.9	3.6	7.1	12.8
	220	81.1	8.0	4.3	6.6	12.1
	300	78.5	11.0	3.7	6.8	12.9
	360	72.4	8.8	5.0	13.7	20.0

3PG						
		Isotope enrichment (%)				Total enrichment (%)
	Cycle time (s)	m+0	m+1	m+2	m+3	
1 <sup>st</sup> cycle	0	87.4	3.7	0.8	8.1	9.9
	20	84.6	4.4	0.7	10.3	12.2
	30	80.5	4.5	1.3	13.7	16.1
	40	82.9	3.2	0.9	13.1	14.7
	150	63.8	3.7	4.5	28.1	32.3
	185	67.1	4.7	5.3	23.0	28.1
	220	66.9	7.3	6.0	19.7	26.2
	260	70.0	6.2	6.1	17.8	23.9
	300	74.6	5.2	4.2	16.1	20.6
	360	71.5	6.8	5.3	16.4	22.2
2 <sup>nd</sup> cycle	0	74.9	5.5	5.0	14.5	19.8
	10	83.3	3.4	0.9	12.3	14.1
	20	83.2	2.5	0.4	13.9	15.0
	60	79.3	3.7	1.0	16.0	17.9
	80	79.0	4.4	0.4	16.2	17.9
	100	78.0	4.9	1.4	15.7	18.3
	120	67.3	2.4	2.0	28.3	30.4
	150	56.7	4.3	4.4	34.6	39.0
	185	61.0	5.1	5.1	28.8	33.9
	300	64.9	6.2	6.8	22.1	28.7
360	66.7	7.1	5.9	20.2	26.5	
3 <sup>rd</sup> cycle	0	64.6	8.7	6.1	20.7	27.6
	10	89.3	3.9	1.1	5.8	7.8
	20	90.3	2.6	1.2	5.9	7.6
	30	92.0	3.0	1.0	4.0	5.7
	60	92.7	2.7	0.6	4.1	5.3
	80	91.2	4.0	0.3	4.5	6.0
	100	89.9	5.2	N.Q.	5.2	6.7
	120	91.7	4.3	0.7	3.3	5.2
	185	83.5	7.2	3.0	6.4	10.7
	220	80.9	7.7	3.5	7.9	12.8
	300	80.8	7.3	3.7	8.1	13.0
	360	77.1	8.4	3.0	11.5	16.3

aKG								
		Isotope enrichment (%)						Total enrichment (%)
	Cycle time (s)	m+0	m+1	m+2	m+3	m+4	m+5	
1 <sup>st</sup> cycle	0	89.8	4.9	N.Q.	0.5	2.3	2.8	5.8
	20	87.4	4.6	4.1	1.3	2.1	0.7	5.6
	30	78.9	6.3	5.5	2.4	4.5	2.5	11.0
	40	78.6	4.1	5.9	2.9	5.0	3.4	12.4
	150	57.7	5.4	7.0	5.0	9.8	15.0	29.8
	185	57.0	4.7	8.2	4.9	11.9	13.3	30.0
	220	61.8	9.0	4.7	5.3	5.7	13.5	24.9
	260	59.4	3.2	10.1	6.2	10.0	11.0	27.4
	300	57.9	5.4	11.6	3.7	10.6	10.7	27.2
	360	56.2	5.2	12.0	7.9	9.3	9.4	27.4
2 <sup>nd</sup> cycle	0	58.0	12.0	8.0	7.0	6.8	8.3	23.5
	10	57.7	4.8	14.2	6.7	6.3	10.4	26.1
	20	45.4	6.7	12.2	9.6	13.1	12.9	35.4
	60	39.2	6.3	14.0	11.6	12.6	16.4	40.3
	80	38.1	4.9	9.5	9.9	16.3	21.3	45.1
	100	44.4	3.6	9.0	7.6	14.2	21.2	41.4
	120	33.7	4.5	9.1	9.2	16.7	26.8	50.3
	150	35.5	4.0	12.0	6.5	18.8	23.3	47.8
	185	46.7	3.5	6.6	6.7	13.9	22.6	41.1
	300	34.6	3.6	12.6	12.9	14.8	21.5	46.8
360	46.2	7.5	11.9	6.9	9.1	18.4	36.1	
3 <sup>rd</sup> cycle	0	46.7	5.6	9.5	6.7	14.1	17.5	37.7
	10	34.9	5.0	12.0	14.1	16.3	17.7	45.0
	20	35.9	3.8	14.1	14.3	12.9	19.1	44.3
	30	33.2	6.9	14.1	12.7	13.5	19.7	45.1
	60	40.3	11.0	10.6	10.8	11.5	15.8	37.9
	80	37.2	12.0	11.3	12.9	12.0	14.5	38.8
	100	40.6	15.8	10.6	10.3	10.3	12.4	34.2
	120	42.3	14.2	10.1	10.7	11.0	11.7	33.8
	185	50.7	12.0	11.4	7.9	6.2	11.6	28.4
	220	50.1	12.1	13.0	6.8	9.2	9.0	28.0
	300	55.8	7.4	8.1	10.5	6.7	11.4	27.8
	360	59.3	10.5	10.3	7.0	6.7	6.2	22.0



Fumarate							
		Isotope enrichment (%)					Total enrichment (%)
	Cycle time (s)	m+0	m+1	m+2	m+3	m+4	
1 <sup>st</sup> cycle	0	90.6	3.6	0.9	4.9	N.Q.	5.0
	20	66.0	4.5	10.4	14.2	4.8	21.8
	30	58.0	2.5	9.7	20.0	9.8	30.2
	40	52.8	3.7	10.3	19.3	13.9	34.4
	150	78.4	3.7	2.0	15.9	N.Q.	13.8
	185	70.2	7.6	8.8	4.7	8.7	18.5
	220	78.3	5.3	4.6	9.0	2.7	13.1
	260	71.5	8.8	4.0	8.0	7.6	17.8
	300	69.9	7.5	2.9	15.6	4.1	19.2
360	67.7	7.5	4.6	16.3	4.0	20.3	
2 <sup>nd</sup> cycle	0	64.4	11.2	5.1	15.9	3.5	20.7
	10	57.7	3.6	6.9	24.6	7.3	30.1
	20	57.5	4.6	10.4	10.1	17.3	31.3
	60	53.2	5.4	6.3	19.6	15.6	34.8
	80	58.3	4.8	4.9	9.2	22.8	33.4
	100	58.6	4.5	2.9	27.1	6.9	29.8
	120	44.5	5.0	5.8	21.2	23.5	43.5
	150	54.4	5.5	6.1	17.2	16.7	34.1
	185	63.5	3.7	2.7	20.9	9.2	27.2
	300	60.4	4.9	6.7	14.7	13.3	28.9
360	61.2	4.1	5.5	24.0	5.1	26.9	
3 <sup>rd</sup> cycle	0	60.1	6.2	3.8	23.6	6.2	27.4
	10	57.9	8.0	8.9	17.0	8.2	27.4
	20	64.4	9.4	4.6	17.3	4.3	21.9
	30	63.6	15.4	6.7	9.2	5.1	19.2
	60	68.4	9.0	3.8	15.2	3.7	19.2
	80	68.9	12.7	4.4	9.4	4.6	17.0
	100	72.2	13.5	4.8	7.3	2.2	13.4
	120	70.7	14.1	5.2	5.9	4.2	14.7
	185	79.1	9.7	5.1	0.6	5.4	10.8
	220	77.9	5.7	4.9	9.2	2.3	13.0
	300	71.3	10.4	4.4	8.9	5.0	16.5
360	75.1	9.3	3.2	8.3	4.1	14.2	

Malate							
		Isotope enrichment (%)					Total enrichment (%)
	Cycle time (s)	m+0	m+1	m+2	m+3	m+4	
1 <sup>st</sup> cycle	0	89.6	7.0	0.5	1.0	1.9	4.6
	20	46.1	3.5	17.4	23.4	9.6	36.7
	30	43.1	7.0	13.6	21.7	14.6	39.4
	40	32.4	7.8	15.6	28.6	15.5	46.8
	150	62.7	3.5	7.3	13.2	13.3	27.7
	185	52.0	7.6	16.6	12.1	11.7	31.0
	220	64.2	3.6	9.3	13.1	9.8	25.2
	260	59.4	10.1	9.4	11.1	10.0	25.5
	300	57.3	14.0	8.0	10.9	9.8	25.5
	360	63.7	9.3	11.0	6.4	9.5	22.1
2 <sup>nd</sup> cycle	0	56.3	14.1	11.3	8.9	9.4	25.3
	10	47.2	13.1	15.6	8.5	15.6	33.0
	20	31.6	8.2	13.7	24.7	21.8	49.2
	60	28.9	8.2	10.9	20.8	31.3	54.3
	80	33.8	3.1	9.0	25.2	28.9	53.1
	100	41.6	1.1	5.0	21.3	31.0	49.8
	120	28.6	4.4	8.0	26.7	32.3	57.4
	150	38.2	3.5	13.4	16.2	28.6	48.4
	185	40.8	7.3	15.9	12.3	23.7	42.7
	300	40.4	8.4	16.0	15.7	19.6	41.4
360	46.7	6.1	12.5	13.3	21.4	39.1	
3 <sup>rd</sup> cycle	0	47.2	9.8	7.2	15.5	20.4	38.1
	10	48.9	10.5	14.8	10.8	15.0	33.1
	20	50.0	21.6	11.7	6.2	10.4	26.4
	30	57.7	17.9	10.8	7.8	5.9	21.6
	60	65.4	19.0	8.6	4.3	2.7	15.0
	80	64.3	16.3	8.9	4.2	6.3	18.0
	100	60.4	19.6	12.6	4.1	3.2	17.5
	120	63.2	20.4	7.3	4.8	4.4	16.7
	185	63.1	13.0	12.4	3.2	8.2	20.1
	220	61.0	17.3	14.5	2.5	4.7	18.1
	300	57.6	13.8	14.9	5.6	8.0	23.1
	360	68.4	2.2	9.9	9.8	9.7	22.5

Rib5P						
		Isotope enrichment (%)				Total enrichment (%)
	Cycle time (s)	m+0	m+1	m+2	m+3	
1 <sup>st</sup> cycle	0	97.5	2.7	N.Q.	0.7	1.0
	20	87.6	3.4	0.7	8.4	10.0
	30	86.4	4.7	0.5	8.4	10.3
	40	83.8	3.7	0.3	12.2	13.6
	150	89.1	2.4	0.6	7.9	9.1
	185	83.5	4.5	0.5	11.6	13.4
	220	91.6	2.3	0.6	5.5	6.7
	260	91.1	4.7	N.Q.	4.1	5.7
	300	95.4	2.8	0.3	1.6	2.7
	360	92.6	4.7	0.8	2.0	4.0
2 <sup>nd</sup> cycle	0	95.6	3.0	N.Q.	1.4	2.4
	10	91.5	3.1	0.2	5.2	6.4
	20	79.8	4.5	0.3	15.5	17.2
	60	85.3	2.1	1.1	11.5	13.0
	80	82.5	2.0	0.8	14.7	15.9
	100	86.3	3.0	0.3	10.4	11.6
	120	75.6	2.8	0.4	21.2	22.4
	150	75.9	2.5	1.3	20.4	22.1
	185	88.9	2.9	0.8	7.4	8.9
	300	92.7	3.4	0.5	3.5	4.9
360	94.0	4.5	N.Q.	1.7	3.1	
3 <sup>rd</sup> cycle	0	95.5	2.4	0.5	1.6	2.7
	10	94.1	3.3	N.Q.	2.8	3.8
	20	93.3	4.7	0.5	1.5	3.4
	30	94.5	3.3	0.1	2.1	3.2
	60	95.3	3.7	N.Q.	1.3	2.3
	80	94.4	3.7	0.5	1.4	3.0
	100	94.6	3.9	N.Q.	1.6	2.8
	120	94.0	4.3	0.2	1.6	3.1
	185	94.2	4.3	N.Q.	1.8	3.0
	220	94.7	2.9	0.5	1.9	3.2
	300	95.1	3.1	0.3	1.4	2.7
	360	95.6	2.5	0.2	1.7	2.6

Trehalose									
		Isotope enrichment (%)							Total enrichment (%)
	Cycle time (s)	m+0	m+1	m+2	m+3	m+4	m+5	m+6	
1 <sup>st</sup> cycle	0	79.5	4.8	1.6	0.4	N.Q.	0.4	13.5	15.3
	20	85.0	5.6	N.Q.	0.3	0.2	0.7	8.3	10.1
	30	84.9	4.4	1.0	0.3	0.1	0.4	8.9	10.5
	40	87.5	6.4	0.2	0.3	0.1	0.3	5.2	6.8
	150	71.0	4.1	1.2	0.1	N.Q.	1.9	21.8	24.5
	185	85.3	5.5	0.8	0.2	0.1	0.6	7.6	9.4
	220	75.7	4.3	0.3	0.3	0.2	1.2	18.0	20.1
	260	84.3	5.1	1.0	0.3	0.1	0.8	8.4	10.5
	300	78.7	5.6	0.6	0.7	0.3	0.9	13.1	15.6
360	69.7	4.4	0.2	0.7	0.4	1.5	23.2	25.8	
2 <sup>nd</sup> cycle	0	83.5	5.2	N.Q.	0.9	0.2	0.8	9.4	11.5
	10	78.8	5.7	0.7	0.8	0.2	1.4	12.3	15.3
	20	82.5	5.9	0.7	0.6	0.3	0.8	9.1	11.6
	60	62.7	4.0	0.3	0.7	0.5	2.5	29.4	32.9
	80	76.9	4.7	0.9	0.7	0.3	1.1	15.4	17.9
	100	64.1	4.3	1.4	1.0	0.1	2.0	27.1	30.5
	120	74.9	5.9	1.2	0.7	0.4	1.4	15.5	18.6
	150	79.5	5.9	0.6	0.9	0.4	1.1	11.5	14.4
	185	75.5	4.9	0.3	1.2	0.3	2.0	15.8	19.2
	300	80.8	5.6	0.6	1.0	0.3	0.9	10.8	13.4
360	70.5	5.6	0.6	0.4	0.4	2.1	20.3	23.7	
3 <sup>rd</sup> cycle	0	74.9	3.9	0.4	1.3	0.3	1.8	17.3	20.4
	10	78.0	5.2	0.8	1.2	0.5	1.2	13.1	16.1
	20	74.2	4.4	0.8	0.9	0.5	1.6	17.6	20.7
	30	76.9	5.1	0.7	1.2	0.5	1.2	14.3	17.3
	60	65.2	3.2	0.5	1.3	0.4	1.7	27.7	30.7
	80	78.8	5.3	0.1	1.3	0.7	1.3	12.4	15.6
	100	77.9	4.1	N.Q.	1.3	0.7	1.4	14.6	17.5
	120	78.2	5.2	0.4	1.2	0.6	1.2	13.3	16.3
	185	76.6	6.2	0.5	1.3	0.6	1.3	13.4	16.8
	220	74.0	3.3	0.7	1.3	0.7	1.2	18.8	21.7
	300	77.5	6.4	1.3	1.1	0.7	1.2	11.8	15.3
360	63.6	5.1	0.3	0.9	0.6	2.1	27.4	31.0	

Glycine					
		Isotope enrichment (%)			Total enrichment (%)
	Cycle time (s)	m+0	m+1	m+2	
1 <sup>st</sup> cycle	0	98.8	1.5	N.Q.	0.4
	30	96.8	4.2	N.Q.	1.1
	150	97.1	3.6	N.Q.	1.1
	220	99.4	1.0	N.Q.	0.1
	300	96.7	3.8	N.Q.	1.4
2 <sup>nd</sup> cycle	10	98.6	1.6	N.Q.	0.6
	60	99.1	1.3	N.Q.	0.2
	100	96.6	4.2	N.Q.	1.3
	185	99.4	1.1	N.Q.	0.1
	360	98.5	1.9	N.Q.	0.5
3 <sup>rd</sup> cycle	0	98.5	1.6	N.Q.	0.7
	20	98.4	1.7	N.Q.	0.7
	60	98.2	2.1	N.Q.	0.7
	100	98.5	1.8	N.Q.	0.6
	150	98.3	2.0	N.Q.	0.7
	220	98.9	1.4	N.Q.	0.4
	360	98.5	1.9	N.Q.	0.5

Cysteine						
		Isotope enrichment (%)				Total enrichment (%)
	Cycle time (s)	m+0	m+1	m+2	m+3	
1 <sup>st</sup> cycle	0	97.0	11.6	N.Q.	N.Q.	N.Q.
	30	94.7	12.4	N.Q.	N.Q.	N.Q.
	150	87.6	13.2	N.Q.	3.4	5.0
	220	89.8	13.2	N.Q.	3.5	3.6
	300	89.7	12.6	N.Q.	2.8	3.6
2 <sup>nd</sup> cycle	10	91.2	13.0	N.Q.	3.1	2.5
	60	85.0	13.1	N.Q.	5.5	7.4
	100	80.0	13.8	N.Q.	7.2	11.2
	185	79.9	14.5	N.Q.	9.1	11.6
	360	81.2	14.2	N.Q.	8.0	10.4
3 <sup>rd</sup> cycle	0	80.7	15.1	N.Q.	8.0	10.5
	20	80.2	13.8	N.Q.	8.3	11.4
	60	79.4	14.0	N.Q.	8.2	11.8
	100	77.3	15.4	N.Q.	9.9	13.2
	150	76.8	15.8	N.Q.	9.9	13.6
	220	76.2	16.0	N.Q.	9.4	13.7
	360	77.1	15.8	N.Q.	8.5	12.8

Threonine							
		Isotope enrichment (%)					Total enrichment (%)
	Cycle time (s)	m+0	m+1	m+2	m+3	m+4	
1 <sup>st</sup> cycle	0	96.2	6.6	N.Q.	N.Q.	N.Q.	0.1
	30	96.7	4.8	N.Q.	N.Q.	0.4	0.6
	150	95.1	5.3	N.Q.	N.Q.	2.2	2.1
	220	95.3	5.3	N.Q.	0.7	1.0	1.7
	300	92.3	7.8	N.Q.	0.6	1.9	3.0
2 <sup>nd</sup> cycle	10	93.5	6.2	N.Q.	0.3	1.4	2.5
	60	93.2	5.9	N.Q.	1.5	1.0	2.8
	100	92.8	4.1	N.Q.	1.7	2.9	4.5
	185	92.9	4.5	N.Q.	0.6	2.1	3.6
	360	90.4	6.5	0.5	0.6	2.0	4.3
3 <sup>rd</sup> cycle	0	90.4	5.9	N.Q.	1.0	2.8	4.9
	20	90.8	6.3	N.Q.	1.3	2.0	4.4
	60	90.8	6.9	N.Q.	2.0	2.3	4.6
	100	92.0	4.2	0.1	1.4	2.3	4.4
	150	92.1	4.5	N.Q.	1.9	2.4	4.5
	220	91.1	5.2	N.Q.	2.3	1.8	4.6
	360	91.2	3.1	0.7	1.8	3.2	5.6

Glutamate								
		Isotope enrichment (%)					Total enrichment (%)	
	Cycle time (s)	m+0	m+1	m+2	m+3	m+4	m+5	
1 <sup>st</sup> cycle	0	95.3	1.3	2.2	0.8	N.Q.	0.4	2.1
	30	82.8	5.2	5.1	2.0	3.3	1.6	8.5
	150	53.5	3.7	11.2	6.2	11.7	13.6	31.9
	220	51.6	4.7	11.6	8.8	11.6	11.8	31.9
	300	50.6	4.7	16.1	1.8	17.1	9.5	31.7
2 <sup>nd</sup> cycle	10	48.0	7.5	13.7	8.8	12.4	9.5	31.7
	60	34.8	8.2	12.1	12.1	13.9	18.9	43.8
	100	27.9	6.6	13.7	13.0	18.9	20.0	49.7
	185	26.9	4.8	13.4	11.9	17.5	25.5	52.9
	360	24.6	4.7	12.6	15.8	19.0	23.3	54.0
3 <sup>rd</sup> cycle	0	25.7	4.3	14.9	14.7	18.1	22.2	52.4
	20	25.2	6.1	14.5	14.2	16.5	23.6	52.3
	60	29.7	9.0	13.7	17.4	12.0	18.1	45.4
	100	36.4	12.7	11.9	13.4	11.9	13.6	38.6
	150	40.4	13.0	13.1	11.4	9.8	12.2	34.8
	220	39.6	14.0	13.5	12.3	8.5	11.9	34.4
	360	39.9	15.3	15.5	12.1	8.3	9.0	32.1

Aspartate							
		Isotope enrichment (%)					Total enrichment (%)
	Cycle time (s)	m+0	m+1	m+2	m+3	m+4	
1 <sup>st</sup> cycle	0	90.5	6.3	N.Q.	3.4	0.6	4.3
	30	53.0	4.8	10.9	21.7	9.5	32.5
	150	46.3	9.8	9.5	16.6	17.7	37.4
	220	47.5	8.1	16.2	14.4	13.8	34.7
	300	49.6	11.2	14.4	12.8	12.0	31.6
2 <sup>nd</sup> cycle	10	50.2	11.7	12.6	11.6	14.0	31.9
	60	47.5	1.7	6.9	21.7	22.2	42.3
	100	42.7	5.2	8.4	17.6	26.1	44.8
	185	29.1	7.3	14.8	18.9	29.8	53.2
	360	29.8	10.7	17.2	16.4	25.9	49.5
3 <sup>rd</sup> cycle	0	29.2	10.0	18.6	18.3	23.9	49.5
	20	52.3	14.8	13.8	7.6	11.5	27.8
	60	66.1	15.1	9.7	3.0	6.1	16.9
	100	64.1	19.0	5.7	5.2	5.9	17.5
	150	56.2	16.6	11.7	6.7	8.8	23.8
	220	52.0	14.5	15.5	7.3	10.7	27.6
	360	50.3	17.1	14.1	9.3	9.2	27.5

Valine								
		Isotope enrichment (%)					Total enrichment (%)	
	Cycle time (s)	m+0	m+1	m+2	m+3	m+4	m+5	
1 <sup>st</sup> cycle	0	86.5	12.3	N.Q.	1.4	0.1	0.7	3.7
	30	73.1	10.6	0.7	3.5	1.8	10.3	16.2
	150	27.3	11.7	2.8	5.7	6.8	45.8	58.0
	220	40.1	7.1	3.4	5.9	5.4	38.1	48.7
	300	48.2	7.8	3.4	5.6	4.4	30.5	40.4
2 <sup>nd</sup> cycle	10	60.5	12.5	1.6	5.0	3.0	17.4	26.0
	60	44.5	7.7	2.5	4.3	5.5	35.6	45.1
	100	37.9	17.6	N.Q.	3.5	5.5	37.6	46.8
	185	28.6	6.2	2.3	5.5	7.0	50.5	61.5
	360	55.8	11.2	0.8	4.4	4.5	23.2	32.0
3 <sup>rd</sup> cycle	0	54.4	14.3	1.1	5.0	4.6	20.7	30.7
	20	64.0	16.5	N.Q.	4.5	2.9	13.1	21.0
	60	74.8	14.7	3.1	3.8	0.9	2.7	9.9
	100	79.9	11.2	3.0	3.0	0.8	2.2	8.0
	150	79.5	11.8	3.4	2.7	0.5	2.0	7.8
	220	76.6	13.7	2.7	3.1	0.7	3.2	9.5
	360	76.2	11.8	3.5	3.4	1.3	3.7	10.6

Proline								
		Isotope enrichment (%)						Total enrichment (%)
	Cycle time (s)	m+0	m+1	m+2	m+3	m+4	m+5	
1 <sup>st</sup> cycle	0	93.9	2.1	N.Q.	3.6	2.8	0.9	4.4
	30	95.6	1.9	N.Q.	2.7	1.0	0.5	2.6
	150	76.9	1.1	0.8	10.9	4.6	5.8	16.5
	220	76.8	0.9	2.8	6.8	6.4	6.4	16.8
	300	73.7	1.1	2.6	11.7	3.4	7.4	18.5
2 <sup>nd</sup> cycle	10	73.7	3.0	3.1	9.5	4.3	6.5	17.4
	60	35.2	1.2	2.6	68.3	N.Q.	1.6	36.7
	100	54.6	2.2	7.3	16.2	8.8	10.9	31.0
	185	47.8	5.0	7.0	7.8	13.5	18.9	38.2
	360	55.5	3.7	6.2	7.8	11.1	15.8	32.5
3 <sup>rd</sup> cycle	0	50.6	2.8	6.9	14.6	9.9	15.2	35.2
	20	30.2	2.6	4.4	56.9	N.Q.	8.2	42.8
	60	44.7	20.7	1.9	12.2	7.5	13.0	31.2
	100	41.8	18.5	2.9	12.5	10.4	13.9	34.6
	150	44.6	4.9	10.0	15.5	11.1	14.1	37.2
	220	43.6	17.1	7.5	11.5	8.8	11.5	31.8
	360	50.1	17.9	6.4	8.1	8.0	9.4	26.8

## References

1. Wahl SA, Dauner M, Wiechert W: **New tools for mass isotopomer data evaluation in (13)C flux analysis: mass isotope correction, data consistency checking, and precursor relationships.** *Biotechnol Bioeng* 2004, **85**:259-268.





Chapter



**Conclusions and Outlook**

## 6.1 Unique contributions and key learnings of this research

Industrial biotechnology applications require cultivating microorganisms in large-scale bioreactors, to enable sufficient production capacity and competitive production costs. Such large-scale environments are commonly characterized by physicochemical gradients, due to mass transfer limitations (mixing), leading to reduced performance (product formation and biomass synthesis), compared to lab-scale cultivation conditions. Following the need to unravel and understand the cellular behavior of microorganisms under changing (dynamic) environments, the effects of dynamic repetitive changes in extracellular substrate concentrations on metabolism of *Escherichia coli* K12 MG1655, were studied. This work enabled to distinguish key cellular functions controlling the cellular long-term (up to 8 generations) adaptation to such dynamics.

In contrast to previous scale-down studies, the quantitative observation and mechanistic description of intracellular metabolism was the main focus of this thesis. Therefore, an experimental platform, generating repetitive dynamic substrate gradients, was chosen. Such defined environment enabled a detailed study of the metabolic network, generating a solid basis of experimental data for kinetic modeling. The quantitative data, together with kinetic modeling, were used to identify key metabolic adjustments during the repetitive cycles.

Repetitive substrate gradients were achieved by block-wise glucose feeding in an aerobic *E.coli* culture. The dynamic cycles, with a duration of 400 s (20 s feeding and 380 s non-feeding) each, allowed for the quantitative monitoring of the physiological responses of the cells, as well as, high frequency metabolome and proteome sampling. A repetitive response was obtained, after 5 residence times of the applied dynamic regime.

Comparing dynamic conditions (feast-famine) to a reference chemostat cultivation (steady-state), highlighted that the biomass specific rates of glucose and oxygen uptake increased, as well as the carbon dioxide production rate. The (average) biomass yield was found to decrease by 30%, which constitutes one of our most significant observations. This observation indicated the increase of ATP-spilling mechanisms. The commonly observed overflow metabolism resulting in production of e.g. acetate was not found (no increase in the concentration of acetate). Interestingly, the cellular ATP concentration was basically homeostatic. According to the measured metabolome and proteome changes, the potential adaptation mechanisms are:

- i. Glycogen and inorganic polyphosphate synthesis and degradation, as revealed by the increase in the abundance of the respective enzymes and the  $^{13}\text{C}$  isotope tracing.
- ii. Increased protein turnover, as indicated by the higher abundance of proteins participating in protein folding (chaperones) and degradation (proteases).

The cellular behavior under dynamic conditions was analyzed using a model-based approach. Using a published *E.coli* kinetic model (calibrated with steady-state data) and the obtained experimental measurements, we could show that significant adjustments are needed to correctly reproduce growth and metabolism under the applied dynamic conditions. The following aspects should be considered:

- i. Significant alterations in the enzymatic kinetics of central carbon pathways when cells are adapted to dynamic conditions.
- ii. The key role of carbon storage metabolism (glycogen production and re-consumption), which allows the cells to handle abrupt changes in the uptake rates, without the detrimental accumulation of glycolytic intermediates. Intracellular glycogen measurements are a necessity, as well as a better description of the kinetics of this mechanism.
- iii. Implementation of ATP-spilling mechanisms in the models to allow for better predictions of energy metabolism.

The first hypothesis (i) was experimentally evaluated using shotgun proteomic analysis on biomass grown under the reference constant feeding and the block-wise feeding conditions. Changes were observed for 23.5% of the total proteome identified. Nevertheless, the magnitude of change was lower than expected, extrapolating from the observed physiological differences. Additionally, main global regulatory proteins did not respond to the switch of conditions and there were no indications of the activation of nutrient stress mechanisms, such as catabolite repression or the stringent response system. Rather than global (stress) responses, *E.coli* cells tuned protein levels related to specific cellular functions. These include biosynthetic pathways and translation processes. Increased levels of ribosomal proteins were assumed to either accommodate higher protein synthesis during phases of rapid growth or compensate for higher protein turnover.

Proteins associated with nutrient transport and catabolism, were down-regulated or remained unchanged during the block-wise feeding. Nevertheless, uptake and catabolic rates were temporarily much higher compared to steady-state conditions, suggesting that there was an enzymatic reserve, for the main fluxes in glycolysis, TCA cycle and pentose phosphate pathway. Such reserve could be beneficial to rapidly enable high fluxes after a switch of nutritional availability (bet-hedging strategies [1]).

## 6.2 Open challenges and recommendations

Research, in all scientific fields, provides answers, but commonly, at the same time generates new ones, with new challenges to solve. The most relevant remaining challenges and the steps which should be taken to obtain a mechanistic understanding of microbial metabolism under dynamic conditions to use this knowledge on optimizing industrial bioprocesses, are summarized below:

- 1) Trade-off between representative scale-down set-ups and data complexity (heterogeneity)

Scale-down experiments are currently best practice to mimic the conditions of bacteria cultivation in large-scale fermenters [2-4]. For a better representation during the scale-down, a quantitative description of the industrial-scale cultivation parameters is necessary. In this work, we showed that the sequence (repetition) of the applied perturbations significantly affects the cellular behavior and suggested that repetitive perturbations are more representative for large-scale conditions, compared to single-pulses. Hence, the relevant industrial mixing and circulation times should be calculated, as accurately as possible, either with online measurements inside the large-scale bioreactors or by using computational fluid dynamic (CFD) models.

At the same time, there is a trade-off between mimicking the large-scale conditions and the “simplicity” of data generation and interpretation. A block-wise feeding regime, generates repetitive cycles, that can be easily sampled and homogeneous conditions can be assumed, meaning that the whole *E.coli* population simultaneously face the same perturbations (substrate excess, limitation or depletion). Nevertheless, the conditions differ in the large-scale cultivations, where individual cells are exposed to different fluctuations, depending on their specific trajectory, i.e. the zones of the reactor they are in time.

This consideration has led to the use of two-compartment systems for scale-down studies. In a recent study, Wang G, *et al.* [5] compared an intermittent feeding regime in one reactor with substrate perturbations in a two-compartment system, as a scale-down for penicillin production. They showed different observations between the two systems, mainly regarding the expression of sugar transporters and carbon storage strategies in *Penicillium chrysogenum*. Subsequently, profound consideration of the experimental setup should be given to interpret results from scale-down experiments and judge how representative they are to real industrial conditions. Several methods have been developed to track subpopulations and define heterogeneity in large-scale cultivations [6-14]. The current challenge is to integrate heterogeneity predictive models with single-cell studies, in order to

answer the following question: Is reduced microbial performance a result of badly performing subpopulations?

In addition, while commonly various gradients are present simultaneously in a large-scale cultivation, their effects on cellular metabolism should be assessed first separately to decipher complexity. When enough understanding on regulation under each condition is acquired, their combination can be further studied experimentally, investigating which gradients provoke more rapid or more drastic responses on the system, by comparing all available observations. Do all gradients affect productivity or growth? Are the effects of different gradients observed in different time intervals and how relevant are they for the industrial process under investigation?

## 2) Application to engineered production strains

In this work, only the *E.coli* wild-type laboratory strain (K12 MG1655) was studied. Studying engineered production strains will give further insights to the impact of dynamics on production performance of microbes in large-scale applications. Combined with predictive, kinetic modelling, novel strategies for robust strain design and engineering can be developed.

## 3) Validation of hypotheses using mutant strains

According to our observations, energy metabolism seemed to play a key role on how cells face substrate perturbations. For *E.coli*, we propose to improve intracellular glycogen and polyphosphate measurements to explore these potential mechanisms of energy homeostasis. In addition, perturbation studies with respective knock-out strains will validate or reject the derived hypotheses.

## 4) Data integration and multi-scale modeling

Multi-omics approaches play a significant role in the quantitative description of cellular behaviour under dynamic conditions but result in large datasets and wide range of information. Not only high quality data are needed in terms of genome, transcriptome, proteome, metabolome and fluxome, but the main challenge lies on the integration of these data to make them useful for answering the scientific questions posed.

The need for predictive dynamic kinetic models and the experimental and computational challenges have been widely discussed in literature, as well as in this work (Chapters 2 and 4). However, small steps shall be taken towards improving the cellular characterization by kinetic models, under dynamic conditions. Here we showed how carbon storage metabolism and energy-spilling reactions undoubtedly affected model predictions. Implementation of these kinetics are indispensable for optimizing dynamic models and should be taken into consideration when constructing new ones. Future studies should also focus on metabolic

pathways beyond central carbon metabolism, using for example untargeted metabolomic techniques with isotope tracing [15, 16]. The choice of these regions, also, depends on the desired product and efforts for a better characterization of them should be made in genetic and regulation level.

Heterogeneity, in other words studying the response of individual cells rather than population averages, has shown that there are broad differences from cell to cell [17]. The effects of cellular heterogeneity on the population response are not well-characterized and represent a challenge for the construction of dynamic models, as current models describe an “average cell”, rather than single cells with different properties.

Additionally, already for the “average cell” kinetic models, the identification of kinetic parameters is challenging (Chapter 4).  $^{13}\text{C}$  tracer experiments can be used to obtain more information, allowing to first quantify intracellular fluxes, including parallel and bidirectional reactions and then kinetic parameters (Chapter 2).

Next to mechanistic modelling, big data analysis and machine learning could offer (non-mechanistic) approaches to improve bioreactor operation and strain design. Several attempts have already been made on the analysis of cultivation data for process optimization [18, 19] and machine learning approaches are also under development [20-23].

The integration of experimental observations and kinetic modelling continues to optimize solutions for microbial performance limitations, during large-scale cultivations, but also providing new insights on cell biology and redefining current knowledge.

And more importantly, close collaboration between academia and industry will shape the future of biotechnology and exploit its benefits on humans and the environment.

## References

1. Veening JW, Smits WK, Kuipers OP: **Bistability, epigenetics, and bet-hedging in bacteria.** *Annu Rev Microbiol* 2008, **62**:193-210.
2. Neubauer P, Junne S: **Scale-down simulators for metabolic analysis of large-scale bioprocesses.** *Current Opinion in Biotechnology* 2010, **21**:114-121.
3. Noorman H: **An industrial perspective on bioreactor scale-down: What we can learn from combined large-scale bioprocess and model fluid studies.** *Biotechnology Journal* 2011, **6**:934-943.
4. Wang G, Tang W, Xia J, Chu J, Noorman H, van Gulik WM: **Integration of microbial kinetics and fluid dynamics toward model-driven scale-up of industrial bioprocesses.** *Engineering in Life Sciences* 2015, **15**:20-29.
5. Wang G, Zhao J, Haringa C, Tang W, Xia J, Chu J, Zhuang Y, Zhang S, Deshmukh AT, van Gulik W, et al: **Comparative performance of different scale-down simulators of substrate gradients in *Penicillium chrysogenum* cultures: the need of a biological systems response analysis.** *Microbial Biotechnology* 2018, **11**:486-497.
6. Kuschel M, Siebler F, Takors R: **Lagrangian Trajectories to Predict the Formation of Population Heterogeneity in Large-Scale Bioreactors.** *Bioengineering (Basel)* 2017, **4**.
7. Haringa C, Tang W, Deshmukh AT, Xia J, Reuss M, Heijnen JJ, Mudde RF, Noorman HJ: **Euler-Lagrange computational fluid dynamics for (bio)reactor scale down: An analysis of organism lifelines.** *Eng Life Sci* 2016, **16**:652-663.
8. Muller S: **Modes of cytometric bacterial DNA pattern: a tool for pursuing growth.** *Cell Prolif* 2007, **40**:621-639.
9. Cheng YH, Chen YC, Brien R, Yoon E: **Scaling and automation of a high-throughput single-cell-derived tumor sphere assay chip.** *Lab Chip* 2016, **16**:3708-3717.
10. Helmstetter CE: **Timing of Synthetic Activities in the Cell Cycle.** In *Escherichia coli and Salmonella Cellular and Molecular Biology*. 2 edition. Edited by Neidhardt FC. Washington, DC, USA: ASM Press; 1996: 1627-1639.
11. Nitta N, Sugimura T, Isozaki A, Mikami H, Hiraki K, Sakuma S, Iino T, Arai F, Endo T, Fujiwaki Y, et al: **Intelligent Image-Activated Cell Sorting.** *Cell* 2018, **175**:266-276 e213.
12. Sassi H, Nguyen TM, Telek S, Gosset G, Grunberger A, Delvigne F: **Segregostat: a novel concept to control phenotypic diversification dynamics on the example of Gram-negative bacteria.** *Microb Biotechnol* 2019, **12**:1064-1075.
13. Lemoine A, Delvigne F, Bockisch A, Neubauer P, Junne S: **Tools for the determination of population heterogeneity caused by inhomogeneous cultivation conditions.** *J Biotechnol* 2017, **251**:84-93.
14. Ho P, Westerwalbesloh C, Kaganovitch E, Grunberger A, Neubauer P, Kohlheyer D, Lieres EV: **Reproduction of Large-Scale Bioreactor Conditions on Microfluidic Chips.** *Microorganisms* 2019, **7**.
15. Kiefer P, Schmitt U, Müller JE, Hartl J, Meyer F, Ryffel F, Vorholt JA: **DynaMet: a fully automated pipeline for dynamic LC-MS data.** *Anal Chem* 2015, **87**:9679-9686.
16. Huang X, Chen YJ, Cho K, Nikolskiy I, Crawford PA, Patti GJ: **X13CMS: global tracking of isotopic labels in untargeted metabolomics.** *Anal Chem* 2014, **86**:1632-1639.
17. Lidstrom ME, Konopka MC: **The role of physiological heterogeneity in microbial population behavior.** *Nat Chem Biol* 2010, **6**:705-712.
18. Nickel DB, Cruz-Bournazou MN, Wilms T, Neubauer P, Knepper A: **Online bioprocess data generation, analysis, and optimization for parallel fed-batch fermentations in milliliter scale.** *Engineering in Life Sciences* 2017, **17**:1195-1201.
19. Suarez-Zuluaga DA, Borchert D, Driessen NN, Bakker WAM, Thomassen YE: **Accelerating bioprocess development by analysis of all available data: A USP case study.** *Vaccine* 2019, **37**:7081-7089.



20. Treloar NJ, Fedorec AJH, Ingalls B, Barnes CP: **Deep reinforcement learning for the control of microbial co-cultures in bioreactors.** *PLoS Comput Biol* 2020, **16**:e1007783.
21. Carbonell P, Radivojevic T, García Martín H: **Opportunities at the Intersection of Synthetic Biology, Machine Learning, and Automation.** *ACS Synthetic Biology* 2019, **8**:1474-1477.
22. Oyetunde T, Liu D, Martin HG, Tang YJ: **Machine learning framework for assessment of microbial factory performance.** *PLoS One* 2019, **14**:e0210558.
23. Costello Z, Martin HG: **A machine learning approach to predict metabolic pathway dynamics from time-series multiomics data.** *NPJ Syst Biol Appl* 2018, **4**:19.





# Acknowledgements



## Acknowledgements

My PhD journey could not have been successful without the help, love and support of all the people to whom this section is dedicated. Sometimes words are not enough to express gratitude, but I can reassure you that they come right out of my heart. I apologise to the non Greek-speaking readers for switching to Greek in some parts, but some feelings are hard to express in English.

My greatest acknowledgements are firstly addressed to my supervisors, for their inspiration and for ensuring the value and quality of this work. **Aljoscha**, my first “thank you” goes to you for giving me the opportunity to come to Delft and follow my dreams. Thank you for your guidance all these years, your insights, which steered me through this project, and mainly for doing your best to promote my critical thinking skills. **Mark**, thank you for “adopting” me, even if I belonged to another research group! I am grateful for your support and for transmitting your passion for research. Thank you for your encouragement and for always being willing to listen. I am, also, profoundly grateful to both of you for your efforts on replying to all my questions, reading all my writing attempts, correcting, suggesting and discussing, during the challenging writing process of this thesis.

I would like to deeply thank the **committee members** for spending time to evaluate my work and for participating in my thesis defense.

I am also grateful to all the **partners** of the ERA-IB funded consortium **DYNAMICS**, which this project was a part of. Thank you all for the fruitful discussions during our meetings, your hospitality and your collaboration.

The next part of acknowledgements is dedicated to all my colleagues at the fantastic research group of Cell Systems Engineering.

Starting with the people who ensured the high quality of this research, I would like to thank the analytical team, performing analysis on literally hundreds of my samples. **Martin, Cor, Patricia** and **Carol**, thank you for your contribution to my experimental work and your persistence on achieving high accuracy in the measurements. I am grateful for your help on optimizing methods and protocols and for being always available for discussions and explanations. **Johan**, thank you for the TOC and TN measurements (being always so fast!) and for making my mood by always being so cheerful! It is even harder to express my gratitude for **Dirk, Rob** and **Yi Song**, the lab “super-heroes”. Saving fermentations from disaster, resisting exploding tubes, fighting angry bacteria foaming inside gas tubes, saving fainting PhD students (Song thank you for that!) and many more. Special thanks to my lovely ladies **Apilena, Astrid** and **Jannie**. No fermentations would have been possible without you. You have taken good care of my reactors and probes and have organized the “kitchen” so well to

make sure that everything would be available when needed. Bedankt for the fun lunch breaks! All of you have been a valuable part of my research and I hope you keep up with the excellent work!

**Sef, Walter and Martin**, I would like to thank you for your advice and for using your experience on supporting this research. **Jenifer**, you also deserve a big acknowledgement for taking care of all my administration issues, finding solutions to every problem I brought on your desk and for being such a joyful member of the team.

To my officemates (older and newer): **Leonor** thank you for your generous support and your true friendship. You were there for me during the whole duration of this journey, with unconditional help and encouragement. Thank you for the short and long discussions, especially during times of “crisis”, and for all the fun we had together in and outside the office! And thanks for the Portuguese hospitality in São Brás de Alportel! **Mariana**, I will always be grateful for teaching me so many things on building my own reactors, especially in my first year. Gracias por todo! To the blond German angel, **Robin**: your directness and extreme honesty were certainly the spices of everyday life in our office! Thank you for offering me so much laugh (especially when fighting with Leonor like kids in the kindergarten) and for sharing your experience and knowledge whenever I needed it. **Jinrui**, thank you for all the generous advice you have given me and for being the influence of calm and tranquillity in the office. **Koen**, thank you for being always enthusiastic and willing to help and for the countless fun moments of hanging around, eating lunch and dropping by our lovely DE coffee machine! Big thanks also for translating the summary of this thesis in Dutch!

There are of course many more people in the group to thank, because we may have not shared offices, but we for sure shared unforgettable moments in and outside the lab! My warmest gratitude to all my PhD colleagues for proving that research is impossible without their support and teamwork. Thank you for assisting me in the lab with many different tasks and special thanks to my <sup>13</sup>C rapid sampling team! My sweet girls **Yaya, Florence and Francisca**, I feel glad meeting you and learning so much next to you. Thank you for your kindness and for always caring about me. **Hugo**, it is really tough to find the right words for you. Thank you for everything you have done for me, for your advice, true care and genuine friendship. **Karel**, it has been a pleasure working with such a wise man. Hearing you singing (almost every day), through the wall of our office, offered really amusing moments in my daily routine. Gracias for teaching me some real biology and for your tips regarding my trip to Cuba, which made it an unforgettable experience! **Lucas, Maxime, Agi, Carla, Ana Sofia and Alex** thank you for your support and all the nice times we had together. You are all very charismatic and I wish you from heart a bright future!

Of course I could not forget people outside the CSE group, who deserve my acknowledgements. **Ana Maria** and **Pablo**, the Colombian lovely couple, thank you for laughing, laughing and laughing together! **Monica**, thanks for all the fun and for walking me through the most optimistic side of life! Keep that great smile and kindness of yours no matter what! **Cristina** mi querida amiga, thank you chica for the crazy moments we had together (including some volcano adventures) and for teaching me how to be a “strong independent woman”! Last but not least, I have to sincerely thank my Greek, super crazy and noisy friend, **Emma**, who was the “sunshine” of the department. Thank you for making me forget what the word “booooooooooring” (as you call it) means! I miss our “frappe” breaks so much, even if they made me a passive smoker! Ευχαριστώ κοριτσάρα!

But more importantly, I would like to thank you all for the great moments we spent together and for the friendship bonds we created. Where could I start from? Coffee and lunch breaks, barbecues, dinners, Christmas gatherings, gifts, trips, parties, conferences, courses, BT sport days, activities like bouldering, bowling, bobsleighbing and surfing, birthdays and many more! So many memories which will remain an unforgettable part in my heart. Hopefully, even more will follow with you guys! THANK YOU ALL!

During my PhD I also had the luck to supervise very talented students. I would like to deeply thank **Yannick**, **Catarina**, **Jacob**, **Frédéric** and **Lotte** for contributing to this project, for their hard work, commitment and for being patient with my lack of experience in supervising! I did my best to support you, as you also did for me and I am grateful I had the chance to work with you!

Being away from home can be hard for many reasons, and missing mum’s food is one of these. Thus, I would like to thank **Dimitris** and **Maria** for opening their canteen in the Fellowship, offering traditional and super tasty Cretan food, which completely changed my lunch breaks the last 2 years. Thank you for your generosity and affection! Μαρία τα σουτζουκάκια σου είναι ένα ανεξίτηλο κομμάτι αυτού του διδακτορικού!

Just before the end of my Chemical Engineering studies, I decided to do my final thesis at the Technical University of Denmark (DTU), as an Erasmus exchange student. In the Bioenergy group, where I worked, I experienced an incredible working environment, which motivated me to pursue a PhD afterwards. The people, who mainly influenced this decision, were my supervisors. **Irini**, **Ingólfur**, **Merlin** and **Ioannis**, thank you for inspiring me with your passion for research and for being great teachers.



And now it is time for the Greek gang to be acknowledged. My friends in the Netherlands who made me feel like home and who enabled me to achieve a good balance between work and personal life during the PhD. The order of the names is random, I anyway consider all of you my second family. Αγαπημένο μου «Φουλ», **Ελένη, Δάφνη, Δάφνη και Δάφνη** (περίμενα πως και πως να το γράψω αυτό!), νονέ μου **Βασίλη, Γιώργο, Ρενάτο, Βίτο, Βάλια, Μάνο, Μαρία, Αντρέα, Ναταλία, Χρήστο, Μιχάλη, Πάνο** (aka Κολιός) και **Αρετή**, thank you for the countless moments of joy and craziness we have experienced in and outside of the Netherlands, for your endless support towards my PhD, even if you thought that my work was just feeding bacteria and then killing them (ok maybe it was not far from that ☺), and most importantly for the enormous love I have received from you! Τόσες παρέες, ταξίδια, γλέντια, στιγμές, συναισθήματα... Ελπίζω αυτοί οι δεσμοί να μας κρατάνε για πάντα κοντά όσο μακριά κι αν είμαστε. Σας ευχαριστώ και σας αγαπώ! **Δήμητρα**, the greatest Dalmuta, you were one of the first real friends I made in the Netherlands, already in my first months here. Thank you for being always by my side and letting me open my heart to you. And of course thank you for all our amazing trips and holidays we spent together! Girls know how to have fun! **Πάνο**, my beloved classmate, we may still struggle to learn some Dutch but these classes were definitely worth for the fun and the memories. Thank you for your love and the endless hours we spent eating pita gyros, soutzoukakia, pastitsio and discussing about eating while we were eating! **Νίκο**, Μέγα αρχι-διδάσκαλε, thank you for trusting me with the responsibility of the Greek dance team, a magical world full of energy and feelings. I am also grateful for the great work you did on designing the cover of this thesis. **Κωνσταντίνα**, αλάτι, thank you as well for helping out with the thesis cover, but also for being the coolest housemate during COVID-19 times, which we spent full of food, Pamela sweat and laughter! **Αρίσταρχε**, crazy boy, thank you for putting so much laughter in my life, for your kindness, the countless bad jokes (freezing temperatures) and of course the sweaty dancing memories, that we both enjoy more than anything else! I would also like to thank all my co-dancers in the “**Kaneloriza**” Greek dance group, with whom I was able to share my love and passion for Greek traditional dances in the Netherlands. This has been the place where I could always forget any problems and release all my stress during the last 5 years.

To the people who never forget me, no matter how far away we are from each other, and support me to the fullest. **Άρη, Δημήτρη** (Μητσούλης), **Νικόλα** (πουρέκκι), **Δημήτρη** (aka Παραλίας), **Δανάη**, μπατσατοομάδα **Δημήτρη και Νίκο, Βασίλη** (λατρεμένη μου Παλιαμπελιώτη), κουμπάρικια **Άντζυ και Άγγελε** ευχαριστώ για όλα! **Νονέ και νονά** ευχαριστώ για τη θερμή σας αγάπη όλα αυτά τα χρόνια!

Reaching the end of this section, the following acknowledgements are the greatest and the hardest to properly address. However, this thesis would be unfinished without them.

To the man who has been patiently standing on the backstage of this journey, my daily encouragement, my daily care, my love. **Νικολάκη** μου, ευχαριστώ που με αντέχεις και με κάνεις καλύτερο άνθρωπο.

This thesis is dedicated with all my heart to my family, my **mum**, my **dad** and my **sister**. Μαμά, μπαμπά και αδερφούλα, σας ευχαριστώ που με βοηθήσατε να ανοίξω τα φτερά μου και να ακολουθήσω το δρόμο που ήθελα. Σας ευχαριστώ για την ακούραστη στήριξή σας και την απέραντη αγάπη σας!

Γιαγιά Ελένη, γιαγιά Ντίνα, παππού Παντελή και παππού Τάκη, ελπίζω να είστε περήφανοι!

**Thank you all!**

**Σας ευχαριστώ όλους!**



## **About the author**



## Curriculum vitae

Eleni Vasilakou was born the 16<sup>th</sup> of March, 1991 in Ioannina, Greece. Driven by her interest on chemistry, she was admitted at the School of Chemical Engineering of the National Technical University of Athens (NTUA), in 2009. There, she acquired the Diploma in Chemical Engineering (5-year studies equal to BSc and MEng), with a specialization in Biotechnology and Food Engineering. For the scope of her studies, Eleni performed her internship at the National Center for Scientific Research “Demokritos”, in Athens, where she did chemical analysis of suspended particulate matter in the atmosphere.



Biotechnology was the field which intrigued her the most during the last years of her studies. Thus, in 2014 she joined the research group of Prof.dr.ir. Irimi Angelidaki at DTU Environment, at the Technical University of Denmark (DTU), as an Erasmus exchange student, for her final diploma thesis. During this 6-month project, she worked on developing a biorefinery approach of macroalgae *Laminaria digitata* for the production of succinic acid, feed rich in proteins and biogas, co-supervised by Prof.dr.ir. Gerasimos Lyberatos (NTUA).

After her graduation, she joined the group of Cell Systems Engineering of the Technical University of Delft (Department of Biotechnology) as a PhD student, in 2015. Her project was funded by the ERA-IB consortium DYNAMICS (ERA-IB-14-081) and the Dutch Research Council (NWO 053.80.724) and was supervised by Dr. Aljoscha S. Wahl and Prof.dr.ir. Mark C.M. van Loosdrecht. The project focused on unravelling the effects of substrate gradients on the metabolism of bacteria *Escherichia coli* and the results are discussed in this dissertation.

Since September 2020, she is working as a Senior Associate Scientist in Janssen Pharmaceutica in Leiden, the Netherlands.

## Scientific Publications

**Vasilakou, E.**, van Loosdrecht, M.C.M., Wahl S.A. (2020). *Escherichia coli* metabolism under short-term repetitive substrate dynamics: Adaptation and trade-offs, *Microbial Cell Factories*, Volume 19, Pages 116.

Giordano, G., de Graaf, L.M., **Vasilakou, E.**, Wahl, S.A. (2019). Unraveling energy homeostasis in a dynamic model of glycolysis in *Escherichia coli*. 18th European Control Conference (ECC), Naples, Italy, Pages 2140-2145.

**Vasilakou, E.**, Machado, D., Theorell, A., Rocha, I., Nöh, K., Oldiges, M., Wahl, S.A. (2016). Current state and challenges for dynamic metabolic modeling. *Current Opinion in Microbiology*, Volume 33, Pages 97–104.

Alvarado-Morales, M., Gunnarsson, I.B., Fotidis, I.A., **Vasilakou, E.**, Lyberatos, G., Angelidaki, I. (2015). *Laminaria digitata* as a potential carbon source for succinic acid and bioenergy production in a biorefinery perspective. *Algal Research*, Volume 9, Pages 126-132.

## Scientific Awards

**1<sup>st</sup> Best Poster Award:** Vasilakou, E., van Loosdrecht, M.C.M., Wahl S.A., “*Escherichia coli* metabolism under short-term substrate dynamics: Adaptation and trade-offs”, Metabolic Pathway Analysis (MPA), Riga, Latvia, 12<sup>th</sup> – 16<sup>th</sup> August 2019

**2<sup>nd</sup> Best Poster Award:** Vasilakou, E., Alvarado-Morales, M., Gunnarsson, I.B., Fotidis, I.A., Angelidaki, I., “Succinic acid production through a novel third generation biorefinery concept”, 2nd International Conference on Algal Biorefinery (ICAB): A potential source of food, feed, biochemicals, biofuels and biofertilizers, Technical University of Denmark (DTU), Lyngby, Denmark, 27<sup>th</sup> – 29<sup>th</sup> August 2014